

Safety-Driven, Time-Sensitive Approach Strategies for Rendezvous with the Lunar Gateway

Tyler F. Rhodes

Thesis submitted to the Faculty of the
Virginia Polytechnic Institute and State University
in partial fulfillment of the requirements for the degree of

Master of Science
in
Aerospace Engineering

Riley M. Fitzgerald, Chair

Kevin K. Schroeder

Shane D. Ross

April 28, 2025

Blacksburg, Virginia

Keywords: Spacecraft Rendezvous, Three-Body Relative Motion, Rendezvous Safety,

Trajectory Optimization, RPOD

Copyright 2025, Tyler F. Rhodes

Safety-Driven, Time-Sensitive Approach Strategies for Rendezvous with the Lunar Gateway

Tyler F. Rhodes

(ABSTRACT)

Spacecraft Rendezvous, Proximity Operations, and Docking (RPOD) is a critical phase in expedition and resupply missions to space stations. These operations have been extensively studied and executed in the two-body dynamic context with the International Space Station (ISS). These operations are subject to numerous operational requirements to reduce the risk of approaches and ensure the safety of the crew and the space station itself. Missions to the planned Lunar Gateway space station will be no different. However, Gateway resides in Near Rectilinear Halo Orbit (NRHO) around the Earth-Moon L2 point in cislunar space. The classical RPOD understandings through models such as the Clohessy–Wiltshire equations break down in a three-body dynamics-based orbit like the NRHO, requiring proven approach strategies currently used for approaching the ISS to be redesigned. This thesis studies trajectory design within a three-body relative motion context under circular restricted three-body problem (CR3BP) dynamic assumptions, resulting in a novel approach strategy for Gateway. The work addresses a hole in the currently proposed strategies by providing nominal and contingent strategies for visiting vehicles (VVs) to execute to safely and efficiently approach the station, regardless of Gateway’s position in its NRHO, enabling a time-sensitive rendezvous. Three key aspects of an approach strategy are addressed: (1) identification of Delta-V-efficient and passively safe approach axes for a VV to approach along; (2) transfers/trajectories design to enable VVs to efficiently “hop” between hold points (HPs) along the identified axis/axes while remaining safe in the event of various failure modes; (3) station-keeping

strategy selection to enable a VV to maintain an HP when required safely yet efficiently. The conducted analysis breaks the NRHO into six unique regions defined by the orbit's dynamics and geometry, creating consistent regions to tailor operational strategies to the orbit's highly variable time-dependent dynamics. An axis is identified for each region that ensures passive safety for VVs while reducing station-keeping fuel costs. Two unique time-driven approach schemes are presented, resulting in one adopted scheme that allows for safe transfers between four selected HP distances. For times when a VV must halt its approach for extended durations, traditional station-keeping alternatives are identified that allow VV operators to reduce fuel consumption without compromising safety. These optimized components of an approach strategy found through CR3BP modeling are implemented in a full ephemeris dynamics model in STK that affirms the simplified modeling results. The work is concluded with a transit diagram that provides a cohesive visual representation of all avenues shown to enable a safe, timely, and ΔV efficient approach with Gateway.

Safety-Driven, Time-Sensitive Approach Strategies for Rendezvous with the Lunar Gateway

Tyler F. Rhodes

(GENERAL AUDIENCE ABSTRACT)

NASA's Artemis Program plans to establish a new crewed space station in an orbit in space near the Moon. This station, known as the Lunar Gateway, enables crew and supply transfers to Earth and the Lunar surface. An essential aspect of missions to space stations, like the International Space Station (ISS) and Gateway, is the rendezvous, proximity operations, and docking phase, colloquially referred to as RPOD. RPOD involves a secondary spacecraft operating near a primary spacecraft to attach itself to the primary spacecraft. This mission phase has been extensively studied and executed for missions to stations near Earth. These stations operate in Low Earth Orbit (LEO), and their motion is generally governed by a simple dynamics model that only includes the gravitational effects of Earth. Gateway's orbit, known as a Near Rectilinear Halo Orbit (NRHO), differs from these LEO-based stations and is governed by the more chaotic dynamics model, which simultaneously considers the Earth's and Moon's gravitational effects. This difference in governing dynamics breaks down the methods currently used to approach LEO stations, requiring new techniques to account for the increased dynamic complexity of Gateway's NRHO. This thesis focuses on the trajectory design of an RPOD approach strategy with Gateway utilizing models incorporating the three-body dynamics. These strategies must adhere to strict requirements pertaining to the safety of the trajectories that are in place to reduce the risk of an approaching vehicle on both the station's crew and the station itself. To create the strategy, Gateway's NRHO is partitioned into six regions defined by the orbit's changing dynamics. For each region, an

approach path is identified that allows the approaching vehicle to transfer between points along the route safely and efficiently from a fuel perspective. The transfers themselves are constructed in this thesis, and their safety is studied in the event one of four potential failures occurs. In anticipation that an approaching vehicle will be required to pause its approach for a given period, strategies for efficiently holding its position relative to the station are identified. These three aspects are stitched together to form the comprehensive approach strategy for a vehicle attempting to rendezvous with Gateway. The presented strategy addresses a current hole in previously proposed strategies by enabling approaches to occur regardless of where Gateway is located within its roughly 6.5-day orbit. Enabling the approach in all portions of the orbit allows vehicles to execute their RPOD phase in case a time-critical scenario arises. The work concludes with a transit diagram that provides a cohesive visual representation of all proposed strategies that have been shown to enable a safe, timely, and fuel-efficient approach with Gateway.

Dedication

*To my parents and family for your unwavering support in spite of not really knowing what
it is I do. The pretty pictures are for you.*

Acknowledgments

First and foremost, I'd like to thank my parents, for whom, without their love and encouragement throughout my life, I would never have reached this point. You are my rock, enabling me to pursue all my life's passions.

This thesis would not have been possible without the guidance of my advisor, Dr. Riley Fitzgerald. You are one of the smartest and most genuine professors/people I have encountered during my tenure at Tech, and it has been a pleasure to have your insights and feedback throughout this process. I am going to miss weekly advising meetings that were often more geek-out sessions on data visualization, obscure units, and graphic presentation than discussions about rendezvous strategy design. Thank you for your wisdom over the past year.

To my committee members, Dr. Shane Ross and Dr. Kevin Schroeder, I have had both of you as professors during my undergraduate and graduate degrees. You are both as passionate and student driven as they come in the AOE department. Thank you for your passion for teaching and for your feedback throughout this project.

To my blended family, you have shaped me into who I am and always provided support and curiosity for my interests and studies. From shenanigans up on the lake to cherished memories across the pond, you take a man with eyes for the stars and make him glad he's down here on Earth.

To the friends I made along the way, from COVID-constrained move-in day at Hoge Hall through the undergrad AOE gauntlet, long days at soy field launch sites, Florida Beaches and NASA-sponsored Vegas trips for senior design, and finally, to those who sat through my weekly rambles in the Fitzgerald Lab, thank you for taking in this Massachusetts-heralding

northerner and making me a better engineer, student, and person.

Thank you to the Virginia Tech Aerospace and Ocean Engineering Department I've called home for five years. The opportunities, experiences, and support the department has given me are second to none.

Finally, to Sam, who has kept me mentally intact this past year. Thank you for listening to me ramble about random topics late at night and being a constant motivator as I hunkered down to push this across the finish line. Thank you for being one of the brightest spots in a very bright year.

Contents

List of Figures	xiv
List of Tables	xxii
1 Introduction	1
1.1 The Lunar Gateway	2
1.2 Spacecraft Rendezvous, Proximity Operations, and Docking	5
1.3 Proposed Work	7
1.3.1 Gateway Orbit Segmentation	9
1.3.2 Hold Point Axes Identification	9
1.3.3 Hold Point to Hold Point Transfer Selection	10
1.3.4 Safety Verification	10
1.4 Thesis Outline	10
2 Background	12
2.1 Motivating Work	13
2.1.1 3-Body Relative Motion	13
2.1.2 Station RPOD Standards	18
2.1.3 Applied Strategies for Rendezvous within the Three-Body Problem	28

2.2	Technical Gap	34
2.3	Approach	36
3	Methodology	38
3.1	The Circular Restricted 3-Body Problem	39
3.1.1	Equations of Relative Motion	42
3.2	Trajectory Construction and Numerical Methods	45
3.2.1	Trajectory Propagation	46
3.2.2	Single Shooting Method	46
3.3	Gateway Orbit Definition	48
3.4	Adopted Rendezvous Standards	49
3.4.1	Safety Regions	50
3.4.2	Visiting Vehicle Safety	52
3.5	Strategy Realization in STK	55
3.6	Strategy Visualization and Communication	57
3.7	Summary of Methods	59
4	Results	61
4.1	Gateway Orbit Analysis	63
4.1.1	Orbit Dynamics	64
4.1.2	Orbit Velocity Segmentation	64

4.1.3	Orbit Velocity-Geometric Segmentation	67
4.2	Hold Point Axes Identification	70
4.2.1	Hold Point Station-Keeping Cost Analysis	71
4.2.2	Hold Point Safety Analysis	77
4.2.3	Region-to-Region Transfers	92
4.3	Station-Keeping Strategy	99
4.3.1	Traditional Station-Keeping	99
4.3.2	Station-Keeping Alternative: Loitering Trajectories	100
4.3.3	Station-Keeping Alternative: “On-Orbit” Loitering	104
4.3.4	Optimal Station-Keeping Approach	109
4.4	Rendezvous Approach Schemes	110
4.4.1	All-in-One Region Approach	112
4.4.2	One Hold Point per Region Approach	123
4.5	Strategy Realization	134
4.5.1	Approach Implementation	134
4.6	A Complete Gateway Rendezvous Approach Strategy	142
4.6.1	Rendezvous Transit Diagram	142
4.6.2	Nominal Approach Example	147
4.6.3	Off-Nominal Approach Example	150

5 Conclusion	153
5.1 Summary of Contributions	153
5.1.1 Motivation and Main Objectives	154
5.1.2 Essential Findings	155
5.2 Limitations	158
5.2.1 Dynamics Simplifications	158
5.2.2 Trajectory Construction	159
5.3 Suggested Continuations	161
5.3.1 Revisions to Presented Work	161
5.3.2 Natural Next Steps	162
5.4 Conclusion	163
Bibliography	165
Appendices	173
Appendix A CR3BP 9:2 NRHO Reference Orbit Look Up Table	174
Appendix B Loiter Station-Keeping Trade Study Heat Maps	194
Appendix C Misfire Safety Monte Carlo Simulation Plots	198
Appendix D Partial Burn Safety Plots	215

Appendix E “On-Orbit” Loiter TOF Optimization Contour Plots	232
Appendix F STK “One HP per” Approach Passive Safety Analysis	236
Appendix G Note on Franzini and Innocenti’s LVLH EORM	239

List of Figures

1.1	Lunar Gateway Configuration	3
1.2	Proposed Artemis Orbit Alternatives	4
1.3	Historic RPOD Mission Examples	8
2.1	Literature Review Diagram	14
2.2	Three-Body Relative Motion System Visualization	16
2.3	Standard Two-Body LVLH Coordinate Frame	20
2.4	Common Approach Strategies for Crewed RPOD Missions	21
2.5	ISS Safety Regions for CRS Missions	22
2.6	Cygnus' Nominal Rendezvous Approach with ISS	24
2.7	Cygnus' Rendezvous Approach Passive Safety	25
2.8	Cygnus' Rendezvous Approach Abort Trajectory Safety	26
2.9	IRSIS Safety Zone Structure.	27
2.10	Proposed Nominal Gateway Rendezvous Approach	30
2.11	Proposed NRHO Rendezvous Region.	32
2.12	Earth Moon 9:2 NRHO Full Ephemeris Monodromy Matrix Eigenvalue Magnitudes	33
2.13	Multi Orbit Hold Trajectory	34

3.1	CR3BP Coordinate Frames	40
3.2	CR3BP Relative Motion System	42
3.3	Single Shooting Method Schematic	47
3.4	9:2 Southern L2 NRHO Orbit Visualization	50
3.5	Approach Safety Regions	52
3.6	Safe v. Unsafe Free Drift Trajectory Illustration	53
3.7	Gateway NRHO NAIF 15 Year Reference Orbit Segment	56
3.8	Massachusetts Bay Transit Authority Rapid Transit Diagram	58
4.1	Approach Strategy Development Flow Diagram	62
4.2	9:2 CR3BP NRHO Position and Velocity	65
4.3	NRHO Velocity Region Segmentation	66
4.4	Velocity-Geometric Region Segmentation Approach Illustration	68
4.5	NRHO Velocity-Geometric Region Segmentation	69
4.6	Region 1 Loiter v. Station-Keeping ΔV Cost Analysis	73
4.7	Region 2 Loiter v. Station-Keeping ΔV Cost Analysis	75
4.8	Region 3 Loiter v. Station-Keeping ΔV Cost Analysis	75
4.9	Region 4 Loiter v. Station-Keeping ΔV Cost Analysis	76
4.10	Region 5 Loiter v. Station-Keeping ΔV Cost Analysis	76
4.11	Region 6 Loiter v. Station-Keeping ΔV Cost Analysis	77

4.12	HP On Axis Departure Failure Analysis Configuration.	78
4.13	Region 1 Optimal Approach Axis Passive Drift Trajectories	80
4.14	Region 2 Optimal Approach Axis Passive Drift Trajectories	81
4.15	Region 3 Optimal Approach Axis Passive Drift Trajectories	82
4.16	Region 4 Optimal Approach Axis Passive Drift Trajectories.	83
4.17	Region 5 Optimal Approach Axis Passive Safety	84
4.18	Region 6 Optimal Approach Axis Passive Safety	85
4.19	Optimal Approach Axis HP Passive Safety	86
4.20	Region 1 Suboptimal Approach Axis Passive Safety	88
4.21	Region 2 Suboptimal Approach Axis Passive Safety	89
4.22	Region 6 Suboptimal Approach Axis Passive Safety	90
4.23	Suboptimal Approach Axis HP Passive Safety.	91
4.24	HP1 Region-to-Region Transfer Between Region 1 and Region 2	93
4.25	HP1 Region-to-Region Transfer Between Region 1 and Region 2 Random Misfire Monte Carlo Simulation	95
4.26	HP1 Region-to-Region Transfer Between Region 1 and Region 2 Random Partial Burn Safety	97
4.27	Region-to-Region Transfer for HP2 and HP4 Between Region 6 and Region One Partial Burn Safety	98
4.28	HP1, 2, 3, and 4 Accumulated Station-Keeping ΔV Cost Over Region Duration	101

4.29	Loiter Visualization	102
4.30	Region 1 Loiter v. Station-Keeping ΔV Benefit Analysis	103
4.31	“On-Orbit” Hold Visualization	106
4.32	On Orbit Hold Transfer TOF Optimization.	107
4.33	Station-Keeping Alternative Comparison for Holds from Region Six through Region 2	108
4.34	VV Rendezvous Approach Illustration	111
4.35	Region 1 “All-in-One” Approach Transfer TOF Optimization	113
4.36	“All-in-one” Region 1 Approach Profile	116
4.37	“All-in-one” Region 2 Approach Profile	117
4.38	“All-in-one” Region 3 Approach Profile	118
4.39	“All-in-one” Region 4 Approach Profile	119
4.40	“All-in-one” Region 5 Approach Profile	120
4.41	“All-in-one” Region 6 Approach Profile.	121
4.42	“One HP per” Approach Profile Beginning in Region 1	126
4.43	“One HP per” Approach Profile Beginning in Region 2	127
4.44	“One HP per” Approach Profile Beginning in Region 3.	128
4.45	“One HP per” Approach Profile Beginning in Region 4	129
4.46	“One HP per” Approach Profile Beginning in Region 5	130
4.47	“One HP per” Approach Profile Beginning in Region 6	131

4.48	“One HP per” Approach Transfer Two Beginning in Region Six Random Misfire Monte Carlo Simulation	132
4.49	15-Year Gateway Reference Orbit Partitioned using Velocity-Geometric Segmentation Approach	135
4.50	LVLH Coordinate System STK Visualization	137
4.51	Region 1 “One HP per” Nominal Approach Implemented within STK	138
4.52	“One HP per” Full Ephemeris Implementation Approach Transfer 3 Passive Safety Analysis	141
4.53	Approach Strategy Transit Diagram Region Transit Example	143
4.54	Approach Strategy Transit Diagram Region Transfer Example	144
4.55	Time Sensitive Rendezvous Approach Strategy With Lunar Gateway Transit Diagram.	146
4.56	Flight Engineer’s Illustrated Nominal Approach Plan	148
4.57	Transit Diagram With Highlighted Examples	149
4.58	Flight Engineer’s Illustrated Off Nominal Contingent Approach Plan	151
B.1	Region 1 Loiter vs Station Keeping ΔV Benefit Analysis	194
B.2	Region 2 Loiter vs Station Keeping ΔV Benefit Analysis	195
B.3	Region 3 Loiter vs Station Keeping ΔV Benefit Analysis	195
B.4	Region 4 Loiter vs Station Keeping ΔV Benefit Analysis	196
B.5	Region 5 Loiter vs Station Keeping ΔV Benefit Analysis	196

B.6	Region 6 Loiter vs Station Keeping ΔV Benefit Analysis	197
C.1	Region 1 to Region 2 Region-to-Region Transfer Random Misfire Fire Monte Carlo Simulations	199
C.2	Region 2 to Region 3 Region-to-Region Transfer Random Misfire Fire Monte Carlo Simulations	200
C.3	Region 3 to Region 4 Region-to-Region Transfer Random Misfire Fire Monte Carlo Simulations	201
C.4	Region 4 to Region 5 Region-to-Region Transfer Random Misfire Fire Monte Carlo Simulations	202
C.5	Region 5 to Region 6 Region-to-Region Transfer Random Misfire Fire Monte Carlo Simulations	203
C.6	Region 6 to Region 1 Region-to-Region Transfer Random Misfire Fire Monte Carlo Simulations	204
C.7	Region 1, HP1, 4 Hour Loiter Random Misfire Fire Monte Carlo Simulations	205
C.8	Region 1, HP1, 3.5 Hour Loiter Random Misfire Fire Monte Carlo Simulations	205
C.9	Region 1, HP2, 4 Hour Loiter Random Misfire Fire Monte Carlo Simulations	206
C.10	Region 1, HP2, 3.5 Hour Loiter Random Misfire Fire Monte Carlo Simulations	206
C.11	Region 1, HP3, 4 Hour Loiter Random Misfire Fire Monte Carlo Simulations	207
C.12	Region 6 to Region 1 38 Hour Loiter Random Misfire Fire Monte Carlo Simulations	208
C.13	Region 1 “One HP per” Random Misfire MC Safety Analysis Plots	209

C.14 Region 2 “One HP per” Random Misfire MC Safety Analysis Plots	210
C.15 Region 3 “One HP per” Random Misfire MC Safety Analysis Plots	211
C.16 Region 4 “One HP per” Random Misfire MC Safety Analysis Plots	212
C.17 Region 5 “One HP per” Random Misfire MC Safety Analysis Plots	213
C.18 Region 6 “One HP per” Random Misfire MC Safety Analysis Plots	214
D.1 Region 1 to Region 2 Region-to-Region Transfer Partial Burn Safety	216
D.2 Region 2 to Region 3 Region-to-Region Transfer Partial Burn Safety	217
D.3 Region 3 to Region 4 Region-to-Region Transfer Partial Burn Safety	218
D.4 Region 4 to Region 5 Region-to-Region Transfer Partial Burn Safety	219
D.5 Region 5 to Region 6 Region-to-Region Transfer Partial Burn Safety	220
D.6 Region 6 to Region 1 Region-to-Region Transfer Partial Burn Safety	221
D.7 Region 6 to Region 1 38 Hour Loiter Partial Burn Safety	222
D.8 Region 1, HP1, 4 Hour Loiter Partial Burn Safety	223
D.9 Region 1, HP1, 3.5 Hour Loiter Partial Burn Safety	223
D.10 Region 1, HP2, 4 Hour Loiter Partial Burn Safety	224
D.11 Region 1, HP2, 3.5 Hour Loiter Partial Burn Safety	224
D.12 Region 1, HP3, 4 Hour Loiter Partial Burn Safety	225
D.13 Region 1 “One HP per” Partial Burn Safety Analysis Plots	226
D.14 Region 2 “One HP per” Partial Burn Safety Analysis Plots	227

D.15 Region 3 “One HP per” Partial Burn Safety Analysis Plots	228
D.16 Region 4 “One HP per” Partial Burn Safety Analysis Plots	229
D.17 Region 5 “One HP per” Partial Burn Safety Analysis Plots	230
D.18 Region 6 “One HP per” Partial Burn Safety Analysis Plots	231
E.1 On Orbit Hold Transfer TOF Optimization: -HP1.	232
E.2 On Orbit HoldTOF Optimization: -HP2.	233
E.3 On Orbit HoldTOF Optimization: -HP3.	233
E.4 On Orbit HoldTOF Optimization: +HP1.	234
E.5 On Orbit HoldTOF Optimization: +HP2.	234
E.6 On Orbit HoldTOF Optimization: +HP3.	235
F.1 “One HP per” Full Ephemeris Implementation Approach Transfer Departure Burn Passive Safety Analysis	237
F.2 “One HP per” Full Ephemeris Implementation Approach Transfer Arrival Burn Passive Safety Analysis	238

List of Tables

1.1	Artemis Architectural Trade Study	5
3.1	Earth-Moon CR3BP System Parameters and Constants	41
3.2	Numeric Integrator Configuration	46
3.3	Single Shooting Solver Configuration	48
3.4	CR3BP 9:2 NRHO Orbit Initial Conditions and Characteristics	49
3.5	Safety Region Definition	51
4.1	NRHO Velocity Segmentation Definitions	67
4.2	NRHO Velocity-Geometric Segmentation Definitions	70
4.3	ΔV -optimal Rendezvous Approach Axes	74
4.4	ΔV Suboptimal Rendezvous Approach Axes	87
4.5	Region-to-Region Transfers.	96
4.6	Adopted Station-Keeping Alternatives	110
4.7	“All-in-One” Approach Scheme Transfers	122
4.8	“One HP per” Approach Scheme Transfers	124
4.9	15-Year Gateway Reference Orbit Region Initial Time Stamps	136
4.10	“One HP per” Approach Scheme Transfers Full Ephemeris Dynamics Comparison	140

A.1 9:2 NRHO CR3BP Reference Orbit 174

List of Abbreviations

AC	Approach Corridor
AE	Approach Ellipsoid
AS	Approach Sphere
ATP	Authority to Proceed
COM	Center of Mass
CR3BP	Circular Restricted Three-Body Problem
CRS	Commercial Resupply Services
DARPA	Defense Advanced Research Projects Agency
DU	Distance Unit
EOM	Equations of Motion
EORM	Equations of Relative Motion
ER3BP	Elliptical Restricted Three-Body Problem
HP	Hold Point
HPOP	High Position Orbit Propagator
IDSIS	International Deep Space Interoperability Standards
IRSIS	International Rendezvous System Interoperability Standards

ISS	International Space Station
JPL	Jet Propulsion Laboratory
KOS	Keep Out Sphere
L1	Lagrange Point One
L2	Lagrange Point Two
LEO	Low Earth Orbit
LOP-G	Lunar Orbital Platform-Gateway
LVLH	Local-Vertical, Local-Horizon
MBTA	Massachusetts Bay Transit Authority
MEV	Mission Extension Vehicle
NAIF	Navigation and Ancillary Information Facility
NASA	National Aeronautics and Space Administration
NRHO	Near Rectilinear Halo Orbit
RPOD	Rendezvous, Proximity Operations, and Docking
RS	Rendezvous Sphere
STK	Systems Tool Kit
STM	State Transition Matrix

TOF	Time of Flight
TU	Time Unit
UTC	Coordinated Universal Time
VV	Visiting Vehicle

List of Symbols

δr	Relative Position Vector in Synodic Frame
$\hat{\delta}_x, \hat{\delta}_y, \hat{\delta}_z$	Relative Synodic Coordinate Frame Basis Vectors
$\hat{X}, \hat{Y}, \hat{Z}$	Inertial Coordinate Frame Basis Vectors
$\hat{x}, \hat{y}, \hat{z}$	Synodic Coordinate Frame Basis Vectors
Φ	Jacobian
ρ	Relative Position Vector
h	Specific Angular Momentum Vector
J	Objective Function
r_C	Chaser Position Vector
r_{em}	Moon Position Vector with Respect to the Earth
r	Position Vector
r_{C1}	Chaser Position Vector Relative to Earth in Synodic Frame
r_{C2}	Chaser Position Vector Relative to Moon in Synodic Frame
r_C	Chaser Position Vector in Synodic Frame
r_{T1}	Target Position Vector Relative to Earth in Synodic Frame
r_{T2}	Target Position Vector Relative to Moon in Synodic Frame

\mathbf{r}_T	Target Position Vector in Synodic Frame
\mathbf{v}	Eigenvector
\ddot{r}	Second Time Derivative of r
\dot{r}	First Time Derivative of r
$\frac{1}{\omega}$	Time Parameter
Λ	Stability Index
λ	Eigenvalue
μ	Mass Parameter
θ	Polar Angle
φ	Azimuthal Angle
L	Length Parameter
m_i	Mass of Body i
J	Jacobi Constant
LR	Lunar Radius
M	Mean Anomaly
T	Orbit Period
t	Time

Chapter 1

Introduction

“Exploration is in our nature. We began as wanderers, and we are wanderers still. We have lingered long enough on the shores of the cosmic ocean. We are ready at last to set sail for the stars.”

Carl Sagan, *Cosmos* [40]

Rendezvous, Proximity Operations, and Docking (RPOD) is a fundamental and critical process for an increasing number of space missions. Docking different vehicles in space has enabled the assembly of large space structures and optimized mission architectures dating back to the Apollo program [22]. Most missions with an RPOD process have occurred within well-behaved two-body dynamics. Here, the dynamics are approximately time-independent, and docking complexity is consistent regardless of position in the orbit. These characteristics are no longer true in a three-body dynamics context, e.g., the Earth-Moon system. Certain orbits in these regimes have dynamics with extreme fluctuations throughout a single period, increasing RPOD risks and complexity.

As missions extend more commonly into cislunar space where three-body dynamics dominate, specifically with the Artemis program and the planned Lunar Gateway station, three-body-based RPOD operations will become commonplace for mission operators. This thesis focuses on developing strategies for handling RPOD in cislunar space with the lens of approaching Gateway. The goal is to design ΔV -efficient approach strategies that adhere to the International Space Station’s (ISS) RPOD safety requirements currently in place that can be executed

regardless of timing/position in the three-body orbit. These strategies enable mission operators to execute approaches for rendezvous within time-critical scenarios when the ideal positioning of the station is not present. The work aims to comprehensively understand the costs and requirements for mission operators to execute an approach anywhere in the orbit.

1.1 The Lunar Gateway

Humanity first set foot on the Moon with the Apollo 11 mission. The United States continued an intermittent crew presence on the Moon through 1972, concluding with the Apollo 17 mission. Humans have not returned to the surface since. In 2017, the National Aeronautics and Space Administration (NASA) established the Artemis program with Space Policy Directive 1, aiming to establish a sustained crewed presence on the surface of the Moon while serving as a staging point for sending Humans onward to Mars in the future [46]. The program completed the Artemis I mission in 2023 and aims to return humans to the surface of the Moon during the Artemis III mission, tentatively scheduled for 2027 at the time of writing.

A critical component of the Artemis program is the Lunar Orbital Platform-Gateway (LOP-G), commonly called the Lunar Gateway. Lunar Gateway will be assembled across multiple missions beginning in 2028 during the Artemis IV mission. The station serves as a transfer interface between Earth and the Lunar surface. Gateway, like the ISS, is an international and commercial effort with various partners supplying unique modules that comprise the entire station. Figure 1.1 shows the proposed module breakdown [38]. The modules will support many functions similar to the ISS, including human habitation and scientific research.

The ISS currently operates in a near circular, regularly maintained Low Earth Orbit (LEO). This orbit is well-behaved and consistent, making rendezvous consistent and minimally

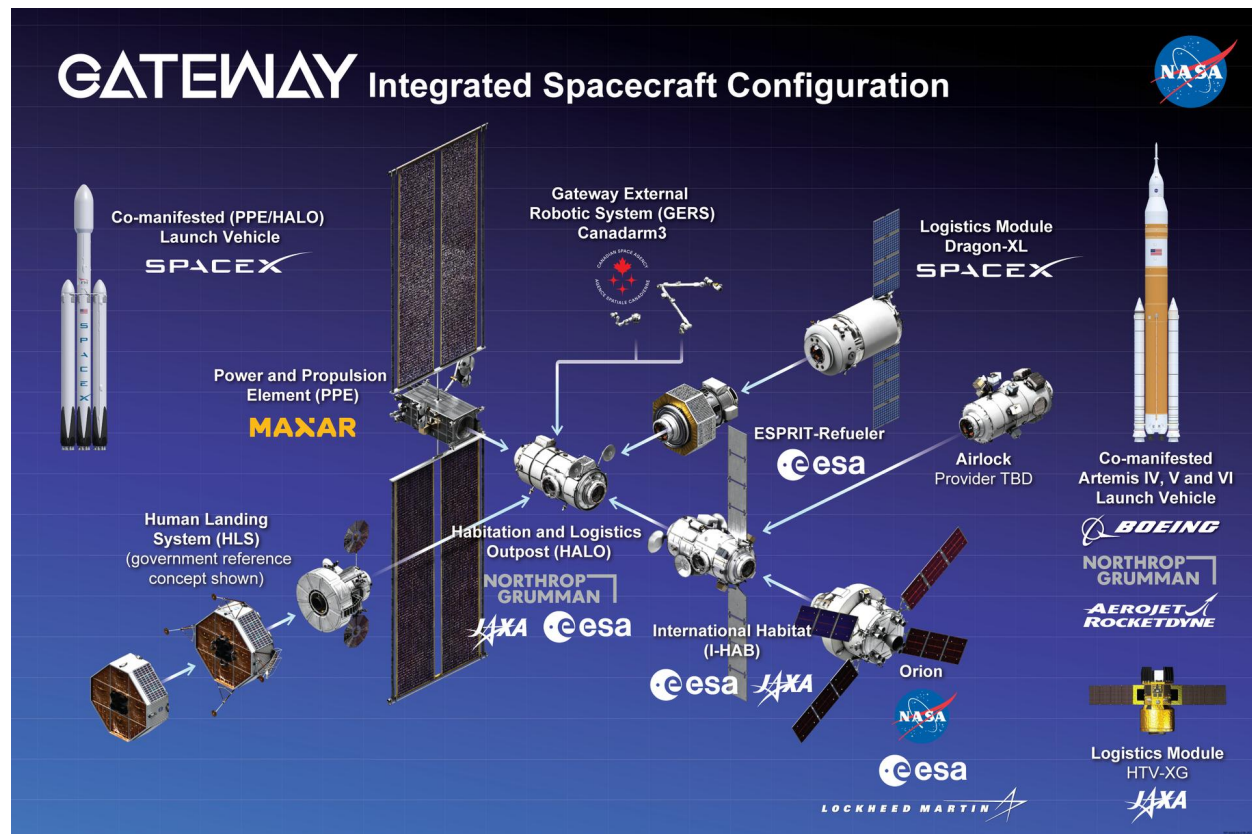


Figure 1.1: Lunar Gateway Configuration. The components of the Lunar Gateway are shown. Gateway is a joint international and commercial effort. Each segment's provider is denoted in the Figure. Figure reproduced from [38].

impacted by perturbations. The Lunar Gateway's proposed Southern Near Rectilinear Halo Orbit (NRHO) around the Earth-Moon Lagrange Point 2 (L2) in cislunar space is different. The NRHO is dominated by classical three-body dynamics where the Moon's pull on the station is also prevalent in addition to the Earth's gravitational pull. NASA selected the NRHO against alternative cislunar orbits. These orbits are visualized in Figure 1.2[4]. The trade between the different three-body orbits considered criteria such as various ΔV metrics, orbit maintenance costs, and RPOD complexity, among others. Table 1.1 [4] shows a qualitative summary of this trade. The NRHO provided an optimal balance between these metrics while being extensible for future crewed Mars campaigns.

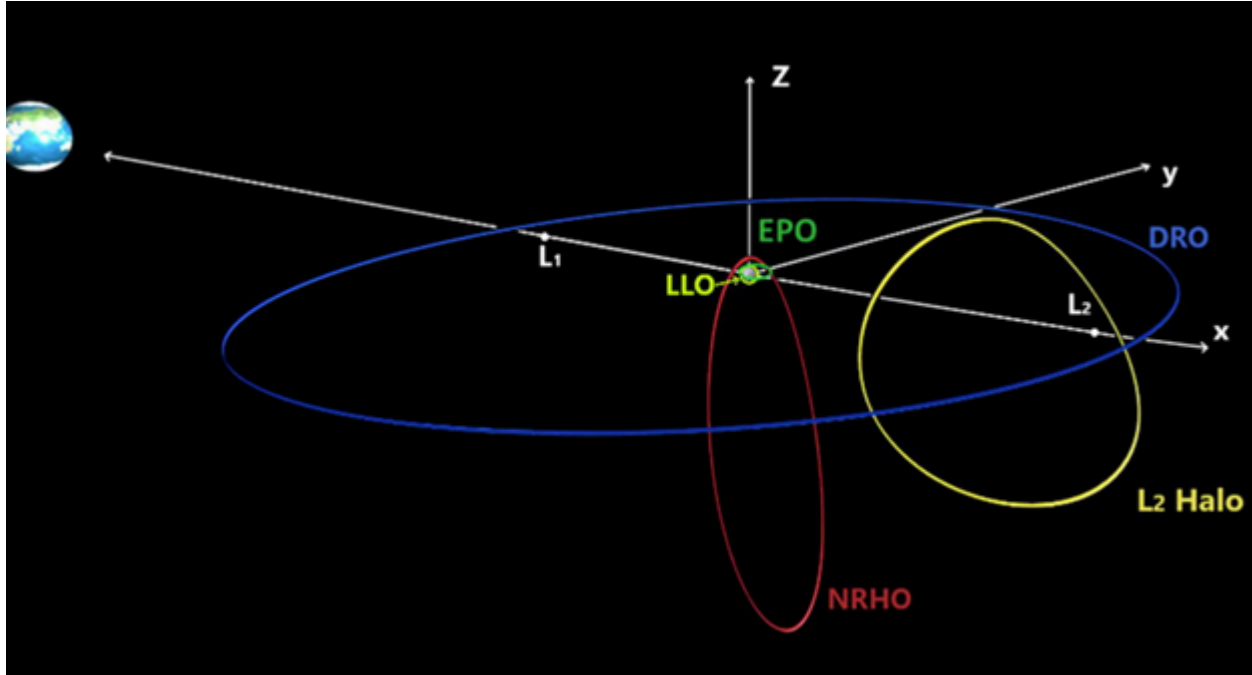


Figure 1.2: Proposed Artemis Orbit Alternatives. The Figure depicts six orbits considered for the Artemis program’s mission architecture. The orbits are visualized in the Earth-Moon synodic frame. The orbits were compared in a trade study shown in Table 1.1. The selected NRHO is traced in red. Figure reproduced from [4].

The NRHO does not come without its caveats. As will be shown later in the thesis, classifying RPOD dynamics within the NRHO as “near linear dynamics” is only valid in specific orbit segments. This characterization becomes invalid in the orbit’s Periselene region. Periselene is the point along the orbit closest to the Moon. This characteristic makes docking with Gateway a more complex process than with ISS. Great care needs to be taken while approaching the station in this region due to the risks associated with its chaotic nature. Minor errors in a vehicle’s state can propagate into significant errors down the line.

Furthermore, the ISS orbits the Earth approximately every 90 minutes. In contrast, the Gateway will complete one orbit about every 6.5 days. This long period makes rendezvous planning challenging to adapt to compared to the ISS for failed attempts or time-sensitive situations.

Table 1.1: Artemis Architectural Trade Study. The table shows NASA’s comparison between multiple cislunar orbit alternatives considered for the Artemis architecture. The orbits were compared using the multiple criteria shown. The cell color is normalized to white to compare against the selected NRHO option. Blue cells indicate better than the NRHO, while orange cells perform worse than the NRHO orbit. Table adapted from NASA NRHO white paper [4].

CISLUNAR ORBITS	Crew Vehicle Access ΔV	Lunar Access ΔV	Gateway Access ΔV	Orbit Maintenance	RPOD	Comm Cutouts	Power Thermal /	Mars Forward
Equatorial LLO	High	Infesible / Short	High	Low / Moderate	Circular Orbit	Moderate	Most Challenging	Minimal
Polar LLO	Highest, Shorter Earth Return	Low / Short Duration	Moderate / High	Low / Moderate	Circular Orbit	Moderate	Challenging	Minimal
EPO with CoLA	Moderate/High	Moderate Short Duration	Moderate / High	Moderate	Challenging	Moderate	Challenging	Minimal
NRHO	Moderate	Moderate Medium Duration	Moderate	Minimal	Near Linear Dynamics	None	Deep Space Equivalent	Extensible
Earth-Moon L2 Halo	Low / Moderate Longer Earth Return	Moderate Long Duration	Low / Moderate	Minimal	Near Linear Dynamics	None	Deep Space Equivalent	Partial Extensibility
DRO	Low / Moderate Longer Earth Return	High Long Duration	Low / Moderate	N/A	Near Linear Dynamics	Infrequent	Deep Space Equivalent	Minimal

Gateway is an exciting endeavor as humanity sets to establish an extended presence on the Lunar surface. However, many challenges exist that have not been encountered in the two-plus decades of ISS rendezvous. Tackling these challenges is an active field of study that this thesis will explore.

1.2 Spacecraft Rendezvous, Proximity Operations, and Docking

RPOD is an essential part of large-scale space operations. Large orbital habitats such as the ISS, Gateway, and proposed commercial LEO stations cannot be launched in a single

vehicle. They are too massive for any currently available and proposed vehicle to carry. The Apollo program was the first to implement a rendezvous to assemble a space structure when the command and service module docked with the lunar module to form a combined vehicle that traveled from Earth's orbit to the Moon [22]. The process was first executed during the Gemini VII mission, seen in Figure 1.3a. The Gemini VII vehicle docked with the Gemini VI vehicle in this demonstration.

Following the Apollo program, spacecraft docking quickly became a common occurrence. The Apollo-Soyuz project was the first instance of two international partners executing a rendezvous, with the USA-flown Apollo Service module joining the USSR-flown Soyuz spacecraft [22]. This collaboration was continued through the Shuttle-Mir program, where the USA sent multiple Shuttle missions to the Russian Mir station and again, today, with the ISS [22].

RPOD has not been limited to orbital stations. The shuttle program performed multiple crewed satellite servicing missions, most notably with the Hubble Space Telescope, to repair and exchange scientific instruments on the observatory [22]. The emergence of uncrewed satellite service vehicles is a rapidly progressing area for instances of RPOD. The Defense Advanced Research Projects Agency (DARPA) first executed an autonomous satellite servicing mission with Orbital Express in 2007 [21]. Northrop Grumman's Mission Extension Vehicle (MEV) has recently executed two autonomous servicing operations on Intelsat satellites [42]. MEV-1's approach is shown in Figure 1.3b [42].

Crewed RPOD with stations has distinct differences from the satellite servicing-focused missions. Safety and minimizing the risk posed to astronauts are always the number one concerns for crewed missions. The protection of the station assets is closely followed, and station docking comes with strict regulations and procedures that must be followed by any visiting vehicle. Vehicle operators traditionally enter joint operations with station controllers,

where station controllers have operational authority over the vehicle, dictating whether it can proceed as it approaches. In autonomous servicing missions, the servicing vehicle can operate with a greater degree of freedom. The operator of the vehicle being serviced may state requirements dictating that its vehicle is uninterrupted from its primary functions. However, its approach is entirely up to the servicer. Missions to Gateway will operate similarly to current ISS missions. Safety is as much of a design factor as fuel costs for mission designers for these missions.

Rendezvous operations enable unique mission and vehicle architectures not otherwise possible from those launched on a single launch vehicle. They enable missions to be extended through servicing operations and large stations to be assembled. The involvement of human life and valuable assets increases the design requirements for rendezvous mission profiles. These safety criteria further complicate the RPOD process in a cislunar context. The work of this thesis applies these safety requirements to the design of three-body-based rendezvous trajectories to form a viable rendezvous approach strategy for the future Lunar Gateway station.

1.3 Proposed Work

This thesis's technical space consists of the overlap of the unique dynamics of Gateway's orbit and the ridged expectations for visiting vehicles approaching a station. An approach strategy for Gateway must address four critical areas: (1) partitioning Gateway's orbit into regions with predictable behavior, (2) identifying an optimal approach axis for each region on which a chaser can remain for an extended period when necessary, (3) implementing non-prohibitive ΔV transfers between points along the approach axis, and (4) validating the safety of (2) and (3) to ensure safety throughout the entire approach.



(a) Gemini VII approaching Gemini VI in 1965. Photo from [39]. (b) Northrop Grumman's MEV-1 approaching Intelsat 901 in 2020. Photo from [42].

Figure 1.3: Historic RPOD Mission Examples. RPOD missions have significantly progressed since the first demonstration in 1965. Gemini VII performed the first docking demonstration in 1965, with Gemini VI in low Earth orbit. Gemini's approach is shown in Figure 1.3a. In 2020, Northrop Grumman's MEV-1 docked with Intelsat 901 in the first commercial autonomous satellite servicing mission. MEV's approach to Intelsat is shown in Figure 1.3b.

The thesis addresses these four areas by answering the following specific questions:

1. How can Gateway's NRHO be segmented into a finite number of regions within which the approach vehicle's behavior is qualitatively consistent throughout the region's duration? Does each region have its own qualities that require a change in operational strategy during the approach?
2. What axes extending outward from the station are both the safest and most efficient to approach along? Do the two-body "V-Bar"/"R-Bar" approach strategies hold in the three-body context, or is the approach skewed from the principal axes of the LVLH frame?
3. Do transfers exist that allow the visiting vehicle to "hop" along the identified approach axes in a time-effective manner without excessive ΔV expenditure?

4. Does the identified approach meet the safety criteria currently in place for the ISS and proposed for Gateway, which are required for visiting vehicles? Is the vehicle safe in the presence of loss of control at any point during the approach?

1.3.1 Gateway Orbit Segmentation

The first objective of the thesis is to identify unique regions within Gateway's orbit. This partitioning creates a set of time-dependent segments where mission operators can alter their decision-making processes to account for the changing dynamic environment of the orbit. Some regions may be more stable, allowing for a more aggressive and streamlined approach strategy. In contrast, other more chaotic regions may necessitate a more cautious approach with contingency plans in the presence of operational malfunctions. The behavior of the chaser should be consistent and predictable within each region.

The first main contribution of this thesis is identifying these regions and formulating a concrete definition for their bounds. Partitioning allows orbit position-dependent strategies to be constrained to unique orbit regions.

1.3.2 Hold Point Axes Identification

With unique regions of the orbit identified, region-specific hold point axes can be determined that allow for the most ΔV -efficient station-keeping for when a visiting vehicle is required to delay its approach. Finding these axes for each region based on ΔV cost and safety metrics is the second contribution of this thesis. It is an open question of whether the standard two-body approach axes will be either fuel-efficient or safe within the NRHO, and identifying the optimal axes serves as the backbone for an efficient approach strategy. This thesis aims to close this question.

1.3.3 Hold Point to Hold Point Transfer Selection

An approach strategy must specify an avenue for how the visiting vehicle approaches the station. Approach transfers during integrated operations between the station and visiting vehicle operators are extensively studied and validated before an RPOD scenario occurs [28]. They are not generated on the fly during an approach; a “go-around” or an abort is performed if the rendezvous cannot be completed via the predefined avenues. The third contribution of this work is to provide a set of transfers along the hold point axes that walk the visiting vehicle toward the station. These transfers cannot be cost-prohibitive to the visiting vehicle but also must conform to the requirements set by the station. The transfers will be generated and analyzed to ensure compliance with Gateway’s requirements.

1.3.4 Safety Verification

The entire RPOD process risks the safety of the station and the visiting vehicle. Space stations are multimillion to multibillion-dollar assets and have a minimal tolerance for risk. Safety is an unfudgeable requirement across the entire process of formulating a rendezvous approach strategy. The fourth contribution of this thesis is the safety verification of the solutions posed to the second and third driving questions for this thesis. The approach strategy must account for non-ideal situations where failure may occur at various instances during the approach.

1.4 Thesis Outline

The thesis is broken into five chapters, which are summarized below:

1. Chapter 1 sets the context for this thesis. It discussed the planned assembly and long-term operations of the Lunar Gateway around Earth-Moon Lagrange Point 2. A discussion of RPOD followed, describing the main features of such missions and their driving considerations.
2. Chapter 2 dives into the background and relevant literature pertinent to this thesis. Background research regarding three-body relative motion, RPOD standards, and applied RPOD strategies is presented. The chapter concludes by identifying the technical gap this work aims to fulfill and the approach taken to address this gap.
3. Chapter 3 outlines the work's methodology. The CR3BP and accompanying relative motion dynamics models are derived. The methods used to construct trajectories within an RPO context are described. Rendezvous safety is defined. The safety guidelines outline how trajectories will be validated to be safe or unsafe. A high-level outline of the strategy's "transit diagram" is provided. Lastly, a full-ephemeris model realization scenario within ANSYS' Systems Tool Kit® (STK) is detailed.
4. Chapter 4 presents the results of the work of the thesis analysis. Gateway's orbit is analyzed and segmented. ΔV -optimal approach hold points are identified and used to find a safe approach scheme for each portion of the station's orbit. Transfers are generated for two procedures, trimmed based on safety, and selected for ΔV efficiency. The adopted strategies are combined into a comprehensive approach transit diagram to provide a streamlined visual of the prescribed methods for a time-sensitive rendezvous. The adopted nominal approaches are then implemented into a complete ephemeris model to compare transfer costs and check safety.
5. Chapter 5 concludes the thesis with a summary of the work's key contributions and the research's limitations. The chapter presents potential continuations for the work and discusses the feasibility of implementing the strategy on real-world spacecraft.

Chapter 2

Background

“Scientific inquiry shouldn’t stop just because a reasonable explanation has apparently been found.”

Neil deGrasse Tyson, *Death by Black Hole: And Other Cosmic Quandaries* [44]

This chapter aims to provide an overview of the relevant background information, prior research, and literature pertinent to the work conducted within this thesis. The chapter begins with a discussion of the literature that motivated the work. The work done on RPOD dates back to the mid-20th century with the Gemini program, but most work has accrued over the past decade for three-body applications. The literature review is broken into three topic areas: “Three-Body Relative Motion Theory,” “RPOD Standard Practices and Regulations,” and “Applied Three-Body RPOD Strategies.” The discussion is followed by an outline of where current literature falls short and the approach taken to address the identified shortfalls.

- Section 2.1 breaks down the relevant research areas from which the thesis draws. Three topics are discussed, beginning with work about three-body Relative Motion Theory, followed by RPOD Standard Practices and Regulations, and concluded with the blend of these topics with Applied three-body RPOD Strategies. Figure 2.1 frames the work that makes up these topics.
- Section 2.2 highlights the current holes in the outlined research domain and emphasizes

the technical gap this thesis aims to fill.

- Section 2.3 outlines the approach taken to address the identified technical gap. It summarizes the planned methodology and resulting contributions of the thesis.

2.1 Motivating Work

Section 2.1 details prior work that has motivated the work of this thesis. The section explores works in building theory within three-body relative motion, rendezvous standard practices and governing operational regulations, and currently proposed strategies for three-body rendezvous that implement the discussion theory within the constraints of the operational standards.

This thesis assumes a solid understanding of restricted three-body problem theory like that discussed in Koon, Lo, Marsden, and Ross' textbook on the matter [29]. Section 3.1 details the concepts used in this work's analysis. Other topics leveraged in the referenced literature may be mentioned in the forthcoming review even if not used explicitly in this work.

2.1.1 3-Body Relative Motion

Relative motion between two or more spacecraft has been an extensively studied field. Missions dating back to the Gemini program necessitated the need to be able to model motion in space between two spacecraft [22]. The majority of this work, however, has been conducted within the two-body context, and until the past decade, there was minimal work done to explore RPOD in the three-body context.

Operating within dynamics dominated by the restricted three-body problems breaks

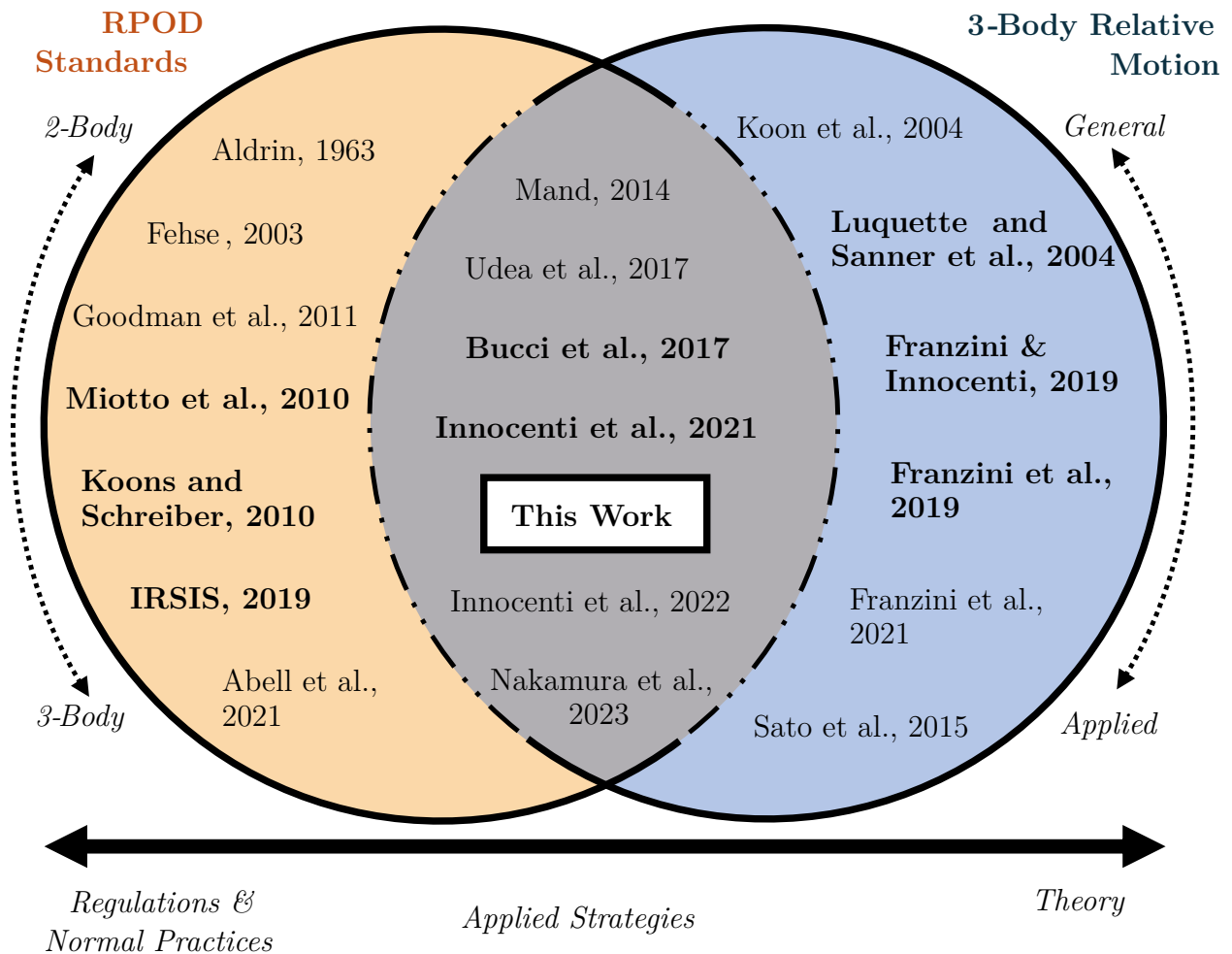


Figure 2.1: Literature Review Diagram. The Venn diagram above categorizes the relevant literature to this thesis [6, 7, 12, 16, 19, 19, 20, 22, 26, 27, 28, 29, 30, 34, 35, 36, 36, 37, 41, 45]. The left half contains works that detail the crewed RPOD standards of the past 60 years. The works are split between standards based on the two-body dynamics at the top and those based on the three-body dynamics at the bottom. The right half of the diagram focuses on works that formulated the theory and equations governing the dynamics of three-body relative motion. The works descend from those more focused on the underlying theory to those focused on exploring potential use cases for the theory. The middle of the diagram forms research that blends the two topics. These works focus on “Applied Strategies,” using the derived theory to design RPOD strategies that follow the standards and regulations. The works in bold are heavily leveraged within this work’s approach.

down the underlying assumptions and simplifications that Clohessy-Wiltshire equations and other two-body-based representations adopt [13]. As missions turn to operate further into cislunar space, using these equations becomes less reliable. Franzini and Innocenti, whose works in this field will be discussed later in Section 2.1.1, showed that the positional error in modeling relative motion with two-body based equations in a three-body context was in the order of kilometers [18]. Such errors are not acceptable if trying to model rendezvous between spacecraft. Relative motion models for missions in cislunar space need to be governed by a set of equations of relative motion (EORM) that account for three-body effects to be reliable.

A representative model for relative motion within a three-body environment necessitates that the force imparted by the second primary body be accounted for in the governing EORM. Early research involving rendezvous scenarios for spacecraft circumvented needing a set of EORM in the Local-Vertical, Local-Horizon (LVLH) frame to describe their rendezvous by simply taking the difference in state vectors obtained from using the restricted three-body problem equations of motion (EOM). In Luquette and Sanner’s paper, the authors define the relative state between a chaser spacecraft as subtracting the chaser’s state from the target’s state. [34]. The same technique is utilized by Ueda and Murakami’s paper and by Mand in his thesis [35, 45].

RPOD is traditionally studied in the LVLH frame. The motion of the chaser with respect to the target is best understood in this frame [22]. An operator can more intuitively relate the guidance readings in this frame, as Aldrin discussed in his dissertation [7]. Readings indicating above and below are truly above and below; those showing in front and behind are truly in front and behind, and those showing to the side are meaning truly to the side. Frames, like those based around barycentric coordinates, lose this intuition. Readings in the LVLH frame are critical for understanding the risk and safety of maneuvers [16]. Some research has taken results from the abovementioned technique and transformed them into an

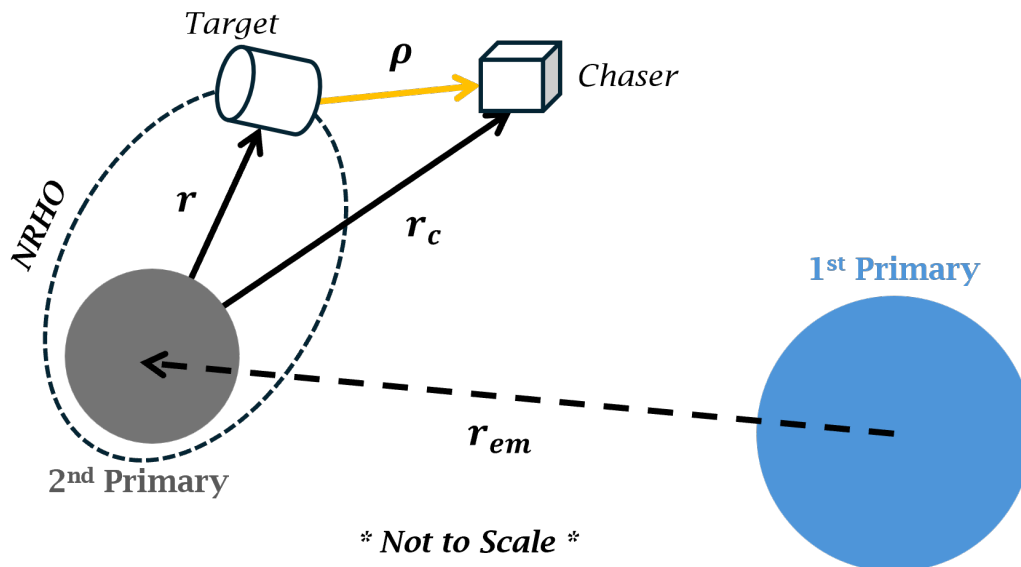


Figure 2.2: Three-Body Relative Motion System Visualization. This visualization of the dynamic system, adapted from [18], shows the bodies of interest within a three-body relative motion scenario. Here, the target is Gateway in its NRHO with a chaser nearby. Its position with respect to the Moon is represented by r . The chaser’s relative position to the target is represented by ρ and position with respect to the Moon by r_c . The Moon’s relative position with respect to Earth is represented by r_{em} .

LVLH representation for visuals post hoc. This approach provides valuable intuition given by the LVLH frame while leaving the underlying dynamics in a more simplified model.

Franzini and Innocenti were the first to derive a set of three-body EORM in an LVLH frame [18]. The equations derived imposed the restricted three-body problem where the system is dominated by two primary bodies, the first more massive than the second, while the third body’s mass is negligible within the system. The third body, in this case, is the target’s spacecraft. The system setup is shown in Figure 2.2 [18]. Their work derives $\ddot{\rho}$ relating the chaser’s position to the target in LVLH coordinates.

The equations are flexible to the user’s desired level of fidelity. Flexibility here means that if a user wants to employ the circular or elliptical restricted dynamics cases, they can do so. Also, the equation’s gravitational term has a linearized variant to speed up computation time

if desired. These assumptions come at the cost of model accuracy, especially in the Periselene region of the NRHO when modeled against an ephemeris model. Their work showed that model simplifications do not lead to insurmountable errors within a region around Aposelene. Franzini and Innocenti’s EORM allows three-body relative motion to be accurately modeled and analyzed without needing constant coordinate transformations.

Franzini and Innocenti’s work defined their *local vertical* as the negative radial vector from the chaser to the center of the Moon. Works since has utilized a solar referenced *local vertical* to align with the International Deep Space Interoperability Standards (IDSIS) International Rendezvous System Interoperability Standards (IRSIS) [28, 37]. The IDSIS’ IRSIS will be discussed more in Section 2.1.2. Utilizing the Sun to define local vertical risks losing the intuition provided to operators as the Sun can be eclipsed in cislunar space and cannot be seen. As such, the work in this thesis follows Franzini and Innocenti’s definition of *local vertical*.

Franzini and Innocenti extensively utilized these equations in later works [19, 20, 26, 27]. From a more theoretical perspective, Franzini used these equations to study rendezvous maneuver design for impulsive and continuous thrust-based trajectories [19, 20]. The EORM written in a state-based form was implemented in an adjoint model to explore performance using an Earth-Moon L1 NRHO as a reference for exploring both types of maneuvers. Both cases showed that computing maneuvers were possible with these equations and that the maneuvers were viable. Innocenti’s work with these equations is discussed later in Section 2.1.3 regarding applied rendezvous strategies.

Franzini and Innocenti’s equations require the computation of higher-order terms, such as the target’s third positional derivative and its specific angular momentum and acceleration at all points in the orbit. These additional terms increase computational complexity and have shown to be burdensome in application [17]. Luquette’s EORM require terms already

obtained through the propagation of the target’s position and velocity terms but are limited to the Circular Restricted Three-Body Problem (CR3BP) assumptions. Franzini’s and Innocenti’s equations best suit an intermediary level of fidelity between the CR3BP and a full ephemeris model, while Luquette’s serves as an efficient model within the CR3BP assumptions.

Two main EORM models have been implemented to date, providing valuable insights into RPOD dynamics in a three-body context. Franzini and Innocenti defined an intuitive frame to keep results consistent with two-body missions with more complex equations. Luquette equations are simplified to a nearly identical structure to the classic CR3BP EOM. They are a viable three-body analog to the two-body models, such as the Clohessy-Wiltshire equations. The work conducted within this thesis will use the more streamlined Luquette equations for the works underlying dynamics modeling while using the LVLH frame posed by Franzini and Innocenti to visualize results.

2.1.2 Station RPOD Standards

The work of this thesis focuses on RPOD with an inhabited station. RPOD takes a different flavor with additional constraints and considerations in this context. Protecting the people’s lives on the station and protecting some of the most expensive assets in all human history is paramount [14, 15]. The literature reviewed regarding RPOD standards focuses on those done with humans involved either on the chaser spacecraft, target spacecraft, or both.

Standard RPOD Approach Profiles

With the space race well into gear in the mid-20th century, engineers and scientists viewed rendezvousing and assembling structures in orbit as a solution to minimizing the required

booster size on the ground [22]. The first successful docking of two objects in space occurred in 1966 during the Gemini VIII mission [22]. The preceding missions and those to follow helped explore approach profiles and set precedents on the best ways to conduct a crewed docking operation.

In the LVLH frame, in a two-body dynamics context, axes are commonly referred to as the R-Bar, V-Bar, and H-Bar: the R-Bar aligned with the radial vector pointing towards the Earth’s center of mass (COM), the H-Bar aligned with the target vehicle’s angular momentum vector, and the V-Bar completes the orthogonal triad to form the LVLH frame [13]. In circular orbits, the V-Bar aligns with the velocity vector of the target vehicle. A diagram of this frame can be seen in Figure 2.3, adapted from [11].

RPOD missions traditionally utilize one of two approach profiles, along the V-Bar or the R-Bar [49]. In a V-Bar approach, the chaser spacecraft proceeds closer to the target by making incremental “hops” along the target’s V-Bar, approaching the target by catching up from behind or falling back into it from ahead. Similarly, in an R-Bar approach, the chaser makes incremental “hops” along the R-Bar, climbing up to the station from below or descending on it from above.

Most profiles combine the two strategies, and either is adopted for a profile segment. Commonly, the chaser-to-target range is closed mainly along the V-Bar. However, in the final approach, the chaser climbs along the R-Bar, taking advantage of a concept known as “orthogonal breaking” to minimize fuel expenditure [22].

Goodman’s documentation of NASA crewed RPOD missions provides a comprehensive overview of crewed missions’ approach profiles and gives examples of the aforementioned approach strategies [22]. Figure 2.4 shows an example of a stable orbit approach and a coelliptic approach [22]. In the stable orbit approach, the chaser “station-keeps,” i.e.,

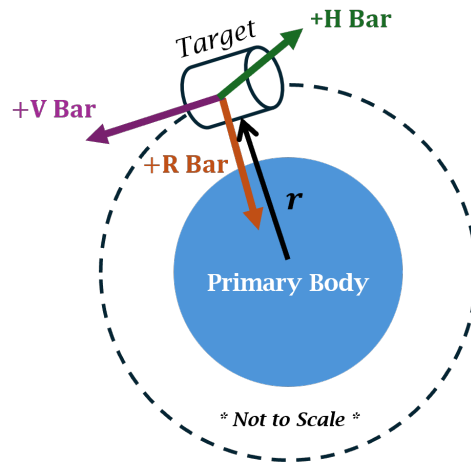


Figure 2.3: Standard Two-Body LVLH Coordinate Frame. The standard two-body LVLH Coordinate Frame is shown. The radial vector from the primary body for which the target body orbits defines the “R-Bar”. The “V-Bar” is the instantaneous velocity vector of the target at a given time in its orbit. The “H-Bar” is given as the cross-product of the R-Bar and V-Bar. This frame is where relative motion is most commonly shown.

maintains relative position and velocity with respect to the target on a stable point within the orbit before injecting itself into a terminal trajectory to rendezvous with the target. The coelliptic approach is made on a coelliptic orbit, primarily characterized by the two orbits being coplanar [22, 50]. The chaser catches up to the object below the V-Bar, tuning its orbit before executing the terminal phase injection to begin docking.

These approach strategies have been the standard of crewed rendezvous for well over half a century. The Shuttle program utilized them, and today, they continue to be utilized by the missions flown under the commercial resupply services (CRS) program [22, 36]. These approach strategies were employed with reducing human/mission risk, operational complexity, and fuel consumption in mind [22]. These two-body-based profiles and their motivations serve as an operational foundation from which to draw design approach strategies for crewed station RPOD profiles within a three-body context.

RPOD approaches depend heavily on sensor and tracking data acquisition for the onboard

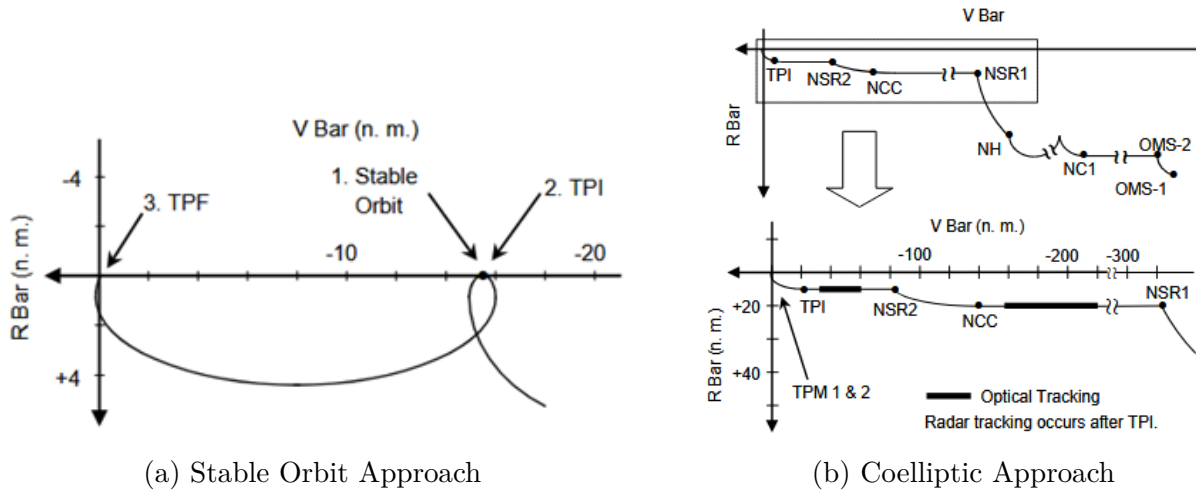


Figure 2.4: Common Approach Strategies for Crewed RPOD Missions. Figure 2.4a shows a stable orbit approach. The chaser vehicle inserts itself at a point ahead or behind the target on the V-Bar and holds till time for terminal phase insertion (TPI). TPI places the chaser on an intercept trajectory for rendezvous. Figure 2.4b shows a coelliptic approach. The chaser incrementally climbs closer to the station in a coelliptic orbit. The chaser occasionally course corrects and makes its TPI close to the target. Figures reproduced from [22].

guidance to be successful. This fact constrained the shuttle rendezvous execution of the profiles. Closed-loop guidance and sensor-driven navigation fall outside the scope of this thesis. As such, the trajectory design itself is of primary interest.

RPOD Safety Standards

The imposed safety requirements that vehicles must adhere to were not discussed above. For visiting vehicles (VV) to the ISS, a strict protocol must be followed [30, 36]. VVs to Gateway will be no different [28].

Like the ISS, Gateway will be visited by nations and numerous commercial entities during its construction and operations [38]. Rendezvous safety and risk mitigation regulations are already standard practice. Koons and Shreiber discuss the risk mitigation adopted by the SpaceX and Orbital Sciences Corporation, presently Northrop Grumman, vehicles for their

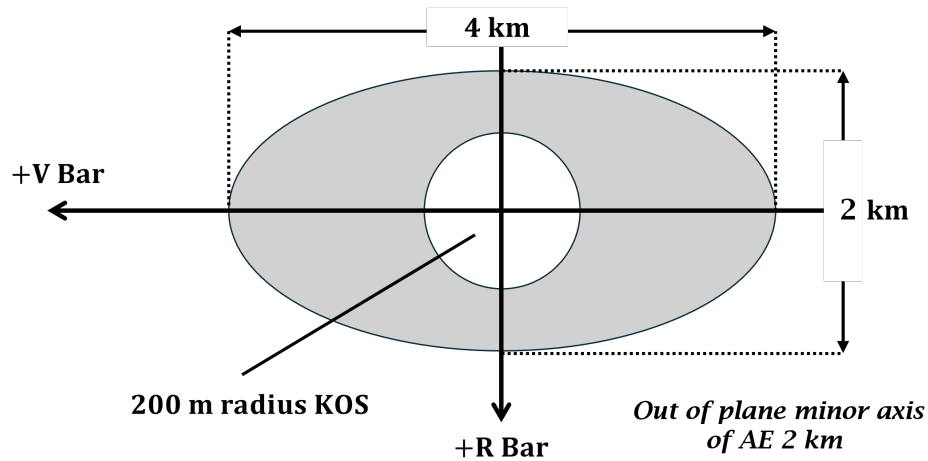


Figure 2.5: ISS Safety Regions for CRS Missions. A V-bar and R-bar cross-section of the ISS safety regions is shown. These regions are in place to mitigate the risk posed by VVs rendezvousing with the station. The AE surrounding the KOS is shown in grey. Figure adapted from [30].

respective CRS missions to the ISS [30]. From a trajectory standpoint, the primary method for risk mitigation is enforced by “safety regions.” The regions Koons and Schreiber show in their paper are depicted in Figure 2.5 adapted from [30]. The outermost region is the “Approach Ellipsoid” (AE), a 4 x 2 x 2 km ellipsoid centered on the ISS with the major axis in line with the station’s V-Bar. The inner region is the “Keep Out Sphere” (KOS), a 200 m sphere centered on the ISS.

Koons and Schreiber continue to discuss how these regions are utilized to mitigate risk to the station [30]. An hour and a half before the VV enters the AE, NASA and the vehicle operator enter integrated operations where NASA has control, but not command, authority over the vehicle. In other words, NASA is not sending commands directly to the vehicle, but they control how the operator can operate it. NASA must give the operator authority to proceed (ATP) before a vehicle enters a region. ATP is granted at various predefined decision points along the vehicle approach profile. ATP is granted based on multiple factors, including but not limited to vehicle status, ISS status, and the presence of potential risks

in the area. If ATP is not granted, the VV must wait outside the region until all issues are resolved. This process is repeated before the vehicle enters the KOS with at least one decision point between the AE and the KOS.

Miotto's paper discusses the work to validate the approach trajectories to the ISS for Northrop Grumman's CRS Cygnus vehicle [36]. Cygnus' nominal approach strategy is shown in Figure 2.6 [36]. The Figure on the right shows the coelliptic approach in the LVLH V-Bar/R-Bar cross-section, while the left shows the timeline of events annotated on the approach profile. The timeline shows the two decision points where ATP is decided. ATP-1 grants Cygnus permission to raise its orbit to and execute burns to approach the R-Bar within the AE. ATP-2 grants Cygnus permission to execute the AD3 burn to "acquire" the R-Bar and begin a series of burns to climb the R-Bar before finally being captured by the station's robotic arm.

Miotto's paper details the extensive analysis to validate this approach profile's safety. Mission faults that had to be accounted for included missed burns, partial burns, drag uncertainty, navigation errors, and the ability to abort at any point during the approach safely. Drag uncertainty is not an issue in Gateway's NRHO, and navigation is outside the scope of this work. However, the burn anomalies are of note for this thesis.

During Cygnus's approach, missed burns must be 24-hour free drift safe. This requirement means that if any burn failed to occur, Cygnus' resulting trajectory had to be shown so that it would not violate any safety regions for 24 hours. This validation for a missed ADV2 burn is shown in Figure 2.7 [36]. In this instance, Cygnus is granted ATP before approach initiation and completes ADV1. However, due to some vehicle anomaly, the ADV2 burn never occurs. The trajectory of Cygnus, with three sigma error bounds, is propagated 24 hours and shows the vehicle never enters either region without control. This kind of verification is completed for all burns in the mission profile.

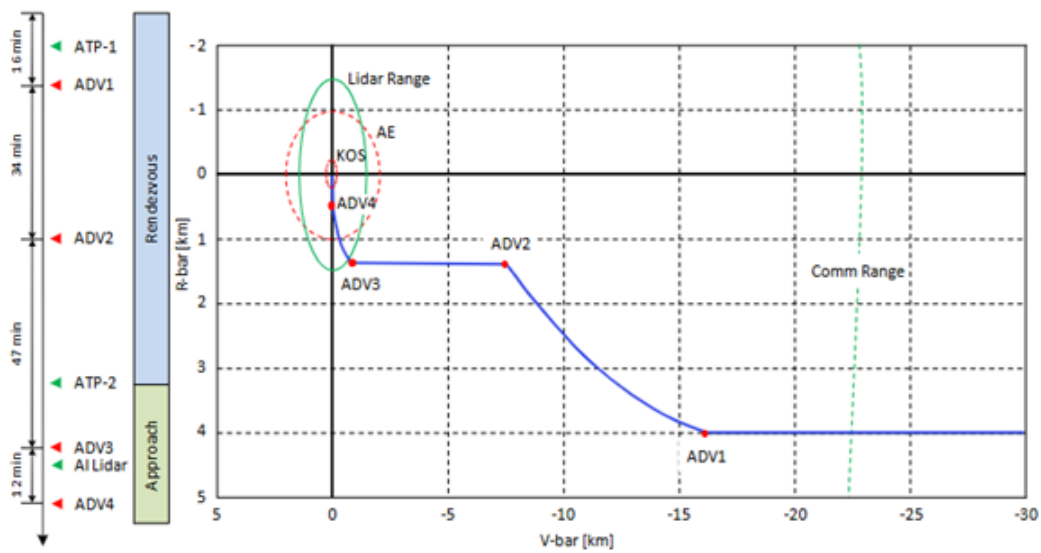


Figure 2.6: Cygnus' Nominal Rendezvous Approach with ISS. Cygnus' nominal approach with the ISS is shown. The autonomous resupply vehicle phases along a coelliptic orbit until it executes ADV1, a rendezvous insertion burn. Cygnus coasts until ADV2, establishing a new coelliptic orbit to phase closer to the R-Bar. ADV3 targets the R-Bar, and the vehicle climbs through the AE until ADV4 when the R-Bar is acquired just before the KOS. A glideslope navigation method controls the final approach inside the KOS. Figure reproduced from [36].

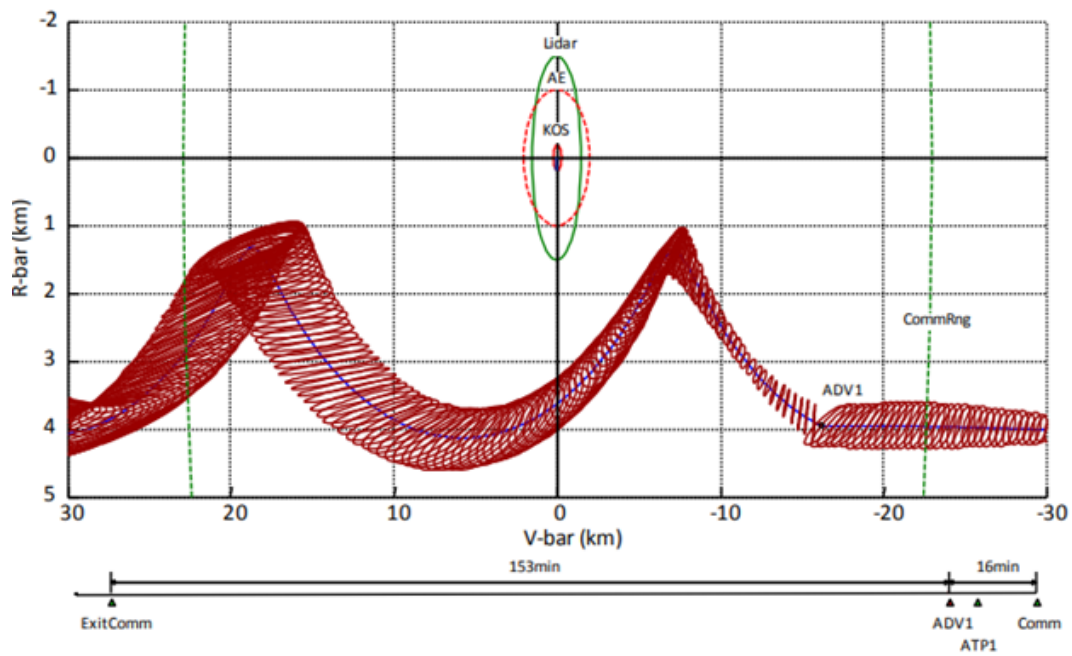


Figure 2.7: Cygnus' Rendezvous Approach Passive Safety. Cygnus' passive safety following the ADV1 burn is shown. If ADV2 were not executed, Cygnus would continue on its orbit caused by ADV1. The orbit's apogee is where ADV2 would occur. This orbit characteristic ensures the vehicle will never get any closer to the ISS along the R-Bar than at this point, ensuring passive safety for the station and vehicle. Figure from reproduced [36].

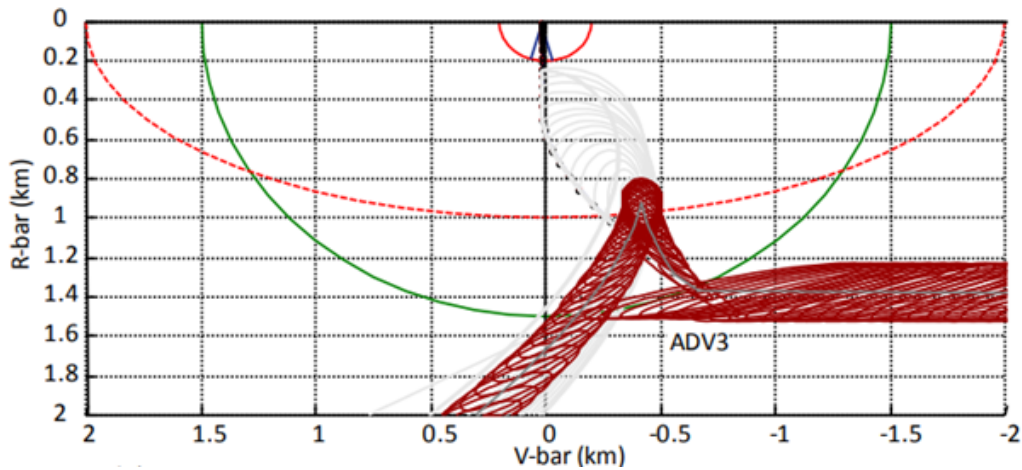


Figure 2.8: Cygnus' Rendezvous Approach Abort Trajectory Safety. Cygnus' trajectory following the ADV3 burn aimed to acquire the R-Bar is shown. At a time following the ADV3 burn, an abort burn is executed. The dispersion of potential resulting trajectories dependent on burn efficiency is plotted in gray. These trajectories meet the KOS safety requirement. Figure reproduced from [36].

The abort requirement for Cygnus mandated that anywhere below the KOS's 200 m floor, the vehicle must be able to abort onto a trajectory that never enters the KOS and leaves the AE in 90 minutes and remain out for 24 hours [36]. Figure 2.8 shows an example of this verification. In this example, Cygnus must abort after its ADV3 burn to acquire the R-Bar [36]. The grey lines show the dispersion of potential resulting trajectories after executing the abort burn. These risks must be accounted for in any Gateway rendezvous approach strategy design.

In 2019, NASA and ISS partner agencies developed the IDSS [28]. Nine standards have been published to date, including the IRSIS. The IRSIS aims to outline requirements for rendezvous operations, specifically within cislunar and deep space environments. The requirements outlined within the IRSIS were adapted from ISS protocol and lessons learned from past missions.

The section of interest pertinent to this thesis is the trajectory safety requirements for VVs

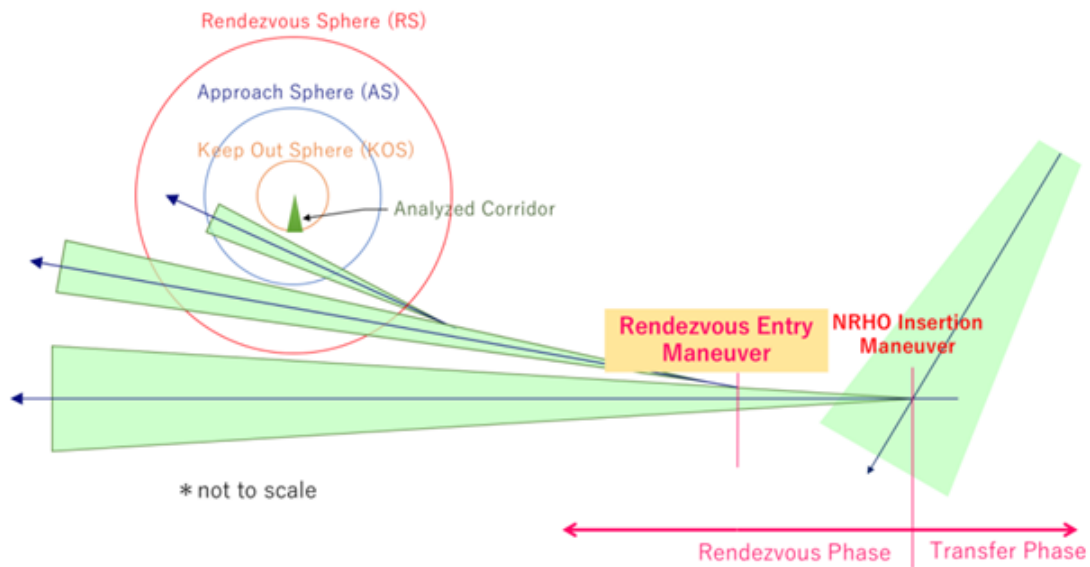


Figure 2.9: IRSIS Safety Zone Structure. The safety zones defined by the IRSIS are visualized. Each sphere is centered around the target. The RS is 10 km, AS is 1 km, and KOS is 200 m. VVs require ATP before entering the next zone. Only the AC is direction-dependent and traditionally is aligned with the station docking port. Figure reproduced from IRSIS [28].

to a station positioned in a cislunar orbit, i.e., a vehicle docking with Gateway. A similar structure to the CRS mission risk mitigation strategy can be seen here. The IRSIS safety zone structure is shown in Figure 2.9 [28]. Here, there are four main zones: a “Rendezvous Sphere,” an “Approach Sphere,” a “Keep Out Sphere,” and an “Approach Corridor” (AC). Not discussed before is the approach corridor. When inside the KOS, the VV must remain inside this cone and adhere to predefined paths inside the AC. The technical details of these zones will be discussed later in Section 3.4. Similar to the ISS rendezvous operations, at least one decision point exists between each zone. ATP must be given at each decision point before entering the next zone. If not given, the spacecraft must be held outside the zone until the reason for the hold is resolved.

The standard details numerous trajectory safety requirements for VVs. These include, among others, abort safety, drift safety, burn anomaly safety, and plume impingement. Burn

anomalies include missed burns, partial burns, and random unexpected burns. In each case, the resulting trajectories must be shown not to enter any safety zones without ATP.

Thruster plume impingement is important, specifically when close to the target, but falls outside the scope of this work. This work will focus on the approach strategy for the “far-field” rendezvous operations phase. This phase encompasses rendezvous orbit insertion to preparation for entry into the KOS [28]. In this phase, thruster plume impingement is a limited concern for VV ranges.

All these standards are in place to minimize mission risk and keep lives and assets safe. The operational protocols and regulations have been standard practice in the industry for decades. They have been executed in numerous missions and are cemented within the foundation crewed-involved docking operations. The protocol will continue to apply to cislunar RPOD missions, and the strategies must adhere to them.

2.1.3 Applied Strategies for Rendezvous within the Three-Body Problem

Work has been done to apply the discussed three-body relative motion theory and use it to design RPOD strategies in cislunar space [6, 12, 26, 27, 35, 37, 41, 45]. Papers have developed strategies for the three main phases of a cislunar rendezvous mission: launch and insertion, transfer, and rendezvous [28]. Specific papers propose mission plans from end to end [26, 37, 41]. However, as discussed in Section 2.1.2, this paper focuses on far-field rendezvous, which occurs in the rendezvous phase of the mission, so that is the portion of these works that will be highlighted.

In his 2023 work, Nakamura details the trajectory design for an uncrewed supply mission to the lunar Gateway in its southern L2 NRHO [37]. The rendezvous scenario occurs in the

Aposelene region of the NRHO, where the orbital dynamics are nearly linear. Aposelene is the point on the orbit furthest from the Moon. The trajectories were evaluated for safety, fuel consumption, and operational feasibility. The paper's safety requirements were that the vehicle's free-drift trajectories should not enter the 1 km AS.

The analysis utilizes Monte Carlo simulations to validate trajectory safety. Initial state error estimates accrued from the previous mission phases were utilized as a bound to perturb the planned initial state of the VV randomly. These initial rendezvous insertion states were propagated for 24 hours to confirm safety. The paper presented validation for the passive safety requirement with this method. The remainder of the paper focuses heavily on sensor-based navigation.

Mand designed a preliminary trajectory for an Orion rendezvous mission on an L2 halo orbit [35]. The L2 Halo orbit has much more consistent dynamics throughout its orbit. It is far less elliptic than a NRHO. The approach developed is a modified double co-elliptic approach analogous to the Orion LEO rendezvous profile. A true co-elliptic approach is not possible here due to the non-planar geometry of the Halo orbit. The double co-elliptic approach strategy was less effective in a Halo orbit than in LEO. However, Mand argued that preserving operational consistency justified the increased fuel costs. Monte Carlo and Linear Covariance simulations validated the vehicle trajectory's passive safety after each burn. The safety requirements were the same as the ISS safety requirements discussed before.

The most applicable and comprehensive paper on Gateway rendezvous trajectory risk mitigation was by Innocenti in 2021 [27]. The paper investigates hold point (HP) safety for three failure modes and proposes a strategy for re-rendezvous after failure. HPs are a stricter form of decision points, requiring the VV to hold before getting ATP. The analysis is built on the EORM derived by Franzini and Innocenti in their work discussed previously. This paper constrains the rendezvous event to the Aposelene region of the NRHO, referencing a paper

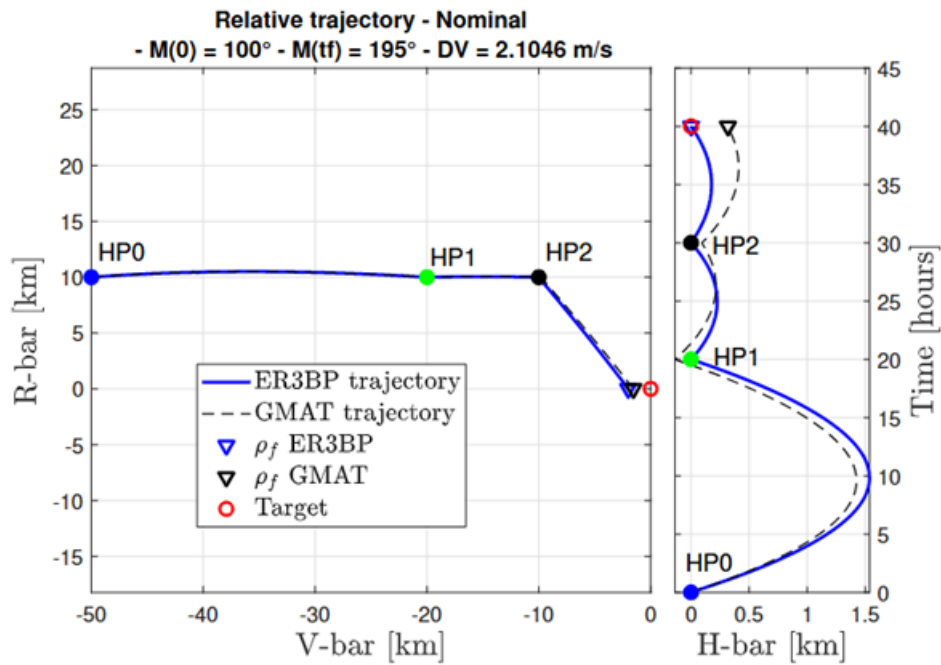


Figure 2.10: A nominal approach strategy for Gateway operating in an elliptical restricted three-body problem (ER3BP) generated NRHO proposed by Innocenti is shown. The approach places HPs (HP#) on unstable manifolds to ensure passive safety in case of an unexpected failure. The trajectory was compared to the result of executing the plan in a full ephemeris dynamics model. Figure reproduced from [27].

by Bucci [12] for the rationale. This work will be discussed later. The nominal trajectories of the proposed approach are shown in Figure 2.10 [27].

The failure modes considered were a missed departure firing from an HP, a missed arrival firing at an HP, and a random thruster firing during transfers between HPs. The aim was to validate the sequence of HPs in their rendezvous profile. Each HP proposed was used as the initial state for departure failure. Then, the resulting trajectory was propagated over one orbit to ensure a 10 km zone was not violated.

The arrival burn failure occurs at the end of a transfer between HPs. The procedure for validating safety is similar to the arrival burn failure; only the initial state is the state of the transfer trajectory at the time of the arrival burn. A random ΔV of 0.05 m/s is applied to

model a misfire at a random point along the transfer. Monte Carlo simulations were run for misfires in between each HP to analyze for potential safety violations.

The paper concludes with a proposed method for selecting a new optimized set of HPs for a re-rendezvous attempt following a failure. The method utilizes the naturally occurring unstable manifolds of the NRHO to ensure the HP's passive safety. This method showed acceptable fuel costs for re-attempt cases that met the paper's safety requirements.

In a later paper, Innocenti ties the far-field approach strategy into a complete three-phase approach starting from the lunar surface and ending at station rendezvous in the Aposelene region [26]. The orbital phasing during the transit face takes advantage of manifold theory drawn from the work of Koon, Lo, and Ross and its application in Ueda's paper of manifold phasing in cislunar space [29, 45]. The rendezvous strategy implements the techniques discussed in his earlier work, now incorporating sensor-based navigation analysis for the proximity of the phase of rendezvous operations.

Noted in the discussion of the strategies above has been the bounding of rendezvous in the Aposelene region of the NRHO [12, 18, 26, 27, 37]. This region is visualized by Franzini and Innocenti in their papers and shown in Figure 2.11 [18]. The bounding to actively performing RPOD strictly within this region is discussed by Bucci [12]. The Aposelene region provides the most linear dynamics within Gateway's NRHO. The orbital velocities are at a minimum here as well. Bucci shows the stability of the Aposelene region through analysis of the NRHO's monodromy matrix's eigenvalues. Figure 2.12 shows the eigenvalue magnitudes of the monodromy matrix evaluated at a range of initial mean anomalies along the NRHO represented in a full ephemeris model. Periselene is located at 360 degrees mean anomaly in this Figure reproduced from Bucci's paper [12]. The spike in eigenvalue magnitude at Periselene emphasizes the instability of this region and its sensitivity to perturbations.

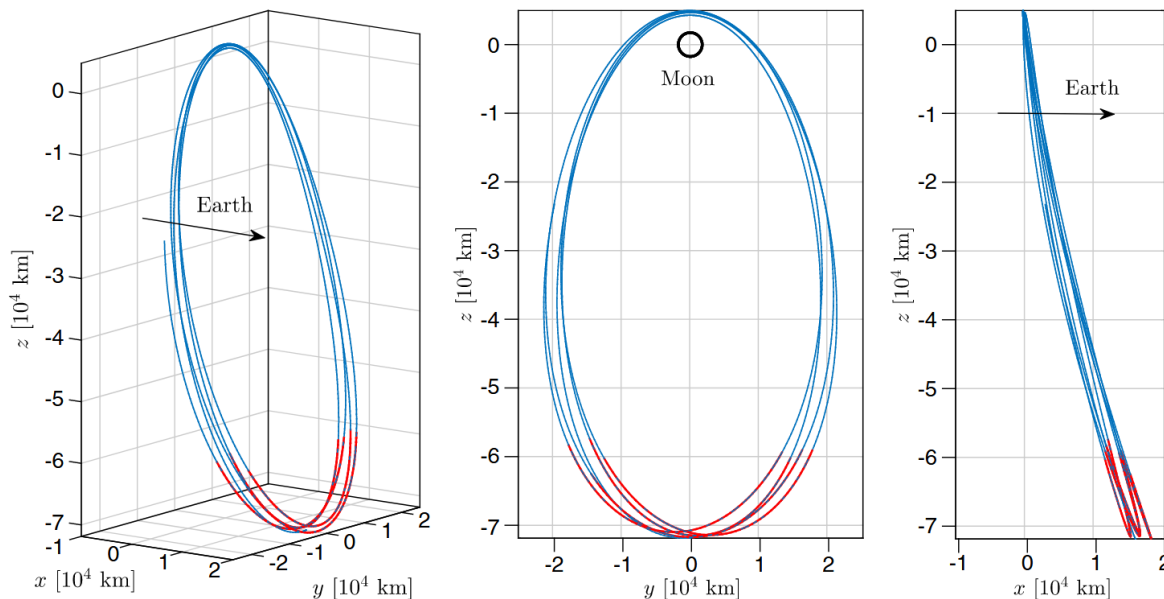


Figure 2.11: Franzizni and Innocenti visualized Bucci's proposed region for safe rendezvous in the NRHO's Aposelene region, highlighted in red [12, 18]. The NRHO is most stable in this region, and the maneuver accuracy required for RPOD increases outside this region. The orbit is shown in an ER3BP dynamics model. Figure reproduced from [18].

This characteristic makes rendezvous safe and predictable in Aposelene. Outside this region, the dynamics grow much more chaotic, and minor inaccuracies can result in drastically different results than desired, necessitating high burn accuracy. The takeaway is that the best practice for having a safe rendezvous with Gateway in the NRHO is to execute it in the Aposelene region. Rendezvous in cislunar space is likely to encounter instances with poor orbit determination that require resulting burns to have an allowable margin of error. This margin is severely limited in Periselene compared to Aposelene.

Bucci's paper uses the dynamic intuition that the monodromy matrix of the orbit state transition matrix provides to seed the design of stable trajectories for rendezvous. His work did not consider safety in the context of operational standards like other works. However, it did consider trajectories to enable the delay of rendezvous to wait for the best opportunity within the Aposelene region. The scalable trajectory, shown in Figure 2.13, is multiple NRHO

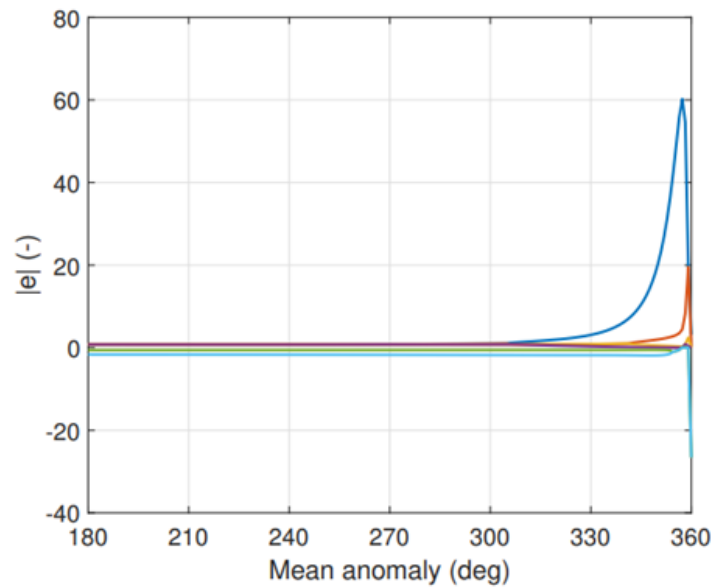


Figure 2.12: Earth Moon 9:2 NRHO Full Ephemeris Monodromy Matrix Eigenvalue Magnitudes. Bucci’s analysis of Gateway’s proposed NRHO monodromy matrix eigenvalues in a full ephemeris dynamics model is shown. The plot graphs the magnitudes approaching the Periselene region of the orbit at 360 degrees mean anomaly. The values spike in this region, indicating the chaotic nature of this region of the orbit. Figure reproduced from [12].

periods in duration and keeps the chaser spacecraft in a stable loop around the target [12]. This orbit was obtained using the unitary eigenvector of the monodromy matrix. Such a trajectory can allow the chaser to inspect, loiter, and wait for the opportune time to begin its final rendezvous approach.

The research has tied together the EORM discussed in Section 2.1.1 and applied it to rendezvous approach strategies that align with the standards shown in Section 2.1.2. The work has given missions a verified approach to rendezvous with Gateway that future missions can implement. However, limiting these strategies to one specific region of Gateway’s orbit creates a limited view of strategies to rendezvous in this orbit. The following section dives into the technical gap in the field.

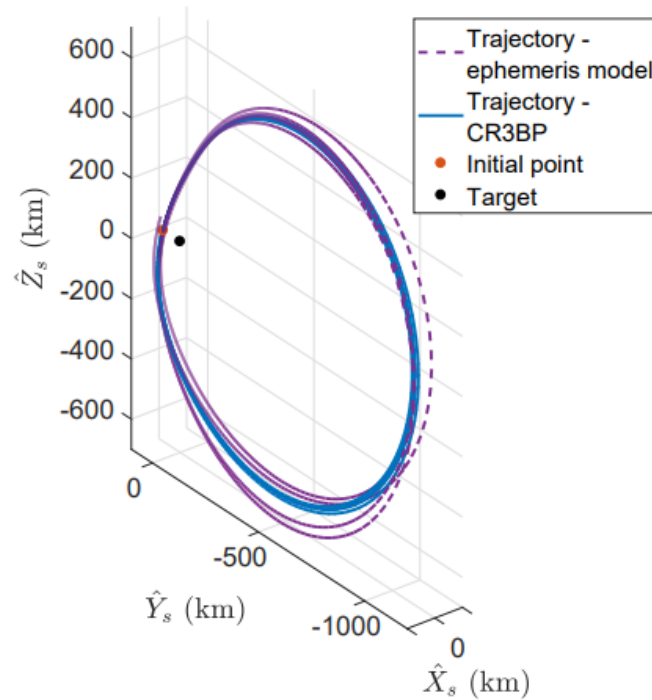


Figure 2.13: Multi Orbit Hold Trajectory. Bucci’s strategy for a long-duration safe hold is shown, reproduced from [12]. The strategy has the chaser park on the NRHO, a set phase lag behind the target. This technique ensures passive safety for multiple orbits in the NRHO. The trajectory was made in a CR3BP dynamics model and compared to a full ephemeris model.

2.2 Technical Gap

The works discussed show that three-body relative motion is a well-studied field with rendezvous strategies proposed for the various orbits Gateway has, at some point, been proposed to reside. The necessary EORM to model RPOD missions in the three-body context has been developed and proven usable in trajectory design for impulsive, finite, and continuous maneuvers. Combined with concepts from the general three-body theory, these equations have been used to optimize approach strategies in all three phases of a rendezvous mission with a crewed station. Lastly, the applicable standards implemented for the ISS and now

adapted for a cislunar station have been implemented into these works to ensure safety compliance.

The currently proposed strategies for Gateway’s planned—at the time of writing—NRHO have leveraged the relative stability of the Aposelene region to mitigate mission risk. However, the Aposelene region only accounts for three days, 45%, of the orbits’ approximately 6.5-day duration. Under the currently presented strategies, over half of the orbit is unaddressed regarding how a mission operator would want to execute RPOD in this region.

The risks associated with conducting RPOD outside of Aposelene. are documented and accurate. Nevertheless, space is a hazardous environment, and time-critical problems have often arisen in the history of human spaceflight [43]. Three documented cases of medical evacuations from the ISS have caused missions to be terminated early and have their crew quickly removed from the station and returned to Earth [43]. As humans plan to return to the Moon, it would be naïve to assume there will not be a scenario where a crew member must swiftly return to Gateway and/or Earth. The current RPOD strategies with Gateway would bottleneck such a time-sensitive scenario if the station positioning did not align with the Aposelene region. Strategies for rendezvous in a time-sensitive scenario are lacking.

This thesis aims to address this hole within the growing catalog of Gateway rendezvous strategies and produce a comprehensive trajectory playbook for docking with Gateway at any point in the Earth-Moon Southern L2 NRHO. Rendezvous approaches still need to comply with the station’s safety standards and are constrained by vehicle performance. Section 2.3 discusses the approach this thesis will take to take steps to achieve this.

2.3 Approach

The work in this thesis will focus on addressing the strategic gap for vehicles attempting to rendezvous with Gateway in a time-sensitive manner, requiring them to attempt RPOD outside the Aposelene region. The work provides applicable mission operators with a situational “transit diagram”. The “transit diagram” will serve as a high-level guide for how vehicles should proceed in a given situation based on their stage in the rendezvous process and Gateway’s current state within its orbit. Initial states throughout the entire orbit, including Aposelene, will be analyzed. The guide will aim to provide a ΔV -efficient path for its prescribed routes while adhering to the governing safety standards for VVs.

The analysis will use the EORM within the synodic frame derived by Luquette [34]. The CR3BP simplifications will be used as the starting point for the research with the aim of producing similar guides in higher fidelity models in the future. The strategies will aim to preserve the current operational procedure VVs follow for the ISS and the requirements outlined in the IRSIS. The trajectory design space will be constrained to the “far field” rendezvous stage. The study will assume that the VV has arrived at a given point in Gateway’s NRHO where relative guidance is feasible and has established a hold awaiting approach initiation. The trajectories will be studied to ensure safety requirements are followed for the failure modes discussed in Innocenti’s paper: HP departure burn failure, HP arrival burn failure, and random misfire [27]. The “transit diagram” will guide operators on how to best approach rendezvous with Gateway, given a specified starting point within the NRHO. The results will be compared against a rough recreation of the proposed strategies within a full ephemeris model.

The results of this research aim to provide a foundational understanding of the techniques and trajectories VVs should expect to encounter if they are required to execute RPOD with

Gateway in a time-critical manner. A mission operator can look at the produced map and gauge a ballpark estimate of necessary burns, trajectories, and contingency plans should they be placed in this situation.

Chapter 3

Methodology

“I could find something sharp in here and poke a hole in the glove of my EVA suit. I could use the escaping air as a thruster and fly my way to you. The source of thrust would be on my arm, so I’d be able to direct it pretty easily.” ... “Hmm,” Lewis said. “Could you get 42 meters per second that way?” “No idea,” Watney said... “But consider this: I’d get to fly around like Iron Man.” ... “Iron Man, Commander. Iron Man.”

Mark Watney, *The Martian* [47]

Chapter 3 discusses the methods, adopted standards, and assumptions used to conduct the analysis for this thesis. The chapter is broken into six main sections outlined below:

1. Section 3.1 introduces the circular restricted three-body problem by deriving its equations of motion (EOM). The governing EOM are followed by introducing the equations of relative motion within the CR3BP dynamics.
2. Section 3.2 describes the numerical methods and accompanying parameters used to propagate trajectories and those used to solve for transfers.
3. Section 3.3 defines the reference orbit for the Lunar Gateway represented in the CR3BP dynamics model generated using the methods shown in section 3.2.
4. Section 3.4 details the adopted safety standards for rendezvousing with Gateway. The methods for checking passive, misfire, and partial burn safety are outlined.
5. Section 3.5 details the setup of the Systems Tool Kit® scenario (STK) used to implement the identified strategy in a full ephemeris model.

6. Section 3.6 outlines the approach to visualizing the strategy through the use of transit diagrams.

3.1 The Circular Restricted 3-Body Problem

Consider an inertial frame $\hat{X}, \hat{Y},$ and \hat{Z} with two primary bodies present. The bodies are assumed to be point masses of m_1 and m_2 , where m_1 is greater than m_2 . The origin of the frame is the barycenter of the two masses. A third body, P , is in the frame with a negligible mass compared to the two primaries. The two bodies rotate around the origin at a rate ω . ω is constant in the circular case. For the second, synodic, frame with the same origin is represented by $\hat{x}, \hat{y},$ and \hat{z} . The \hat{x} axis passes through the two primary bodies' COM, going from the first through the barycenter to the second primary. The \hat{y} axis passes through the system origin perpendicular to \hat{x} in the $\hat{X}-\hat{Y}$ plane. The \hat{z} axis completes the orthogonal triad of the frame passing through the system origin. Assume the rotation of the two primaries is circular and lies in the $\hat{x}-\hat{y}$ plane. These two frames are visualized in Figure 3.1.

The system will be discussed with nondimensionalized units. The conversions of distance, velocity, and time between the dimensionalized and nondimensionalized forms are

$$d' = Ld$$

$$s' = \omega Ls$$

$$t' = \frac{1}{\omega}t$$

where $'$ denotes the nondimensional state. d, s and t represent distance, velocity, and time respectively. L is the distance between the COM of the two primary masses. L and

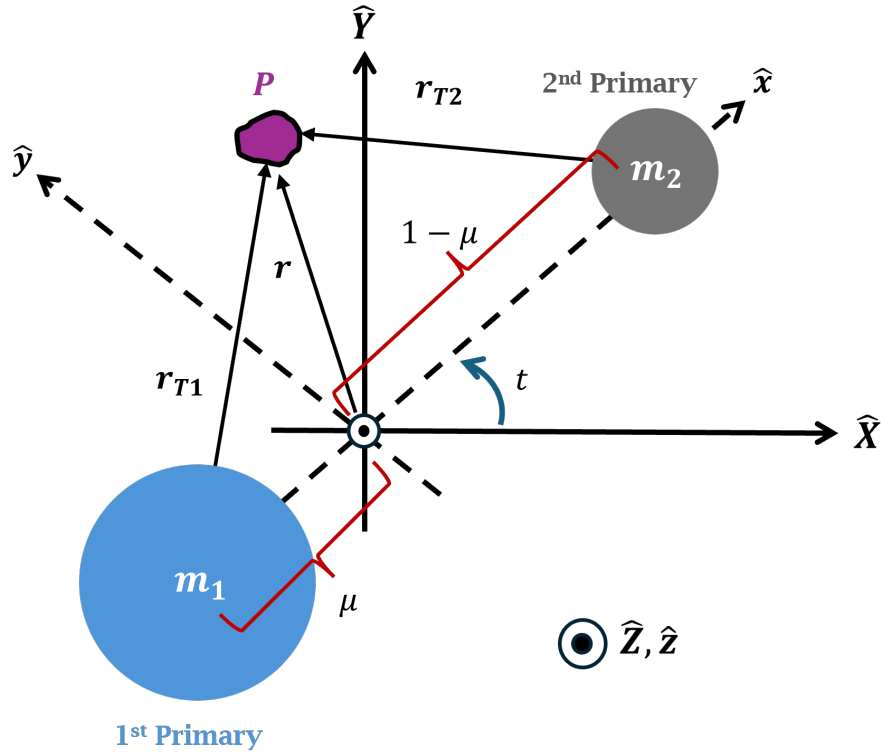


Figure 3.1: CR3BP Coordinate Frames. A top-down view of the inertial and synodic coordinate frame for the circular restricted three-body problem is shown. The two primary bodies with masses denoted m_1 and m_2 rotate around the system's barycenter located at the frame's origin. The inertial frame is formed by the \hat{X} , \hat{Y} , and \hat{Z} axes, and the synodic frame is formed by the \hat{x} , \hat{y} and \hat{z} axes. The third body is denoted as P in the system at a distance r from the origin. The third axes for both frames, \hat{Z} , and \hat{z} , point out of the page orthogonally.

$\frac{1}{\omega}$ are referred to as the systems distance unit (DU) and time unit (TU). The system is parameterized by the mass parameter μ ,

$$\mu = \frac{m_2}{m_1 + m_2}.$$

Following the earlier assumption that $m_1 > m_2$, the placements of m_1 and m_2 along the x axis are $-\mu$ and $1 - \mu$ respectively. The values of L , ω , and μ for the Earth-Moon system studied in this thesis are listed in Table 3.1 and were sourced from the Jet Propulsion Laboratory

Table 3.1: Earth-Moon CR3BP System Parameters and Constants. The three parameters/constants used to parameterize and nondimensionalize the system are listed. The constants are sourced from the Jet Propulsion Laboratory three-body orbit database [32].

Parameter	Standard [km, s]	Normalized [DU, TU]		
L	389703	km	1	DU
ω	$\frac{1}{382981}$	s^{-1}	1	TU $^{-1}$
μ	1.2150×10^{-2}	—	—	—

three-body orbit database [32].

In this work, m_1 and m_2 represent the Earth and Moon, respectively. P , a body with negligible mass in the system, represents either the Lunar Gateway or the visiting vehicle approaching the station. From a Newtonian-based derivation, the equation of motion of P is shown in Eq. 3.1. Equation 3.1 is used to propagate orbits within the synodic frame for this work.

$$\ddot{\mathbf{r}} = \begin{bmatrix} 2\dot{r}_y \\ -2\dot{r}_x \\ 0 \end{bmatrix} + \begin{bmatrix} r_x \\ r_y \\ 0 \end{bmatrix} - \frac{1-\mu}{r_{1T}^3} \begin{bmatrix} r_x + \mu \\ r_y \\ r_z \end{bmatrix} - \frac{\mu}{r_{2T}^3} \begin{bmatrix} r_x + \mu - 1 \\ r_y \\ r_z \end{bmatrix} \quad (3.1)$$

where

$$r_{1T} = \sqrt{(r_x + \mu)^2 + r_y^2 + r_z^2}$$

$$r_{2T} = \sqrt{(r_x + \mu - 1)^2 + r_y^2 + r_z^2}$$

ρ_1 and ρ_2 are the distances from the first and second primaries to P respectively.

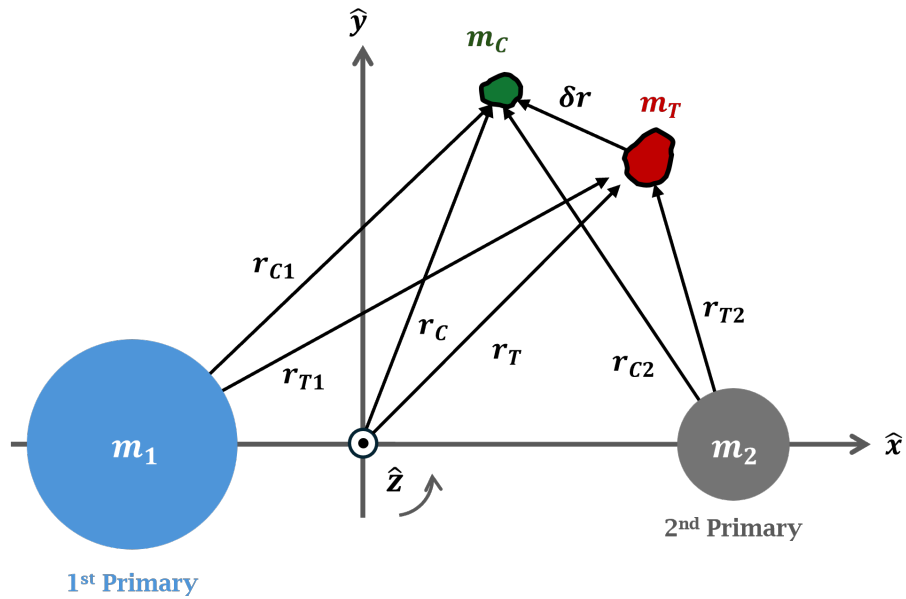


Figure 3.2: CR3BP Relative Motion System. In the restricted three-body system, m_t represents a target spacecraft while m_c represents a chaser spacecraft. The relative position of the chaser is $\delta \mathbf{r}$.

3.1.1 Equations of Relative Motion

As discussed in section 2.1.1, Luquette and Sanner's equations of relative motion will be used to model RPOD in this thesis. The following presents these equations.

Reconfiguring the CR3BP system to represent a relative motion scenario adds a second body of negligible mass. This modified system is shown in Figure 3.2. The equations of relative motion relating the motion of a chaser spacecraft to a target spacecraft are obtained by subtracting the equations of motion of the target from the chaser. This is shown in Eq. 3.2.

$$\delta \mathbf{r} = \mathbf{r}_C - \mathbf{r}_T \quad (3.2)$$

\mathbf{r}_T and \mathbf{r}_C are the target and chaser state relative to the system origin. Expanding this equation using Eq. 3.1 results in

$$\begin{aligned}
\delta\ddot{r}_x &= 2\delta\dot{r}_y + \delta r_x + (1 - \mu) \left(\frac{r_{Tx} + \mu}{\|\mathbf{r}_{1T}\|^3} - \frac{r_{Tx} + \delta r_x + \mu}{\|\mathbf{r}_{1T} + \boldsymbol{\delta r}\|^3} \right) \\
&\quad + \mu \left(\frac{r_{Tx} - \mu - 1}{\|\mathbf{r}_{2T}\|^3} - \frac{r_{Tx} + \delta r_x + \mu - 1}{\|\mathbf{r}_{2T} + \boldsymbol{\delta r}\|^3} \right) \\
\delta\ddot{r}_y &= -2\delta\dot{r}_x + \dot{r}_y + (1 - \mu) \left(\frac{r_{Ty}}{\|\mathbf{r}_{1T}\|^3} - \frac{r_{Ty} + \delta r_y}{\|\mathbf{r}_{1T} + \boldsymbol{\delta r}\|^3} \right) \\
&\quad + \mu \left(\frac{r_{Ty}}{\|\mathbf{r}_{2T}\|^3} - \frac{r_{Ty} + \delta r_y}{\|\mathbf{r}_{2T} + \boldsymbol{\delta r}\|^3} \right) \\
\delta\ddot{r}_z &= (1 - \mu) \left(\frac{r_{Tz}}{\|\mathbf{r}_{1T}\|^3} - \frac{r_{Tz} + \delta r_z}{\|\mathbf{r}_{1T} + \boldsymbol{\delta r}\|^3} \right) + \mu \left(\frac{r_{Tz}}{\|\mathbf{r}_{2T}\|^3} - \frac{r_{Tz} + \delta r_z}{\|\mathbf{r}_{2T} + \boldsymbol{\delta r}\|^3} \right)
\end{aligned} \tag{3.3}$$

where

$$\begin{aligned}
\mathbf{r}_{1T} &= [r_{Tx} + \mu, r_{Ty}, r_{Tz}]^\top \\
\mathbf{r}_{2T} &= [r_{Tx} + \mu - 1, r_{Ty}, r_{Tz}]^\top \\
\boldsymbol{\delta r} &= [\delta r_x, \delta r_y, \delta r_z]^\top.
\end{aligned}$$

Equation 3.3 is referred to as the nonlinear equations of relative motion (NLEORM). As this is the only set of relative motion equations used in this work, it is referred to as the equations of relative motion (EORM) for short. Luquette shows that the EORM can be written in a linearized state-space form as shown in Eq. 3.4. This system's Jacobian is the 6×6 matrix in Eq. 3.4. Integrating this matrix over a duration of the trajectory results in the state-transition matrix (STM). The STM denoted as $\boldsymbol{\Phi}$, will be utilized in assisting the numerical methods discussed in Section 3.2 and in checking the validity of the rendezvous approach axes discussed in Section 2.3 and Section 4.2. The STM structure can

be decomposed into Eq. 3.5.

$$\delta \dot{\mathbf{r}} = \begin{bmatrix} 0_{3 \times 3} & I_3 \\ \Xi(t) - [n \times][n \times] & -2[n \times] \end{bmatrix} \delta \mathbf{r} \quad (3.4)$$

where

$$\Xi(t) = - \left(\frac{1-\mu}{r_{1T}^3} + \frac{\mu}{r_{2T}^3} \right) I_3 + \frac{3(1-\mu)}{r_{1T}^5} [\mathbf{r}_{1T} \mathbf{r}_{1T}^\top] + \frac{3\mu}{r_{2T}^5} [\mathbf{r}_{2T} \mathbf{r}_{2T}^\top]$$

$$[n \times] = \begin{bmatrix} 0 & -1 & 0 \\ 1 & 0 & 0 \\ 0 & 0 & 0 \end{bmatrix}$$

$$[n \times][n \times] = \begin{bmatrix} -1 & 0 & 0 \\ 0 & -1 & 0 \\ 0 & 0 & 0 \end{bmatrix}.$$

The Jacobian from Eq. 3.4 can be decomposed into

$$\Phi(\Delta t) = \begin{bmatrix} \Phi_{rr} & \Phi_{rv} \\ \Phi_{vr} & \Phi_{vv} \end{bmatrix} \quad (3.5)$$

LVLH Frame

Franzini and Innocenti's LVLH formulation of a set of relative motion equations were implemented and tested for this thesis. However, they were not used for the complete analysis due to

the complexity of calculating the angular acceleration, necessitating the target’s positional jerk derivative. If it interests the reader, the derivation of these equations can be found in Appendix G. Nevertheless, as discussed in Section 2.1.1, relative motion results are commonly viewed in the LVLH frame.

Approach plans within this thesis will be visualized in the LVLH frame. This LVLH frame will use Franzini and Innocenti’s definition visualized in Figure 2.2. The frame’s basis vectors are stated in Eq. 3.6. *Local-Vertical* is defined as the unit negative radial vector. The radial vector, \mathbf{r}_{T2} , points from the Moon’s COM to the Target. *Local-Horizontal* is the negative unit specific angular momentum vector. The specific angular momentum, \mathbf{h} , is with respect to the Moon and defined as $\mathbf{h} = \mathbf{r}_{T2} \times \dot{\mathbf{r}}_{T2}$. The third vector, called the “V-Bar”, is the cross-product of the two other vectors.

$$\begin{aligned}\hat{\mathbf{k}} &= -\frac{\mathbf{r}_{T2}}{\|\mathbf{r}_{T2}\|} \\ \hat{\mathbf{j}} &= -\frac{\mathbf{h}}{\|\mathbf{h}\|} \\ \hat{\mathbf{i}} &= \hat{\mathbf{j}} \times \hat{\mathbf{k}}\end{aligned}\tag{3.6}$$

3.2 Trajectory Construction and Numerical Methods

The equations of motion discussed in Section 3.1 serve as the mathematical backbone for propagating trajectories and constructing transfers to design the rendezvous approach strategy. Section 3.2.1 discusses the setup of the numerical integrators implemented to propagate the trajectories, and Section 3.2.2 discusses the single shooting method used to solve for transfers.

Table 3.2: Numeric Integrator Configuration.

Integrator Setup	
Integrator	ode78 [25]
Absolute Tolerance	10^{-12}
Relative Tolerance	10^{-10}

3.2.1 Trajectory Propagation

The orbits/trajectories in the CR3BP synodic and CR3BP relative synodic frames were propagated via numeric integration. MATLAB's `ode78` integrator was implemented using the constraints listed in Table 3.2 [25]. This setup was utilized in the propagation of trajectories in both systems. MATLAB's `ode78` implements a Runge-Kutta 7th and 8th order method to complete the numeric method.

3.2.2 Single Shooting Method

All transfers in this work are modeled with impulsive burns. Assuming one Hold Point (HP) per safety region, the rendezvous safety regulations, discussed in more detail in Section 2.1.2, require the ATP before a VV can transfer to the following HP. To account for likely holds at each HP, each transfer will assume zero relative velocity in the synodic frame at the beginning and end of each transfer. These transfers will require at least two burns: one to initiate the transfer and one to establish a hold at the end of the transfer. A single shooting method, illustrated in Figure 3.3, was implemented to solve for transfer trajectories between two points given a desired time of flight (TOF).

The single shooting method implemented uses MATLAB's `fsolve` function to solve Eq. 3.7 [24]. The solver is provided the initial position, $\delta \mathbf{r}_0 = [\delta r_{x0}, \delta r_{y0}, \delta r_{z0}]$, the desired final position, $\delta \mathbf{r}_f = [\delta r_{xf}, \delta r_{yf}, \delta r_{zf}]$, the transfer TOF, and an initial guess for the design vector.

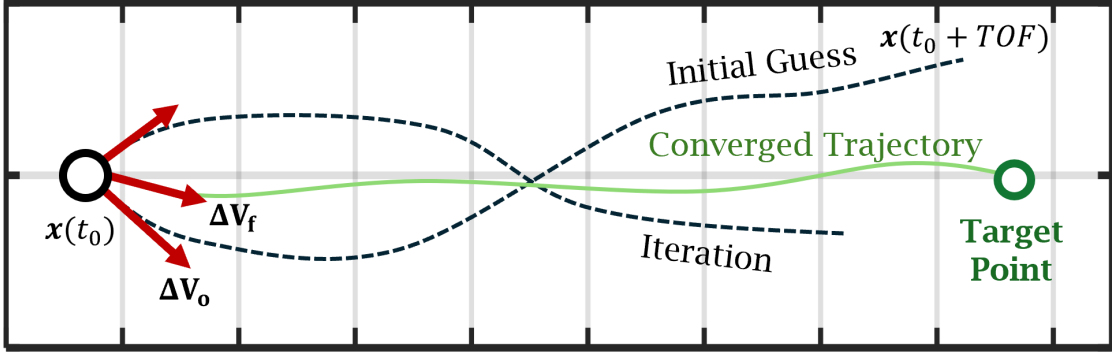


Figure 3.3: Single Shooting Method Schematic. The method searches for a converged trajectory that begins at $\mathbf{x}(t_o)$ and ends at the target point after a prescribed TOF. The method iterates the design vector until the trajectory converges to the target point within a specified tolerance.

The design vector, shown in Eq. 3.8, is the impulsive burn's ΔV vector at transfer initiation.

$$\text{Objective Function } (\mathbf{J}) = \delta \mathbf{r}_f - \delta \mathbf{r}_{fi}(\delta \mathbf{r}_0, \Delta \mathbf{V}_i, \text{TOF}) \quad (3.7)$$

$$\Delta \mathbf{V}_i = \begin{bmatrix} \dot{\delta r}_{x0} & \dot{\delta r}_{y0} & \dot{\delta r}_{z0} \end{bmatrix}^T \quad (3.8)$$

The solver was configured with the options in Table 3.3. Each iteration propagates the relative state of the chaser vehicle using the method discussed in Section 3.2.1 with the initial state of the chaser being $[\delta \mathbf{r}_0, \Delta \mathbf{V}_i]$, where $\Delta \mathbf{V}_i$ is the current iterations design vector. After propagating the trajectory for the duration of TOF, Eq. 3.7 is evaluated to see if the specified solver tolerances are met. If the tolerances are not met, the solver iterates using the STM upper right quadrant, $\Phi_{rv}(\text{TOF} + t_0, t_0)$, to calculate the functions Jacobian. Once a solution satisfies the solver tolerances, a transfer's ΔV cost can be computed using Eq. 3.9.

Table 3.3: Single Shooting Solver Configuration. MATLAB’s *fsolve* function was implemented within a single shooting method. The following parameters were used.

Solver Setup	
Solver	<code>fsolve</code> [24]
Algorithm	Levenberg-Marquardt
Function Tolerance	10^{-8}
Step Tolerance	10^{-6}

$$\Delta V_{\text{Transfer}} = \|\Delta \mathbf{V}_i\| + \|\dot{\delta \mathbf{r}}_f\| \quad (3.9)$$

3.3 Gateway Orbit Definition

The reference orbit utilized to model the Lunar Gateway was seeded from NASA’s Jet Propulsion Laboratory’s (JPL) Three-Body Periodic Orbit Database [32]. Gateway will operate within an Earth-Moon Southern L2 Halo Orbit with an orbital period of roughly 6.56 days [32]. The seed orbit from JPL was selected from the libraries Earth-Moon Southern L2 Halo orbit family database with a period of 6.52 days. The orbit’s initial conditions and relevant characteristics within the nondimensionalized three-body frame discussed in Section 3.1 are listed in Table 3.4. T is the orbit period, J is the Jacobi constant, and Λ is the stability index.

Table A contains the full list of states for one complete revolution of the NRHO and can be found in Appendix A. The list was generated by propagating the initial conditions for one period. This list of states was utilized as a lookup table to provide the numeric integrator the values for \mathbf{r}_T in Eq. 3.3 to represent Gateway’s trajectory. One period of the trajectory is visualized in Figure 3.4. The orbit’s initial condition is the Aposelene of the orbit. This point is defined as the furthest point from the Moon’s COM. The mean anomaly of the orbit

Table 3.4: CR3BP 9:2 NRHO Orbit Initial Conditions and Characteristics. Orbit initial conditions were taken from the JPL three-body periodic orbit database [32].

Parameter:	[DU,TU]	Value:
x_0	DU	1.0190
y_0	DU	-2.8484×10^{-27}
z_0	DU	-1.7992×10^{-2}
\dot{x}_0	DU/TU	-3.2158×10^{-13}
\dot{y}_0	DU/TU	9.6564×10^{-2}
\dot{z}_0	DU/TU	-4.8653×10^{-12}
T	TU	1.4711
J	DU ² /TU ²	3.0496
Λ	n/d	1.2354

is referenced from the Aposelene point in this work. The mean anomaly of the NRHO is defined by Eq. 3.10, where t is the time passed since Aposelene passage. This definition differs from many referenced works, which define $M(0) = 0$ at Periselene.

$$M(t) = 2\pi \frac{t}{T} \quad (3.10)$$

3.4 Adopted Rendezvous Standards

Crewed and station rendezvous has a heightened level of operational scrutiny. With the ISS, VVs enter integrated operations with the station and must abide by the rendezvous safety standards adopted by the station. VVs rendezvousing with Gateway will experience a similar situation. The IDSS published the IRSIS, which outlined rendezvous standards with cis-lunar space stations, which Gateway is classified as. The IRSIS are nearly identical to current ISS standards with slight modifications due to the difference in station location. The following outlines the safety standards for VV safety during station approach. Section 3.4.1 defines the safety regions, while Section 3.4.2 defines VV safety in the presence of various

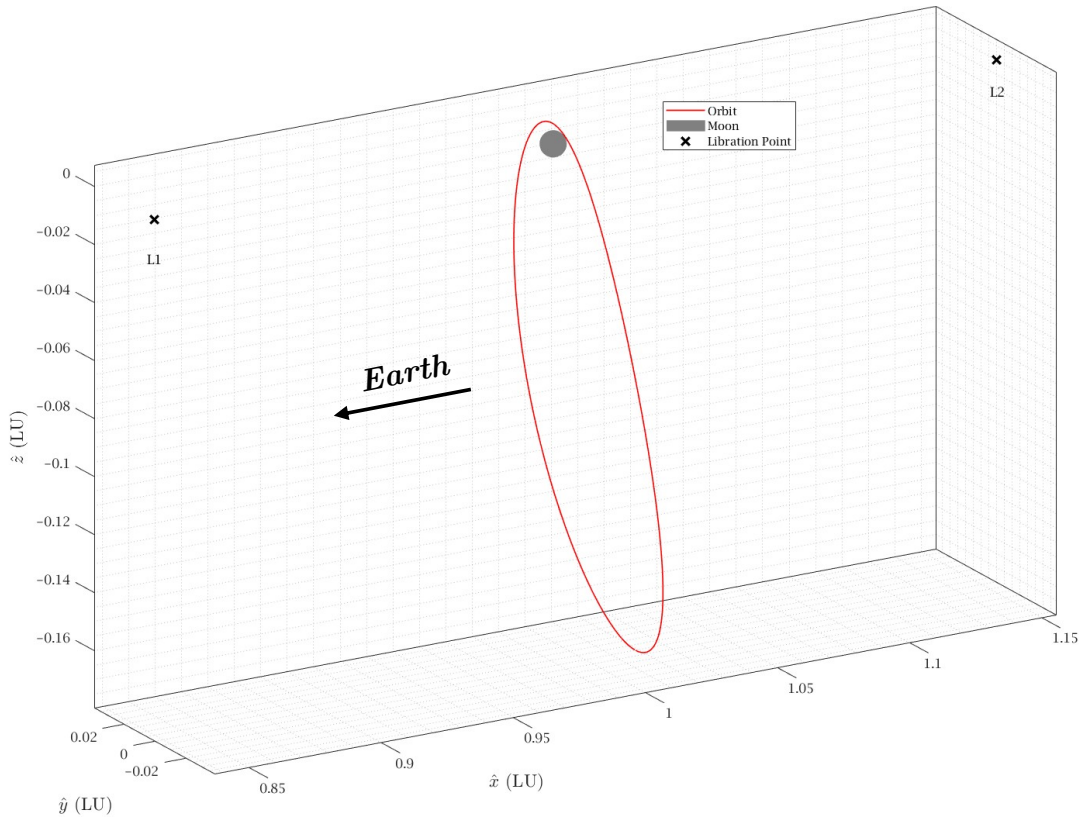


Figure 3.4: 9:2 Southern L2 NRHO Visualization. One orbit period is shown in 3D space. The plots are shown in the nondimensional synodic frame. This orbit serves as a CR3BP representation of Gateway’s orbit.

failure modes of the VV.

3.4.1 Safety Regions

The ISS has three safety regions for VV: an approach ellipsoid (AE), a keep-out sphere (KOS), and an approach corridor (AC). The zones are centered around the station. Operations within the AE are more relaxed than in the KOS; the vehicle can operate anywhere in this region, given that its trajectories do not violate any safety rules. The AC is nested within the KOS, and operations within the AC are much more constrained. AC operation rules are VV-specific. Each VV has a predefined path to the final station rendezvous, and any

Table 3.5: Safety Region Definition

Region:	Definition:
Rendezvous Sphere (RS)	10.0 km sphere centered on the station.
Approach Sphere (AS)	1.0 km sphere centered on the station.
Keep Out Sphere (KOS)	0.200 km sphere centered on the station.
Approach Corridor (AC)	Cone centered around station docking axis extending from station to KOS. Semi-vertical angle of 5 degrees.

deviations from this path usually result in an abort. This work provides a generalized strategy for VVs, so operations within the AC/KOS are not considered.

From the IRSIS, a similar zonal structure is defined. The IRSIS defines four safety regions, with the additional being an outer rendezvous sphere (RS). The approach ellipsoid is substituted for an approach sphere. Gateway does not experience atmospheric drag like the ISS, so the in-track positional uncertainty of the station is reduced, reducing the region's size and changing from an ellipsoid to a sphere. The dimensions of the safety regions are listed in Table 3.5 and visualized in Figure 3.5.

These safety regions serve as gates for VVs. The station operator must grant authority to proceed (ATP) before a VV can enter the next region. A VV approach plan consists of various hold points (HPs); the proposed strategy of this work places one hold point within each region. So, the VV will begin its approach at an HP outside the RS. The vehicle will wait for ATP to enter the RS and then “hop” to the following HP somewhere inside the RS and establish a new hold while it waits for ATP to enter the AS. This process repeats for the forthcoming regions. A transfer between HPs is deemed unsafe if it enters a region without ATP or if it enters a region without ATP in the event of a failure. The following section defines the failures that concern this thesis.

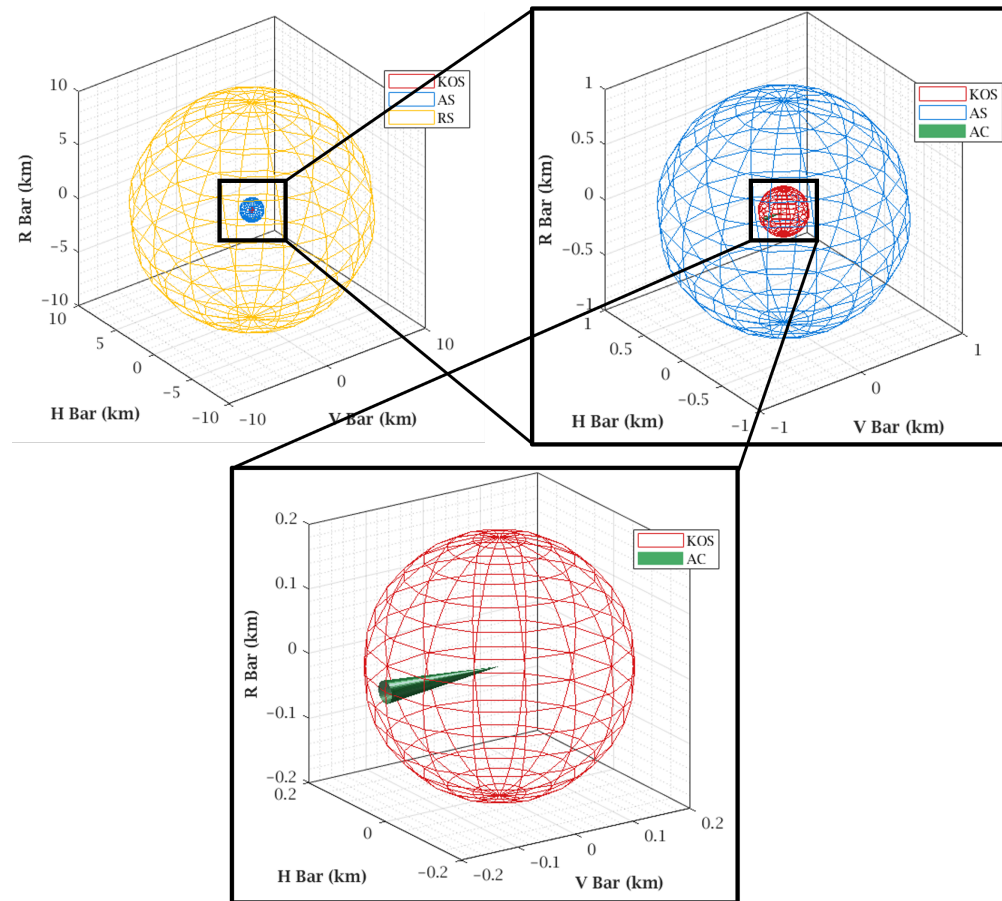


Figure 3.5: Approach Safety Regions. The four safety regions are shown in the series of zoomed-in snapshots. The three outer regions are spheres centered around the target, while the approach corridor is a cone with a semi-vertical angle of 5 degrees centered on the docking axis.

3.4.2 Visiting Vehicle Safety

Spacecraft encounter numerous off-nominal scenarios during operations. These issues are usually not mission critical, but when approaching a multi-billion dollar asset like the ISS or Lunar Gateway, failures that pose any risk to them must be mitigated. Failure risk during the rendezvous approach can be mitigated through trajectory design. The safety regions defined above are in place to reduce risk to the station. Trajectories must be tested under various failure scenarios to ensure the resulting trajectory does not violate the safety regions.

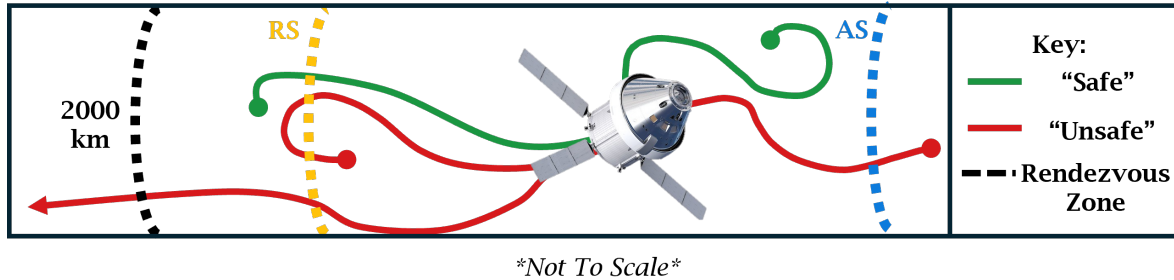


Figure 3.6: Safe v. Unsafe Free Drift Trajectory Illustration. Examples of safe (green) and unsafe (red) trajectories are shown. A VV can drift around in and go into the preceding safety region. However, a VV cannot enter the next region without ATP and cannot reenter a zone after exiting if drifting. An additional case of an unsafe drift is if the VV drifts far away from the station. “Far away” is defined as 2000 km in this work.

Trajectories considered for the proposed approach strategy were analyzed under four different failure modes: an arrival or departure burn failure, a random misfire, and a partial burn. Arrival and departure burn failures fall under the umbrella of passive safety.

Passive Safety

Arrival and departure burn failures occur when a vehicle fails to execute the burn to depart an HP and when a vehicle fails to execute the burn to “break” at the next HP. To model these failures, the vehicle is simulated as having lost all control and entering a free drift. A drift is deemed safe if it meets the following criteria, illustrated in Figure 3.6, throughout a 24-hour loss of control. A VV is safe in either failure if it remains in its current region and does not cross into the next region. A departure burn occurs after a VV has received ATP, so the “current region” is defined as the region the targeted HP is located in, not the region the VV departed. A VV is also deemed safe if it drifts to a preceding region. That is, a VV can drift from the AS to the RS and be deemed safe. However, a VV can not drift from the AS to the RS and then reenter the AS. Once the VV leaves the inner region, it must regain ATP to reenter the inner region.

While not inherently unsafe, far drifts away from the station can lead to VV not having the resources to reach the station and ending up on a runaway trajectory. Drifts that result in the VV drifting greater than 2000 km were classified as unsafe. The 2000 km threshold is not codified in literature but was chosen based on the author's intuition. This failure mode was rarely encountered in the forthcoming analysis and only occurred near the Periselene region of the NRHO.

Misfire Safety

Thruster misfire is when the VV thrusters unexpectedly fire during a transfer between HPs. This failure is simulated by inducing a fixed $\|\Delta\mathbf{V}\|$ of 0.05 m/s in a random direction at a random time during the transfer. The VV then enters a free drift for 24 hours, and the resulting trajectory must meet the same criteria as the departure and arrival burn failures to be classified as safe. The fixed magnitude of the misfire is taken by a similar analysis run by Innocenti during the safety analysis of his proposed approach strategy [26].

Monte Carlo simulations were run to quantify a trajectory's safety under a random misfire. Each proposed trajectory for the approach strategy was simulated 1000 times, with each instance being placed at a random point along the transfer and the burn being directed in a random direction. The misfire safety of a transfer is quantified as the percentage of safe instances to total simulations. There is no defined threshold in prior literature for a required misfire safety percentage. A low misfire safety percentage will not reject a trajectory. However, it will need to be noted that executing said transfer comes with added risk.

Partial Burn Safety

A partial burn occurs when, during either the departure or arrival burn at an HP, only a certain percentage of the burn is completed. Transfers were analyzed to consider if only 10, up through 90, percent of the burn's $\|\Delta\mathbf{V}\|$ was imparted on the vehicle. The resulting trajectory was analyzed for 72 hours and met the above criteria to be deemed safe. The increase in duration compared to passive safety failures is to account for the longer transfer TOFs that will be considered. Arrival failures are propagated 24 hours from the missed burn, while partial burns are propagated from the initial burn. The longest transfer duration considered in this work is just under 48 hours. A 72-hour propagation ensures that the initially considered TOF plus an added day is incorporated into the safety analysis for the partial burn.

3.5 Strategy Realization in STK

The approach strategy is designed under the CR3BP assumptions, simplifying the rendezvous dynamics compared to what an approaching vehicle would experience under a full ephemeris model. To compare the approach strategy's results to a full ephemeris model, ANSYS® Systems Tool Kit® (STK), version 12.5.0, was utilized to reconstruct the proposed approaches [8].

The scenario utilized a 15-year reference orbit provided by NASA's Navigation and Ancillary Information Facility (NAIF) [31, 33]. The scenario used a seven-day segment of this orbit spanning from January 2nd 2020 13:18:26.000 UTC through January 9th 13:18:26.000 UTC. This time was determined from the orbit segmentation presented later in Chapter 4. Figure 3.7 visualizes a portion of the reference orbit.

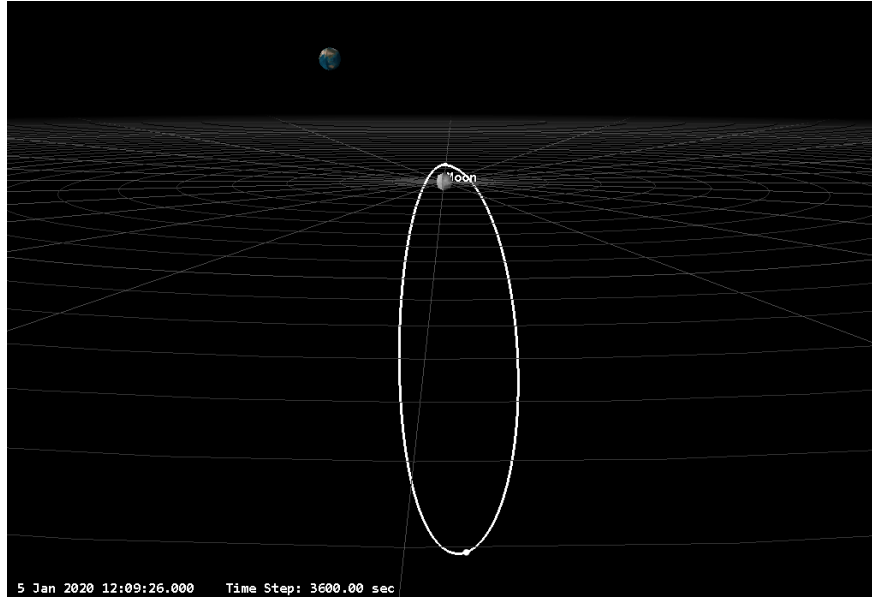


Figure 3.7: Gateway NRHO NAIF 15 Year Reference Orbit Segment. A seven-day segment of a 15-year propagation in a full ephemeris model implemented in STK is shown. Orbit provided by NASA’s NAIF [31].

STK’s Astrogator was used to implement the selected approach plan from the CR3BP-based analysis. Franzini’s LVLH coordinate system was established on the Gateway satellite object. The transfers were generated using Astrogator’s targeting sequence differential corrector. For each sequence, the TOF from the CR3BP approach plan was fixed, and the targeted HP position was set as the targeting sequence goal with an objective tolerance of 0.10 m. The Lunar High Position Orbit Propagator (HPOP) was set as the trajectory propagator. This targeting sequence setup was the same for all transfers. A burn summary report was generated for each approach strategy to compare the $\|\Delta\mathbf{V}\|$ of the maneuvers to the CR3BP values.

STK was also used to test passive safety in a full ephemeris model. The free drifts were simulated with a 24-hour propagate segment placed in the mission control sequence where the failure would occur. A range report of each failure instance was exported to check the appropriate safety criteria. The random misfires and partial burns were not implemented

in the full ephemeris model due to the required time to thoroughly recreate these failures in STK. However, future work should tackle this and can be streamlined through STK automation.

The strategy is designed to be generalized and not vehicle-specific. As such, ΔV and the passive safety metrics are the only results of interest. These are vehicle-independent, so the trajectory modeling does not require any specific vehicle settings implemented in the scenario.

3.6 Strategy Visualization and Communication

One of the main deliverables of this thesis is an approach “transit diagram” to visualize the approach strategy. This will be designed referencing common metro system transit diagrams. Boston, Massachusetts’ transit diagram is shown in Figure 3.8 as an example [9]. These diagrams provide transit riders with a condensed view of the “lines” that connect all the stations in the network. The Boston diagram has five main lines: blue, green, orange, red, and silver. Each line serves a different geographic region of the city. Riders can easily see what lines and transfers they need to make to reach their desired destination based on where they currently are within the system. It is independent of the user’s particular perspective in space and time, meaning that a rider can find the best path to its destination no matter when and where a rider starts. Rendezvous scenarios with Gateway should be able to begin at any point in the NRHO in a time-sensitive scheme, so a good visual should preserve this characteristic.

A high-level diagram breakdown is described here, but a more detailed breakdown of the diagram’s specific cartography will be provided in Section 4.6.1. The results of this work will segment the NRHO into different regions. These regions will be visualized as different



Figure 3.8: Massachusetts Bay Transportation Authority (MBTA) Rapid Transit Diagram. The Transit diagram from Boston’s “T” is shown. The transit diagram shows the various available subway lines of the network. Transit diagrams like this effectively show pathing between different points to riders. Diagram provided by MBTA [9].

“lines” on the approach strategy visual. There will be four concentric loops representing the four HPs of the approach. Each loop will be segmented into different regions, each with a tailored approach to transit through the region. Each region can be transited by traditional station-keeping or through forced loitering. Forced loitering here will entail the VV entering a trajectory that departs a hold point and, after a desired TOF, returns to that hold point to establish a hold.

The trajectories of the selected approach scheme will connect the loops. The trajectories allow all VVs to hop to the inner loops along a safe trajectory. In conjunction with the region transit approaches, the HP to HP transfer trajectories encompass the approach strategy. Combining the two describes how to approach Gateway for any given point along the NRHO and how to hold through a specific duration when the ATP is not granted to the VV.

The diagram will provide a qualitative representation of each adopted strategy for approaching and holding near Gateway. Only actions shown to be safe and relatively optimized will be included in the diagram. Critical quantitative information, such as a prescribed action’s ΔV cost and duration, will be displayed with each segment of the diagram. Like an Earth-based transit diagram, key geographic features will be present on the diagram to help orient the reader to their location in the orbit. These elements enable operators to parse the key details for the approach efficiently to quickly determine the best course of action based on their present situation.

3.7 Summary of Methods

This chapter presented the governing equation for modeling the dynamics in the CR3BP synodic frame with Eq. 3.1 and the equation for modeling the relative motion of two vehicles in the frame with Eq. 3.3. The numeric integration method for propagating orbits was

outlined and implemented into a single shooting method to solve for transfers between two points in the relative motion frame. With this propagation method and initial conditions provided by JPL, a 9:2 reference trajectory was generated to serve as the reference state for Gateway at any point around the NRHO.

Furthermore, the adopted safety standards were detailed. The work will consider the four regions defined by the IRSIS to serve as gates along a VV's approach. The definitions of a safe and unsafe trajectory were defined and illustrated. These definitions are used to analyze trajectories for four possible failure modes. The transfers' safety and ΔV cost are used to identify an optimal approach strategy to rendezvous with Gateway in a time-sensitive scenario. The method for realizing these CR3BP-based approaches in a full ephemeris model utilizing STK was described. Finally, the way in which the selected approach plan will be visualized was framed. The methods described in this chapter are utilized for all the results presented in Chapter 4.

Chapter 4

Results

“It’s a weird feeling, scientific breakthroughs. There’s no Eureka moment. Just a slow, steady progression toward a goal. But man, when you get to that goal it feels good.”

Andy Weir, *Project Hail Mary* [48]

Chapter 4 presents the analysis and results used to develop a time-sensitive rendezvous strategy with the Lunar Gateway. The strategy is developed step-by-step and presented as a transit diagram. The analysis follows the flow chart illustrated in Figure 4.1. The first step in developing the rendezvous strategy begins with partitioning Gateway’s NRHO into distinct regions characterized by orbit dynamics. With consistent regions defined, each region’s approach axes are identified. Due to Gateway’s highly variable dynamics throughout a single orbital period, the ΔV -optimal approach axes constantly drift. As a result, a well-tuned strategy should account for this.

With axes defined for each region, the passive safety of various points along each axis is studied. This analysis results in the specific placement of the four approach hold points (HPs) along each axis. Basing the placement of the HPs their on passive safety analysis ensures that any departure failure from a HP during the approach will be safe. The visiting-vehicle (VV) may need to transfer between axes if the VV is required to hold for longer than one region. These region-to-region transfers are constructed and analyzed to conclude the HP axes identification analysis.

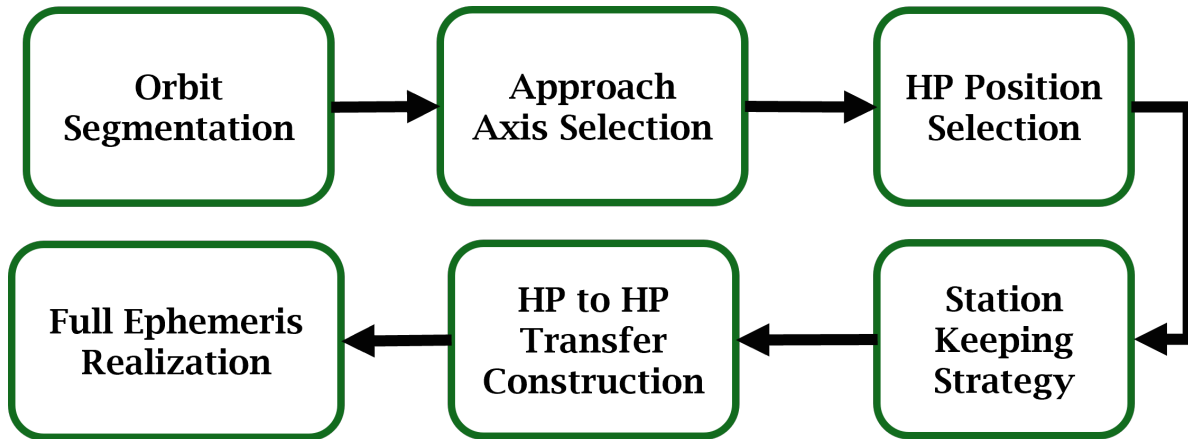


Figure 4.1: Approach Strategy Development Flow Diagram. Key phases in developing the rendezvous approach are shown. The chapter is presented following this flow. Each phase builds off the results of the prior phases. Orbit segmentation begins with analyzing the reference orbit presented in Section 3.3.

Following the axes selection, the station-keeping strategy at each HP is then studied, comparing two alternatives to the traditional station-keeping approach. This study identifies how, when needed, a VV operator should maintain its current position for a given duration. This analysis dictates the optimal approach a VV should take to perform extended holds.

The transfers between hold points are then studied. Two approach schemes, constrained by the time-sensitive nature of the problem, are considered. One considers rendezvousing with Gateway within the duration of one orbit region, while the other considers one transfer per region duration. These schemes are called the “All in One” approach and the “One Hold Point per” approach. All trajectories designed for these schemes and those for the steps above are selected based on a balance of their ΔV cost and their safety in the presence of arrival burn, random misfires, and partial burn failures. These criteria trim the viable approaches forming the adopted approach strategy.

Following the CR3BP-based analysis, the strategy is studied in the full ephemeris dynamics model within STK. The nominal approach schemes are implemented utilizing the HP placement and transfer durations found from the prior analysis. These plans are studied to see anticipated

burn ΔV changes and transfer safety changes. The full ephemeris realization concludes the simulation-based analysis to formulate the time-sensitive rendezvous approach strategy with the Lunar Gateway.

With an identified approach strategy, each nominal strategy can be visualized. The complete strategy transit diagram enables VV operators to identify the best operational route for getting their vehicle to the Station based on the current location in the NRHO, the time needed to get there, and acceptable ΔV margins to complete the approach phase of their docking operation. This visualization ties together all the prior analyses into one cohesive diagram.

The Chapter concludes with the presentation of a nominal and off-nominal approach scenario. The scenarios mimic the flow of real-world rendezvous operations. At each step in the approach, the identified approach strategy is leveraged to determine the best course of action for the hypothetical VV operator to safely perform the approach phase of the rendezvous operation with Gateway.

4.1 Gateway Orbit Analysis

The reference orbit for Gateway modeled in the CR3BP was presented in Section 3.3, and its states are tabulated in Appendix A. The analysis of Gateway's orbit is broken into a study of its dynamics, followed by the partitioning of the orbit based on its dynamics. Two approaches are studied. Section 4.1.2 presents a velocity-based segmentation of the orbit, while Section 4.1.3 presents a velocity-geometric-based segmentation that aligns the regions with being consistent with those already present in current literature.

4.1.1 Orbit Dynamics

The nonlinear dynamics of the NRHO are the primary reason traditional RPOD models break down. However, there are regions of the orbit that have nearly linear dynamics. Approaching rendezvous in these regions is safer due to the stability of the dynamics. The chaotic dynamics outside these regions require increased caution when executing. This section analyzes the orbit dynamics to determine the best way to define distinct orbit regions. The goal is to have each region be characterized by its distinct dynamics.

Figure 4.2 shows the components of the position and velocity vectors over one period of the 9:2 CR3BP NRHO in the synodic frame. The orbit is periodic in the CR3BP dynamics and repeats every 6.52 days. Aposelene is at 71 159 km, and Periselene is at 2853 km measured from the Moon's COM. Analyzing the Figure shows that the dominating terms defining the Station's motion are the \dot{r}_y and \dot{r}_z components of the velocity vector. The \dot{r}_x component remains relatively consistent over the orbit. These two terms of the velocity vector serve as the basis for the first segmentation method explored.

4.1.2 Orbit Velocity Segmentation

The orbit's velocity terms motivate the first approach to segment the NRHO. The first region begins at Aposelene when the \dot{r}_z component is zero with a positive acceleration. This definition distinguishes this point from $\dot{r}_z = 0$ at Periselene. The first region lasts until the \dot{r}_y component flips sign, changing from negative to positive. Region Two runs from this point until the dynamics fully transition into a more chaotic regime. This transition point is defined at $\dot{r}_y = 0.5$ km/s, selected due to the rapid acceleration in both \dot{r}_y and \dot{r}_z components at this point. The third region runs until the transition point at max \dot{r}_y Periselene where \ddot{r}_y transitions from positive to negative and \dot{r}_z rapidly transitions from positive to negative sign.

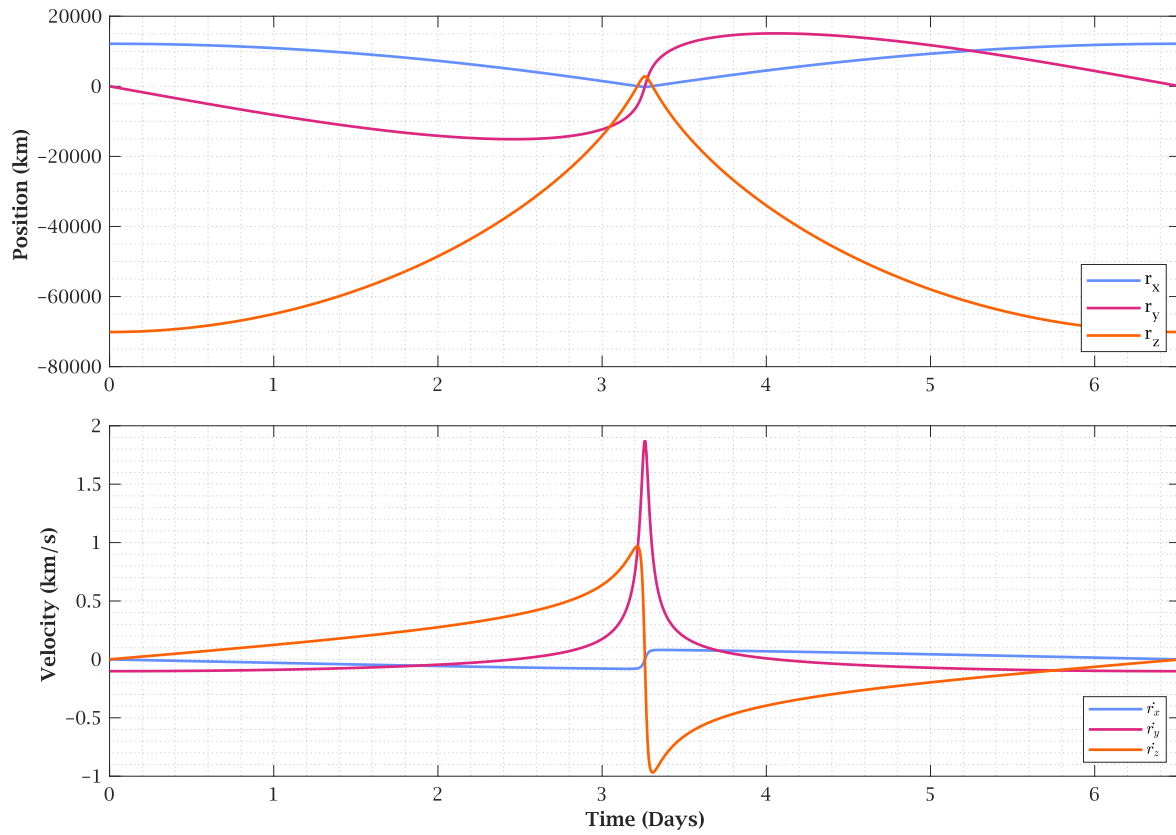


Figure 4.2: 9:2 NRHO Position and Velocity. The 9:2 CR3BP NRHO Position and Velocity are shown in terms of their vector components in the synodic frame. The terms are shown over one orbit period, which repeats every 6.52 days.

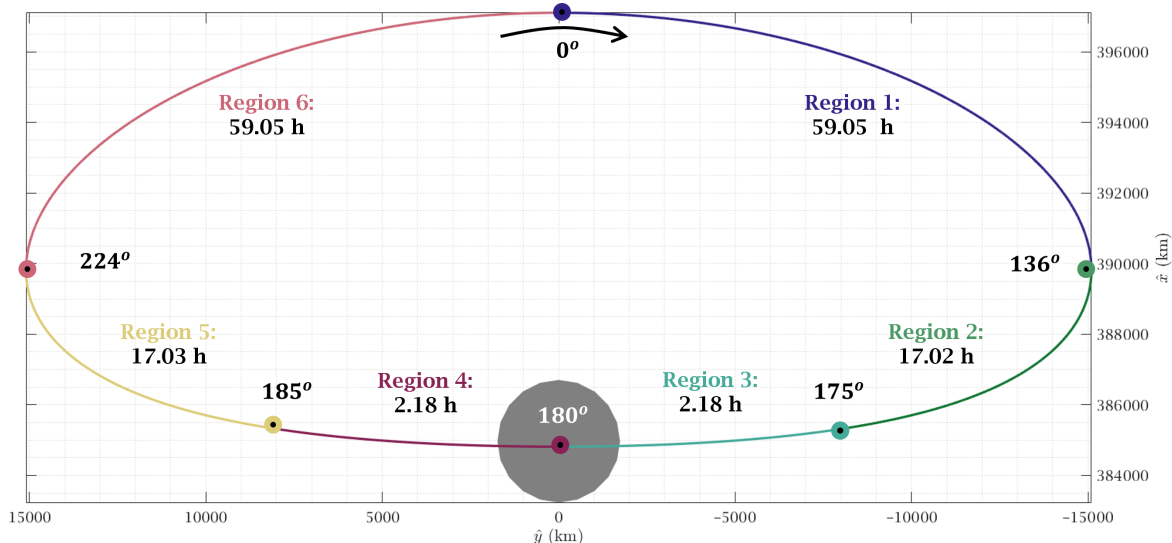


Figure 4.3: NRHO Velocity Region Segmentation. A 2D projection of the segmented NRHO broken into six regions based on the orbit’s velocity behavior on the \hat{x} - \hat{y} plane, is shown. There is a nonzero \hat{z} component to the NRHO. Region One begins at Aposelene and continues until $\dot{r}_y = 0$. The second region runs from this point until the magnitude of $\dot{r}_y = 0.5$ km/s. A third region runs from the end of two until Periselene. Regions Four through Six mirror the first three regions

The fourth, fifth, and sixth regions mirror the first three. The region definitions, resulting initial mean anomaly, rounded to the nearest integer, and duration are listed in Table 4.1. Furthermore, the segmentation is visualized in Figure 4.3.

Regions Six and One are characterized by their stability. The dynamics through these two regions are reasonably consistent, with minimal acceleration compared to the rest of the orbit. Region Two and its mirror of Region Five are transitional regions. The early portion of two and the end of five resemble the stable Aposelene-straddling regions. However, closer to Periselene, the Station rapidly accelerates. This extreme acceleration characterizes Regions Three and Four, which straddle Periselene.

This approach to segmentation achieves the objective of creating distinct dynamics-driven regions. However, these definitions break up the Aposelene region which is kept as a

Table 4.1: NRHO Velocity Segmentation Definitions. The first segmentation approach segmented the NRHO into six distinct regions defined by the orbits' dynamics. The dominant \dot{r}_y and \dot{r}_z terms drive the definitions. The initial mean anomaly and total duration of each region are listed.

Region	Initial Point Definition	M_0 (deg)	Duration (h)
1	$\dot{r}_z = 0 \wedge \ddot{r}_y > 0$	0	59.05
2	$\dot{r}_y = 0 \wedge \ddot{r}_z > 0$	136	17.02
3	$\dot{r}_y = 0.5 \wedge \ddot{r}_y > 0$	175	2.18
4	$\max \dot{r}_y$	180	2.18
5	$\dot{r}_y = 0.5 \wedge \ddot{r}_y < 0$	185	17.02
6	$\dot{r}_z = 0 \wedge \ddot{r}_y < 0$	224	59.05

continuous region in literature. Similarly, Periselene is broken down into two regions. These splits are not perfect from an operational perspective, as the two critical regions of the orbit are broken into two similar regions and would be more easily referred to as just one combined region. A modified approach is considered to align the segmentation with prior research into Gateway rendezvous and to create more operational continuity.

4.1.3 Orbit Velocity-Geometric Segmentation

The alternative approach aims to preserve the continuity of the Periselene and Aposelene regions and align the Aposelene region more consistently with prior literature. A velocity-geometric segmentation approach is adopted, preserving dynamics as the primary driver of region definition. This approach is illustrated in Figure 4.4.

The velocity-geometric segmentation leverages the symmetry of the NRHO to create cohesive Periselene and Aposelene regions. Beginning with Region Six, as with Region Two under the prior approach, the initial point is defined by when $\dot{r}_y = 0$ while having positive acceleration in the \hat{y} component. Region Six continues until $r_z = -2\text{LR}$, where LR represents a lunar radius of 1737 km. At this point, Region One begins and is referred to as the Periselene

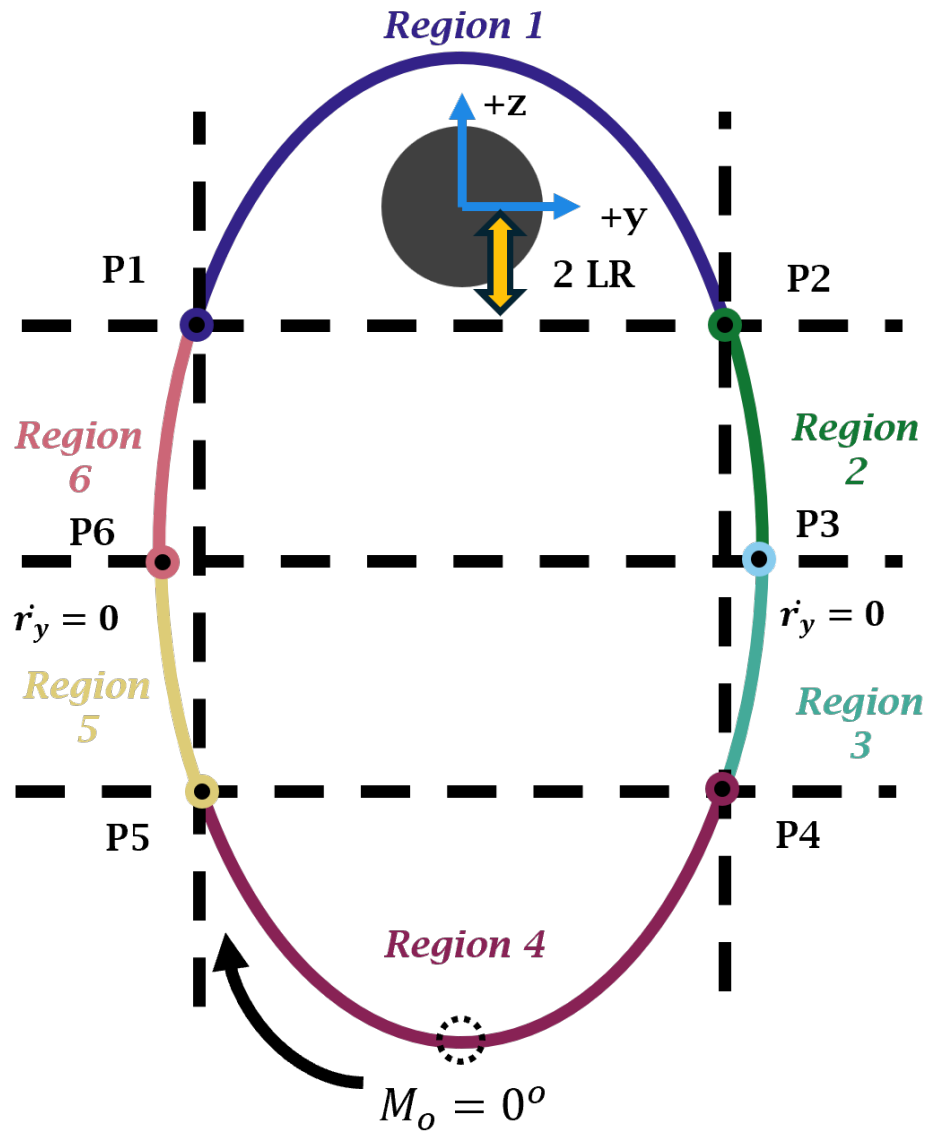


Figure 4.4: Velocity-Geometric Region Segmentation Approach Illustration. The geometry and symmetry leveraged to adapt the velocity-driven approach are shown. P1 and P2, defined as the points 2LR below the Moon's center, serve as the bounds of the Periselene region. These points are then reflected across the midline of the orbit defined by the line connecting P3 to P6 where $\dot{r}_y = 0$ forms the Aposelene region bounds.

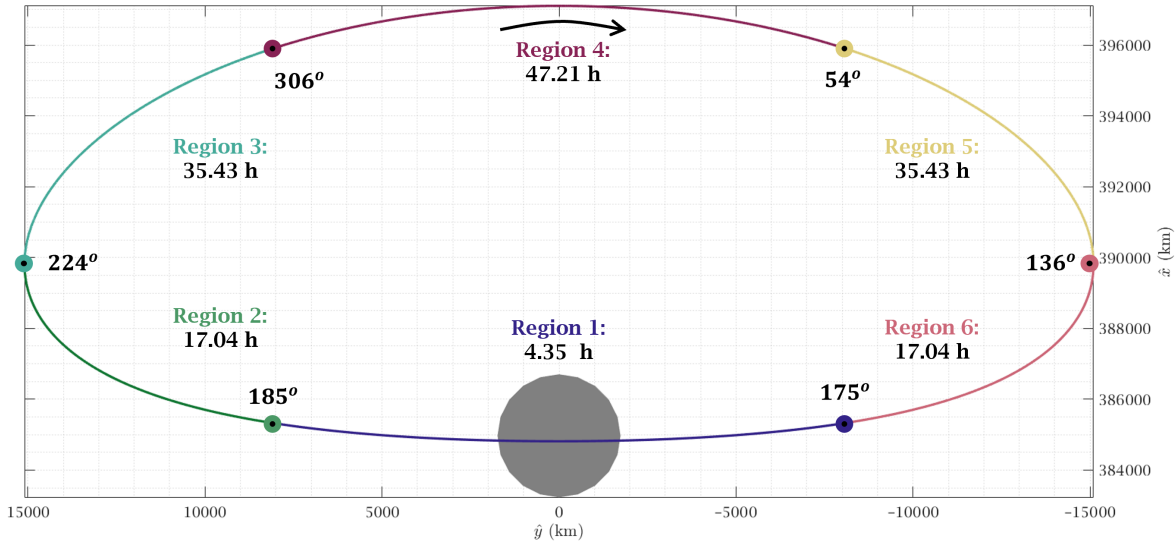


Figure 4.5: NRHO Velocity-Geometric Region Segmentation. The segmented NRHO, broken into six regions according to the velocity-geometric-based approach, is shown. Region One, encompassing Periselene, is the shortest in terms of duration, while Region Four, encompassing Aposelene, is the longest. The four transition regions come in pairs, (two/six) and (three/five), reflected across the \hat{y} -axis, each with an equal duration. These regions exhibit similar behavior but in reverse order concerning time.

region. The Periselene region continues until r_z returns back to $-2LR$. Region Two is a mirror of six ending when $\dot{r}_y = 0$. Region Three is analogous to Region Six, beginning at $\dot{r}_y = 0$ but ending when $r_y = r_y(r_z = -2LR \wedge \ddot{r}_y < 0)$. That is, Region Three ends when the r_y returns to the same value as r_y , defining Region Two's beginning. Regions Two and Four have identical initial r_y components. Region Four is called the Aposelene Region and runs until $r_y(R4_0)$ returns to the same value. Region Five is a mirror of Three. This segmentation symmetry can be seen in a visualization of the approach in Figure 4.5. The region definitions, resulting initial mean anomaly, rounded to the nearest integer, and duration are listed in Table 4.2.

This segmentation of the NRHO aligns Region Four to be close to the Aposelene region discussed in prior works. The Aposelene region is characterized by its stable dynamics, while the Periselene region is defined by its extreme acceleration. Regions Two and Six are

Table 4.2: NRHO Velocity-Geometric Segmentation Definitions. The second of two segmentation approaches considered segmenting the NRHO into six distinct regions defined by the orbits’ geometry and dynamics. The orbit’s dominant velocity terms and natural symmetry define the region. Region One represents the Periselene region, while Region Four represents the Aposelene region. The initial mean anomaly and total duration of each region are listed.

Region	Initial Point Definition	M_0 (deg)	Duration (h)
1	$r_z = -2LR \wedge \ddot{r}_y > 0$	175	4.35
2	$r_z = -2LR \wedge \ddot{r}_y < 0$	185	17.04
3	$\dot{r}_y = 0 \wedge \ddot{r}_z < 0$	224	35.43
4	$r_y = r_y(r_z = -2LR \wedge \ddot{r}_y < 0)$	306	47.21
5	$r_y = r_y(r_z = -2LR \wedge \ddot{r}_y > 0)$	54	35.43
6	$\dot{r}_y = 0 \wedge \ddot{r}_z > 0$	136	17.04

transitioning into and out of the Periselene region. Regions Three and Five are transition regions into and out of the Aposelene region. The velocity-geometric approach achieves the goal of being driven by the NRHO dynamics while obtaining regional continuity throughout both defining portions of the orbit. This method allows the entire approach strategy to be broken into segments. Instead of a “One size fits all” approach, a tailored strategy for each region can be developed and then stitched together into an entire approach strategy for Gateway that enables rendezvous throughout the entirety of Gateway’s orbit. For these reasons, this segmentation method will be utilized for this work.

4.2 Hold Point Axes Identification

The approach strategy for each region begins with identifying each region’s approach axis. In the two-body context, the approach is done along, or parallel to, one of the LVLH frame basis vectors: the V-bar, R-bar, and, less commonly, the H-bar. For this strategy, a region’s approach axis is chosen by its station-keeping ΔV and the passive safety of hold points along the axes. The goal is to find the axis within each region that balances the cost to remain at a

given HP on the axis while ensuring that said HP is safe in the presence of a station-keeping failure. Section 4.2.1 presents the analysis for identifying the optimal station-keeping ΔV cost approach axis. Section 4.2.2 follows with the safety analysis along the identified axes. In cases where the optimal axis is unsafe, suboptimal axes are analyzed to find safe axes. The suboptimal axis choice leverages the station-keeping cost analysis to choose an axis that, while not the most ΔV -efficient, is close to optimal.

4.2.1 Hold Point Station-Keeping Cost Analysis

The ΔV required to station-keep for one region duration at points along a sphere of radius ρ were calculated to find the optimal axes, generating a station-keeping ΔV cost map. Each point on the map is associated with an approach axis defined by the vector pointing from the station center to the point on the sphere. The coordinate transformation shown in Eq. 4.1 defines the points along the sphere. φ is the azimuthal angle measured counter clockwise from the $+\hat{x}$ axis and θ is the zenith angle measured counter clockwise from the $+\hat{z}$ axis. Analyzed points were evenly spaced in 5° increments.

$$\begin{bmatrix} \delta r_x \\ \delta r_y \\ \delta r_z \end{bmatrix} = \begin{bmatrix} \sin \theta \cos \varphi & \cos \theta \cos \varphi & -\sin \varphi \\ \sin \theta \sin \varphi & \cos \theta \sin \varphi & \cos \varphi \\ \cos \theta & -\sin \theta & 0 \end{bmatrix} \begin{bmatrix} \rho \\ \theta \\ \varphi \end{bmatrix}, \quad \begin{array}{l} \varphi \in [0, 2\pi] \\ \theta \in [0, \pi] \end{array} \quad (4.1)$$

The ΔV cost for station-keeping at a given hold point is determined by integrating the acceleration of the target vehicle for the duration of a specified hold. This calculation is done via Eq. 4.2. In this equation, t_f is a given region's total duration. It should be noted that this is an estimate to the station-keeping cost. A real-world mission would not constantly fire its thruster to maintain the HP. A range tolerance would be prescribed, and

after the VV drifts outside the tolerance, it would burn to adjust and maintain the HP. However, this study will use this approximation to evaluate the cost for a given axis.

$$\Delta V = \int_0^{t_f} \|\delta \dot{\mathbf{r}}\| dt \quad (4.2)$$

The STM, calculated using Eq. 3.4, was also analyzed to check the validity of the identified axes from the heat maps. The eigenvector, \mathbf{v} , associated with the minimum eigenvalue, $\min \lambda$, of $\Phi_{rv}(t_f, 0)$, where t_f is a region's duration, provides an estimate of the vector that experiences the least change in velocity based on the initial position. This vector should align relatively close to the identified axis from the heat maps. There will be variations between the two for a given region, as the STM is a linearized model for the EORM. The linearization errors are nonnegligible and will produce differences between the STM vector and heat map axis vector, primarily expected in Region One, where the errors are most significant.

The station-keeping cost for a region heavily depends on the VV relative acceleration, which is governed by Gateway's location in the NRHO. Station-keeping becomes more fuel-intensive the closer the Gateway is to Periselene. As a result, Region One has the highest station-keeping cost map out of the six regions, while Region Four has the lowest due to its position around Aposelene.

Region One's station-keeping ΔV cost map for a $\rho = 5$ km is shown in Figure 4.6. This map, and subsequent ones shown later, implement a Robinson protection to visualize the station-keeping data for every point on the analyzed sphere. This region has a worst case ΔV of 7.76 m/s and a best case of 5.03 m/s. The optimal axis is aligned with the $\delta \mathbf{r}_x$ basis vector. Holding along the $\delta \mathbf{r}_x$ axis provides significant savings compared to other axes. Between 7.76 m/s and 5.03 m/s over a four hour region to only station-keep is a significant cost but not prohibitive. Alternatives to traditional station-keeping are explored later in Section 4.3

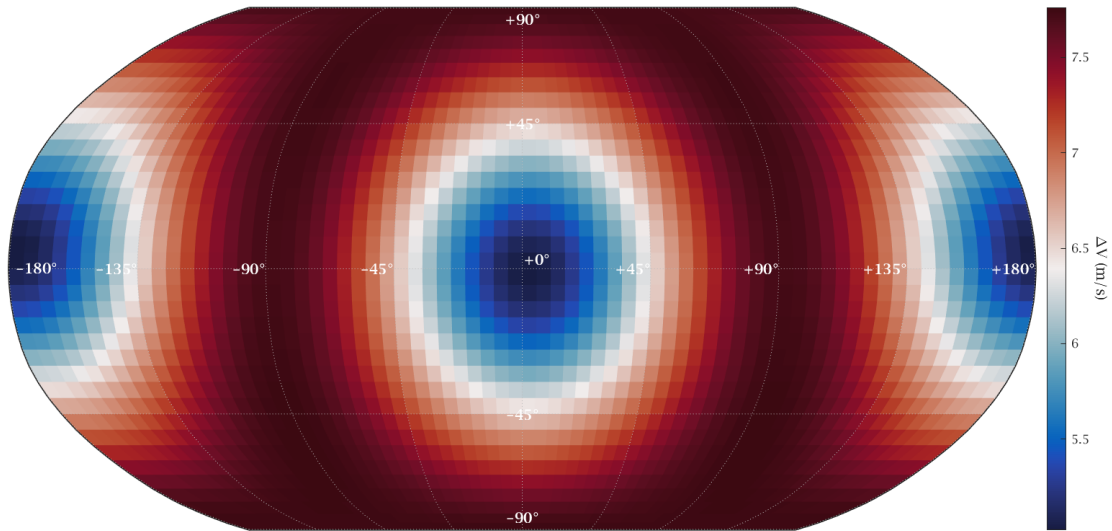


Figure 4.6: Region 1 Loiter v. Station-Keeping ΔV Benefit Analysis. The ΔV is required to hold at various points along a sphere with a 5 km radius for the duration of Region One. Analyzed points were spaced along the sphere’s surface at 5° increments. Based on this analysis, the optimal ΔV approach axis for this region is aligned with the $\delta \mathbf{r}_x$ basis vector defined by $\delta \mathbf{r}_x = [1, 0, 0]$ in the relative synodic frame. Holding on this axis results in a necessary ΔV reduction of over 2.74 m/s compared to holding on the worst axis for this region.

to identify methods to reduce the cost of maintaining a HP.

The linearization error of the Periselene region can be seen through the analysis of the STM for this region. The \mathbf{v} associated with $\min \lambda$ of this region has a 87.20° difference in direction. This difference is significant, but it is assumed that the extreme nonlinearities in the dynamics within this region are the source of the error. The following regions align more closely with the identified optimal axis.

The remaining five regions see a significant reduction in required ΔV . These regions’ heat maps are shown in Figures 4.7, 4.8, 4.9, 4.10, and 4.11. The best case axes identified from the heat maps for each region, along with their associated best case ΔV , are listed in Table 4.3. Regions Two and Six see a $10\times$ magnitude reduction in ΔV for the worst-case axis, while Three through Five see a $100\times$ reduction compared to Region One.

Table 4.3: ΔV -optimal Region Rendezvous Approach Axes. The components of each region's identified approach axes in the relative synodic frame are listed. The axes were identified through station-keeping ΔV cost analysis. The required station-keeping ΔV at the identified axis is listed for a HP at 5 km.

Region	φ ($^\circ$)	θ ($^\circ$)	δr_x	δr_y	δr_z	ΔV (m/s)
1	0	90	1.000	0.000	0.000	5.03
2	350	100	0.970	-0.171	-0.174	0.22
3	350	110	-0.925	0.163	0.342	1.12×10^{-2}
4	0	120	-0.866	0.000	0.500	9.033×10^{-4}
5	10	110	-0.925	-0.163	0.342	1.12×10^{-2}
6	10	80	-0.970	0.171	0.174	0.22

These reductions are numerically significant. Holding on a nonoptimal axis in Region Four requires, while not many, some station-keeping burns to occur. Holding on the optimal axis requires tenths of millimeters per second per second, effectively zero from an operator's perspective. Holding on these axes reduces the amount of fuel and station-keeping burns required to maintain the HP, increasing the operational efficiency of the approach. Holding on a suboptimal axis is not prohibitive either. While it would increase fuel costs, the increases are not debilitating from a ΔV budget perspective, enabling the suboptimal axis to increase HP passive safety.

Regions Two through Six have varying levels of agreement with their STM eigenvector (\mathbf{v}). The angle between each region's \mathbf{v} and the identified axes are 10.2° , 52.6° , 54.5° , 28.7° , 13.6° respectively. The Φ_{rr} quadrant of the STM showed worse agreement across the board. Regions Three and Four have higher than anticipated differences, given their relative dynamic stability. Two and Six closely agree with the STM but are lower than expected, given their relative dynamic instability. Furthermore, it was anticipated that the mirrored regions would have similar differences. Regardless, \mathbf{v} s and identified axes were relative to each other, giving confidence in the identified axes from station-keeping simulations.

These axes serve as a first iteration for identifying the best approach axes for rendezvousing

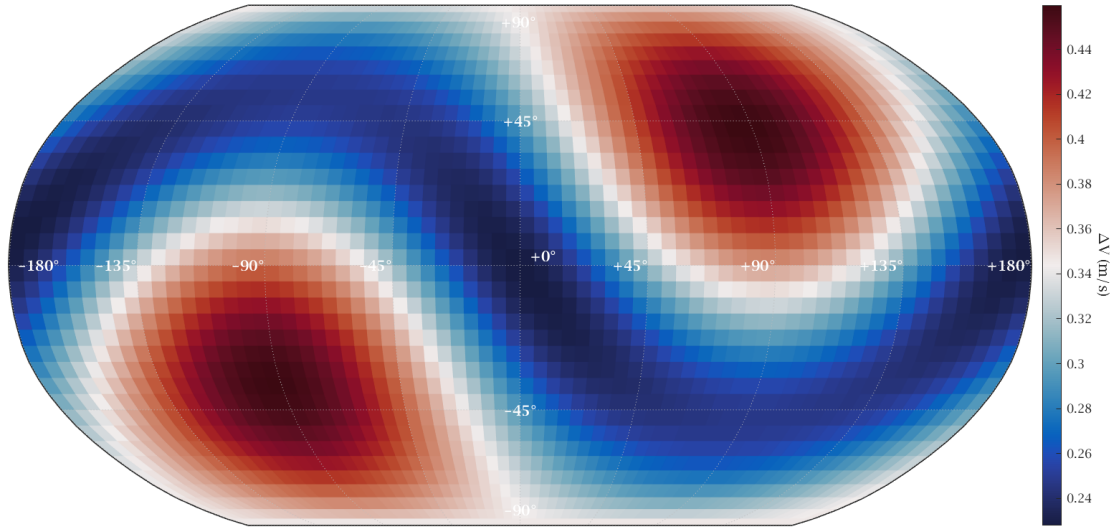


Figure 4.7: Region 2 Loiter v. Station-Keeping ΔV Cost Analysis. The ΔV is required to hold at various points along a sphere with a 5 km radius for the duration of Region Two. Analyzed points were spaced along the sphere's surface at 5° increments. Based on this analysis, the optimal ΔV approach axis for this region is a vector defined by $\delta\mathbf{r} = [0.981, -0.086, 0.174]$ in the relative synodic frame. Holding on this axis results in a necessary ΔV reduction of 0.23 m/s compared to holding on the worst axis for this region.

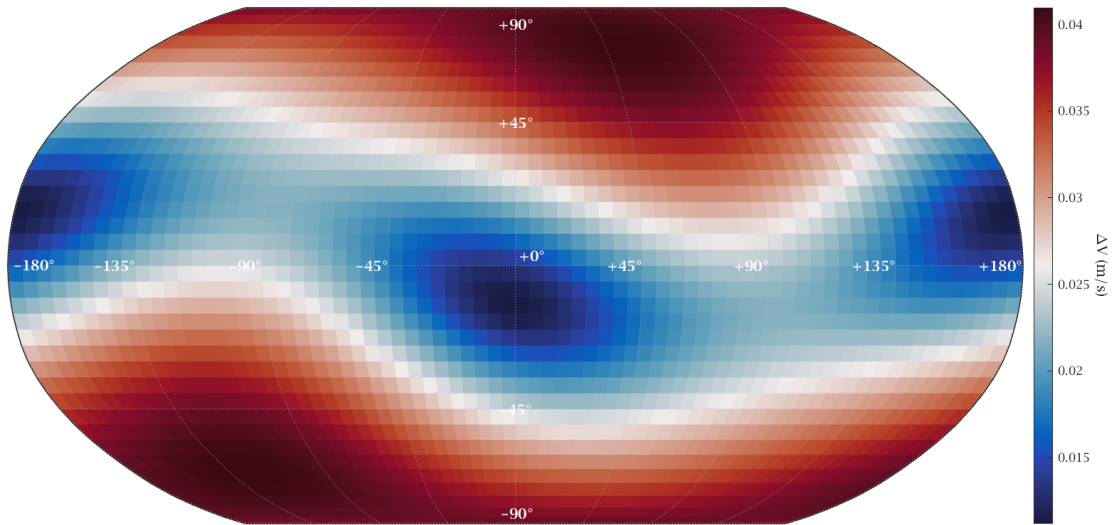


Figure 4.8: Region 3 Loiter v. Station-Keeping ΔV Cost Analysis. The ΔV is required to hold at various points along a sphere with a 5 km radius for the duration of Region Three. Analyzed points were spaced along the sphere's surface at 5° increments. Based on this analysis, the optimal ΔV approach axis for this region is a vector defined by $\delta\mathbf{r} = [-0.925, 0.163, 0.342]$ in the relative synodic frame. Holding on this axis results in a necessary ΔV reduction of 3.00×10^{-2} m/s compared to holding on the worst axis for this region.

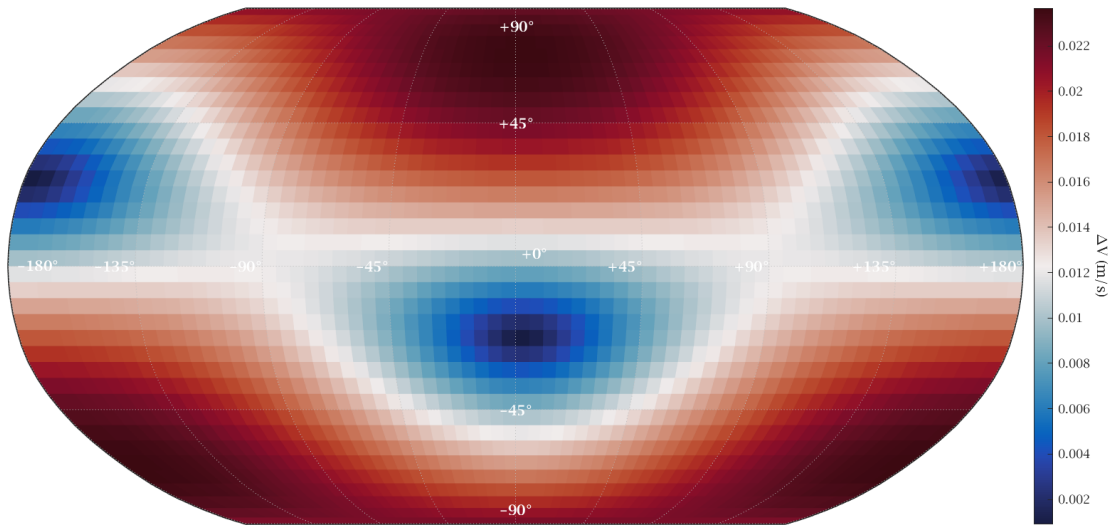


Figure 4.9: Region 4 Loiter v. Station-Keeping ΔV Cost Analysis. The ΔV is required to hold at various points along a sphere with a 5 km radius for the duration of Region Three. Analyzed points were spaced along the sphere's surface at 5° increments. Based on this analysis, this region's optimal ΔV approach axis is a vector defined by $\delta \mathbf{r} = [-0.866, 0.00, 0.500]$ in the relative synodic frame. Holding on this axis results in a necessary ΔV reduction of 5.1×10^{-2} m/s compared to holding on the worst axis for this region.

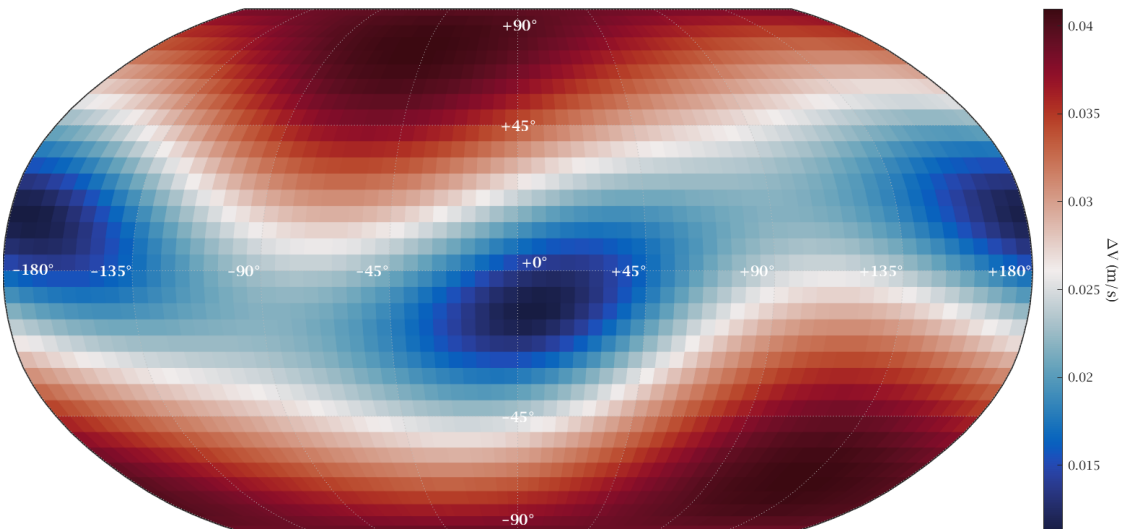


Figure 4.10: Region 5 Loiter v. Station-Keeping ΔV Cost Analysis. The ΔV is required to hold at various points along a sphere with a 5 km radius for the duration of Region Five. Analyzed points were spaced along the sphere's surface at 5° increments. Based on this analysis, the optimal ΔV approach axis for this region is a vector defined by $\delta \mathbf{r} = [-0.925, 0.163, 0.342]$ in the relative synodic frame. Holding on this axis results in a necessary ΔV reduction of 3.00×10^{-2} m/s compared to holding on the worst axis for this region.

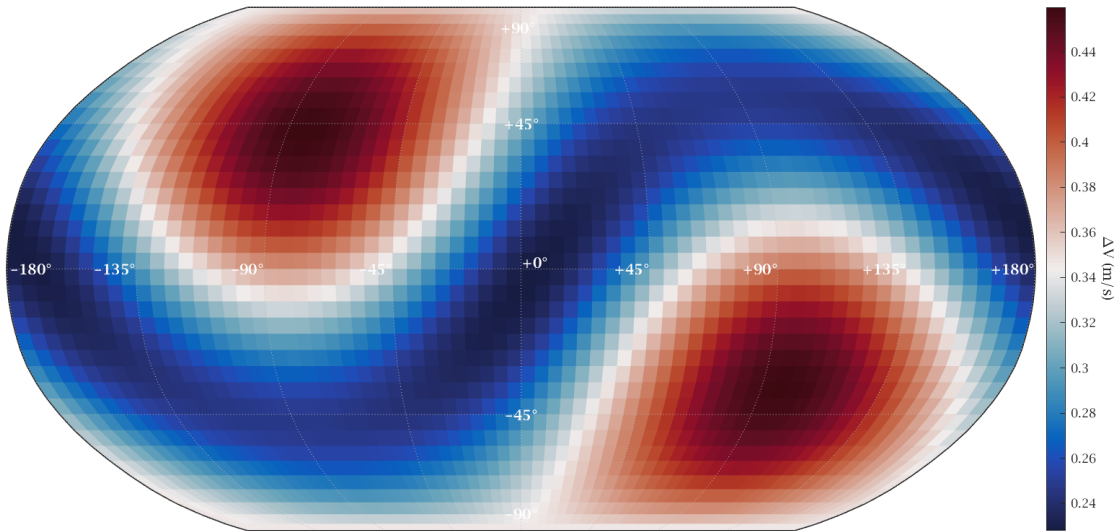


Figure 4.11: Region 6 Loiter v. Station-Keeping ΔV Cost Analysis. Region 6 Loiter v. Station-Keeping ΔV Cost Analysis. The ΔV is required to hold at various points along a sphere with a 5 km radius for the duration of Region Six. Analyzed points were spaced along the sphere's surface at 5° increments. Based on this analysis, the optimal ΔV approach axis for this region is a vector defined by $\delta\mathbf{r} = [-0.981, -0.086, 0.174]$ in the relative synodic frame. Holding on this axis results in a necessary ΔV reduction of 0.23 m/s compared to holding on the worst axis for this region.

with Gateway within each region. The second piece of the axis identification process analyzes each axis' passive safety. The following section simulates the passive safety of HPs along this iteration of approach axes.

4.2.2 Hold Point Safety Analysis

After identifying the axis with the minimum station-keeping ΔV cost, points along the axes were analyzed for passive safety in the presence of a VV departure failure. As described earlier, a departure failure occurs when a VV is scheduled to depart the HP but shuts down at the planned burn. To simulate safety if a departure failure occurs, the vehicle is simulated as if it were on a free drift starting at this failure, where operators have no control over the vehicle for 24 hours. The safety criteria detailed in Section 3.4.2 were used to determine the

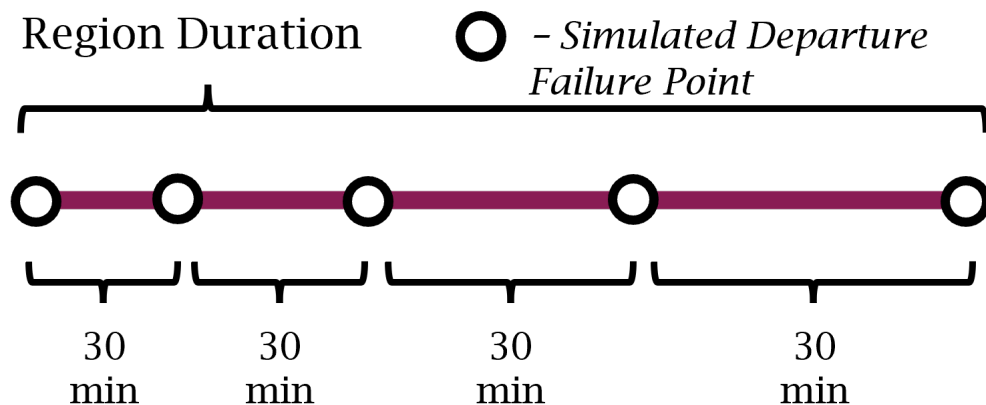


Figure 4.12: HP On Axis Departure Failure Analysis Configuration. HPs were tested at different points spaced 30 minutes apart, spanning the duration of a given region. Testing multiple points in a region is necessary due to the changing dynamics within a region. The variation could lead to a safe result for the first HP tested, but then, under slightly different dynamics, the same HP could become unsafe.

safety of one of these drifts.

While the regions are segmented to try and maintain consistent dynamics, there is still variation. Because of this, a safe departure failure at time t_i may become unsafe if initiated at time t_{i+1} . The variable dynamics necessitate each HP on each axis to be tested at times and distributed across the duration of a given region. For this analysis, HP departure failures were simulated at 30-minute increments beginning at the start of a region. This setup is visualized in Figure 4.12. This configuration provides complete coverage of the entire orbit, giving a comprehensive measure of the passive safety of the HPs along axes. HPs were spaced 5 km apart spanning from -50.5 km to 50.5 km.

The following passive safety analysis is presented in two parts: the analysis done on the identified ΔV -optimal axes and the analysis done on three suboptimal axes tested to provide a safe alternative to optimal axes determined to be unsafe. The analysis aims to ensure there are four HPs, two outside the RS and one within the RS and AS, respectively, that are safe. The HPs outside the AS must be 100% safe to be considered. The HP inside the AS should

be close to 100% but is given some leeway in Regions One, Two, and Six due to the chaotic nature of those regions.

Optimal Axes

Region One's ΔV -optimal axis HP passive safety is shown in Figure 4.13. The Figure shows each propagated trajectory in the δr_x - δr_y plane. There is a nonzero δr_z component to each trajectory, which is not shown for simplicity. Each trajectory was propagated 24 hours if safe and terminated once deemed unsafe. The green trajectories represent safe drifts, while the dark red represents unsafe drifts. Each safety region is shown with yellow representing the RS, blue representing the AS, and bright red representing the KOS. Each HP candidate is shown as a black dot.

Region One (Periselene) was a primarily unsafe region. The trajectories initially break away slowly from the Station, and the VV runs out of time to drift away and intersects with a safety region. Only HPs far from the RS had enough time to drift off the δr_x axis and not cross into any regions. The safety percentage of each HP is shown in Figure 4.19. No HP had a safety percentage above 70% for this region. Region One needs a suboptimal approach axis because of this. Based on Figure 4.6, a suboptimal axis, defined as $[-0.750, -0.433, 0.500]$. This was selected because it oriented the axis to allow the streamline-like drifts to pass above and to the side of the safety regions without venturing into the more expensive zones in the heat map.

Region Two's optimal axis was the second of three determined to be unsafe. Region Two's passive drift trajectories can be seen in Figure 4.14. The drifts behave similarly to Region One, breaking slowly away from the δr_x axis. However, due to the optimal axis being skewed from the δr_x axis, the trajectories can now drift away without intersecting. The HPs

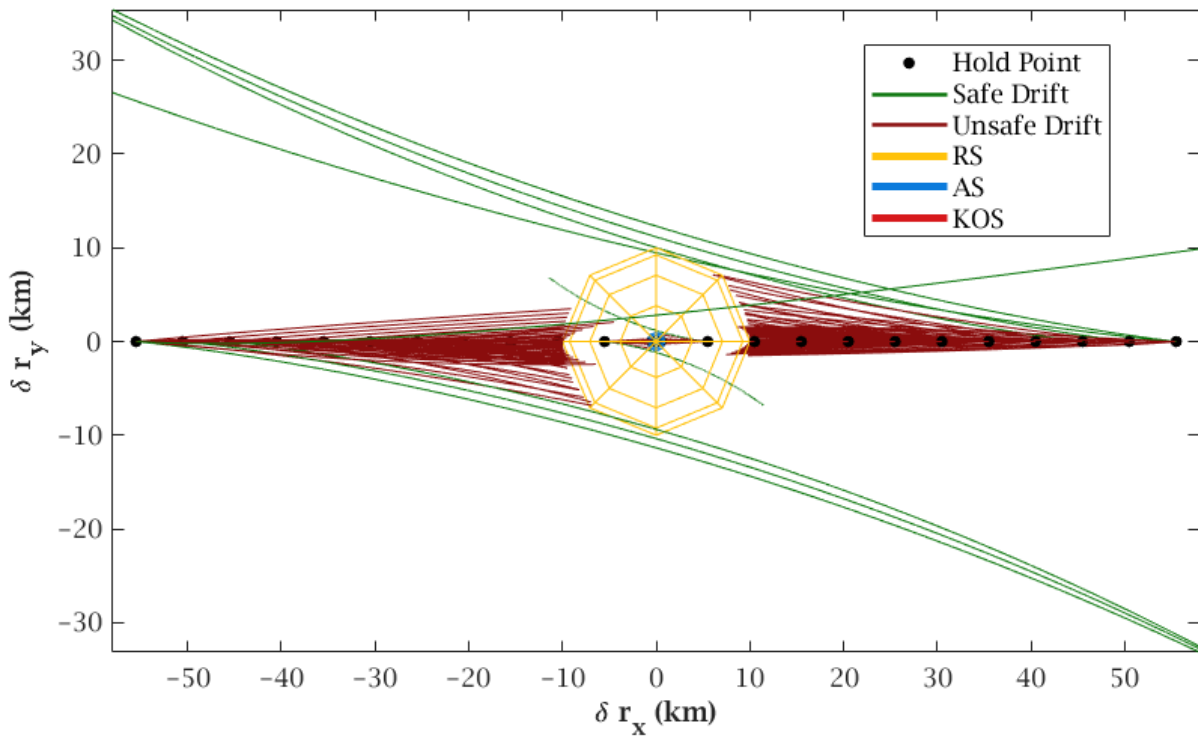


Figure 4.13: Region 1 Optimal Approach Axis Drift Trajectories. Region One’s passive safety trajectories are shown. Each trajectory begins after a departure failure and is propagated for 24 hours or until deemed unsafe. Safe trajectories are shown in green, and unsafe trajectories are shown in dark red. The RS, AS, and KOS are shown in yellow, blue, and bright red, respectively. This plot is a 2D slice along the δr_x - δr_y plane to show the behavior best. There is a nonzero δr_z component to each trajectory. Region One’s axis was deemed unsafe, and a second suboptimal axis was identified.

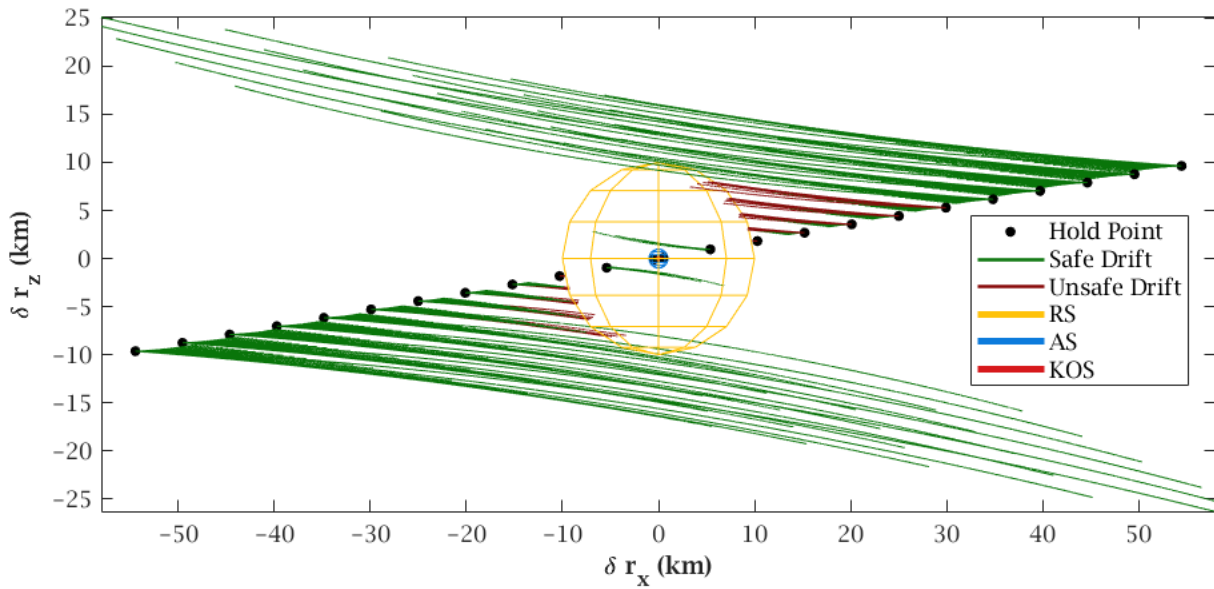


Figure 4.14: Region 2 Optimal Approach Axis Passive Drift Trajectories. Region Two’s passive safety trajectories are shown. Each trajectory begins after a departure failure and is propagated for 24 hours or until deemed unsafe. Safe trajectories are shown in green, and unsafe trajectories are shown in dark red. The RS, AS, and KOS are shown in yellow, blue, and bright red, respectively. To show the behavior best, this plot is a 2D slice along the δr_x - δr_z plane. There is a nonzero δr_y component to each trajectory. Region Two’s axis was deemed unsafe, and a second, suboptimal axis was identified.

for Region Two are 100% safe up until $\delta r = \pm 30.5$ km away from the Station. The safety margin drops down to 0% for the HP right outside the RS but returns to 100% at ± 5.5 km. However, the safety drops below 80% inside the AS. This level is below the author’s comfort level, even considering the region’s proximity to Periselene. The safety of this innermost HP required a suboptimal axis to be chosen for Region Two. Based on Figure 4.7, a suboptimal axis, defined as $[-0.854, -0.354, 0.383]$, was selected.

Region Three, Four, and Five axes were shown to be 100% safe except for Region Five, which had two HPs close to the RS boundary dip below 100%. Each regions’ trajectories can be seen in Figures 4.15, 4.16, and 4.17 respectively. Regions Three and Four show minimal drift after failure. The VV departs its HP and drifts no more than 10 km. Region Five exhibits

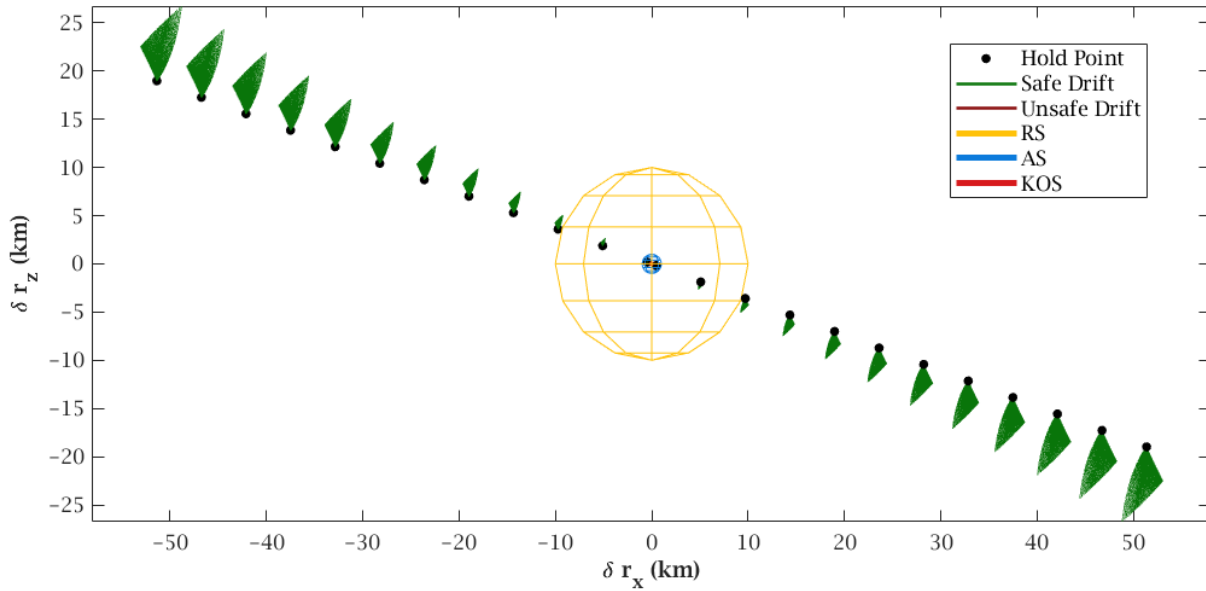


Figure 4.15: Region 3 Optimal Approach Axis Passive Drift Trajectories. Region Three’s passive safety trajectories are shown. Each trajectory begins after a departure failure and is propagated for 24 hours or until deemed unsafe. Safe trajectories are shown in green, and unsafe trajectories are shown in dark red. The RS, AS, and KOS are shown in yellow, blue, and bright red, respectively. To show the behavior best, this plot is a 2D slice along the δr_x - δr_z plane. There is a nonzero δr_y component to each trajectory

more dramatic VV behavior as the orbit approaches closer to Periselene. The points with failure occurring closer to the region’s initial time drifts behave similarly to Regions Three and Four. However, as the failures occur closer to the start of Region Six, the drifts become more extreme. Each Figure is shown as a 2D slice to best view the behavior; each trajectory has a nonzero out-of-plane component.

Region Six’s passive drift trajectories are shown in Figure 4.11. This region’s drifts closer to the beginning of the region have a more pronounced bend around the Station, avoiding any safety violations. However, as the failures occur closer to the start of Region One, the drifts become more streamlined, shooting straight into the safety boundaries. This behavior causes the HP’s to have reduced safety across the board, with no single HP being more than

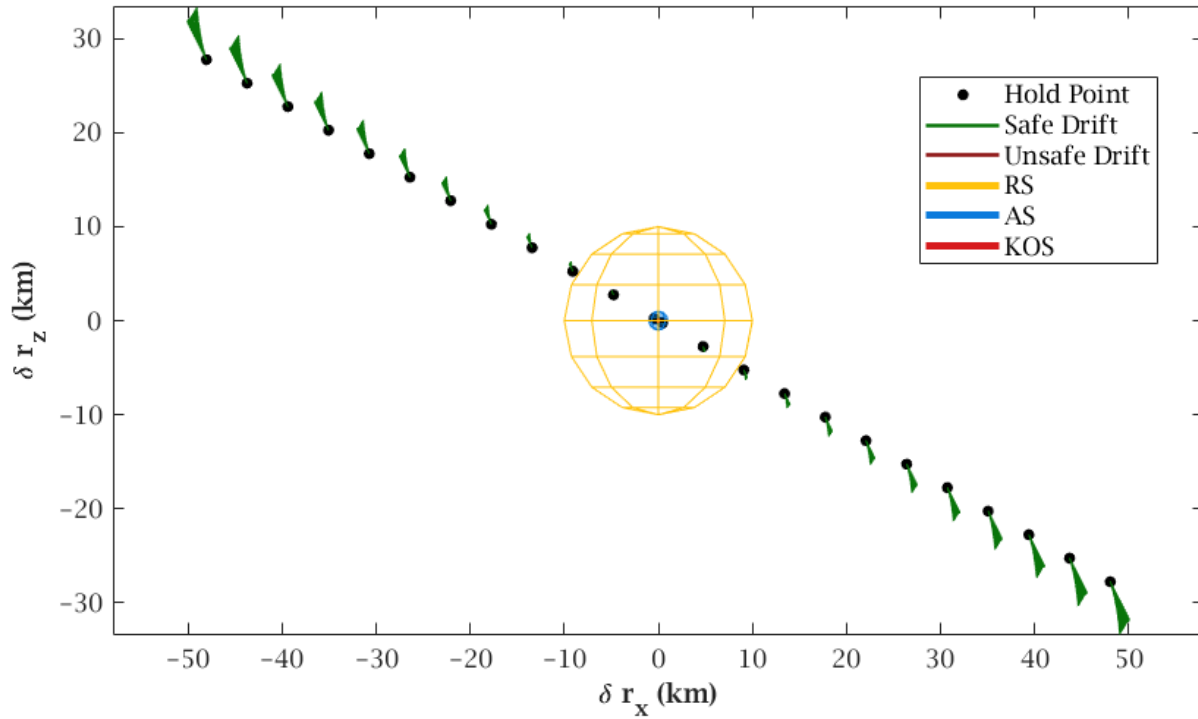


Figure 4.16: Region 4 Optimal Approach Axis Passive Drift Trajectories. Region Four's passive safety trajectories are shown. Each trajectory begins after a departure failure and is propagated for 24 hours or until deemed unsafe. Safe trajectories are shown in green, and unsafe trajectories are shown in dark red. The RS, AS, and KOS are shown in yellow, blue, and bright red, respectively. To show the behavior best, this plot is a 2D slice along the δr_x - δr_z plane. There is a nonzero δr_y component to each trajectory

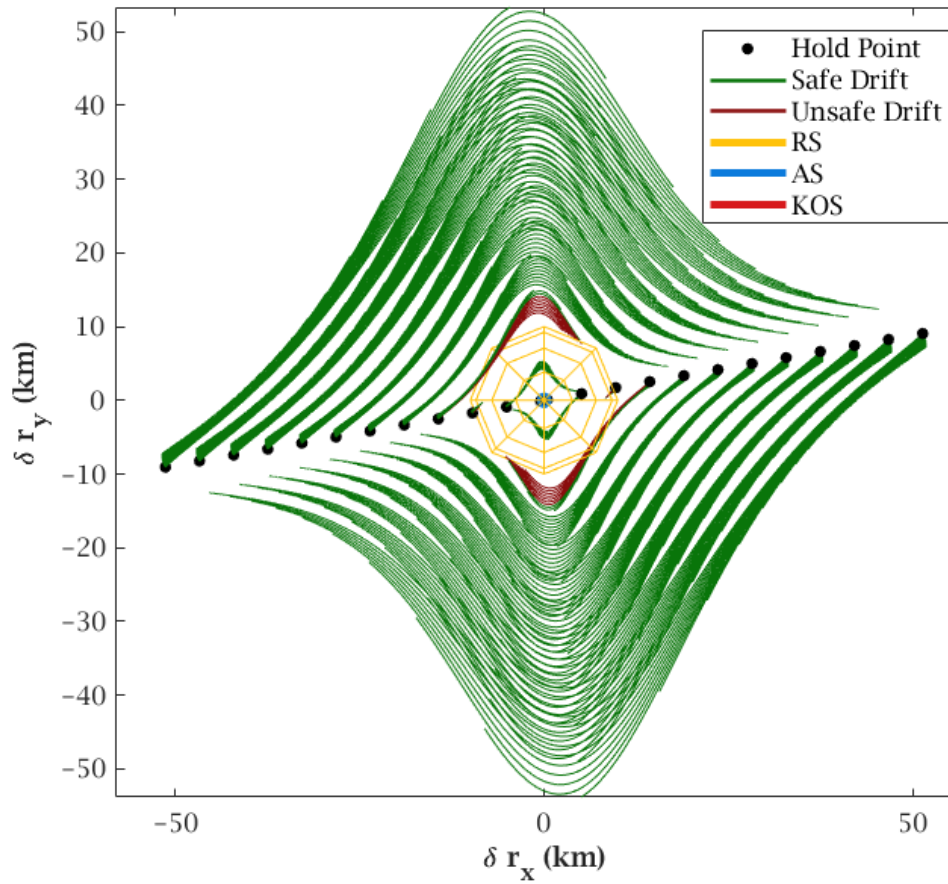


Figure 4.17: Region 5 Optimal Approach Axis Passive Drift Trajectories. Region Five's passive safety trajectories are shown. Each trajectory begins after a departure failure and is propagated for 24 hours or until deemed unsafe. Safe trajectories are shown in green, and unsafe trajectories are shown in dark red. The RS, AS, and KOS are shown in yellow, blue, and bright red, respectively. This plot is a 2D slice along the δr_x - δr_y plane to show the behavior best. There is a nonzero δr_z component to each trajectory

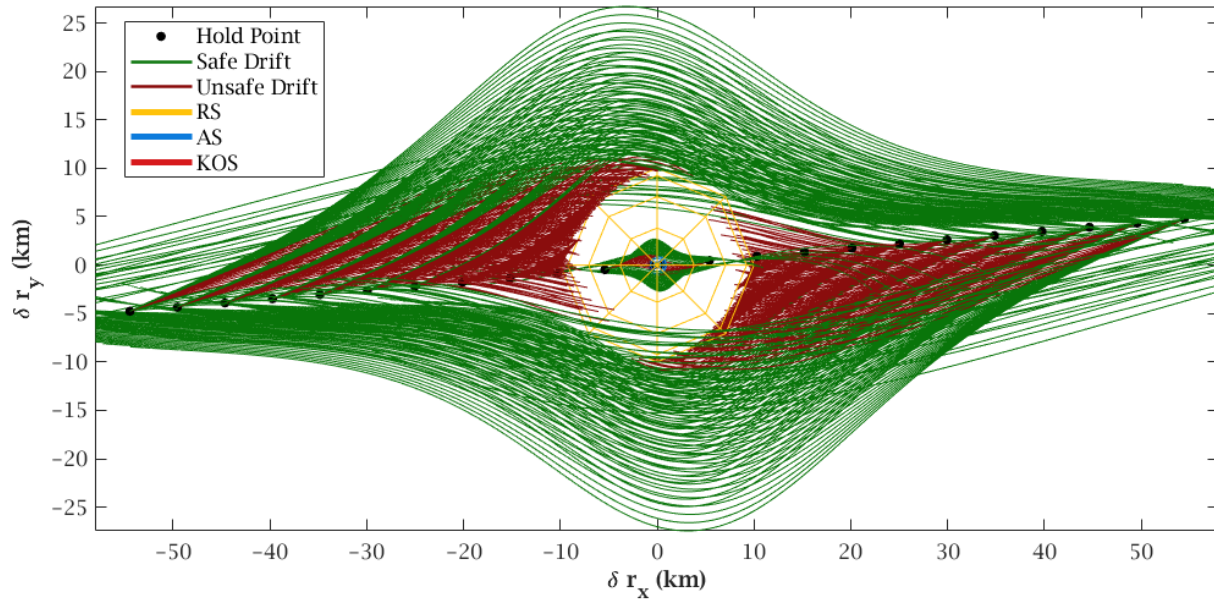


Figure 4.18: Region 6 Optimal Approach Axis Passive Drift Trajectories. Region Six's passive safety trajectories are shown. Each trajectory begins after a departure failure and is propagated for 24 hours or until deemed unsafe. Safe trajectories are shown in green, and unsafe trajectories are shown in dark red. The RS, AS, and KOS are shown in yellow, blue, and bright red, respectively. This plot is a 2D slice along the δr_x - δr_y plane to show the behavior best. There is a nonzero δr_z component to each trajectory. Region Six's axis was deemed unsafe, and a second, suboptimal, axis was identified.

75% safe. The HPs become increasingly unsafe closer to the Station, bottoming out at 0% at ± 20.5 km. Safety increases once the HP is placed within the AS and KOS, but both HPs are still primarily unsafe. As with Regions One and Two, a suboptimal axis must be selected for Region Six. Based on Figure 4.11, a suboptimal axis, defined as $[-0.500, 0.500, 0.707]$, was selected.

Figure 4.19 shows the HP safety percentage for each HP analyzed. Here, the strong safety of Regions Three, Four, and Five can be seen. Each of these regions is consistently safe across all HP distances. Region Five sees a dip closer to the RS boundary, which should be anticipated when starting so close to the boundary. The poor safety of Regions One, Two, and Five can also be seen. Region Two is the safest of the three but is deemed unsafe due to

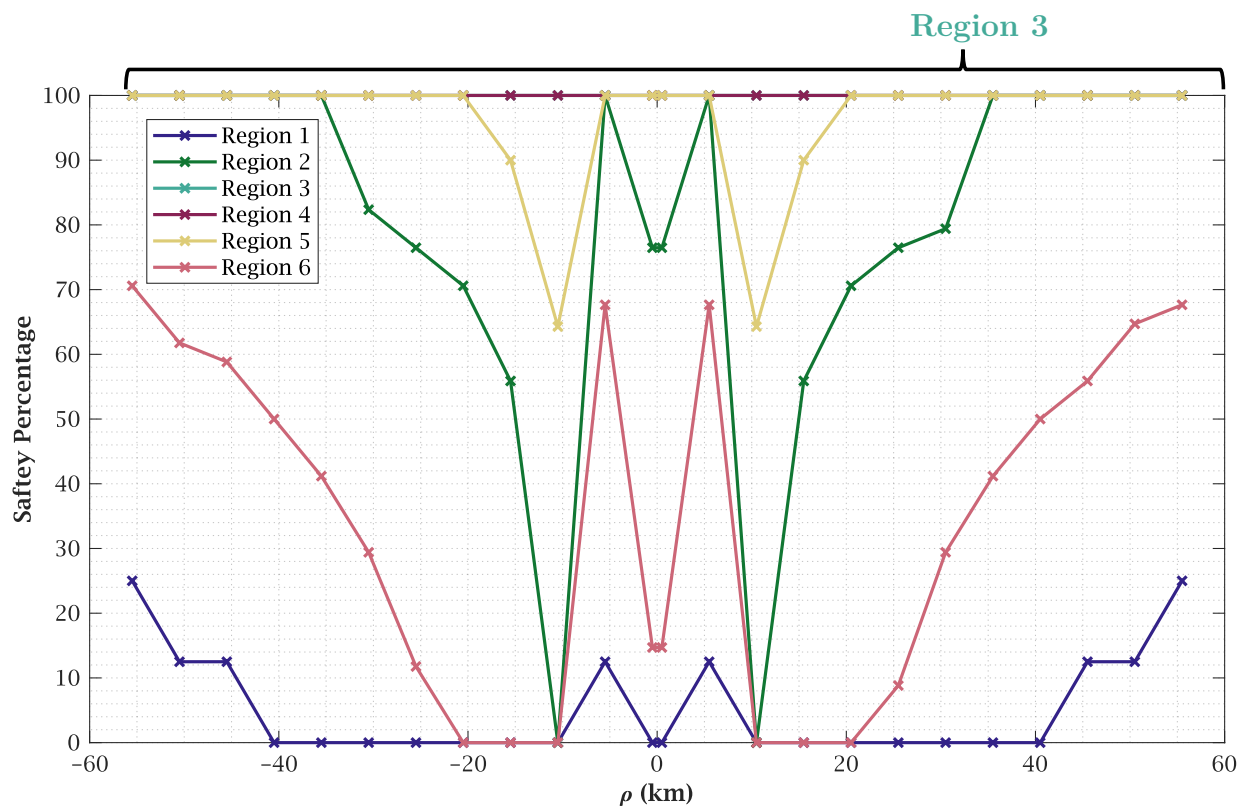


Figure 4.19: Optimal Approach Axis HP Passive Safety. The HP safety percentage for HPs along the identified optimal axes is shown. The safety percentage is the percent ratio of safe drifts to total drifts. These drifts simulate a departure failure and quantify the passive safety of each HP. HPs ranging from -50.5km to 50.5km in steps of 5km were tested. Regions One, Two, and Six were determined to be unsafe. Suboptimal axes were identified for these regions.

its low safety for the HP within the AS. All of Regions One and Six HPs are unsafe. These regions' optimal axes are not suitable for an approach scheme. Suboptimal axes must be evaluated to settle on a selected axis for each region.

Safe, Suboptimal Axes

The suboptimal axes for Regions One, Two, and Six were chosen based on the station-keeping heat maps in Section 4.2.1. These axes are listed in Table 4.4 with their associated ΔV

Table 4.4: ΔV Suboptimal Rendezvous Approach Axes. The components of each region’s identified suboptimal approach axes in the relative synodic frame are listed. The suboptimal axes were required due to the poor safety of the optimal axes for the listed regions. These axes were identified through station-keeping ΔV cost analysis. The required station-keeping ΔV at the identified axis is listed for a HP at 5 km.

Region	δr_x	δr_y	δr_z	ΔV (m/s)
1	-0.750	-0.433	0.500	6.50
2	-0.854	-0.354	0.383	0.32
6	-0.500	0.500	0.707	0.41

required to hold for the region duration. These must be safe to be finalized as approach axes for the rendezvous strategy. The suboptimal axes identified in the section above were tested using the same parameters.

Region One’s suboptimal axis results are shown in Figure 4.20. The altered axis dramatically improves the safety results. The outermost HPs now achieve 100% safety for departure failures. After ± 30.5 km, there is a drop in safety to roughly 60% as the HPs get closer to the RS. The safety returns to 100% within the RS and KOS except for the +0.55 km HP, which has a safety of about 85%. The safety percentages for each HP can be seen in Figure 4.23. These results show that this suboptimal axis is suitable for the approach strategy for Region One.

Region Two’s and Six’s results can be seen in Figures 4.21 and 4.22, respectively. Both regions’ suboptimal axes significantly improve HP safety percentage for departure failures. Region Two and Six are 100% safe for all tested HPs. These axes result in increased ΔV but guarantee passive safety. These axes will be utilized for Regions Two and Six for the approach strategy.

The HP safety percentages for each region, including the optimal axes results from before, can be seen in Figure 4.23. These suboptimal axes for Regions One, Two, and Six enable operators’ safe holding optimized for ΔV efficiency. HPs for this strategy will be placed at

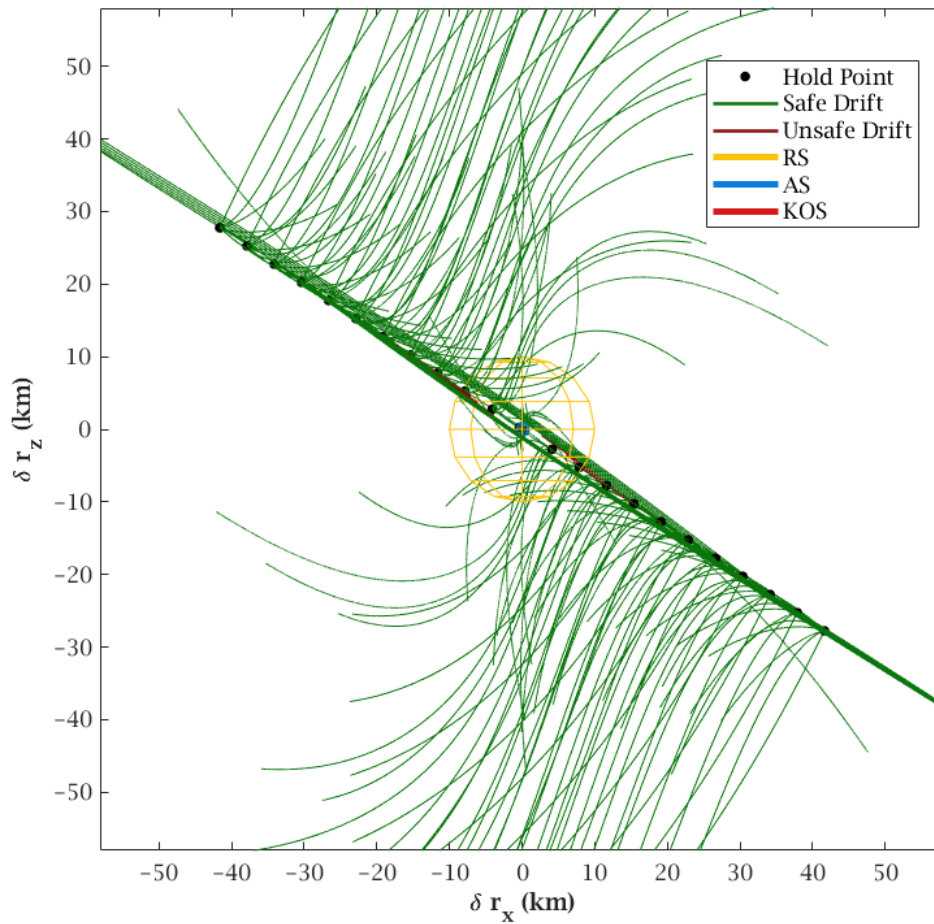


Figure 4.20: Region 1 Suboptimal Approach Axis Passive Drift Trajectories. Region One’s passive safety trajectories are shown for the suboptimal axes. Each trajectory begins after a departure failure and is propagated for 24 hours or until deemed unsafe. Safe trajectories are shown in green, and unsafe trajectories are shown in dark red. The RS, AS, and KOS are shown in yellow, blue, and bright red, respectively. To show the behavior best, this plot is a 2D slice along the δr_x - δr_z plane. There is a nonzero δr_y component to each trajectory. This suboptimal axis improved the safety of the HPs compared to the optimal axis.

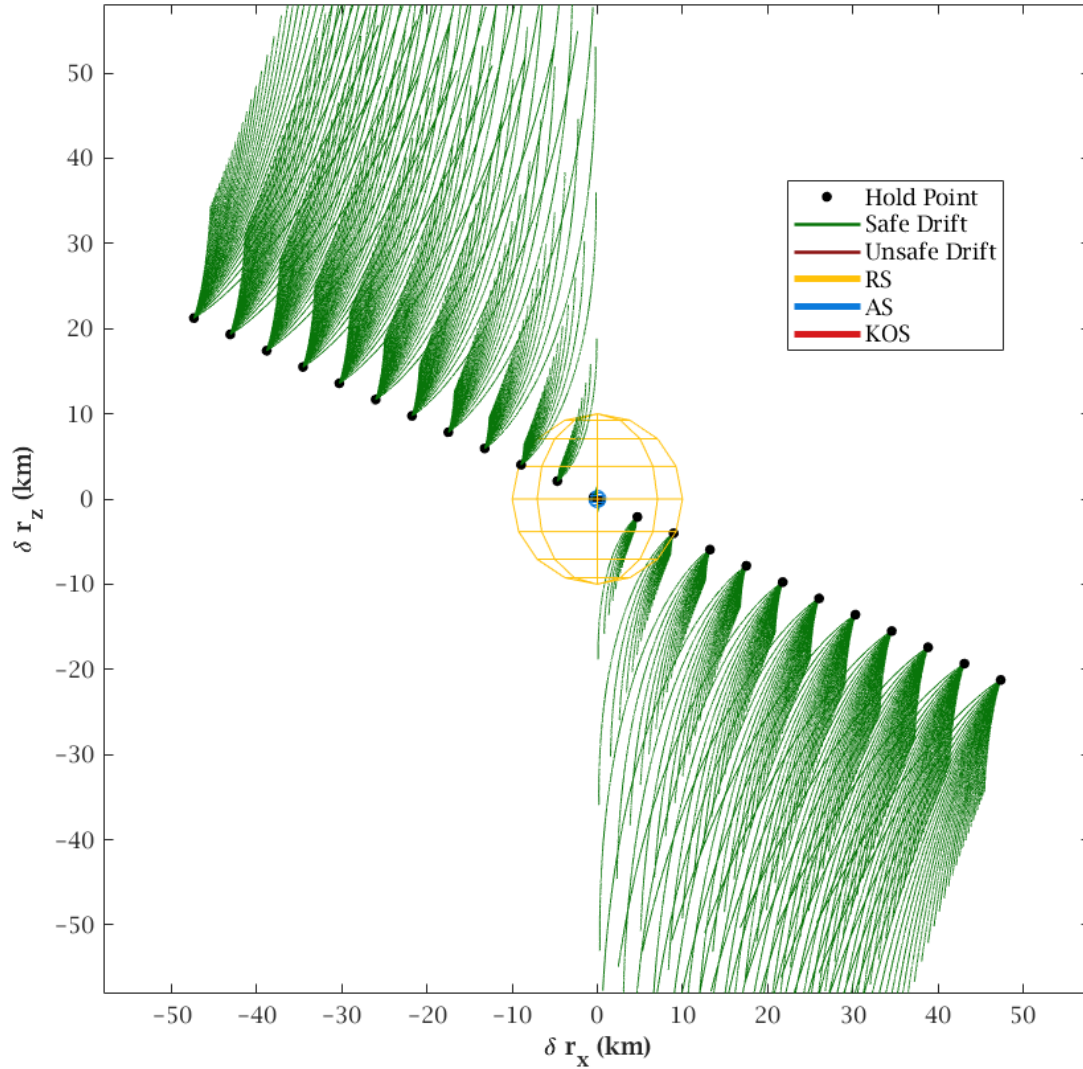


Figure 4.21: Region 2 Suboptimal Approach Axis Passive Drift Trajectories. Region Two's passive safety trajectories are shown for the suboptimal axes. Each trajectory begins after a departure failure and is propagated for 24 hours or until deemed unsafe. Safe trajectories are shown in green, and unsafe trajectories are shown in dark red. The RS, AS, and KOS are shown in yellow, blue, and bright red, respectively. To show the behavior best, this plot is a 2D slice along the δr_x - δr_z plane. There is a nonzero δr_y component to each trajectory. This suboptimal axis improved the safety of the HPs compared to the optimal axis.

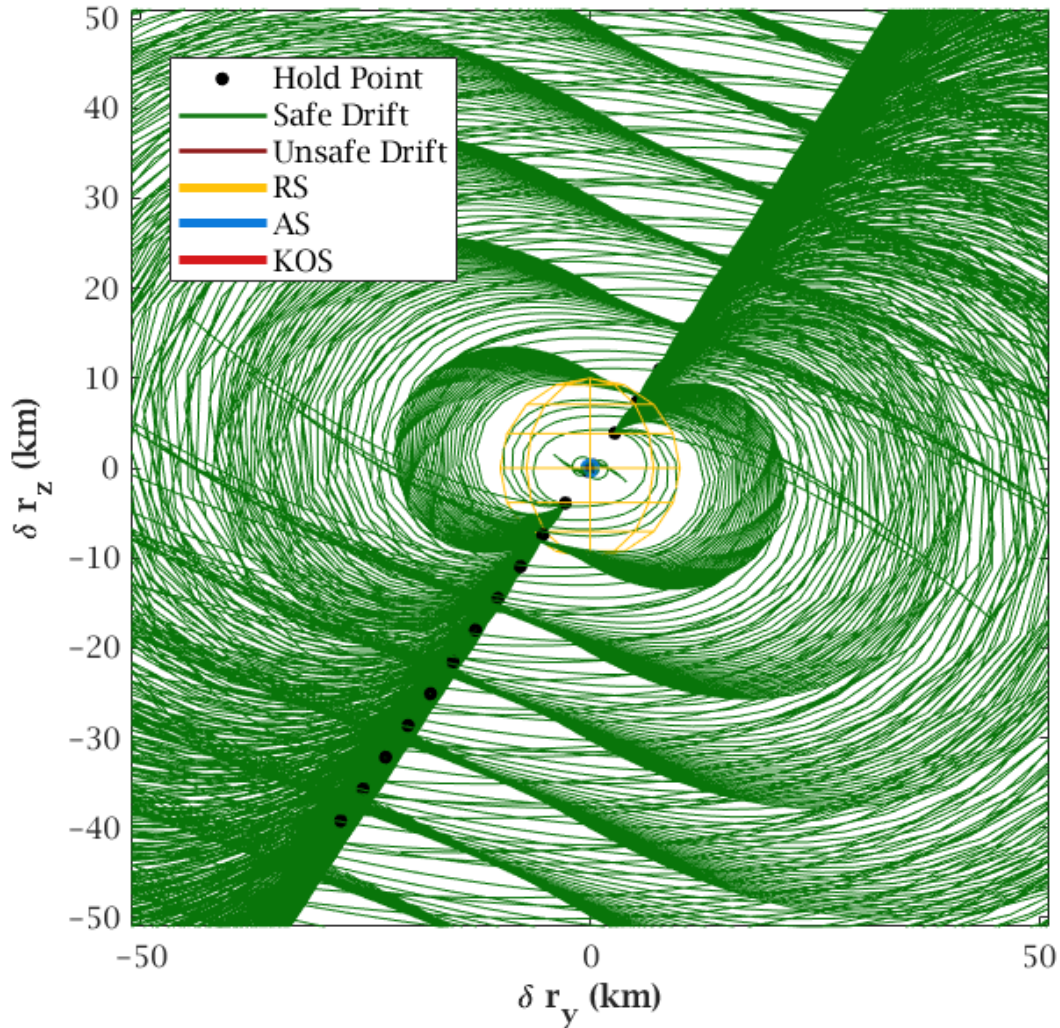


Figure 4.22: Region 6 Suboptimal Approach Axis Passive Drift Trajectories. Region Six’s passive safety trajectories are shown for the suboptimal axes. Each trajectory begins after a departure failure and is propagated for 24 hours or until deemed unsafe. Safe trajectories are shown in green, and unsafe trajectories are shown in dark red. The RS, AS, and KOS are shown in yellow, blue, and bright red, respectively. To show the behavior best, this plot is a 2D slice along the δr_y - δr_z plane. There is a nonzero δr_z component to each trajectory. This suboptimal axis improved the safety of the HPs compared to the optimal axis.

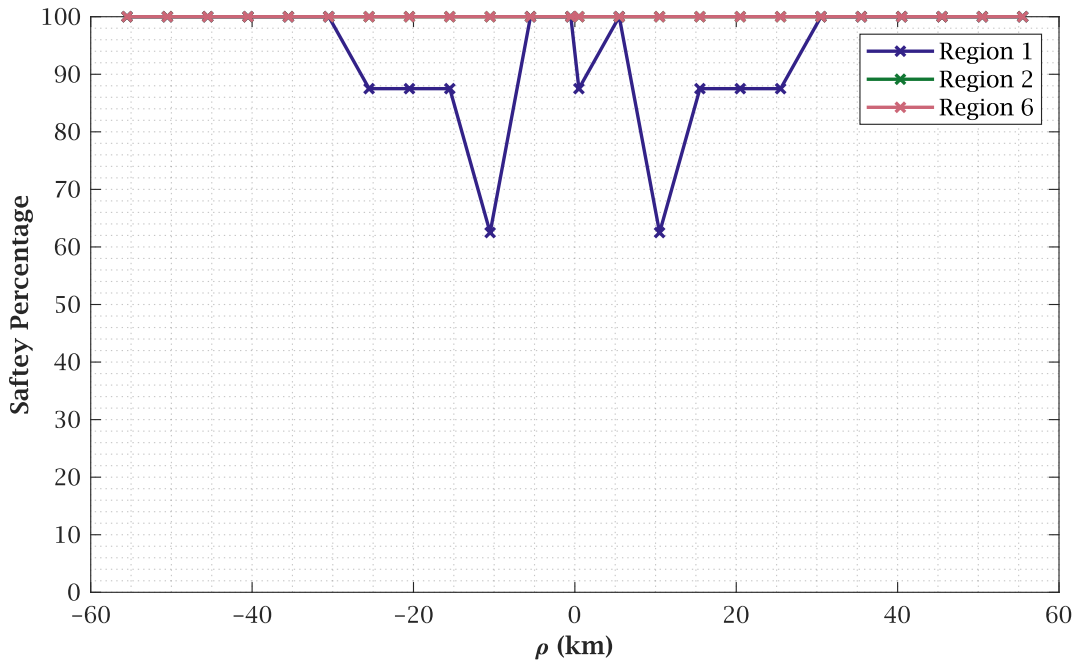


Figure 4.23: Suboptimal Approach Axis HP Passive Safety. The HP safety percentage for HPs on the identified suboptimal axes for Regions One, Two, and Six. Region Two and Six have 100% safety for all HPs. The safety percentage is the percent ratio of safe drifts to total drifts. These drifts simulate a departure failure and quantify the passive safety of each HP. HPs ranging from -50.5 km to 50.5 km in steps of 5 km were tested. Regions One, Two, and Six new axes were deemed safe and will be adopted for the overall rendezvous strategy.

± 50.5 km, ± 30.5 km, ± 5.5 km, and ± 0.5 km. These HPs will be called HP1, HP2, HP3, and HP4. HP2 was placed at ± 30.5 km because of Region One's safety percentage dip after this point. HP1 designates the rendezvous initiation point for the strategy. VV will be assumed to have transferred from either a cislunar or a low lunar orbit to position themselves at HP1 along a given axis. From HP1, the VV can follow the strategy developed in the following sections.

The analysis above has identified six axes based on station-keeping ΔV costs. Each axis was analyzed to quantify its passive safety in a departure failure occurring at various times within an axes' respective region. Three of the optimal axes were safe, while three were

unsafe. Suboptimal axes were identified for the unsafe regions, and these new axes were safe. Based on the safety percentage for HPs on all six axes, four distances were chosen for the four HPs for each axis.

4.2.3 Region-to-Region Transfers

These axes and HP placements serve as the foundation of the approach strategy. The first step in implementing the axes is to design transfers between them. While a nominal plan efficiently “walks” the VV incrementally closer to Gateway, there will be situations where the VV has to hold, and said hold may span multiple regions. As the ΔV maps for station-keeping showed, holding on a nonoptimal axis can increase fuel costs. To prevent this, the VV should transfer between axes when needed. This final portion of the axes identification process constructs these region-to-region transfers and analyzes their safety.

A transfer’s ΔV cost is heavily influenced by its duration. Designing short transfers requires the VV to accelerate and rapidly travel the required distance. Long transfers risk being negatively affected by uncooperative dynamics that the trajectory has to fight to reach its target. Later analysis in this work tackles this optimization problem for specific transfers. However, from an operations perspective, the region-to-region transfers should be of equal length with uniform placement at the beginning and end of each region. Doing so makes them a seamless part of the operations that can be easily anticipated while also preserving the structure of the regions.

The region-to-region transfers were set to be one hour long evenly divided between two regions, i.e., the transfer begins 30 minutes before the end of Region X and arrives at the HP of equal distance from the station in Region X+1 30 minutes after the start of Region X+1. 30 minute long transfers were considered but resulted in transfer ΔV s exceeding 100 m/s. An

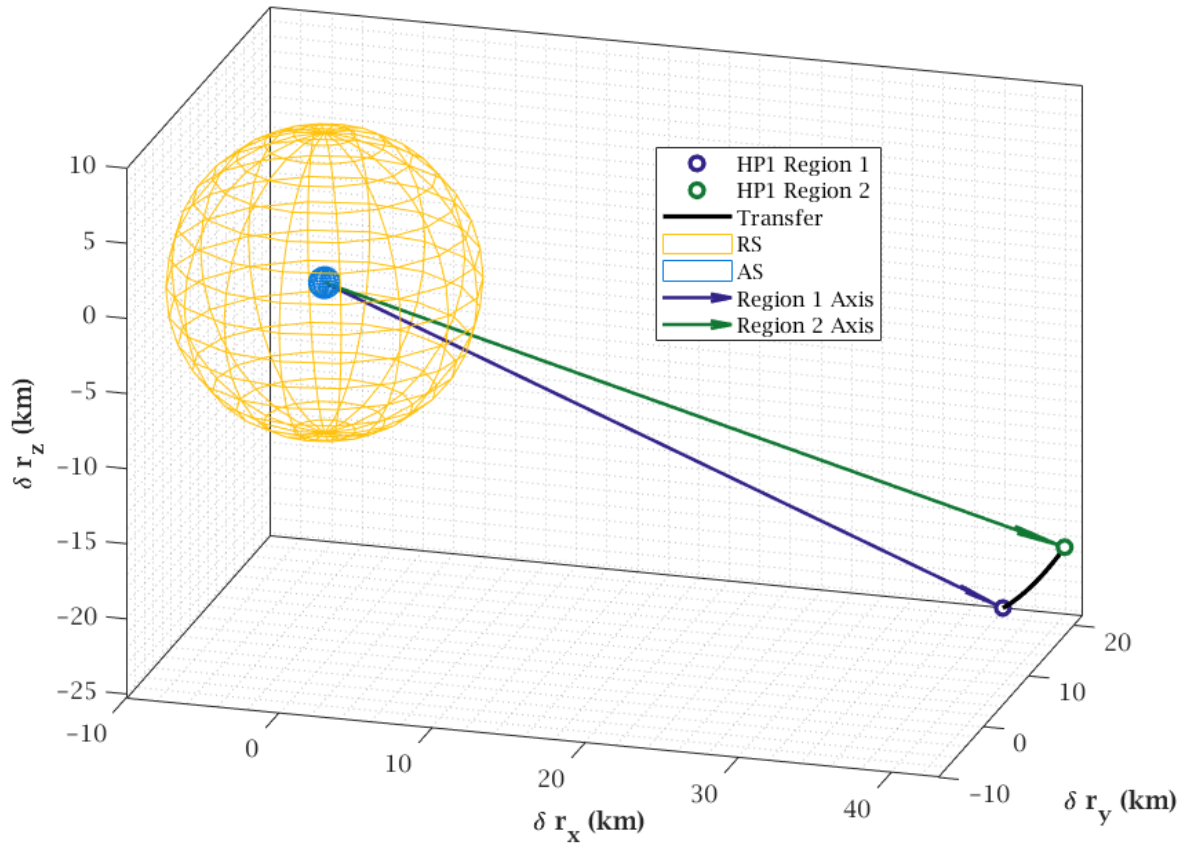


Figure 4.24: HP1 Region-to-Region Transfer Between Region 1 and Region 2. The transfer between HP1 on Region One's axis to HP1 along Region Two's axis is shown. The transfer allows the VV to hold along the optimal axis for each region when it is required to hold for extended durations. This transfer requires 5.40 m/s to execute.

example transfer is shown in Figure 4.24 with the transfer represented in the relative synodic frame. The transfer is between HP1 of Region One and HP1 of Region Two, which requires 5.40 m/s to perform. This transfer enables the VV to transition from holding optimally holding on Region One to optimally holding on Region Two.

All 24 region-to-region Transfers, six regions with four HPs per axis, are listed in Table 4.5 with their random misfire safety percentage and applicable must-complete burn range. The transfers have already been shown to be passively safe in the event of a departure failure

because their starting points are the HPs that have already been analyzed. Their arrival burn safety, as well as their random misfire and partial burn safety, is not. The arrival burn safety can be seen in the partial burn analysis below. The following analysis will determine the safety of these transfers if any failures occur.

Transfer Random Misfire Safety

As discussed in Section 3.4.2, a random misfire occurs when a ΔV is applied in a random direction at a random moment along the transfer. These simulations assume a constant ΔV magnitude of 0.05 m/s consistent with prior works' analysis [27]. This failure helps simulate potential random perturbations of the trajectory along with the unlikely event that a thruster randomly misfires. The failure is simulated with 1000 Monte Carlo simulations, where the events are placed randomly along the trajectory. At each event, a random unit vector is generated and multiplied by the ΔV magnitude and added to the current state's velocity components. That new state is then propagated out 24 hours and analyzed to see if it violates any safety criteria.

For example, the random misfire results for the same HP1 region-to-region between Region One and Region Two are shown in Figure 4.25. Here, 100% of the random misfires are safe. The misfires are vertically distributed along the y-axis, showing their random placement along the transfer. The dispersion of resulting trajectories remains consistent for all instances, with the misfire's placement and direction being largely ineffectual on the trajectory. The range would drift below the applicable safety threshold if an instance were unsafe.

All the misfire safety percentages are listed in Table 4.5. The Monte Carlo simulations are plotted in Appendix C. The lowest misfire safety percent for any region-to-region transfer was 95.4% for a transfer between HP4s from Region One to Region Two. Only three transfers

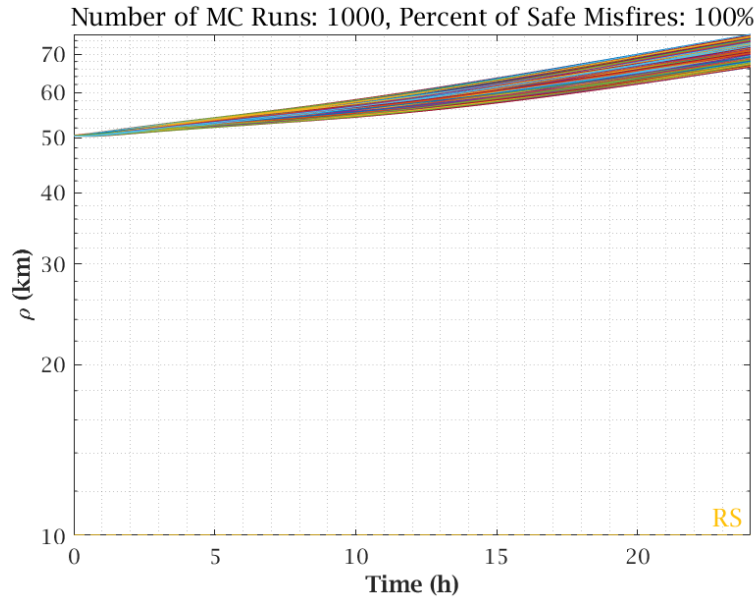


Figure 4.25: HP1 Region-to-Region Transfer Between Region 1 and Region 2 Random Misfire Monte Carlo Simulation. One thousand instances were simulated. This transfer was between HP1s, setting its safety threshold at 10 km. Any transfers that crossed this boundary would be considered unsafe.

had a safety percentage lower than 100%. With 95.4% being the lowest and only one of three nonperfect simulations, it provides strong confidence in the safety of these transfers should a random misfire occur.

Transfer Partial Burn Safety

A partial safety burn analysis is done to see what occurs if, during a burn, the main thruster shuts down, leaving only a fraction of the burn completed. This may result in an unsafe trajectory. As a result, the VV must attempt to correct this and complete the remaining percentage of the burn, which would result in a safe trajectory. A common approach is to designate a portion of the burn as “must complete”. For example, if completing 0-44% of the burn results in a safe drift but 45-75% of the burn results in an unsafe trajectory, the VV operator will deem that once 44% of the burn is complete, no matter what, the vehicle

Table 4.5: Region-to-Region Transfers. Each region-to-region transfer is listed with designations for the HP number the transfer is between, the initial and ending regions, the required ΔV , the random misfire safety percentage, and, when applicable, the percentage range where the VV should operate under a “must complete state”.

Region ₀	Region _f	HP#	ΔV (m/s)	Misfire Safety (%)	“Must Complete” Range (%-%)
1	2	1	5.40	100.0	—
1	2	2	3.26	100.0	—
1	2	3	0.58	100.0	—
1	2	4	0.05	95.5	—
2	3	1	15.08	100.0	—
2	3	2	9.11	100.0	—
2	3	3	1.64	100.0	—
2	3	4	0.15	100.0	—
3	4	1	6.76	100.0	—
3	4	2	4.09	100.0	—
3	4	3	0.74	100.0	—
3	4	4	0.07	96.4	—
4	5	1	6.76	100.0	—
4	5	2	4.08	100.0	—
4	5	3	0.74	100.0	—
4	5	4	0.07	96.4	—
5	6	1	25.02	100.0	—
5	6	2	15.11	100.0	—
5	6	3	2.72	100.0	—
5	6	4	0.25	100.0	—
6	1	1	28.79	100.0	—
6	1	2	17.39	100.0	10-30
6	1	3	3.14	100.0	—
6	1	4	0.29	100.0	10-40

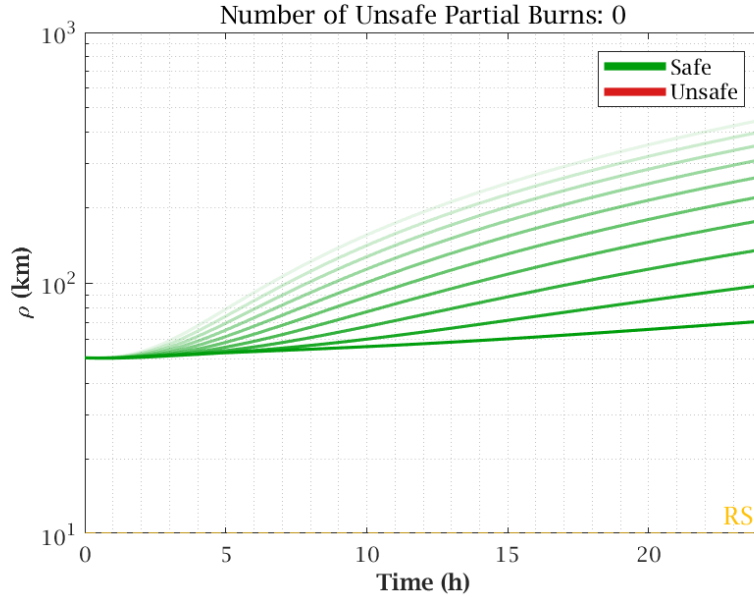


Figure 4.26: HP1 Region-to-Region Transfer Between Region 1 and Region 2 Random Partial Burn Safety. Partial burns ranging from 10% to 100% are shown. Each line represents a partial burn and is inversely transparent to the burn percentage.

must use all resources to complete the next 30% of the burn in the event the main thruster fails. Whether its attitude thrusters are used or a backup engine is used, the 30% must be completed to ensure at least 75% of the burn is complete to ensure the trajectory becomes safe.

For example, the partial burn safety analysis for the same HP1 Region One to Region Two transfer is shown in Figure 4.26. The completion percentages for burns from 10% to 100% are shown with the percentage represented by the transparency of the line. 100% completed burns have zero transparency, while a 10% partial burn is 90% transparent. If 0% of the burn is completed this results in a departure burn failure accounted for in the axis selection in Section 4.2. For this transfer, all partial burns resulted in safe drifts. These plots also show the arrival burn failure for each transfer. Looking at the 100% burn line shows the drift if an arrival burn failure were to occur. All the partial burn simulation plots can be found in Appendix D.

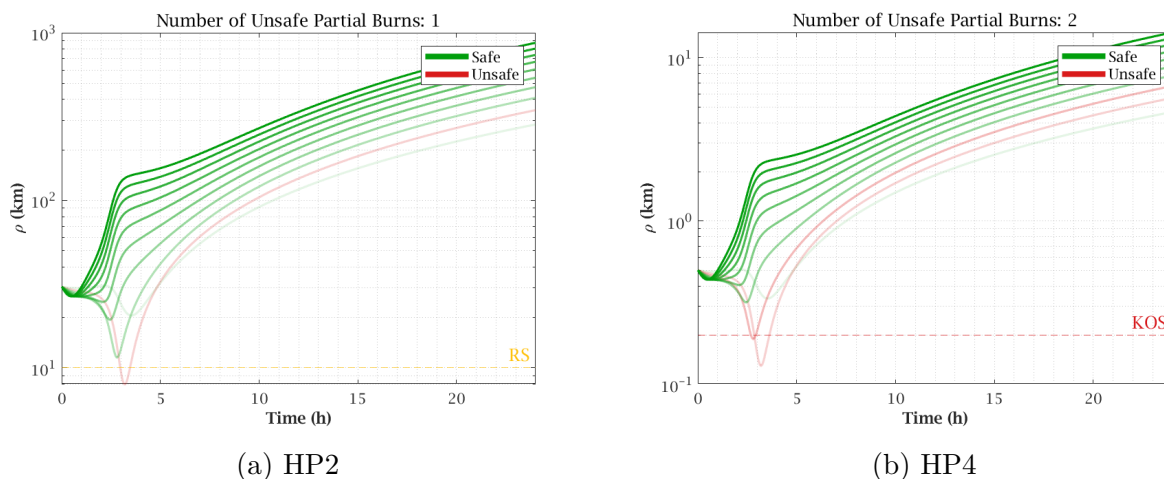


Figure 4.27: Region-to-Region Transfer for HP2 and HP4 Between Region 6 and Region One Partial Burn Safety. Both transfers require the VV to enter a “must complete” operating mode where, if the main thruster fails, the VV must use all available resources to ensure the necessary amount of burn is completed to ensure a safe drift. For HP2’s transfer, this is required to be between 10 and 30 percent, while for HP4’s, it is required to be between 10 and 40 percent.

Two of the 24 transfers have portions of their burn that require the VV to operate under a must-complete state. These transfers are for HP2 and HP4, between Region Six and Region One. The partial burn results for these transfers are shown in Figures 4.27a and 4.27b, respectively. From the simulations, taken at steps of 10%, HP2’s transfer is unsafe at 20% completion, and HP4’s is unsafe at 20% and 30% completion. As a result, once the VV completes 10% of the burn, it should enter the “must complete” until 30% of the burn is complete for the HP2 transfer and until 40% of the burn is complete for the HP4 transfer. Doing so ensures that a VV will bring its unsafe drift range above the safety region threshold into a safe drift.

This analysis concludes the HP and axes identification. Axes were selected and then adjusted to provide safe ΔV -optimal holding points within each region when required due to poor passive safety. Transfers were constructed between HPs along the axes of neighboring regions to enable the VV to jump from axis to axis in order to allow it to hold when a hold spans

multiple regions optimally. These transfers were analyzed for arrival burn, partial burn, and random misfires to ensure their safety in these situations.

4.3 Station-Keeping Strategy

Returning back to Region One's suboptimal station-keeping axis ΔV results, Region One had a best-case station-keeping cost of 7.76 m/s at 5.5 km away from the station. Expending this amount of ΔV is feasible for one phase of an RPOD mission. However, alternative approaches should be considered to identify avenues to reduce the required ΔV to hold through Periselene. Three methods for station-keeping were considered: traditional station-keeping, loitering, and on-orbit loitering. Traditional station-keeping was used to determine the optimal approach axes. Loitering in place of station-keeping is defined as performing a transfer with the VV departing the HP only to return the VV to the same HP after a desired TOF. on-orbit loitering is when the VV establishes itself onto Gateway's own NRHO, defined in the full nonlinear dynamics, a set phase lag behind or ahead of the VV.

Traditional station-keeping is studied in greater depth than before to serve as a baseline for comparing the alternatives. The two proposed alternatives were analyzed for passive safety and ΔV cost of executing these alternatives. The alternatives' costs were compared against the traditional approach for cases determined to be safe.

4.3.1 Traditional Station-Keeping

Each HP within each region is analyzed to determine the ΔV required to hold for a 15-minute duration. The results for HP one, two, three, and four are plotted in Figures [4.28a](#), [4.28b](#), [4.28c](#), [4.28d](#) respectively. These Figures show the accumulated station-keeping ΔV over the

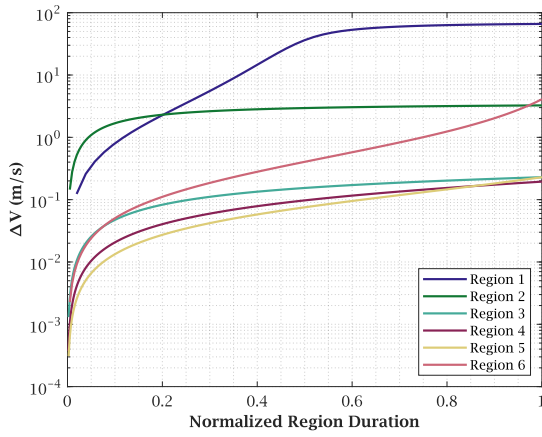
duration of each region. The region durations are normalized while ΔV is plotted on a log scale to compare the overall behavior and magnitudes of the regions across the four HPs. The behavior is identical for each region across HPs. However, ΔV required decreases as the HPs get closer to the Station. All regions except Region Six have most of their ΔV accumulated in the first half of the region, while Region Six is more evenly distributed across the region duration.

Station-keeping at HP4 within the KOS is below 1 m/s for all regions. However, Region One, Two, and Six exceed 10 m/s, with Region One reaching 66.08 m/s for its total duration at HP1. These regions are the intended targets for the station-keeping alternatives as they have the largest room for savings. Savings may be found in the other regions but may not be worth implementing due to increased operational complexity for marginal ΔV savings.

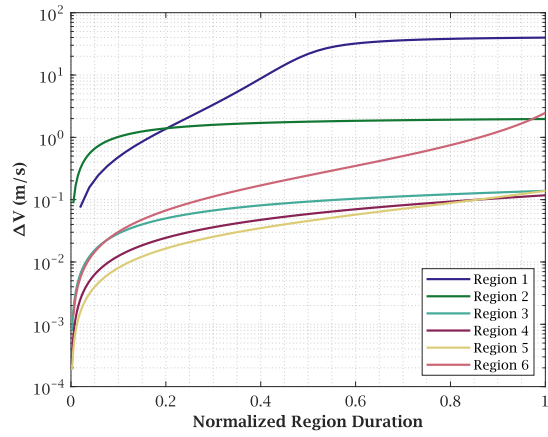
4.3.2 Station-Keeping Alternative: Loitering Trajectories

The first alternative considered is performing a loiter. A loiter trajectory begins at a HP. The VV performs a burn, placing it on a trajectory that returns to the same HP after a designed TOF. This alternative requires only two burns, compared to the multiple pulses needed while performing traditional station-keeping. In chaotic regions like near Periselene, the loiter trajectory can leverage the natural dynamics to bring the VV back to the HP, reducing burn costs. An example of a loiter can be seen in Figure 4.29.

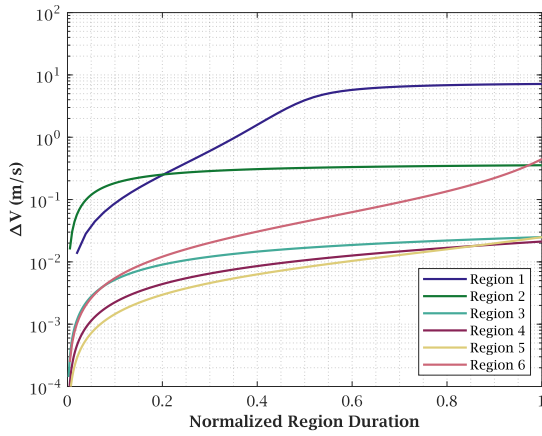
The single-shooting method discussed in Section 3.2.1 is used to generate candidate loiter trajectories. Each loiter's ΔV cost was the sum of its departure and arrival burn. Candidateloiters were discarded if the missing the arrival burn resulted in an unsafe trajectory. The passive safety criteria determined the arrival burn failures' safety. Loiters were generated at 30 min increments, all beginning at the start of a region. Loiters deemed viable and



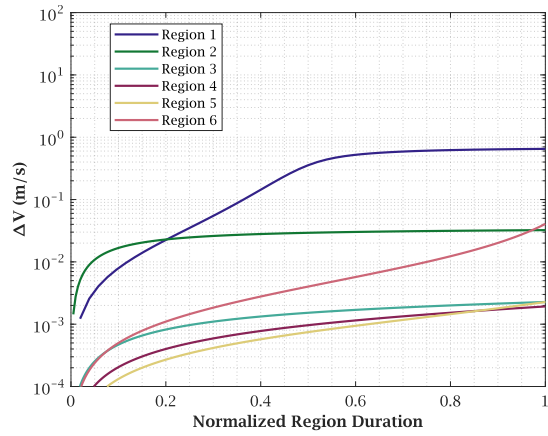
(a) HP1



(b) HP2



(c) HP3



(d) HP4

Figure 4.28: HP1, 2, 3, and 4 Accumulated Station-Keeping ΔV Cost Over Region Duration. Each region station-keeping cost v. fraction of region duration is shown. Cost behavior does not change based on HP distance, but ΔV magnitude does, decreasing as distance from station decreases.

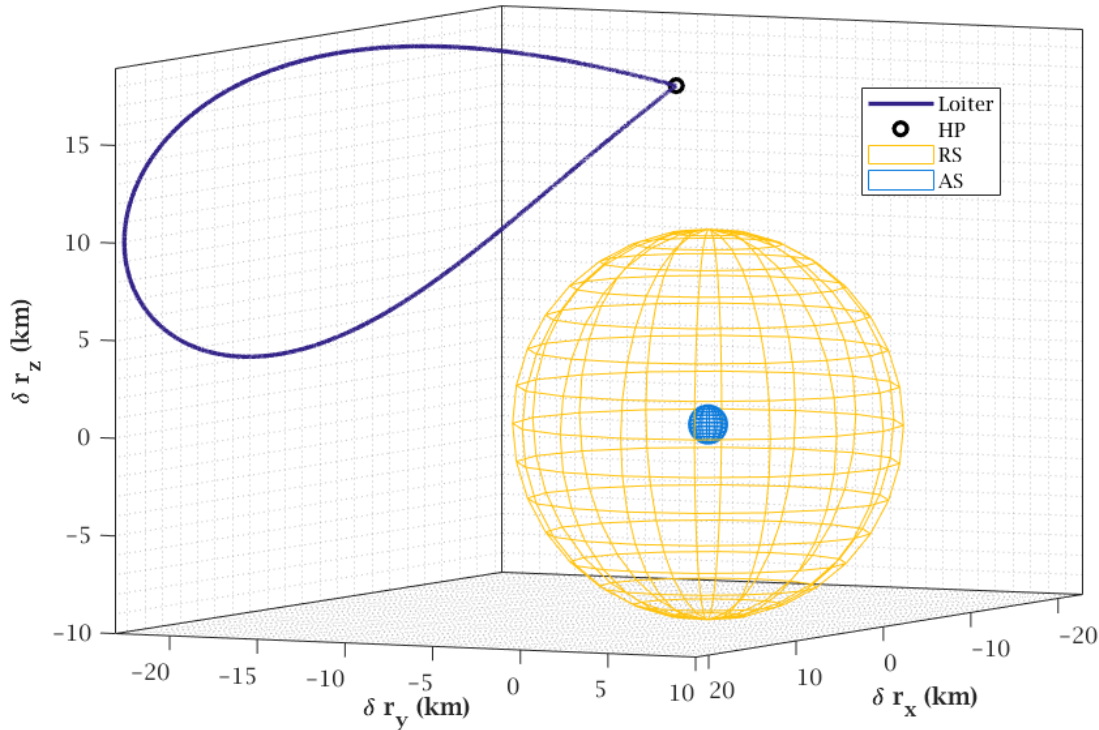


Figure 4.29: Loiter Visualization. An example of a Loiter is shown in the relative synodic frame. The VV begins at HP2 in Region One and performs a single burn to place itself on a four hour loiter trajectory. The VV performs a second burn to reestablish the synodic hold after the four hour duration.

worthwhile were adopted as alternative operators could use instead of traditional station-keeping.

Loiters are worthwhile if they provide significant enough ΔV savings to make departing the HP worthwhile. Entering a loiter removes the ability to approach the Station, so an extended loiter should only occur if the operator knows the VV will not be granted ATP in that time frame. If ATP may be granted soon, traditional station-keeping may be operationally preferred, even if a loiter may save ΔV .

The trade study between traditional station-keeping and loitering for Region One is shown in Figure 4.30. This heat map is partitioned into boxes representing the difference in ΔV

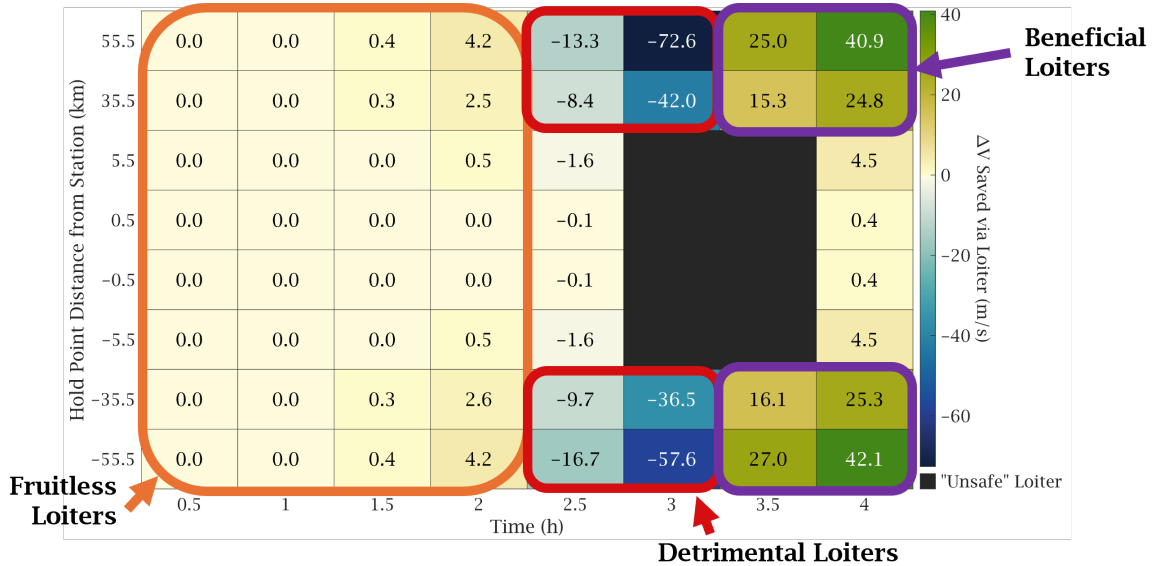


Figure 4.30: Region 1 Loiter v. Station-Keeping ΔV Benefit Analysis. Loiter trajectories were generated for the denoted durations for each HP. The ΔV required to perform the loiter was compared to the ΔV required to perform traditional station-keeping. Blue boxes show when traditional station-keeping is better, while green shows when performing a loiter is better. Off-white boxes show when the two approaches are equal. The longer loiters at the outer HPs are shown to be worthwhile alternatives to traditional station-keeping saving over 40 m/s of ΔV

required to execute a loiter versus station-keep at a specified distance for a specified time. The deeper shade of green a box is, the more favorable it is to execute a loiter. The deeper shade of blue a box is, the more favorable performing traditional station-keeping is. The more off-white boxes represent instances where performing either is near equal. The exact ΔV difference is inscribed in each box, with positive values being favorable towards loiters and negative being favorable towards traditional station-keeping. Black boxes represent loiters that were discarded due to poor safety.

Region One saw the largest number of worthwhile loiters. Specifically, loiters of 3.5 hours and four hours produced meaningful savings at HP1, HP2, and HP3. HP4's loiter savings were only 0.4 m/s, which is not significant enough to warrant a loiter. The outer HPs had significant savings with a full region loiter providing over 42.1 m/s in ΔV reduction. The

ΔV saved decreases to around 25 m/s if the loiter is reduced by 0.5 hours. Most loiters shorter than 2.5 hours are nonsignificant and have no bias toward either method, meaning traditional station-keeping is operationally favorable. The analysis showed that loiters of 3.5 hours should be avoided as they are costly compared to traditional station-keeping costing over 72.6 m/s of ΔV for HP1. From this analysis, loiters for HP1, HP2, and HP3 of 3.5 and four hours were identified as worthwhile loiters that should be implemented by operators when appropriate.

Analyzing loiters generated for the remaining five regions shows no other instances when a loiter is worthwhile or when a loiter should be strictly avoided. The most beneficial loiters for Regions Two and Six produce ΔV savings of 0.3 m/s and 0.7 m/s, respectively. The two methods are nearly equivalent in all other instances across these and the other regions. As such, traditional station-keeping should be employed for these instances. Each region's heat map and visualization of each HP's viable loiter trajectories are in Appendix B.

4.3.3 Station-Keeping Alternative: “On-Orbit” Loitering

The second alternative was reacquiring the NRHO at a desired phase lag from the Station. The VV transfers from its HP at the beginning of Region Six and, after an initial TOF, TOF_1 , reaches the point on the NRHO at the same relative distance away from the Station as the initial HP. At this point, the VV executes a burn to establish itself on the NRHO. The VV then freely drifts around the Station for the duration of Region One with guaranteed safety as the drift is along the NRHO. After surviving Region One, the VV executes a burn of TOF_2 to transfer itself to the same HP number within Region Two. After this transfer the VV executes a final burn to establish a hold. This method, called an on-orbit loiter, takes the VV out of the active approach for three regions and would only be implemented

for long-duration holds.

An example of a transfer to the NRHO insertion point and the proceeding on-orbit loiter can be seen in Figure 4.31. The Figure shows the relative motion in the relative synodic frame. The VV begins at HP1 in Region One and transfers to the on-orbit insertion point which is the same relative distance from the Station as HP1. The VV executes a burn at this point to establish itself on the NRHO. The VV then freely drifts, shown in purple, along the NRHO, remaining in the vicinity of the Station for the entire drift duration. After the drift, the VV transfers to the HP of the same distance located on the new region's axis. The method of holding on the NRHO was shown in Bucci's work discussed earlier in Chapter 2 [12]. These on-orbit loiters can be advantageous for holds that last multiple NRHO periods, allowing minimal ΔV expenditure over a multi-week long hold. However, due to the time-sensitive nature of the motivating scenario of this thesis, these extended holds are limited to a couple of orbit regions.

The two transfers pose a TOF optimization problem. The bounds for the first transfer are that the initial burn occurs just after the start of Region Six and that the NRHO is acquired before the start of Region One. The second transfer is the reverse. The first burn must occur after the end of Region One, and the next HP must be acquired at the end of Region Two. The ΔV of this process is given by the following equation:

$$\sum \Delta V = \Delta V_{\text{Burn 1}} + \Delta V_{\text{Burn 2}} + \Delta V_{\text{Burn 3}} + \Delta V_{\text{Burn 4}}.$$

The burns' ΔV are dependent on the time between burns. The optimization of the TOFs for the two transfers for an on-orbit loiter transferring the VV from HP1 of Region One, riding the NRHO, and transferring to HP1 of Region Two is shown in Figure 4.32. The figure shows the total ΔV required to perform this alternative for a given combination of TOFs.

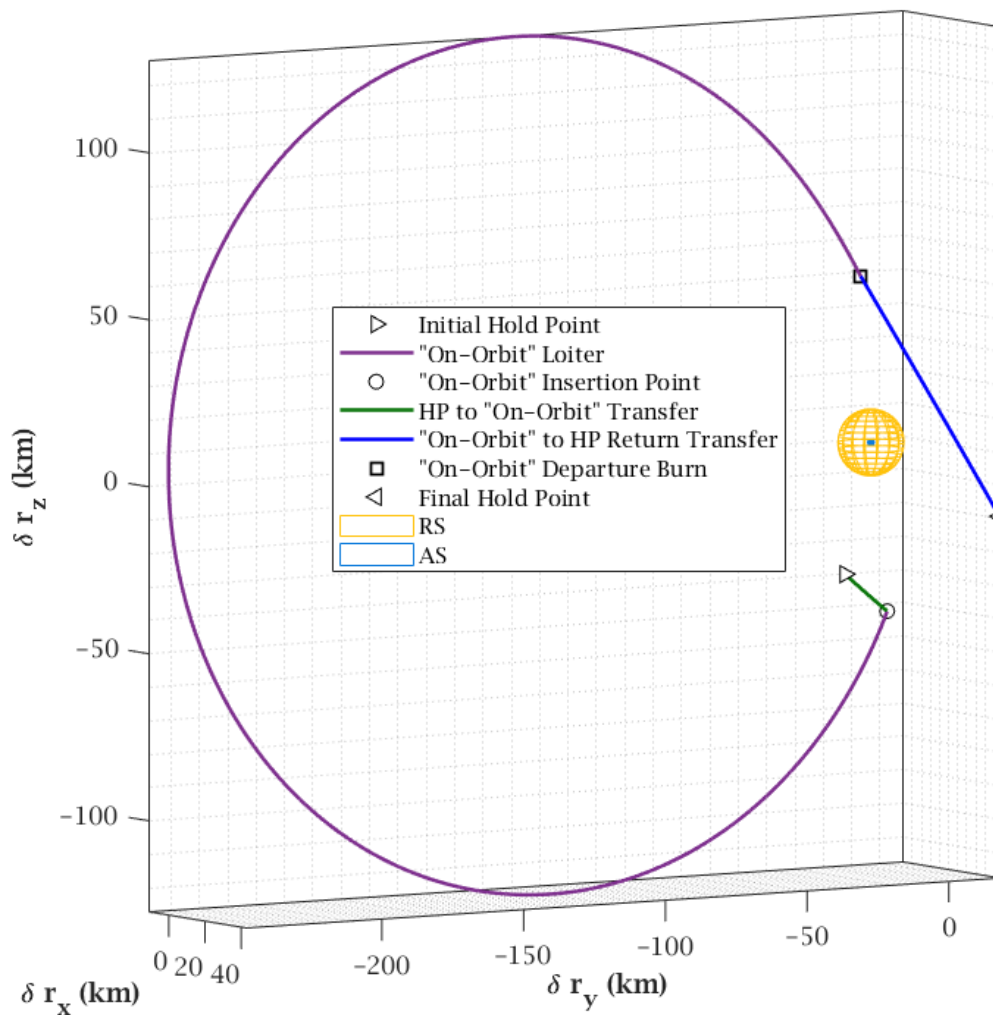


Figure 4.31: “On-Orbit” Hold Visualization. An example of an on-orbit Loiter is shown in the relative synodic frame. The VV begins at HP1 and transfers to the insertion point at the same relative distance from the Station. The VV burns to enter the NRHO phased behind the Station. The VV then freely drifts for a fixed desired duration along the NRHO, remaining in the vicinity of the Station. At the end of the drift, the VV transfers back to the HP of the same distance in the new region.

The white space in the contour plot shows combinations that required unsafe burns and the optimal combination is noted with the star marker. TOFs were tested in 0.5 hour increments from 0.5 to 16.5 hours. For all HPs, the optimal combination of TOFs was 16.5 hours TOF_2 with TOF_1 having some variance on the positive HPs. The contour plots for the remaining HP combinations are in Appendix E.

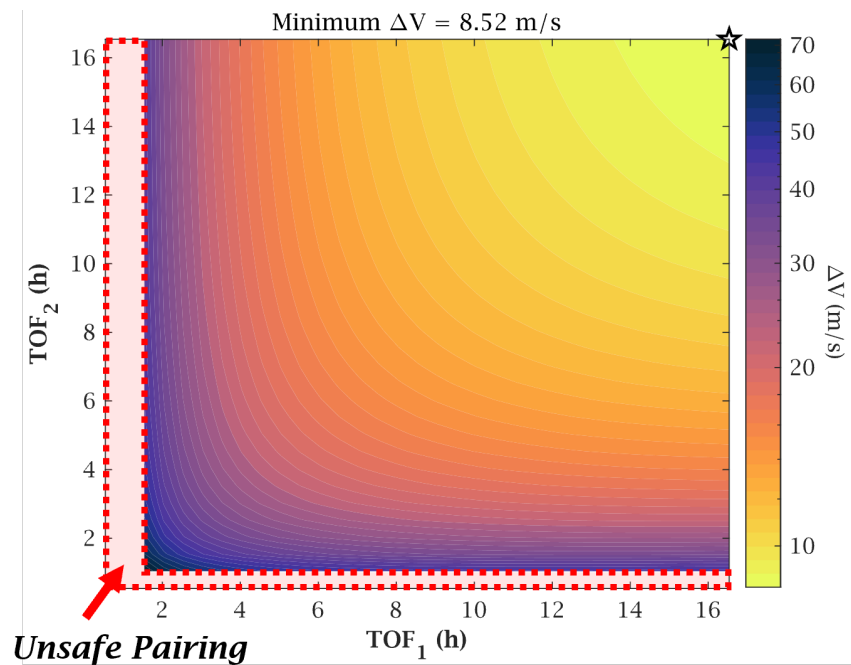


Figure 4.32: On Orbit Hold Transfer TOF Optimization. The contour plot shows the ΔV required to execute the on-orbit station-keeping alternative between Region Six HP1 and Region One HP1 utilizing the NRHO for different TOF combinations. TOF_1 represents the TOF for the first transfer starting in Region Six and ending at the NRHO insertion point. TOF_2 represents the TOF for the transfer from the NRHO exit point to Region Two HP1. The white space represents combinations that resulted in unsafe transfers and the optimum is noted with the star marker. This plan was for HPs on the negative approach axis.

Each on orbit loiter ΔV was compared against the required ΔV for traditional station-keeping and a loiter spanning the three regions. The traditional loiter can also be considered a phasing maneuver along the NRHO due to its long duration. The comparison of the three methods can be seen in Figure 4.33. The difference in magnitudes of the ΔV required for each HP can be seen. Traditional station-keeping is the worst option for holding from Region Six through

Region Two for an extended duration. The on-orbit loiter provides significant improvement but is not nearly as effective as performing a pure loiter.

On-Orbit loitering provides significant ΔV savings when compared to traditional station-keeping. However, traditional loiter provides even greater ΔV savings of 77.99 m/s, 47.45 m/s, and 8.60 m/s for loiters starting at HP1, HP2, and HP3 respectively. The on-orbit loiters are close to the traditional loiters but require twice the amount of burns to be performed, increasing operational complexity. For extended holds spanning the duration of Region Six through Region One, a traditional loiter, as described in Section 4.3.2, should be executed in order to minimize the required ΔV for each HP. Furthermore, as discussed previously, this loiter should only be performed if an operator knows ATP will not be granted during the loiter.

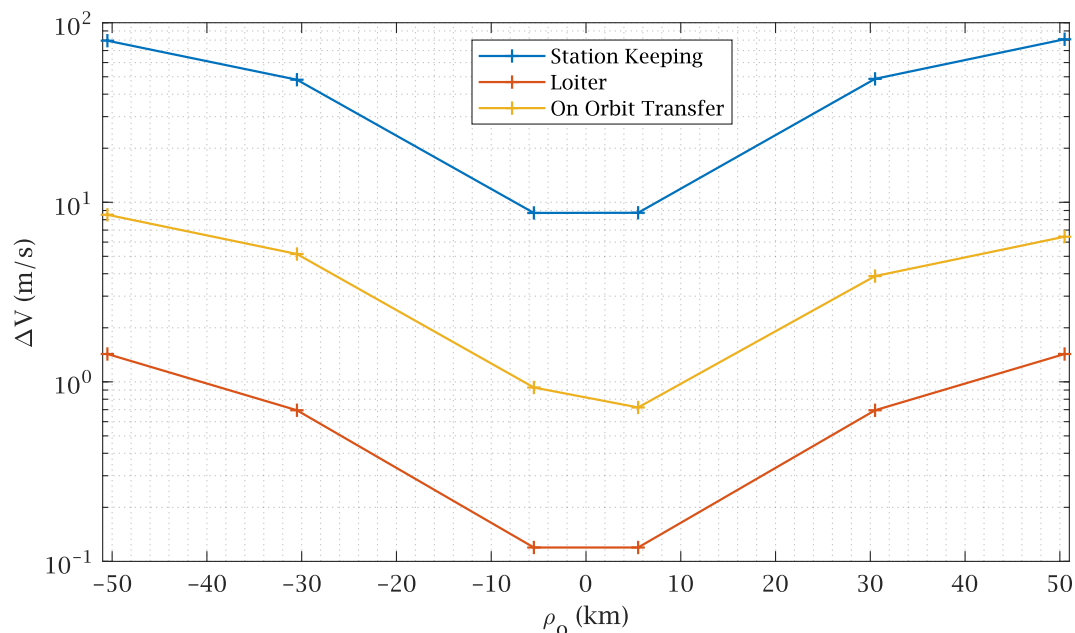


Figure 4.33: Station-Keeping Alternative Comparison for Holds from Region Six through Region 2. The required ΔV to perform an extended hold from the beginning of Region Six through the end of Region Two is compared between the three proposed alternatives. Traditional station-keeping is the worst option from a ΔV perspective, while a more traditional loiter is the best. On-Orbit loitering provides improved performance but requires more ΔV and requires more burns to be performed.

4.3.4 Optimal Station-Keeping Approach

The analysis of the alternatives to traditional station-keeping identified multiple instances where an alternative can be implemented to reduce the necessary ΔV to hold while a VV awaits ATP. Traditional station-keeping was a viable approach to holding but became costly when performed over extended periods. Loitering was a more efficient approach for extended durations, specifically within Region One and when holding from Region Six through Region Two. The instances when a loiter should be executed are listed in Table 4.6 with the amount of ΔV saved by performing the loiter over traditional station-keeping. To preserve operational flexibility, a VV operator may stick with traditional station-keeping for loiters with smaller ΔV savings. However, executing a loiter for loiters with significant ΔV savings is strongly advised.

For the safety of these alternatives, the misfire safety of these alternatives was all above 98%, with only the extended loiters being below 100%. All alternatives had zero unsafe partial burns. These metrics solidify their benefit as safe alternatives and save mission operators ΔV . All the misfire Monte Carlo simulations and partial burn plots can be found in Appendix C and Appendix D, respectively.

These alternative methods allow operators to preserve fuel when appropriate during their approach towards Gateway. Holds are not ideal for an approach from a time perspective, but they are common in current Station rendezvous operational practice. Traditional station-keeping remains the flavor of choice in the more stable regions of the orbit near Aposelene. However, these methods can be enacted when the VV enters the regions near Periselene. Doing so can decrease operational complexity for operators and preserve ΔV for their vehicles. With the holding strategy determined for the region across all four HPs, the approach strategy can be developed to walk the VV from the outer HPs inwards towards Gateway.

Table 4.6: Adopted Station-Keeping Alternatives. Instances when one of the alternatives to station-keeping should be performed to reduce ΔV required to hold. Alternatives are listed with when, represented by the initial mean anomaly, M, where represented by the HP the operator may be at, how long the alternative lasts, the ΔV saved from the hold, and the misfire safety of the alternative.

Alternative	M ($^{\circ}$)	Where	Duration (h)	ΔV Reduction (m/s)	Misfire Safety (%)
Loiter	175	HP1	3.5	25.0-27.0	100.0
Loiter	175	HP2	3.5	15.3-16.1	100.0
Loiter	175	HP1	4.0	40.9-42.1	100.0
Loiter	175	HP2	4.0	24.8-25.3	100.0
Loiter	175	HP3	4.0	4.5	100.0
Loiter	136	HP1	38.0	78.0	99.3
Loiter	136	HP2	38.0	47.5	99.8
Loiter	136	HP3	38.0	8.6	98.3

4.4 Rendezvous Approach Schemes

The next step in building up a comprehensive rendezvous strategy is the construction of transfers between HPs. The transfers walk the VV from the outer HPs, starting at HP1, to the edge of the RS at HP2, into the RS with HP3, and finally into the AS and just outside the KOS at HP4. This “walk” is illustrated in Figure 4.34. Starting at HP2, the VV operator must receive authority to proceed (ATP) from the station operator before entering the RS and again at HP3 before entering the AS. The transfers must abide by similar safety criteria tested during region Axis selection. However, as the VV will be granted ATP to enter the upcoming safety region, the criteria are slightly modified. The VV’s trajectory can cross into the approved safety region, but the prior safety criteria apply once the boundary is crossed. It cannot cross into the next safety region, and if it drifts back outside the region for which it was granted ATP, it can not reenter. Each transfer constructed for this approach must meet the criteria. This section aims to design approach schemes that perform and execute this “walk” safely.

Two approach schemes were considered based on the time-sensitive nature of the problem.

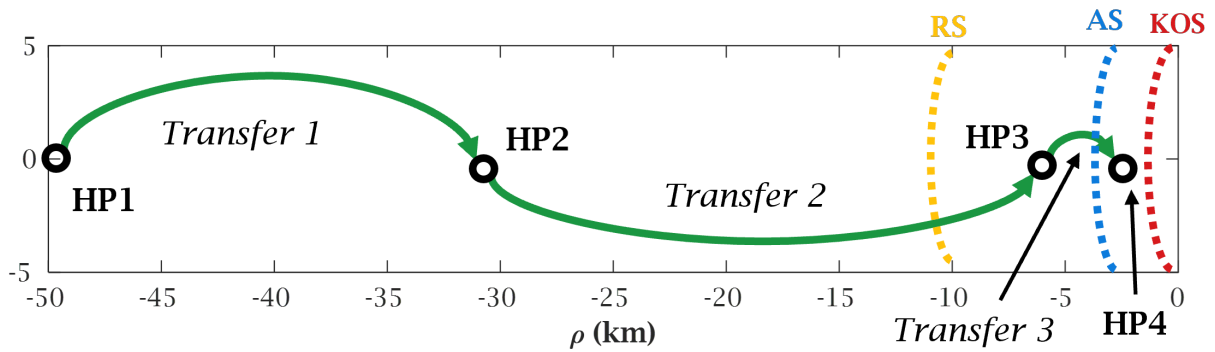


Figure 4.34: VV Rendezvous Approach Illustration. HPs are represented by black circles, transfers by green lines with arrows denoting direction, and the safety regions are shown by colored dashed arcs. The VV begins its approach at HP1 and performs its first transfer to HP2. After being granted ATP, the VV performs transfer two, bringing it inside the AS. Again, after being granted ATP, transfer three, bringing it inside the AS where it would then wait to begin its final approach into the KOS.

The two schemes vary in the timing of the transfers. The first scheme is referred to as the “all-in-one” approach. This scheme executes all three transfers with the duration of a single region. This scheme’s analysis focuses on optimizing the three transfers’ TOF. The second scheme is called the “One HP per Region” approach. This scheme is a more patient scheme where each transfer takes the duration of a region, i.e., if the VV begins in Region Four, transfer one is Region Four’s duration, and transfer two is Region Five’s duration, and so on. Each region’s duration fixes the TOF for these regions. This approach was taken to ensure consistent traceability at the expense of restricting the design space.

These two schemes encompass the most basic spacing of transfers while preserving operational symmetry. One could combinatorially optimize an approach scheme by placing two transfers in one region and the third in a different area. However, doing so would make the scheme more single-mission optimized, losing the comprehensive rendezvous strategy’s general applicability. These two schemes keep the approach organized and can be executed in a standard manner.

4.4.1 All-in-One Region Approach

The three transfers of the all-in-one approach are constrained by their duration. All three transfers must occur within the duration of a single region. Furthermore, time must be given to allow station operators time to grant ATP. To model this, 15 minute holds are placed before each transfer. This results in the TOFs being constrained by the following equation:

$$\text{TOF}_1 + \text{TOF}_2 + \text{TOF}_3 + 45 \text{ min} \leq T_{\text{Region}}$$

This equation was used for each region to generate a list of possible TOF combinations. Step sizes of 15 minutes for Region One and one hour for the other regions was used to increment each TOF combination set. For each combination, the ΔV required for each transfer was calculated along with the ΔV to station-keep for the 15 minute hold in between transfers. This calculation can be seen in the following equation:

$$\sum \Delta V = \Delta V_{\text{SK}1} + \Delta V_{\text{T}1,1} + \Delta V_{\text{T}1,2} + \Delta V_{\text{SK}2} + \Delta V_{\text{T}2,1} + \Delta V_{\text{T}2,2} + \Delta V_{\text{SK}3} + \Delta V_{\text{T}3,1} + \Delta V_{\text{T}3,2}$$

where $\Delta V_{\text{SK}i}$ is the ΔV to station-keep before transfer i . $\Delta V_{\text{T}i,j}$ is the ΔV of transfer i 's j^{th} burn. Recall that each transfer has a departure burn to depart the HP and an arrival burn to reestablish zero relative motion. The optimal transfer has the combination of TOFs that requires the lowest amount of ΔV to execute.

The results of this optimization for an all-in-one approach within Region One are shown in Figure 4.35. Each line spanning the width of the parallel axis plot represents a combination of TOFs that met the outlined constraints. Each line terminates at the ΔV axis, denoting that combination's ΔV . The optimal combination for this region was a TOF_1 of 75 minutes, a TOF_2 of 60 minutes, and a TOF_3 of 68 minutes. This combination had an associated ΔV

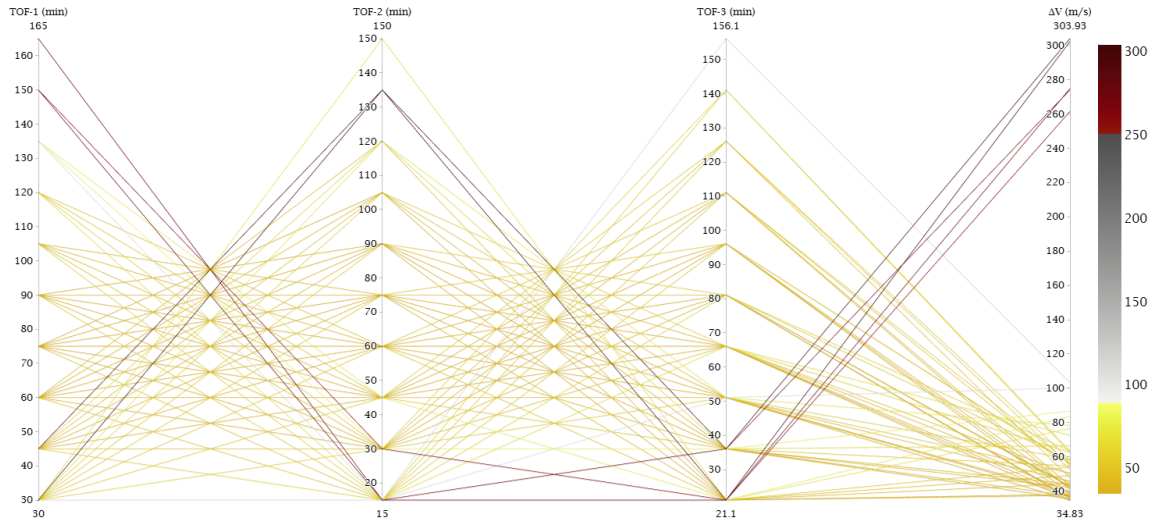


Figure 4.35: Region 1 “All-in-One” Approach Transfer TOF Optimization. This parallel axis plot shows the ΔV associated with a given pairing of transfer TOFs. The minimum ΔV combination for this region was 34.83 m/s. However, all transfers resulted in unsafe trajectories in the case of an arrival burn failure at one of the three transfers.

cost of 34.83 m/s to execute.

To confirm these candidates as a viable approach, their passive safety was simulated in the event of arrival burn failure. All candidates resulted in one or more of the three transfers becoming unsafe in the event of one of these failures. Because of this, none of these results can be considered for an approach strategy for Region One.

The same analysis was conducted in all five other regions. Like Region One, all candidate combinations of TOF resulted in one or more transfers becoming unsafe and unable to be considered for the final approach strategy. This result ruled out the all-in-one approach scheme as a possible safe strategy to rendezvous with Gateway in a time-sensitive manner.

Emergency Situation: Flight Rules Waived

On Boeing’s Starliner spacecraft’s first crewed mission on June 5th, 2024, the spacecraft came within one thruster failure of losing six degrees of freedom control during approach with the ISS [10]. The near emergency scenario caused NASA to waive standard approach flight rules to ensure the two astronauts would not be forced to abort and make it safely to the station [10]. A time-critical scenario that causes mission control to waive flight rules demands a time-critical approach, like the all-in-one scheme, regardless of the potential safety risk involved.

While a more patient approach must be considered to develop a safe approach scheme, the ΔV optimal all-in-one approach plans are shown as a “break glass in case of emergency” approach. Figures 4.36-4.41 visualize the six unsafe but most time-critical plans. Each approach plan is shown in three different perspectives: the trajectory in the synodic frame, a 2D projection on the V-Bar R-Bar plane in the LVLH frame, and a time history of the plan’s H-Bar component from the LVLH frame. The synodic frame provides an understanding of what portion of the orbit is being traversed throughout the approach. The LVLH V-Bar R-Bar projection gives the classical view of the rendezvous profile. The H-Bar time history shows the spacing of the burns along with the relative lateral movement over time of the VV with respect to the Station.

The symbols on the plot designate key events during the approach. The red triangles designate the location of the departure and arrival burns. Six are placed on each plot for all six burns. The 15-minute spacing between burns dwarfs in comparison to the full duration approach plans, so they appear onto each other in most cases. If the plot were in the relative synodic frame, these points would be exactly on top of each other, as the VV does not move during the hold. However, due to the rotation of the LVLH frame with respect to the synodic

frame, a synodic station-keeping process appears as a drift in the LVLH frame, causing the circles to be slightly misaligned.

The \triangle and ∇ symbols denote the approach plan's start and end, respectively. The safety regions are shown in color by dashed lines, while the black dashed line shows the reference NRHO. These figures aim to provide the reader with a complete picture of the VV behavior during each approach.

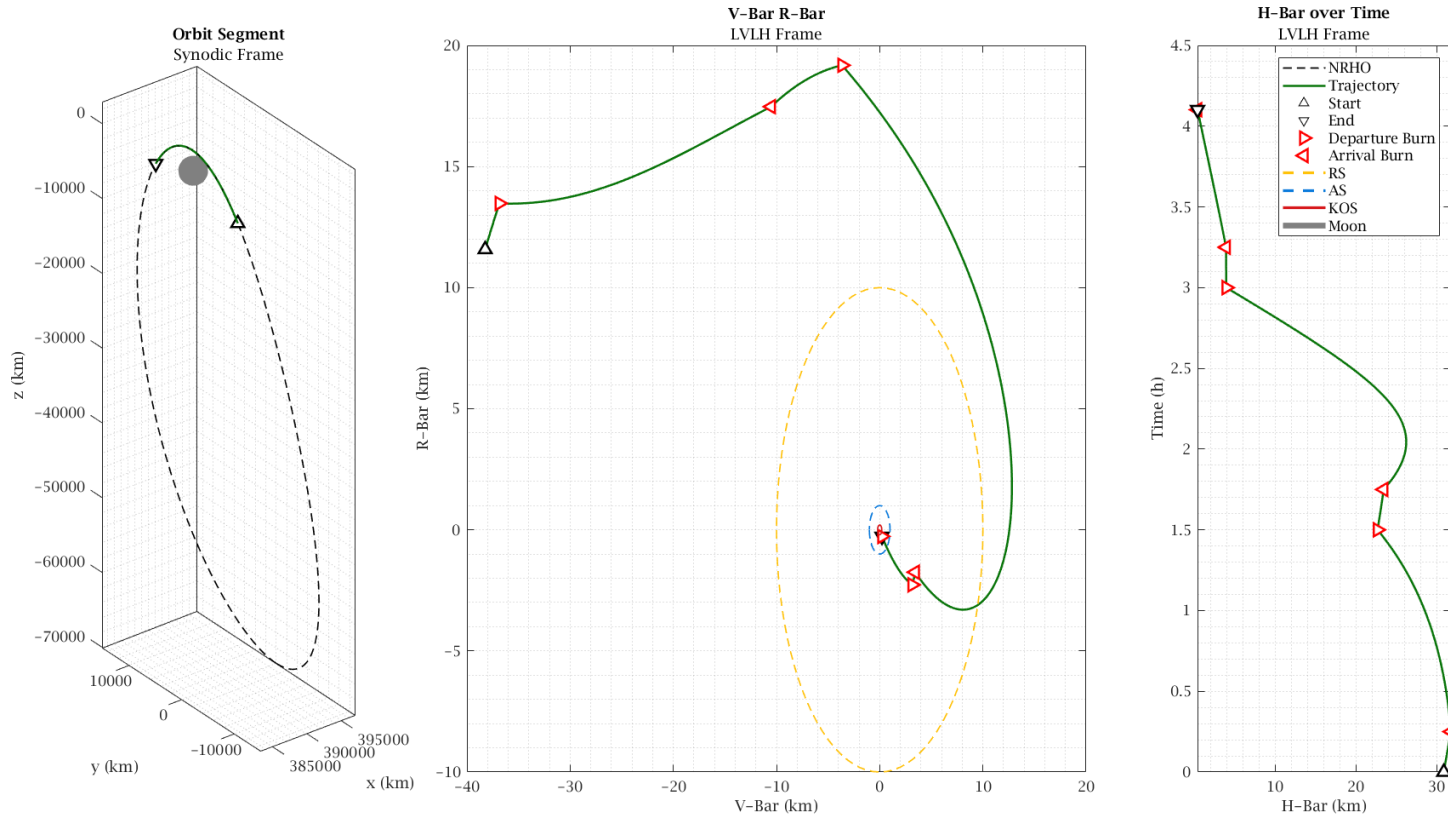


Figure 4.36: “All-in-one” Region 1 Approach Profile.. The approach plan is shown from three perspectives: a synodic view of the plan, a V-Bar R-Bar LVLH view, and an LVLH H-Bar view plotted against time for the plan duration. This plan requires 30.18 m/s to execute nominally.

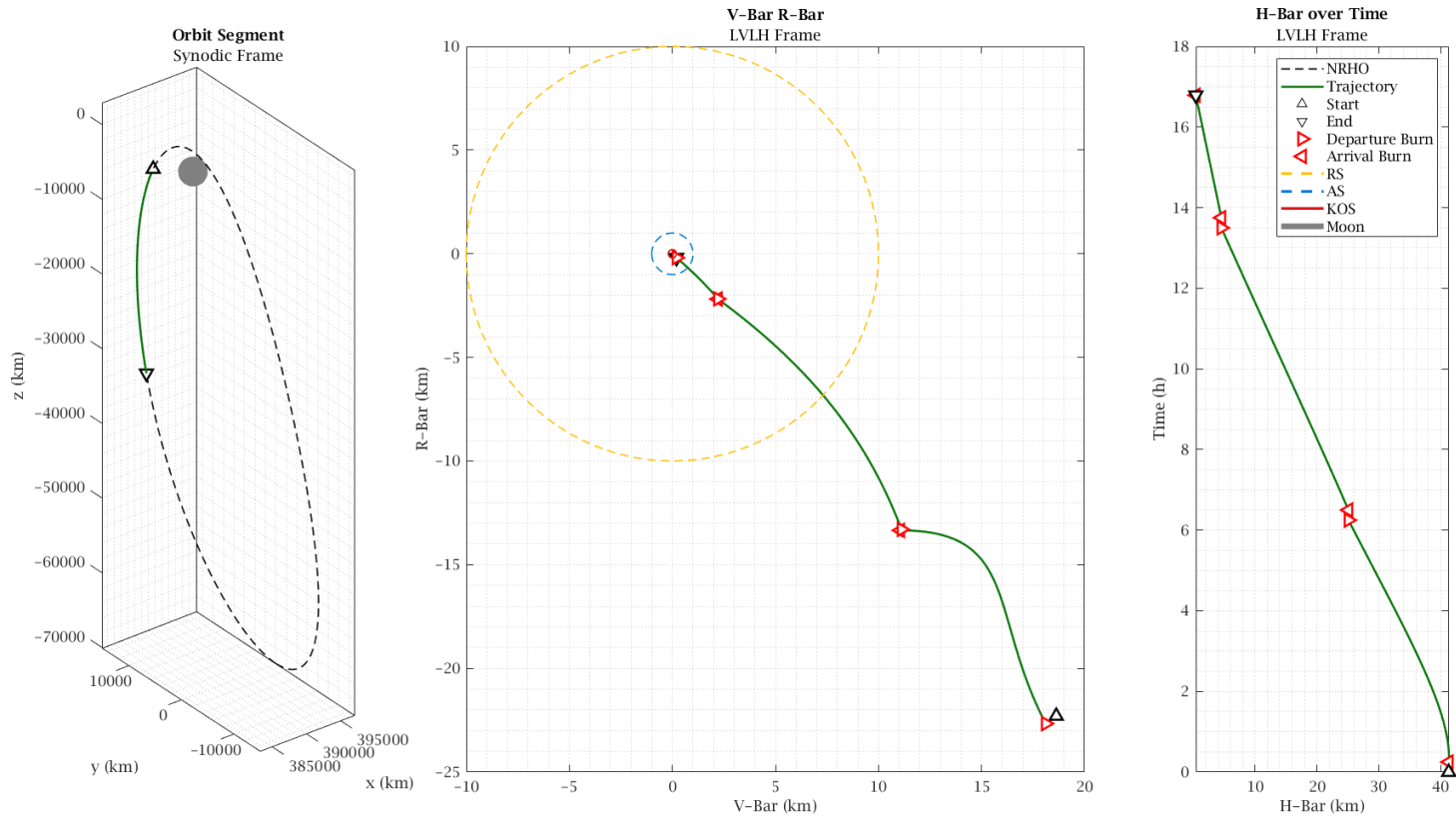


Figure 4.37: “All-in-one” Region 2 Approach Profile. The approach plan is shown from three perspectives: a synodic view of the plan, a V-Bar R-Bar LVLH view, and an LVLH H-Bar view plotted against time for the plan duration. This plan requires 7.69 m/s to execute nominally.

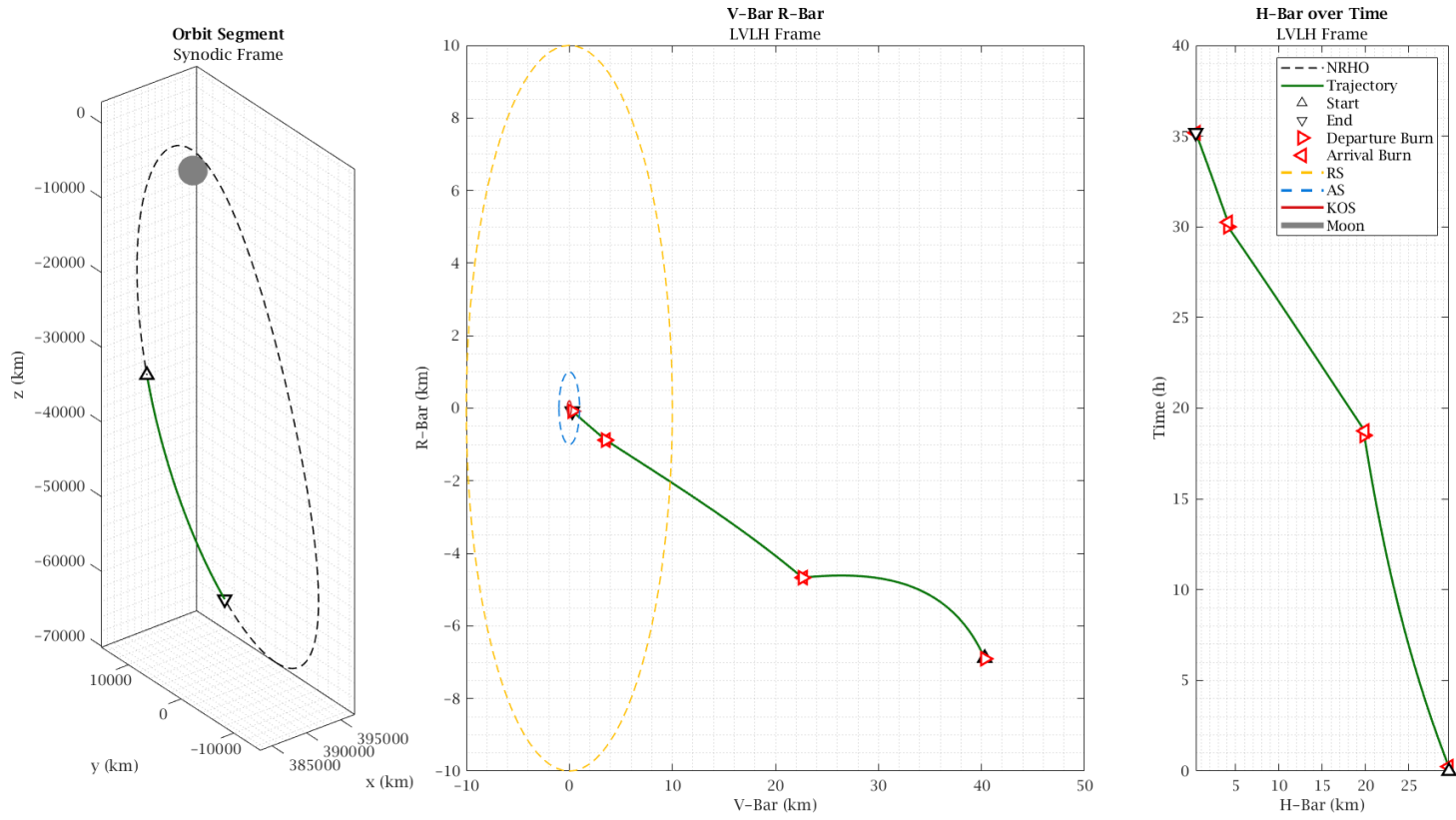


Figure 4.38: “All-in-one” Region 3 Approach Profile. The approach plan is shown from three perspectives: a synodic view of the plan, a V-Bar R-Bar LVLH view, and an LVLH H-Bar view plotted against time for the plan duration. This plan requires 2.17 m/s to execute nominally.

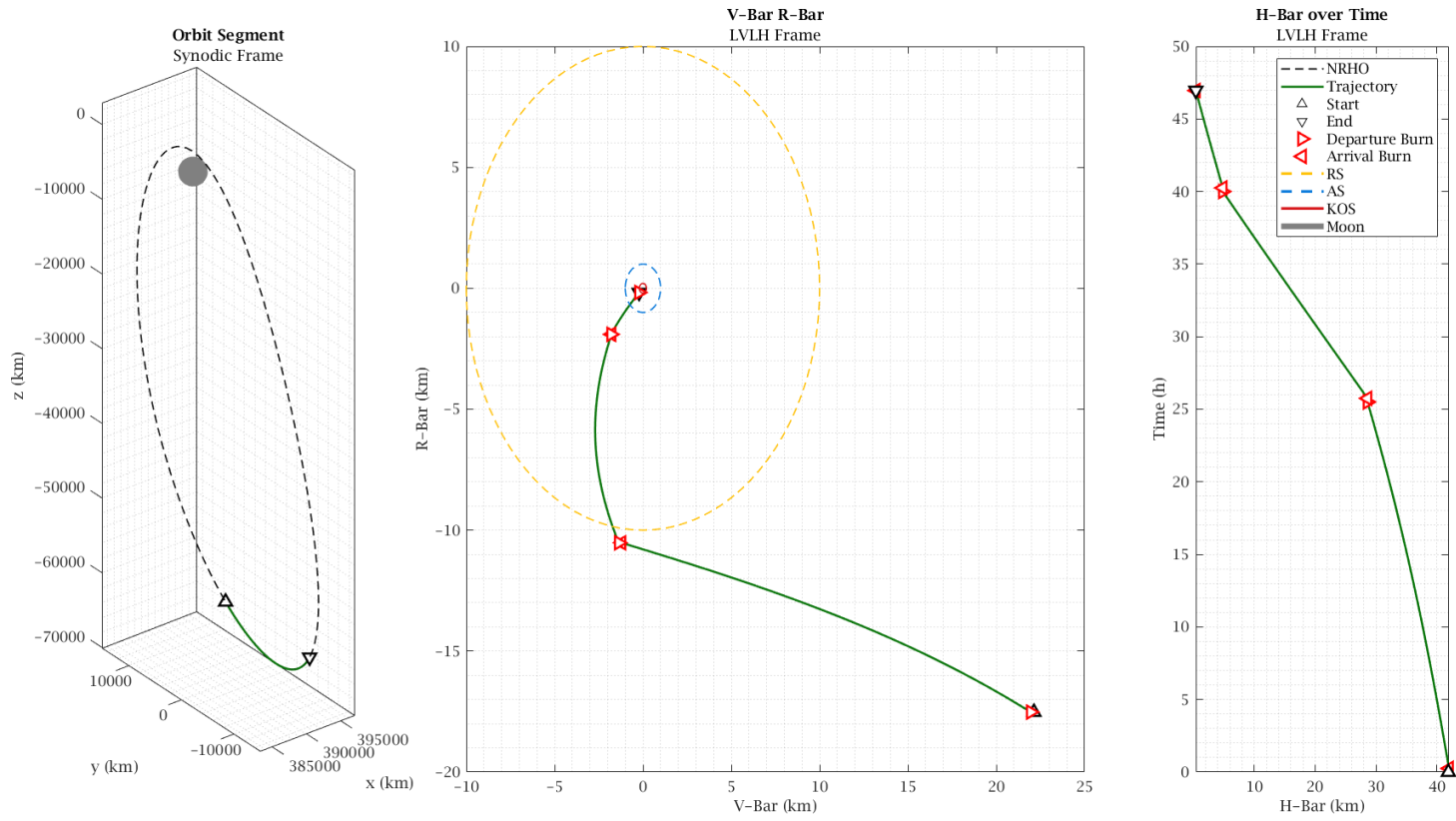


Figure 4.39: “All-in-one” Approach Profile Beginning in Region 4. The approach plan is shown from three perspectives: a synodic view of the plan, a V-Bar R-Bar LVLH view, and an LVLH H-Bar view plotted against time for the plan duration. This plan requires 1.70 m/s to execute nominally.

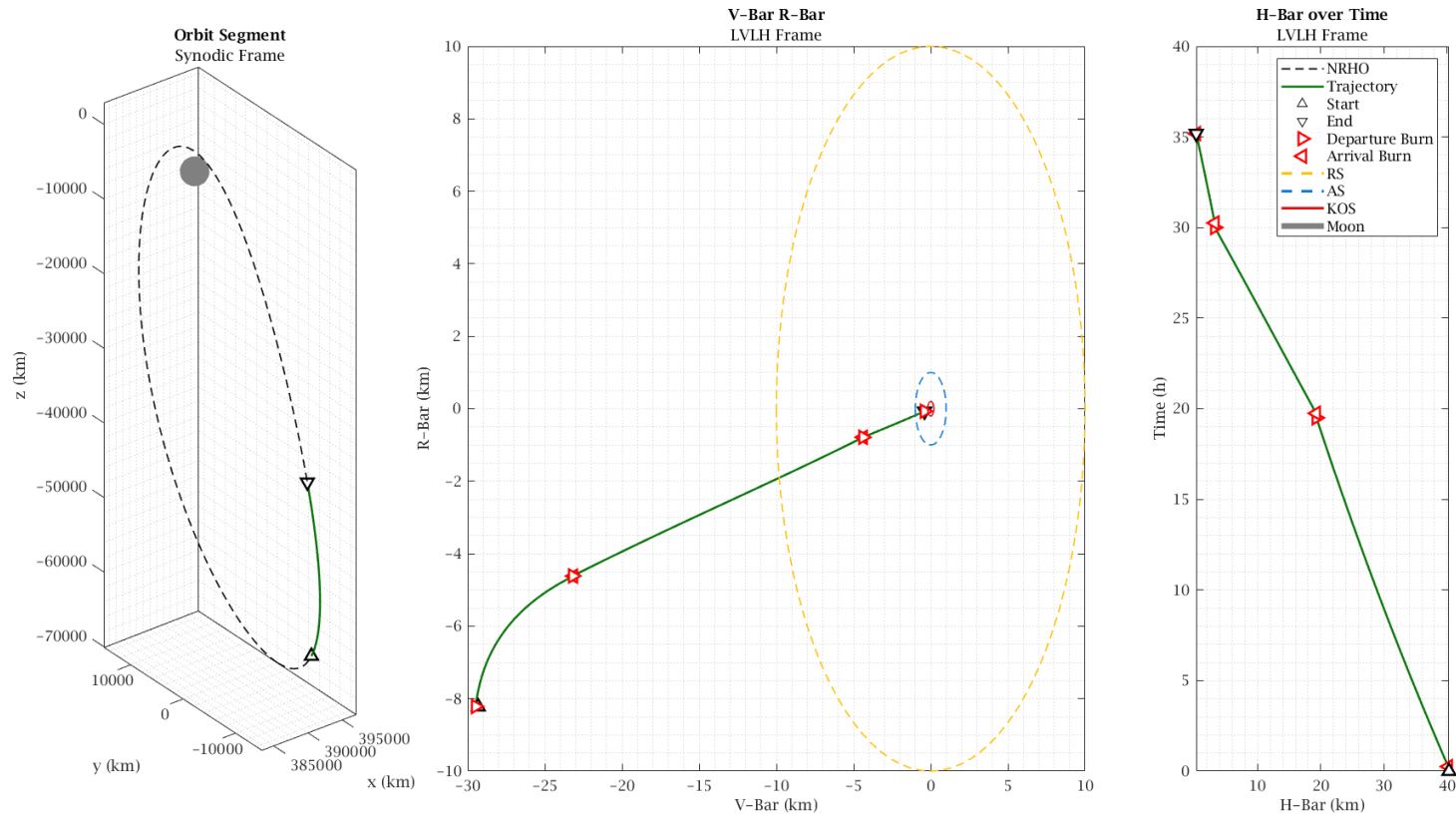


Figure 4.40: “All-in-one” Region 5 Approach Profile. The approach plan is shown from three perspectives: a synodic view of the plan, a V-Bar R-Bar LVLH view, and an LVLH H-Bar view plotted against time for the plan duration. This plan requires 2.21 m/s to execute nominally.

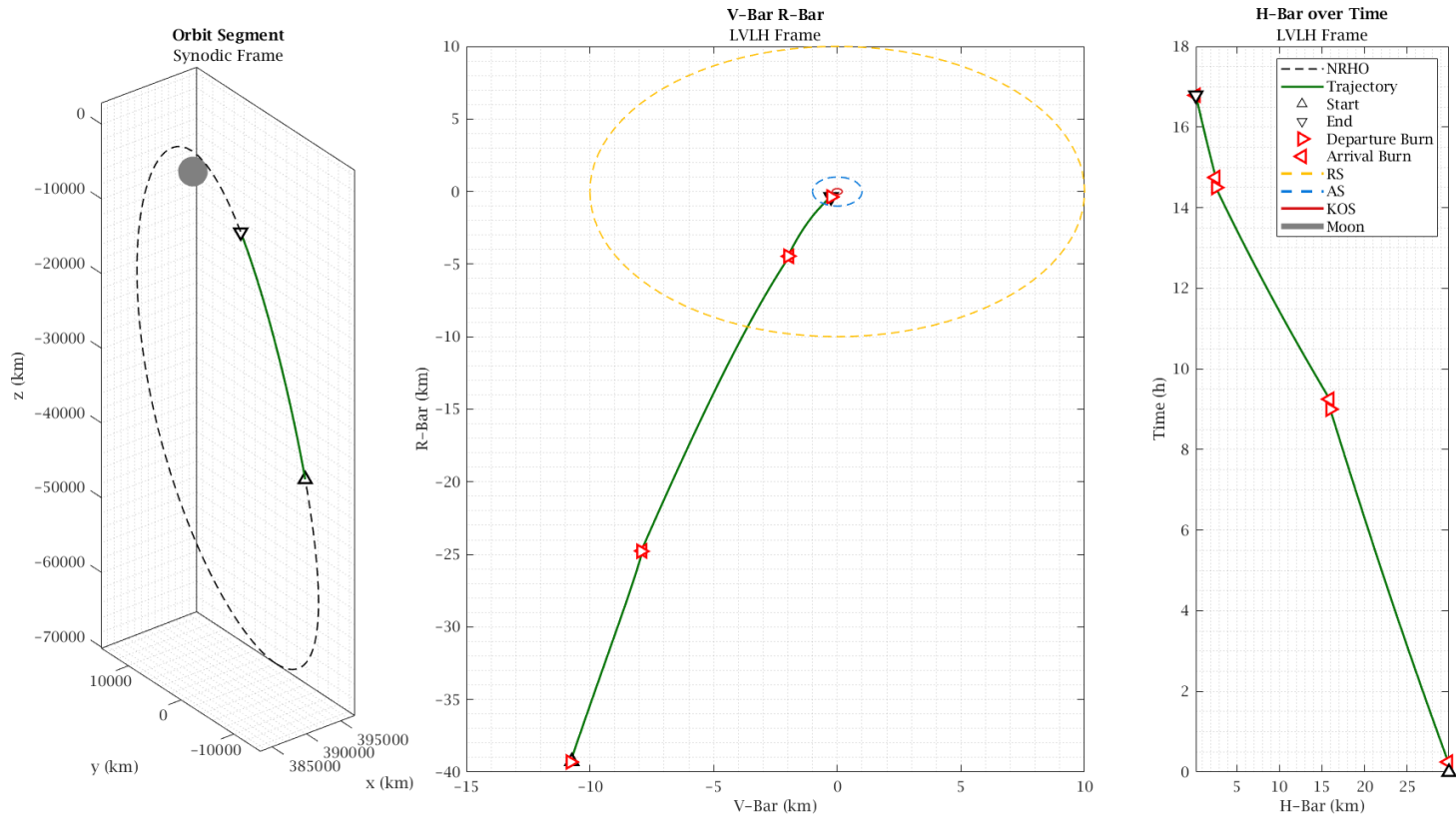


Figure 4.41: “All-in-one” Region 6 Approach Profile. The approach plan is shown from three perspectives: a synodic view of the plan, a V-Bar R-Bar LVLH view, and an LVLH H-Bar view plotted against time for the plan duration. This plan requires 4.75 m/s to execute nominally.

All transfers for these plans are listed in Table 4.7 with their corresponding TOF, initial Mean Anomaly (M_0), and required ΔV . Region One’s profile is the most fuel-demanding approach plan requiring 30.18 m/s of ΔV to execute all six burns. Region Two through Six’s plans require significantly less ΔV , with Region Two dropping to 7.69 m/s and all other regions requiring less than five m/s. These plans are not ΔV intensive, making them achievable by most vehicles. Due to their short TOFs, some burns are unlikely to be executed by low-thrust vehicles. However, they do not meet the passive safety requirements dictated by the IRSIS requirements. So, while the approaches are dynamically valid and enable a swift approach, they can only be used if the flight rules are discarded in extreme circumstances.

Table 4.7: “All-in-One” Approach Scheme Transfer. All 18 transfers that makeup the six unsafe approach plans for the all-in-one scheme are listed. The initial mean anomaly where the transfer begins is listed along with each transfer’s TOF and ΔV .

M_0 ($^\circ$)	HP ₀	TOF (h)	ΔV (m/s)
175.6	1	1.25	10.39
179.0	2	1.25	14.38
182.5	3	0.85	5.42
185.6	1	6.00	2.82
200.0	2	7.00	2.71
216.6	3	3.04	2.17
224.8	1	18.25	0.63
267.3	2	11.25	0.94
293.8	3	4.93	0.60
306.3	1	25.25	0.46
4.9	2	14.25	0.76
38.3	3	6.71	0.48
54.9	1	19.25	0.60
99.7	2	10.25	1.01
123.9	3	4.93	1.29
136.4	1	8.75	1.98
157.1	2	5.25	2.01
169.7	3	2.04	1.45

4.4.2 One Hold Point per Region Approach

The one HP per scheme offers a safer slower-paced approach. One transfer occurs within the duration of one region, which means the VV will hop between one HP per region. Each hop transfers the VV onto the next region's approach axis, allowing it to hold optimally if it is not granted ATP to execute the next transfer.

Similarly to the all-in-one scheme, the transfers will have a buffer between them. A 15 minute hold will be placed at the start and end of each region, bracketing the transfers. This scheme requires no TOF optimization like the all-in-one scheme, as each transfer is governed by the following equation fixing each transfer's duration:

$$\text{TOF}_i + 30 \text{ min} \leq T_{\text{Region},i}$$

There were 18 transfers generated as a result of this scheme: six starting regions with three transfers per approach. Unlike the all-in-one scheme, all 18 transfers were passively safe in the presence of arrival failures. All arrival burn failure analysis can be seen represented by the 100% burn completion trajectory range in the partial burn plots found in Appendix D. These plots are discussed further in Section 4.4.2.

The 18 transfers are tabulated in Table 4.8 where the initial region of the approach, the initial hold point, TOF, and ΔV for each transfer are listed. The transfers' ΔV is the sum of the departure and arrival burns. Also listed are the random misfire safety percentages determined from Monte Carlo simulations for each transfer, which will also be discussed later in Section 4.4.2.

These transfers enable the VV to hop from HP-to-HP. They also do not need to be executed in order. For example, the operator may begin in Region Five and execute the transfer

Table 4.8: “One HP per” Approach Scheme Transfers. All 18 transfers that makeup six nominal approach plans for the one HP per scheme are listed. The initial region where the nominal approach begins is listed along with each transfer’s initial HP. Each respective transfer is also listed with its TOF and required ΔV and random misfire safety percentage.

Region ₀	HP ₀	TOF (h)	ΔV (m/s)	Misfire Safety (%)
1	1	3.85	21.70	96.8
1	2	16.54	12.07	91.3
1	3	34.93	11.60	98.7
2	1	16.54	2.84	100.0
2	2	34.93	2.47	98.7
2	3	46.71	2.28	98.5
3	1	34.93	0.39	100.0
3	2	46.71	0.32	99.2
3	3	34.93	0.23	98.8
4	1	46.71	0.30	100.0
4	2	34.93	0.43	100.0
4	3	16.54	0.29	96.6
5	1	34.93	0.70	100.0
5	2	16.54	0.76	100.0
5	3	3.85	0.96	98.9
6	1	16.54	1.98	100.0
6	2	3.85	5.00	100.0
6	3	16.54	1.15	95.9

according to plan. However, after arriving at HP2 and entering Region One, the operator is told that their vehicle must be held for Region One. The operator can then employ the loiter prescribed in Section 4.3 to wait out the region optimally. After the hold, they are granted ATP to HP3 and perform the HP2 to HP3 burn that is a part of the one HP per plan that nominally begins in Region One.

The following visualizes each approach plan in Franzini and Innocenti’s LVLH frame. The transfers are then scrutinized under the two additional failure modes of interest outlined in Section 3.4.2: random misfire safety and partial burn safety. Only nominal and notable instances of either are shown in this section. To see all of the plots for the random misfire Monte Carlo simulations and the partial burns simulations, see Appendix C and Appendix

D, respectively.

Approach Plans

All six nominal approach plans are visualized in Figures 4.42-4.47. The figures are structured similarly to the all-in-one approach plan figures. Each approach plan had viable ΔV requirements. The approach beginning in Region One had the most expensive plan requiring 46.09 m/s of ΔV to execute fully. The remaining regions have significantly reduced ΔV requirements of 8.00 m/s, 0.94 m/s, 1.02 m/s, 2.47 m/s, and 8.36 m/s for Regions Two, Three, Four, Five, and Six respectively. These requirements should be achievable by most vehicles designed to make it to Gateway via finite burns. In Chapter 5, continuous thrust vehicles are touched on.

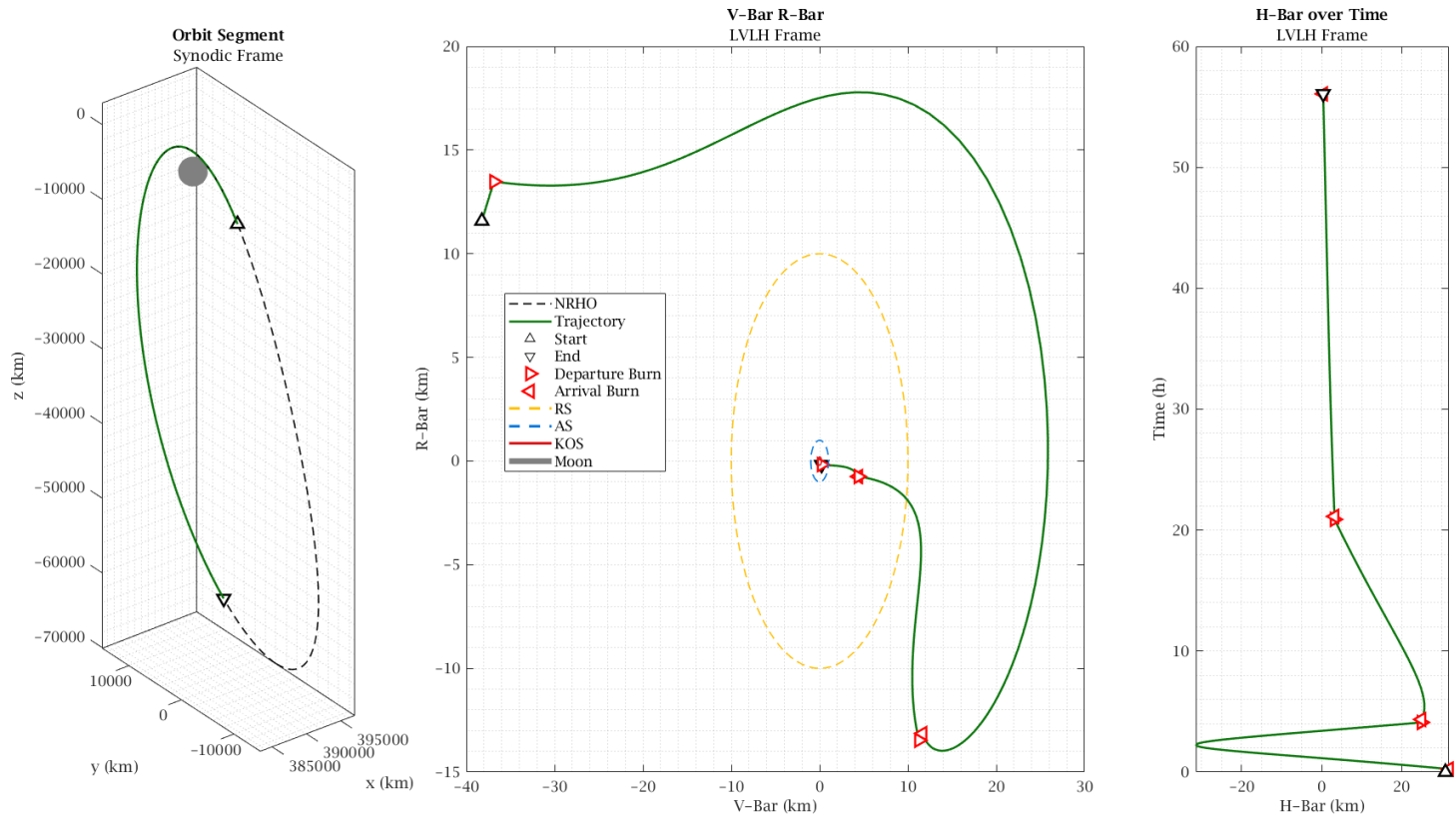


Figure 4.42: “One HP per” Approach Profile Beginning in Region 1. The approach plan is shown from three perspectives: a synodic view of the plan, a V-Bar R-Bar LVLH view, and an LVLH H-Bar view plotted against time for the plan duration. This plan requires 46.09 m/s to execute nominally.

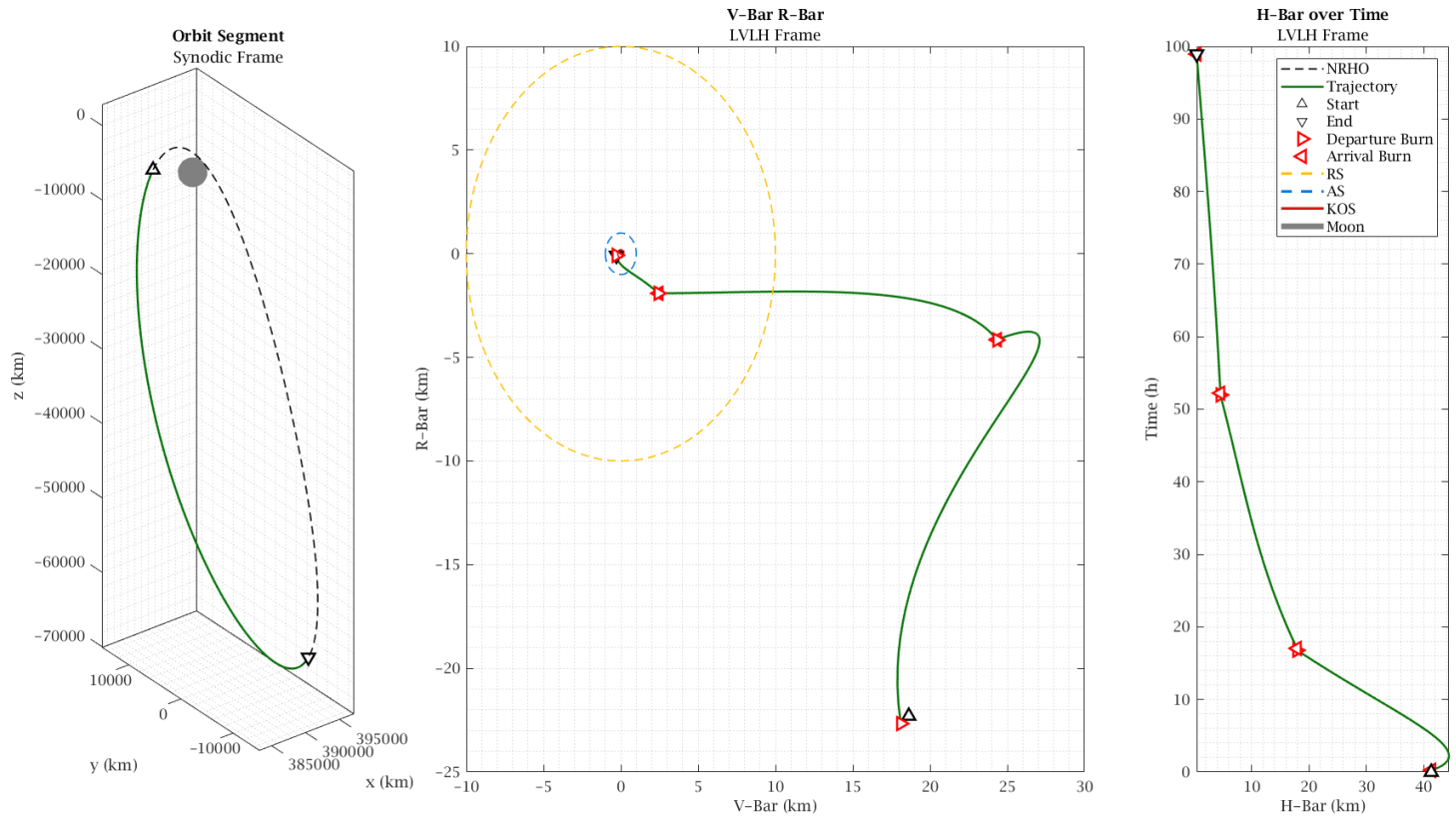


Figure 4.43: “One HP per” Approach Profile Beginning in Region 2. The approach plan is shown from three perspectives: a synodic view of the plan, a V-Bar R-Bar LVLH view, and an LVLH H-Bar view plotted against time for the plan duration. This plan requires 8.00 m/s to execute nominally.

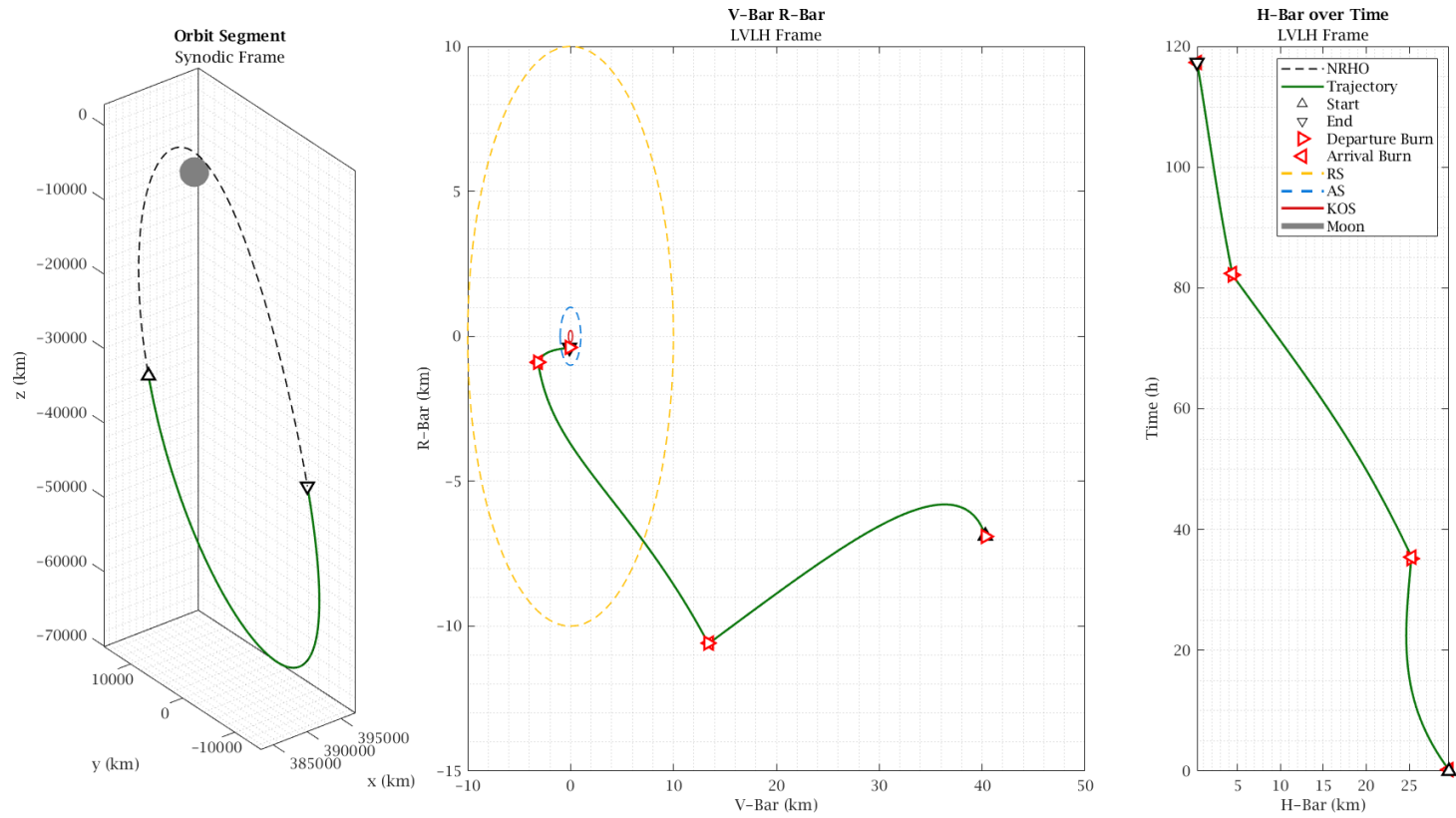


Figure 4.44: “One HP per” Approach Profile Beginning in Region 3. The approach plan is shown from three perspectives: a synodic view of the plan, a V-Bar R-Bar LVLH view, and an LVLH H-Bar view plotted against time for the plan duration. This plan requires 0.94 m/s to execute nominally.

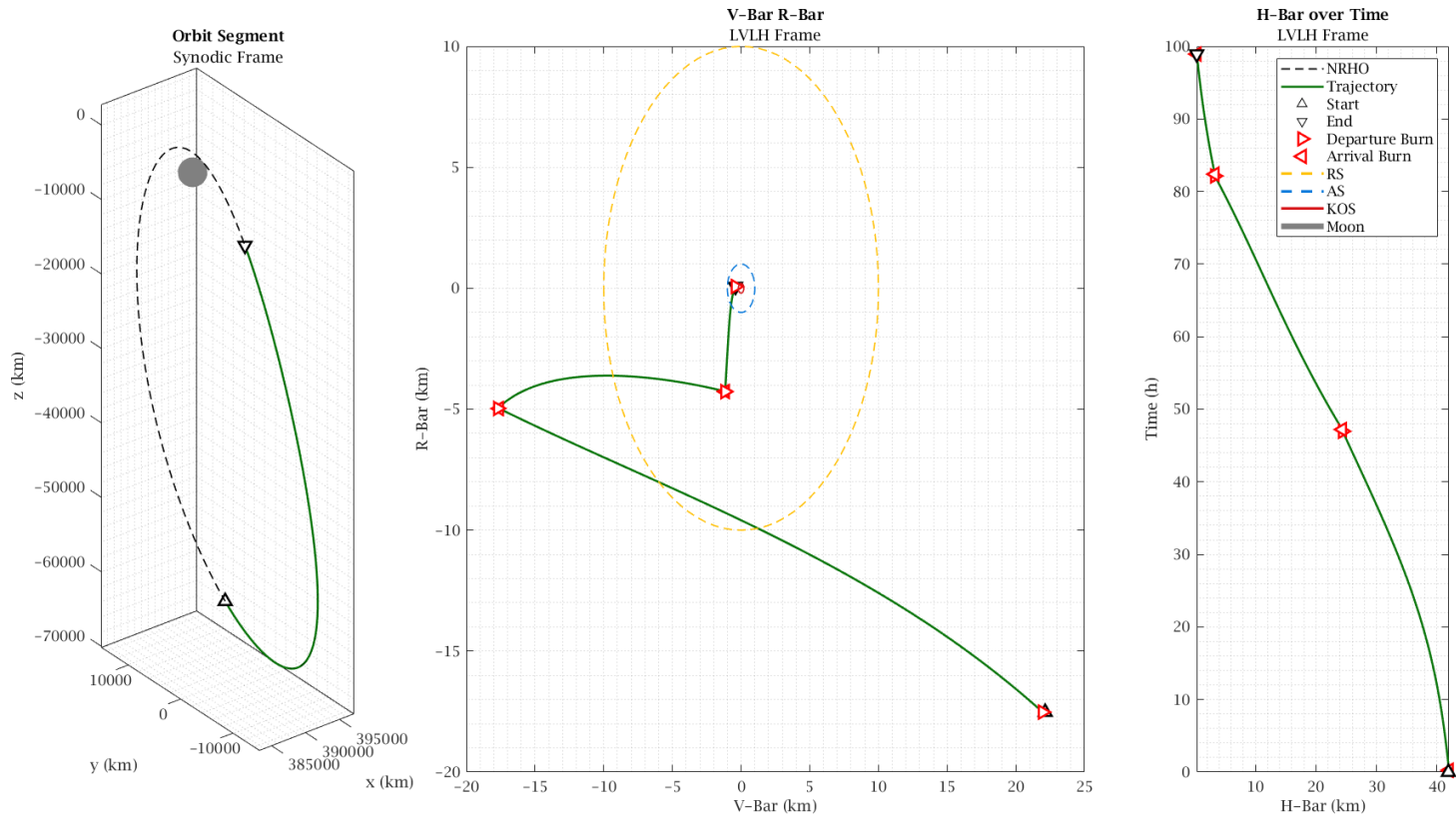


Figure 4.45: “One HP per” Approach Profile Beginning in Region 4. The approach plan is shown from three perspectives: a synodic view of the plan, a V-Bar R-Bar LVLH view, and an LVLH H-Bar view plotted against time for the plan duration. This plan requires 1.02 m/s to execute nominally.

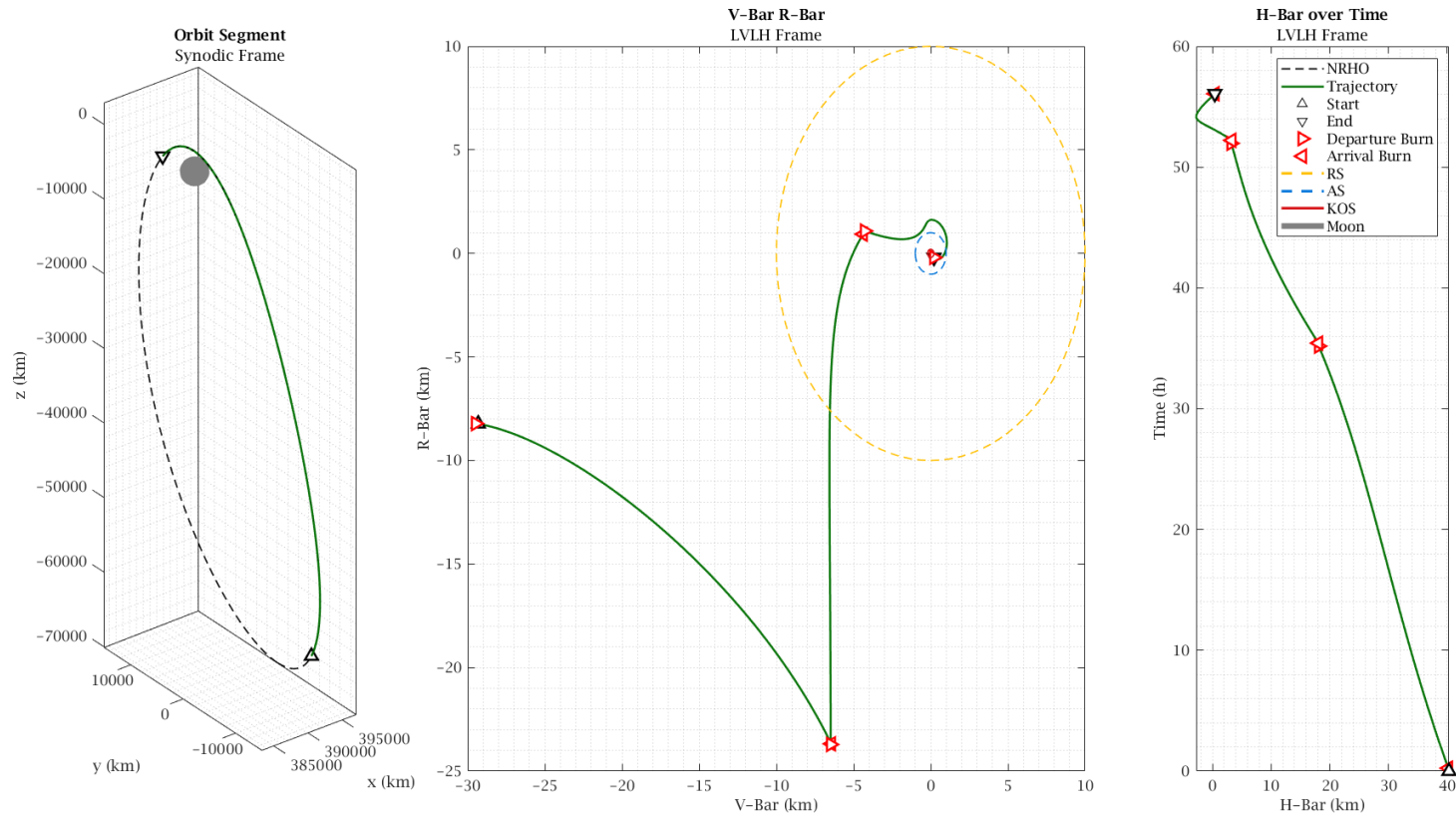


Figure 4.46: “One HP per” Approach Profile Beginning in Region 5. The approach plan is shown from three perspectives: a synodic view of the plan, a V-Bar R-Bar LVLH view, and an LVLH H-Bar view plotted against time for the plan duration. This plan requires 2.47 m/s to execute nominally.

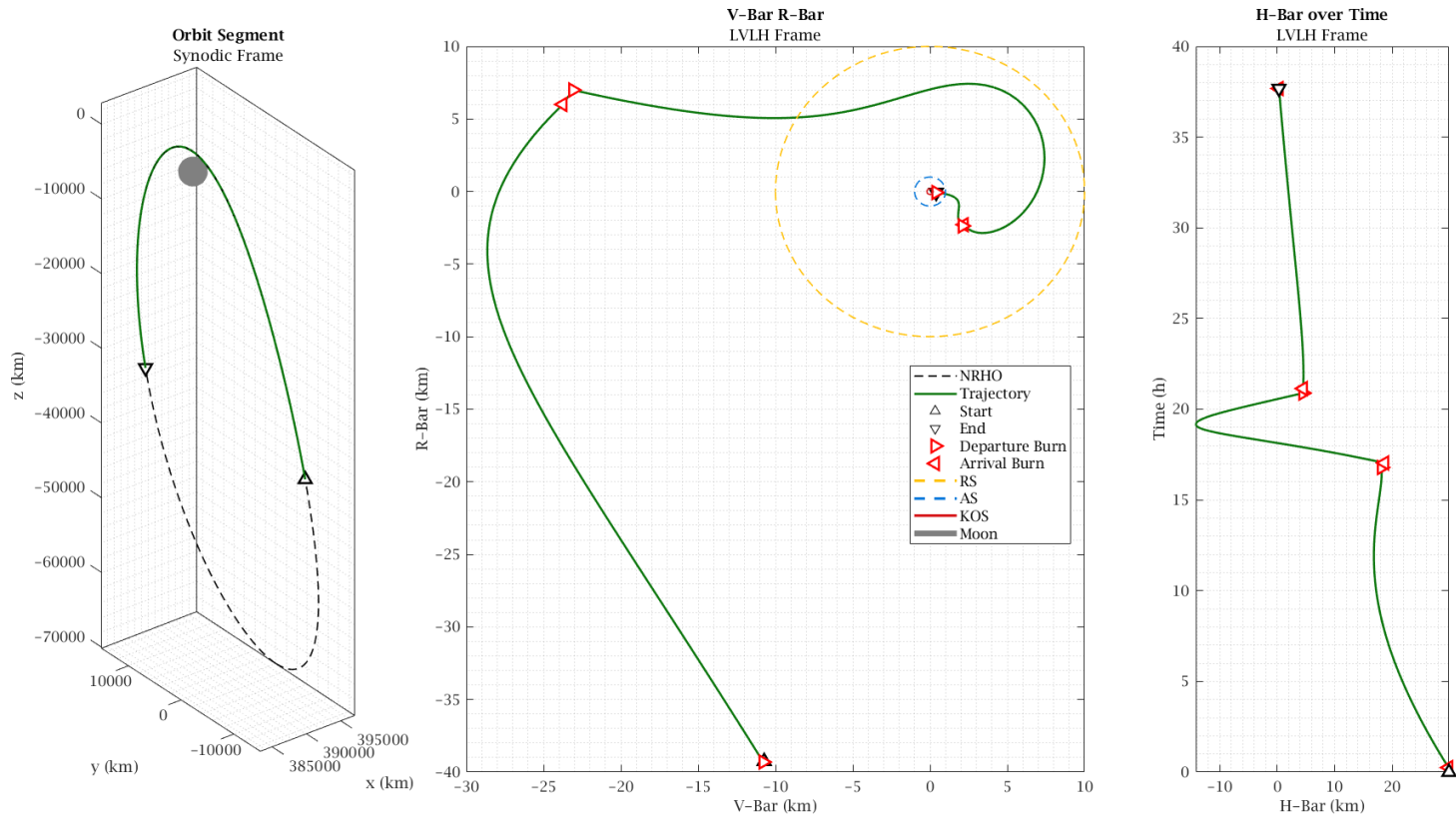


Figure 4.47: “One HP per” Approach Profile Beginning in Region 6. The approach plan is shown from three perspectives: a synodic view of the plan, a V-Bar R-Bar LVLH view, and an LVLH H-Bar view plotted against time for the plan duration. This plan requires 8.36 m/s to execute nominally.

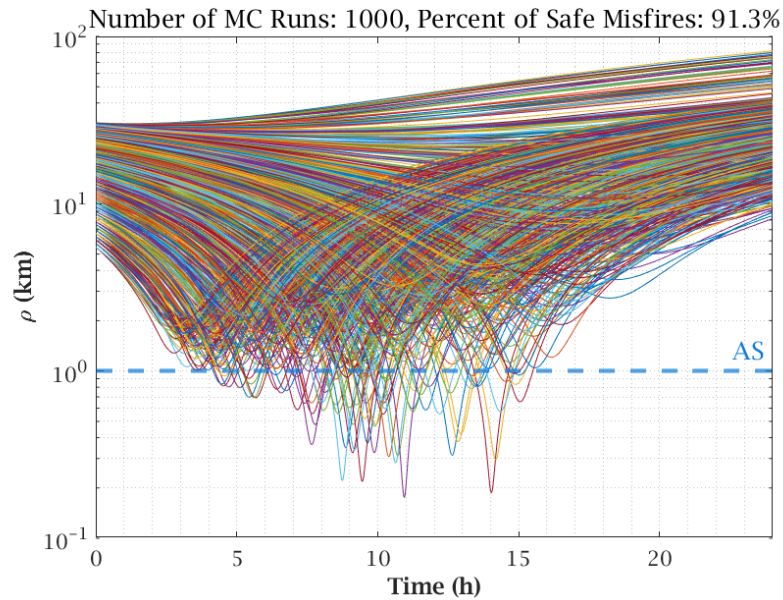


Figure 4.48: “One HP per” Approach Transfer Two Beginning in Region Six Random Misfire Monte Carlo Simulation. One thousand instances were simulated. This transfer was between HP2 and HP3, setting its safety threshold at 1 km. This transfer was the unsafest of the scheme’s 18 total transfers with a safety percentage of 91.3%.

Transfer Random Misfire Safety

Random misfires were analyzed for each transfer. As with the other transfers studied, a random misfire assumes a ΔV of 0.05 m/s applied in a random direction at a random time along the transfer. Each transfer was tested with 1000 Monte Carlo simulations, which tested the random thruster fires. The resulting trajectory after each misfire was propagated 24 hours and analyzed to see if it violated any of the safety criteria.

All transfers between HPs for this scheme had a random misfire safety percentage above 90%. Each safety percentage can be found in Table 4.8, while all Monte Carlo simulation plots can be seen in Appendix C. All but one transfer had a safety percentage above 95%. This transfer was between HP2 and HP3 for the approach, which initially began in Region One. The Monte Carlo Simulation for this transfer is shown in Figure 4.48 with a safety percentage of 91.3%. Most of the unsafe misfires were minor, barely skirting past the threshold, with

some having significant safety breaches. All transfers having above a 90% safety percentage further reinforce the safety of this approach scheme and are significant improvements on previously proposed strategies in the literature. Transfers studied in Innocenti's proposed strategy in 2022 had safety percentages of 56.7% and 46.4% for transfers modeled in the ER3BP [26]. Innocenti's work showed that these percentages decreased to 0% in a full ephemeris dynamics model, signifying the effect dynamic simplifications can have on the results. For most transfers, having lower than a 5% chance of an unsafe random misfire is deemed acceptable by the author, and these transfers are deemed misfire safe for this approach scheme.

Transfer Partial Burn Safety

Partial burn safety criteria was the final safety analysis conducted on these transfers. As before, it is done to see if the transfer remains safe if, during the execution of a departure burn, the main thruster shuts down, leaving only X% of the burn executed. If certain percentages cause the resulting trajectory to be unsafe drift in free drift, the VV must enter a "must complete" state to make the trajectory safe. Some of these transfers are longer than 24 hour, and so the 24 hour safety criteria after failure is not suitable for this partial burn study. For this analysis, the trajectories are propagated for 72 hours, being roughly 24 hours longer than the longest prescribed transfer.

Simulating partial burns for each transfer resulted in zero instances of an unsafe partial burn. All of the partial burn plots, which contain the 100% burn failure visualizing an arrival burn failure, can be found in Appendix D. These results once again solidify the safety of this approach scheme. While this scheme is not as time efficient as the all-in-one scheme proposed above, it is 100% safe in the presence of departure burn, arrival burn, and partial burn failures. Furthermore, it is above 90% safe for all random misfires, with a majority

being above 95% safe. This approach scheme is the adopted strategy for walking the VV through the HPs and towards the Station.

4.5 Strategy Realization

The preceding sections of this chapter have analyzed and presented all the requirements for performing an approach toward the Lunar Gateway. However, all analyses were conducted using the simplified dynamic modeling assumptions of the CR3BP. This lower-fidelity modeling provided a first guess of the costs and risks associated with performing an approach anywhere in the NRHO, but how good of a guess remains to be determined. This section concludes the thesis simulations by studying the approach scheme implemented in a full ephemeris dynamics model.

As outlined in Section 3.5, STK will be utilized to realize the strategy within a higher-fidelity model. The one HP per approach scheme will be recreated within the STK scenario utilizing Gateway's 15-year reference orbit as a starting point [33]. STK's Astrogator will take the scheme's transfers' initial and final states and solve for a transfer with the same TOF using a differential corrector numeric process. The converged STK approaches will then be compared against the CR3BP results from Section 4.4.2. The comparison will focus on the necessary ΔV for each transfer and the transfers' passive safety.

4.5.1 Approach Implementation

The approach recreation began with identifying the NRHO regions in the 15-year reference orbit. A 6.66 day state report in the Moon-centered synodic frame was extracted, and then applying the region definitions from Section 4.1.3, the orbit was segmented into the six

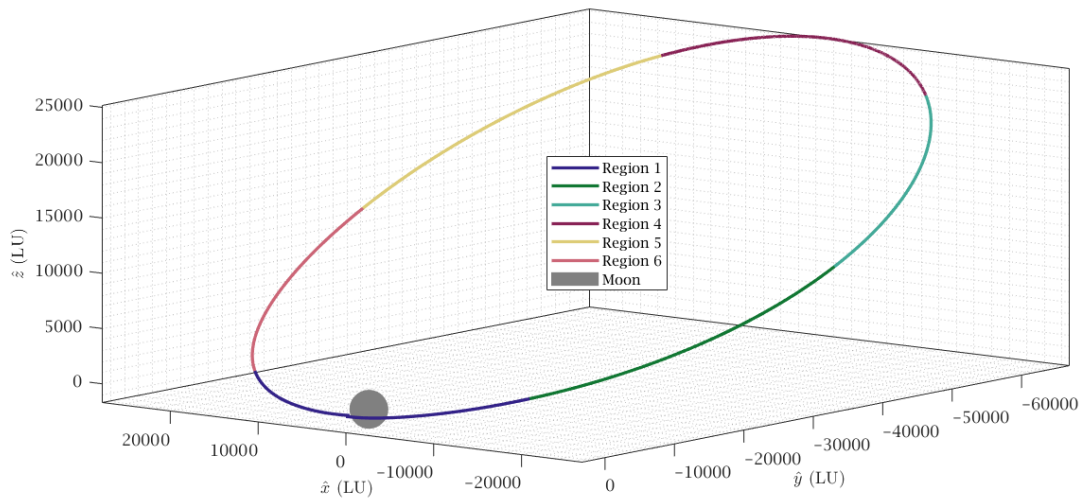


Figure 4.49: 15-Year Gateway Reference Orbit Partitioned using Velocity-Geometric Segmentation Approach. A 6.66 Day portion of Gateway’s 15-year reference orbit was used to identify the six regions of the NRHO in STK. The region spanned from The time stamps of these regions were used to initialize the six one HP per approaches.

regions. Figure 4.49 visualizes the reference orbit segmentation. Note STK’s change in reference frame axes swapping the \hat{y} and \hat{z} axes in comparison to the earlier presentation of the orbit.

The time stamps for each region’s beginning were recorded from this segmentation and used to initialize six VV rendezvous satellite objects. One for each of the six nominal one HP per approach schemes. The initial time for each region is listed in Table 4.9. The times are listed in Coordinated Universal Time (UTC) following a Day-Month-Year Hour-Min-Second format.

The LVLH coordinate system was created centered on Gateway. The system axes are visualized in STK overlaid on Gateway near Periselene in Figure 4.50. The system definition followed the exact definition as earlier for Franzini and Innocenti’s LVLH frame. In this Figure, the LVLH-MoonZcentered Z axis is the negative radial vector from the Moon’s COM to Gateway. The LVLH-MoonZcentered Y axis is aligned with the orbit’s angular momentum

Table 4.9: 15-Year Gateway Reference Orbit Region Initial Time Stamps. The initial times for each region within one 6.66 day span of the 15-year reference orbit are listed.

Region	Day	Month	Year	hh:mm:ss (UTC)
1	8	January	2020	18:44:26.000
2	2	January	2020	13:18:26.000
3	3	January	2020	07:51:26.000
4	4	January	2020	14:55:26.000
5	6	January	2020	14:02:26.000
6	7	January	2020	23:00:26.000

vector with respect to the Moon, and the `LVLH-MoonZcentered X` axis is the resulting cross product between the `LVLH-MoonZcentered Y` and `LVLH-MoonZcentered Z` axes.

With the region time stamps and the LVLH frame implemented onto Gateway, each VV Satellite objects approach scheme were constructed in Astrogator. The HP locations for the start and end of each transfer were taken from the results of Section 4.4. For a given region’s approach, that region’s HP1 position in the LVLH frame and each region’s start time defined the object’s initial state. The 15 minute station-keeping gaps were implemented with Astrogator `Hold Mission Control Sequence (MCS) Segments` of the same length. All transfers were constructed using Astrogator `Targeting Sequence` segments. Each `Targeting Sequence` used a differential corrector to target a `Maneuver` segment, modeled as impulsive, to aim for the following HP after the desired TOF. The TOF was implemented with a `Propagate` segment set to the TOF. The `Propagate` segment was set to use STK’s Moon High Precision Orbit Propagator. The differential corrector tuned all three thrust axes to achieve a final position within a 1 meter tolerance of the target HP. Following the transfer burn, a second `Targeting Sequence` tuned the arrival burn to achieve zero relative velocity within a tolerance of 0.10 m/s.

This Astrogator MCS structure was the same for all three transfers. All six schemes’ MCS converged for all six burns, realizing all the nominal approach plans in a full ephemeris

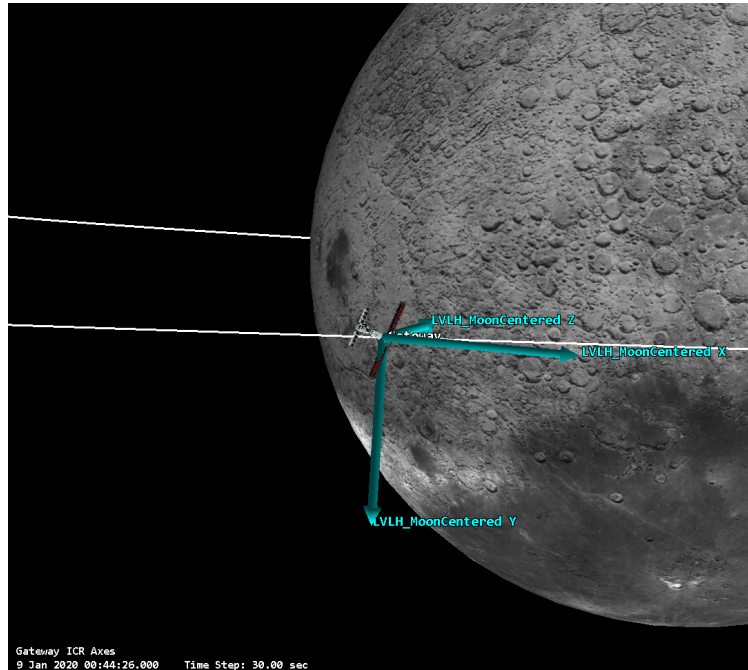


Figure 4.50: LVLH Coordinate System STK Visualization. Franzini and Innocenti’s LVLH frame was constructed within STK to enable the HPs to be placed in the same position as the CR3BP modeling positions.

dynamics model. Figure 4.51 shows the approach beginning in Region One. The purple curves show each transfer phase of the approach, while the holds are shown in orange. As mentioned in Section 4.4, the holds are visible as they are held in the synodic frame, which the LVLH frame rotates within over time. The three safety region spheres are also visualized centered on Gateway. With realized nominal approaches in a full ephemeris model, they can be compared to the CR3BP results.

Transfer ΔV Comparison

STK maneuver summary reports provided each transfer’s ΔV , which listed each impulsively modeled burn’s magnitude. The magnitude of each burn is listed in Table 4.10. Each burn’s percent difference compared to the CR3BP transfers is also shown with positive

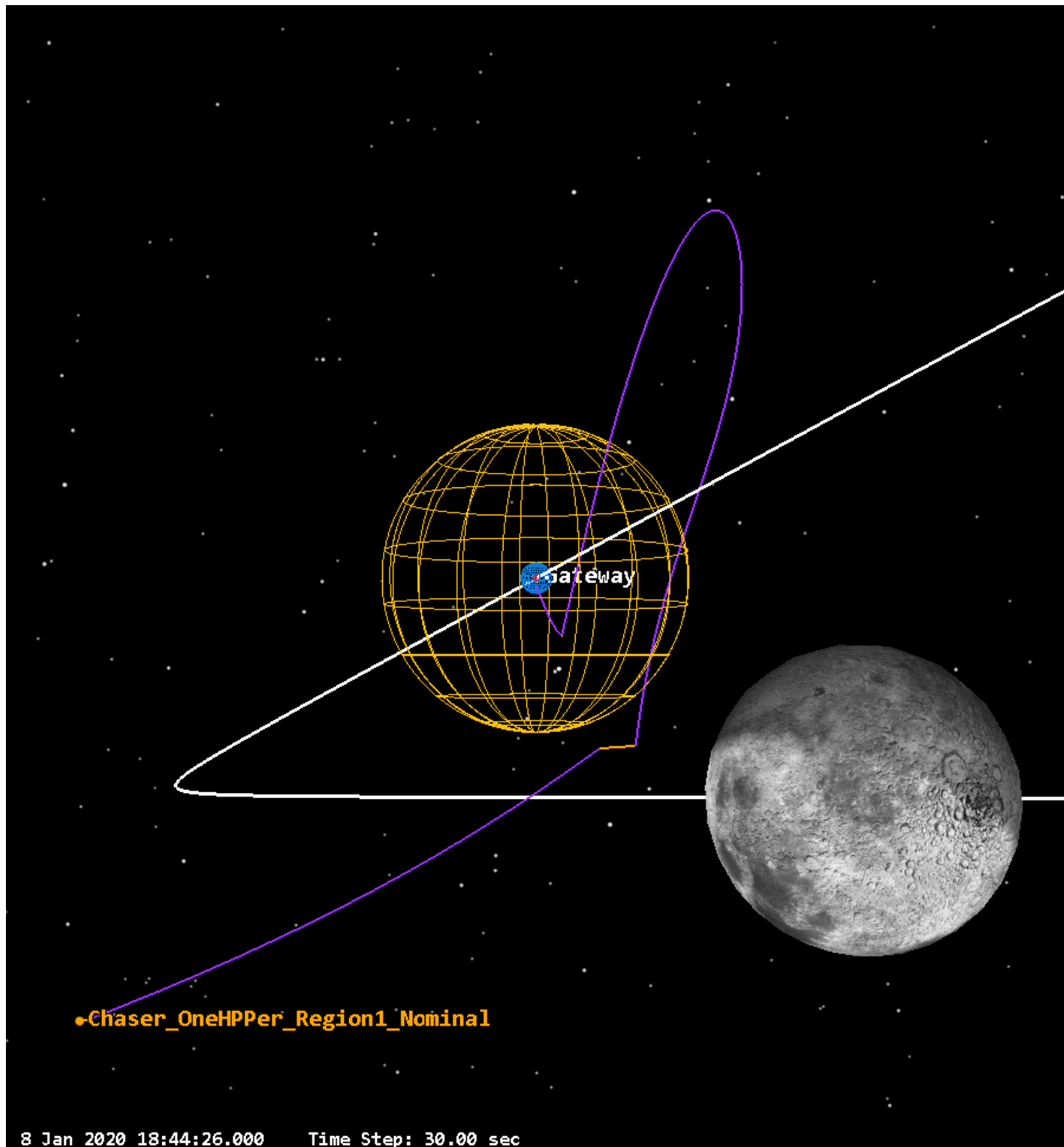


Figure 4.51: Region 1 “One HP per” Nominal Approach Implemented Within a Full Ephemeris Dynamics Model. Transfers are shown in purple while station-keeping holds are in orange. Gateway is centered within the three safety spheres and placed on the NRHO in white.

values denoting when the CR3BP magnitude was higher and negative denoting when STK's magnitude was higher. The burns had a wide range of percentages, with the best agreement being 6.1% and the worst being 190.9%. Note that the large percentage instances occur with plans with minor ΔV requirements, resulting in a small divisor in the percent error calculation.

The source of error could come from a wide range of areas, from differences in trajectory construction methods to the dynamic models themselves. The more significant errors are most likely due to the differences in approach for constructing the trajectories, leading to more drastic differences. In comparison, more minor errors are likely cases when the solvers produced analogous solutions, with dynamic modeling providing the majority of the errors. The magnitudes of the STK burns themselves are encouraging results. Most transfers required less ΔV than the CR3BP trajectories, making implementation of the approaches less costly. All are feasible magnitudes for any VV attempting this operation to achieve.

Transfer Passive Safety Simulation

The transfer passive safety was the second characteristic of each approach analyzed in the complete ephemeris dynamic realization. The arrival burns, and departure burn failures were studied at each HP for each transfer. The failures were modeled by running each transfer's MCS up until the point of failure. In place of executing the following action in the nominal plan, the MCS was given a 24 hour **Propagate** segment. The VV range report was then extracted and analyzed to see if the VV's resulting drift violated the applicable safety criteria.

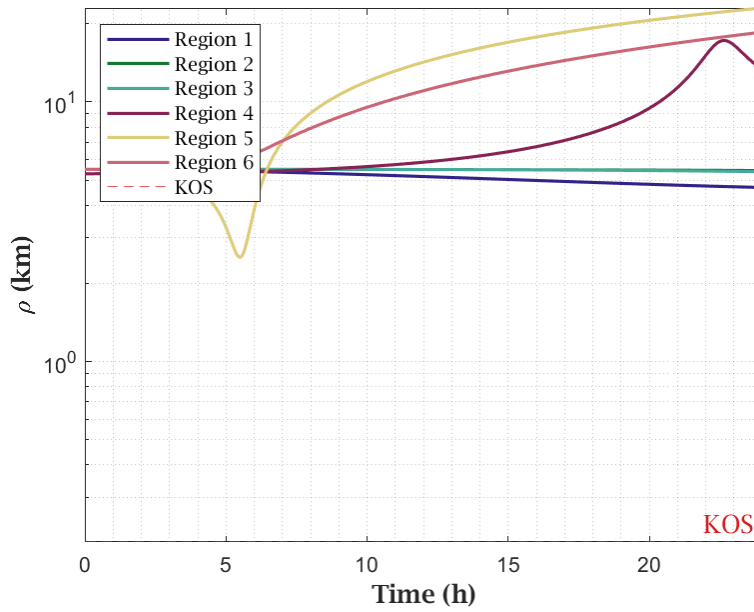
Figure 4.52 presents one transfer for the passive safety analysis. The remaining passive safety plots are in Appendix F. A departure and arrival failure are shown for the third transfer

Table 4.10: “One HP per” Approach Scheme Transfers Full Dynamics Ephemeris Comparison. All 18 transfers comprising six nominal approach plans for the one HP per scheme were implemented within STK’s full ephemeris dynamics model. The transfers’ required ΔV were compared. Positive ΔV differences represent CR3BP overestimates, and negative differences represent CR3BP underestimates compared to the full ephemeris implementation. The initial region where the approach begins is listed along with each transfer’s initial HP.

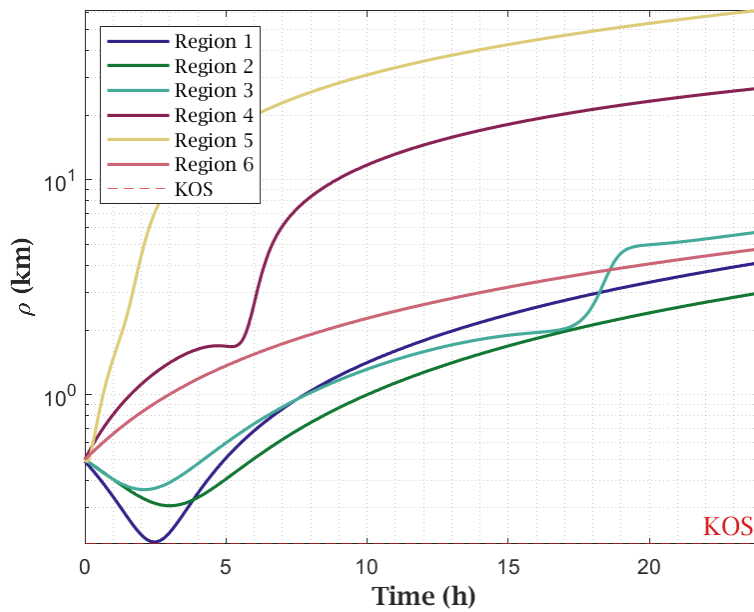
Region ₀	HP ₀	TOF (h)	STK ΔV (m/s)	CR3BP ΔV (m/s)	Percent Difference
1	1	3.85	10.58	21.70	51.24
1	2	16.54	15.63	12.07	-29.49
1	3	34.93	0.27	11.60	97.67
2	1	16.54	2.27	2.84	20.07
2	2	34.93	0.39	2.47	84.21
2	3	46.71	0.06	2.28	97.37
3	1	34.93	0.98	0.39	-151.29
3	2	46.71	0.34	0.32	-6.25
3	3	34.93	0.09	0.23	60.87
4	1	46.71	0.43	0.30	-43.33
4	2	34.93	0.54	0.43	-25.58
4	3	16.54	0.20	0.29	31.03
5	1	34.93	1.16	0.70	-65.71
5	2	16.54	0.90	0.76	-18.42
5	3	3.85	0.81	0.96	15.63
6	1	16.54	1.71	1.98	13.64
6	2	3.85	4.66	5.00	6.80
6	3	16.54	0.18	1.15	84.35

for all six region’s approaches. All cases were safe. Region One’s Arrival burn failure came within 6.25 meters of the KOS boundary. These simulations affirm the axes safety presented in Section 4.2.2 with the departure burn failure analysis and affirm the trajectory design safety through the arrival burn failure analysis.

These simulations confirm the passive safety of the designed approach schemes. More analysis is needed in the future to simulate the other failure modes, but these serve as a strong foundation. With these approaches’ improved ΔV efficiency, this full ephemeris implementation shows their validity as a safe rendezvous approach strategy that opens up



(a) Departure Burn Failure



(b) Arrival Burn Failure

Figure 4.52: “One HP per” Full Ephemeris Implementation Approach Transfer 3 Passive Safety Analysis. The nominal Astrogator MCS for each approach was modified to introduce failures at the beginning and end of each transfer. These two figures show the 24 hour drift of the VVs after a departure and arrival burn failure for the third transfer in the approach for all six nominal plans. No VV violates the safety criteria. Region Six’s arrival failure comes within 6.25 meters of the KOS.

rendezvous to regions outside Aposelene.

4.6 A Complete Gateway Rendezvous Approach Strategy

Chapter 3 introduced the idea of using a transit diagram to represent the approach strategy. The diagram designed for the approach strategy implements the loiters selected in Section 4.3 and the approach scheme selected in Section 4.4. This section first details how to interpret the diagram before presenting the entire diagram in Figure 4.55. After the diagram is presented, two scenarios are proposed to show how a VV operator would execute it in a mission application. The first scenario is a nominal case with no unexpected holds, and the operator is promptly granted ATP. The second scenario is an off-nominal scenario where an unexpected error on Gateway requires the operator to decide the best course of action to hold for the duration. These two scenarios encompass most of the nuances regarding properly using the diagram.

4.6.1 Rendezvous Transit Diagram

The transit diagram has two key elements: region transit strategies and HP-to-HP transfers. The region transit strategies show how a VV should optimally operate through the duration of a region at a set hold point. These strategies leverage the results of the traditional station-keeping and station-keeping alternatives. The HP-to-HP transfers are developed by deconstructing each nominal one HP per approach plan and stitching individual transfers around the diagram. A breakdown of how each of these elements is visually represented follows.

Figure 4.53 illustrates how the diagram details transiting a region. The white dots represent

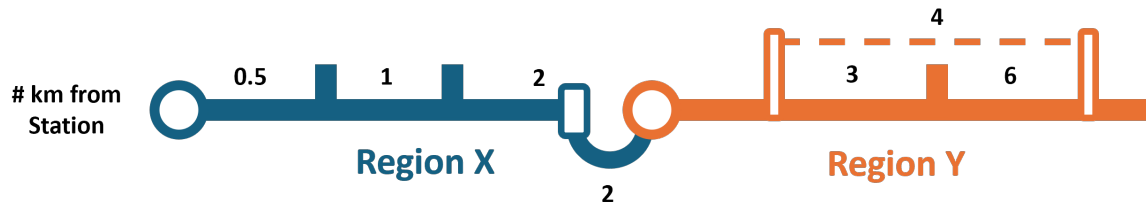


Figure 4.53: Approach Strategy Transit Diagram Region Transit Example. This figure outlines how a VV transiting two regions of the NRHO will be visualized. Each tick mark represents either 30 60 or 120 minutes of the region. The number in-between ticks shows the ΔV required to keep on the hold point away from the station. In some cases, a forced loiter may be more efficient. These are represented by the straight dashed lines connecting two filled ticks. ΔV s below 0.10 m/s are omitted from the diagram. The one hour region-to-region transfers are shown by the small arc connecting a region end to an region start.

the beginning of a new region of the NRHO. The ticks represent either 30, 60, or 120 minute intervals dependent on region. Region One has 30 minute ticks, Two and Six have 60 minute ticks, while Three, Four, and Five, have 120 minute. Solid lines between ticks represent that traditional station-keeping should be employed for that duration of the region if a transfer is not being executed. Dashed lines departing a tick and running parallel to the line before eventually returning to the same loop represent a forced loiter. These are present when analysis shows that a forced loiter is more ΔV -efficient than traditional station-keeping if a VV is expected to hold on a line for the prescribed duration. The number above either line segment is the ΔV required to perform station-keeping or execute the loiter maneuver. If a number is not present between the ticks, the station-keeping cost is below 0.10 m/s. The one hour region-to-region Transfers are shown represented by the arc connecting a region's end to the following region's beginning.

The goal of the VV is to walk inwards through the loops, each loop representing a HP distance, bringing it to the station. Figure 4.53 shows how the map visualizes this process. Transfers depart a tick mark, curve down and run parallel between loops before curving again to connect to the next loop. The two numbers centered on the transfer line represent

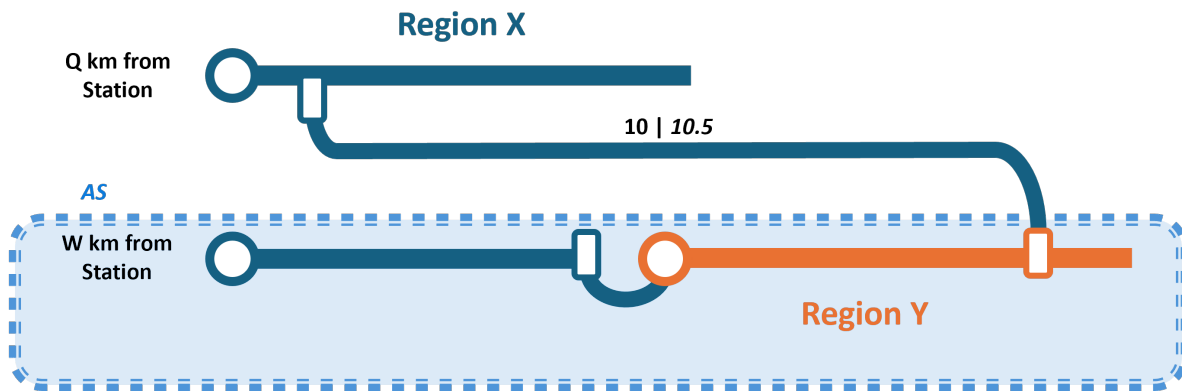


Figure 4.54: Approach Strategy Transit Diagram Region Transfer Example. This figure shows how transfers between hold points will be visualized. A thinner, solid, curved line connecting two loops will show a transfer. The numbers below the transfer represent the ΔV of the transfer and the TOF of the transfer. Safety regions are shown as dashed lines running unattached in between loops.

the transfer ΔV and transfer TOF. The transfer ΔV , in meters per second, is written in Roman, and the TOF, in hours, is italicized. Dashed lines with shading beneath between the four loops represent the placement of the safety regions surrounding the station. All transfers, station-keeping, and loiters flow clockwise around the figure.

These two elements are blended to create the complete transit diagram. The VV operator can take where their vehicle is in the NRHO and draw out nominal and contingent approach plans that meet their rendezvous time and fuel requirements. Each potential action illustrated is safe across the multiple failure modes relevant to trajectory design and execution.

Lastly, this diagram addresses the key motivation of this thesis. The diagram is not limited to operations within the Aposelene region. 100% of the orbit is covered, enabling VVs to approach Gateway at any time throughout its NRHO safely. Following one of the lines all the way around the diagram represents one NRHO period with actions available all the way around. The various approaches provide multiple solutions to the hypothetical time-sensitive rendezvous scenario for a VV that must rapidly return to Gateway and cannot afford to wait

for perfect Gateway positioning in the orbit that may take on the order of days to occur.

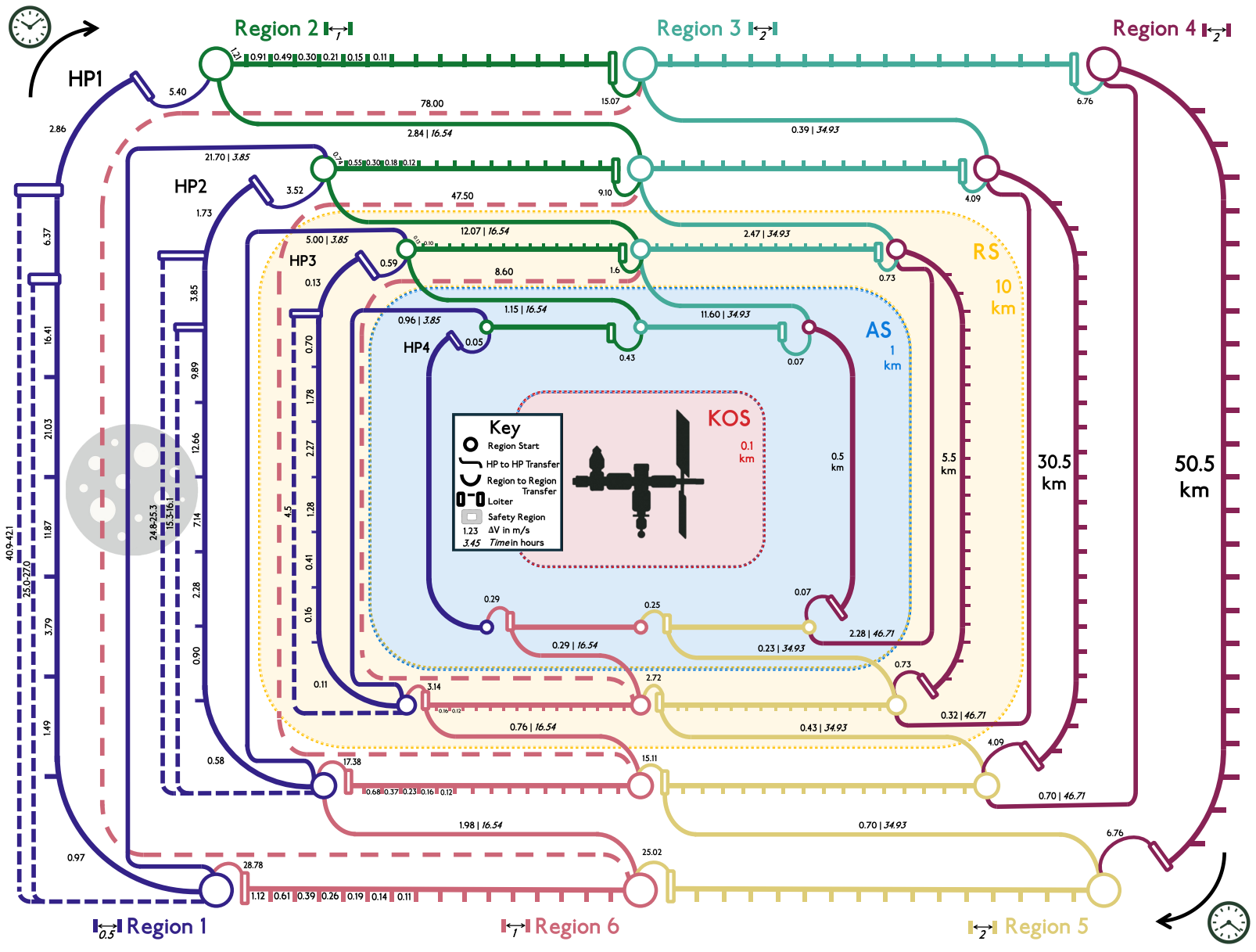


Figure 4.55: Time Sensitive Rendezvous Approach Strategy With Lunar Gateway Transit Diagram.

4.6.2 Nominal Approach Example

Consider the following hypothetical approach scenario: Resupply launches from Earth to the Lunar Gateway have experienced consecutive failures, similar to the string of ISS resupply mission failures in the 2010s [1, 5, 23]. These launch failures have resulted in critically low supply levels on Gateway's, which must be addressed urgently.

The autonomous cargo resupply spacecraft has just completed its transfer phase and established itself on HP1 50.5 km away from Gateway 3.5 hours after the station entered Region One of the NRHO. In integrated ops with NASA, the cargo supply operators are finalizing the rendezvous approach phase.

The flight dynamics engineer, referencing the adopted strategy diagram, illustrates the approach in Figure 4.56. The vehicle has 30 minutes of station-keeping remaining in Region One. Before then, two transfers should be uploaded to the vehicle to execute. First is a region-to-region transfer to align the vehicle with Region Two's approach axis. If the transfer succeeds and the vehicle remains healthy, it will execute a HP-to-HP transfer, walking it to HP2 along Region Three's axis. The engineer passes this plan to the flight controller, who green-lights the plan and sends the commands to the vehicle. The portion of the diagram this nominal plan is taken from is shown in highlighted in red in Figure 4.57. The off-nominal example discussed later is shown in orange.

18 hours have passed, and the vehicle has successfully performed the two commanded transfers. The cargo craft sits 30.5 km away from Gateway, which has just entered Region Three in the NRHO. The operators confirmed the vehicle's healthy status with NASA officials, who granted ATP to the flight team to enter the RS. Continuing with the nominal plan, the operators command the HP-to-HP transfer, walking the vehicle from HP2 to HP3. This transfer takes under a day and a half to complete, and operators monitor the vehicle's

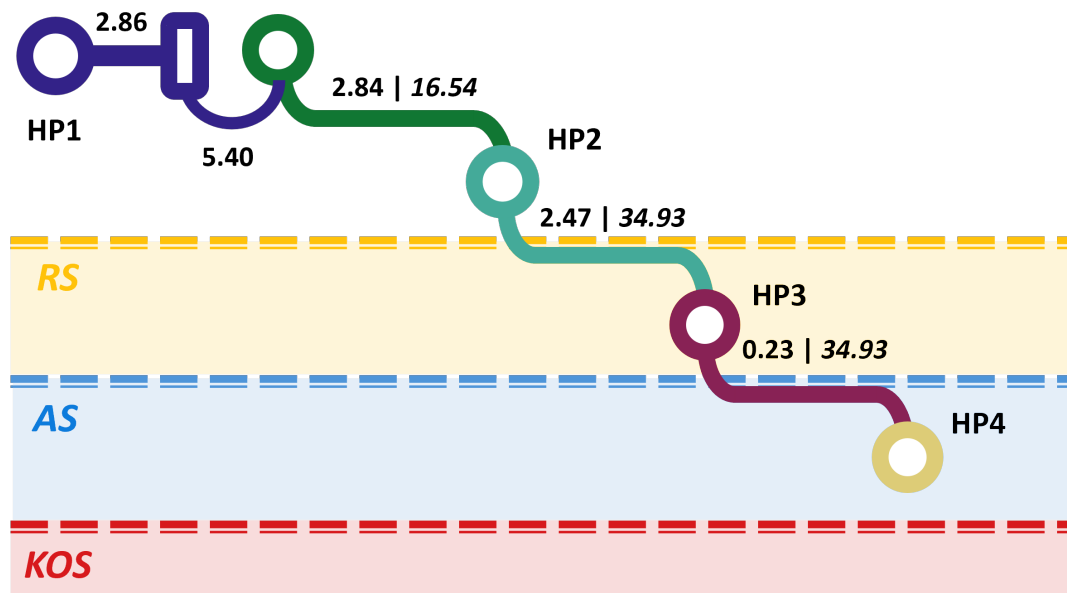


Figure 4.56: Flight Engineer's Illustrated Nominal Approach Plan. Transit diagram illustration of nominal approach determined based on the current status of approach. Vehicle begins approach 3.5 hours into Region One and transfers to HP1 in Region Two before executing the one HP per approach scheme beginning in Region Two.

health.

All goes according to plan upon arrival at HP3, and the final transfer to HP4 in within Region Five is commanded after receiving ATP to enter the KOS from NASA. This transfer takes 46.7 hours and will place the resupply vehicle outside the KOS. From here, autonomous guidance algorithms will perform the final rendezvous and docking actions within the approach corridor within the KOS, bringing the necessary cargo to Gateway.

This scenario represented a nominal approach. No hiccups on the VV operator's side nor station setbacks from NASA's side prevented the VV from following the streamlined path taken by the flight engineer from the transit diagram. Holds were completed between transfers to confirm vehicle health before ATP was granted and the supplies made it to the station. The vehicle was allowed to conduct an efficient approach even though it began its rendezvous phase just after Periselene passage. However, few approaches in practice are

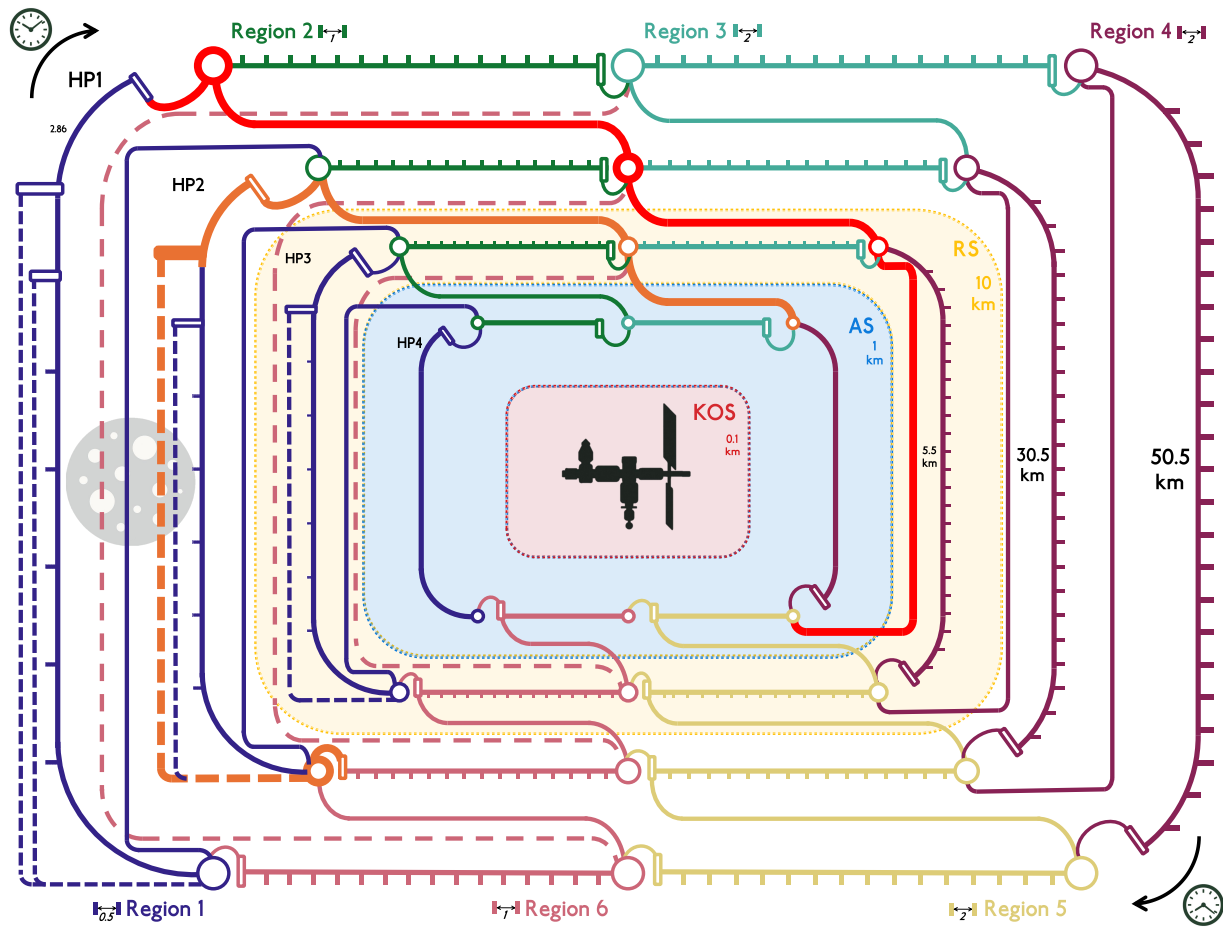


Figure 4.57: Transit Diagram With Highlighted Examples. The nominal scenario is highlighted in red while the off-nominal plan is in orange.

as seamless as the one just described.

4.6.3 Off-Nominal Approach Example

An analogous vehicle is halfway along its approach in a less time-critical context. It sits at HP2 30.5 km from Gateway within Region Six. Gateway is operating nominally, but the avionics engineer on duty within the flight operations center notices depleted power levels on the cargo due to an undiagnosed issue. The engineer needs time to confirm his hypothesis fully but believes it to be a faulty sensor reading.

NASA is unwilling to risk the vehicle losing power midway through its approach and denies ATP until the issue is resolved. The flight dynamics engineer was expecting to tell the flight controller to perform the HP-to-HP transfer between Region Six and One entering the RS, but this can no longer occur. Talking to the avionics engineer learns that this bug may not be resolved until Gateway enters Region Two.

Given the information before him, the flight engineer plans the approach seen in Figure 4.58. The engineer concludes the best course of action is to transfer to Region One's axis and execute a four hour loiter burn to wait out Region One. This action returns the vehicle to the axis, ready to transfer to Region Two. By then, the avionics engineer and their team will have hopefully addressed the power level issue. If the issue is still not addressed, the vehicle can station-keep through Region Two, giving more time to debug. The flight controllers agree and plan the transfers and loiters.

After successfully completing a region-to-region transfer to HP2 in Region One, a loiter burn, and another region-to-region transfer to HP2 in Region Two, the avionics engineer confirmed the issue as a faulty sensor. NASA, satisfied with the findings, granted the operators ATP, allowing them to complete the HP-to-HP transfer entering the RS. From here, the team

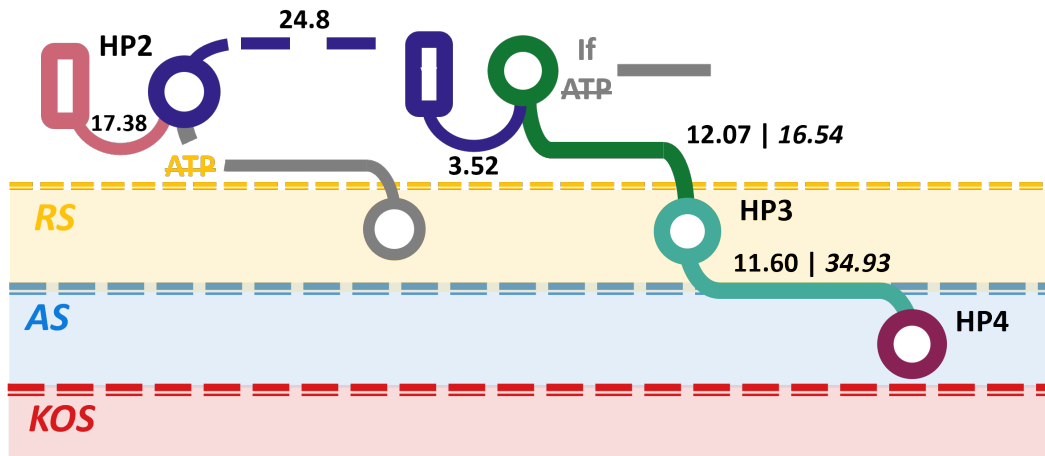


Figure 4.58: Flight Engineer’s Illustrated Off Nominal Contingent Approach Plan. Transit diagram illustration of contingent approach determined based on the ATP rejection and ongoing vehicle issues. The vehicle sits at HP2 in Region Six, waiting for ATP to enter the RS transfers to HP2 in Region 2 to execute a loiter through Region One. After the loiter and another transfer to HP2 of Region Six, the engineer will either station-keep through Region Six or, if granted ATP, execute the two transfers, bringing the vehicle to HP3 and, subsequently, HP4.

experiences no issues and executes the nominal HP-to-HP transfer to bring the vehicle to HP4 within Region Four.

This scenario presented a more realistic approach from an operations perspective. An issue with an unclear timetable arose, requiring contingent actions. The actions were evident in the transit diagram, allowing for a streamlined comparison between viable options for the flight engineer. If more issues arose or the power reading issue persisted, the diagram provided the information needed to determine how to proceed best.

In summary, the transit diagram presented in Figure 4.55 is a cohesive visualization combining all the results of this thesis into one chart. The region segmentation breaks the orbit into its distinct regions. The station-keeping and subsequent alternative analysis form the transit strategy for the vehicle through each region around the entire NRHO. The six one HP per approach plans are stitched together around the diagram, enabling the vehicle to walk

inwards toward Gateway. Each action shown has been simulated to be passively safe in the presence of departure burn, arrival burn, random misfires, and partial burn failures. This diagram fills the hole in the present literature, enabling a timely approach to Gateway anywhere along the NRHO.

Chapter 5

Conclusion

“No man should escape our universities without knowing how little he knows.”

J. Robert Oppenheimer

This Chapter summarizes the work and takeaways presented in the thesis. Limitations and continuations to the work are discussed. The Chapter follows the structure below:

- Section 5.1 states the motivations alongside the driving questions that this work set out to address. The findings of the work that address these questions are discussed at a high level.
- Section 5.2 addresses the limitations of the work due to simplifications in the underlying dynamics assumptions and trajectory.
- Section 5.3 explores potential continuations of the work and areas of the presented work that could be reiterated.

5.1 Summary of Contributions

This section summarizes the motivations that drove the thesis. The key contributions of the thesis that addressed these motivations are reviewed.

5.1.1 Motivation and Main Objectives

This thesis is driven by the planned Lunar Gateway space station in orbit around the Earth-Moon Lagrange Point 2 in cislunar space [38]. Gateway's orbit is a special classification within the family of Halo orbits known as a Near Rectilinear Halo Orbit (NRHO) [4]. This orbit creates unique dynamics-driven challenges that break down the classical assumptions that drive current approach strategies for near-Earth rendezvous operations like those with the ISS [13, 18]. These unique orbital dynamics have required researchers to develop new rendezvous, proximity operations, and docking (RPOD) strategies to enable the necessary RPOD missions required to assemble and operate Gateway [12, 18, 19, 20, 26, 27, 35, 37, 45]. These proposed strategies limit rendezvous to a region surrounding the orbits Aposelene. This bounding restricts operations to just 45% of the entire orbit, leaving just over 3.5 days of the orbit unaccounted for.

This limitation forms the first motivation of the work. This motivation is to create an approach strategy encompassing the entire NRHO duration. An efficient strategy that achieves this must answer four driving questions: How can the NRHO be segmented to allow for consistent visiting vehicle (VV) behavior within each region? What are the ΔV -optimal approach axes within each region that allow for safe but non-costly holding? Do transfers exist between HPs placed along each region's axis that allow for a time-effective ΔV efficient approach? Lastly, can each piece of the strategy meet the currently published rendezvous safety requirements for crewed deep space station RPOD?

The last of these questions encompasses the second motivation of the thesis: ensuring the time-sensitive approach strategy is safe in the presence of four main failure modes that a VV may experience. These failure modes are departure and arrival burn failures occurring at the beginning and end of a transfer, a random misfire that occurs along a transfer, and

a partial burn. The International Deep Space Interoperability Standards (IDSIS) published the International Rendezvous System Interoperability Standards (IRSIS) in 2019 detailing the safety requirements for rendezvous with deep space stations such as Gateway [28]. The current ISS standards motivated these standards, which provide a rigid operational protocol for vehicles [30, 36]. These regulations heavily restrict the operations of VVs in the station’s proximity, requiring them to receive permission before entering various safety regions surrounding the station. Any usable approach strategy must meet the safety regulations outlined in these regulations, requiring all adopted strategies to be shown to be compliant with these regulations.

These two aspects above motivate this thesis. The goal is to develop a safe, time-sensitive rendezvous approach strategy that enables an approach with Gateway. This approach is not limited to just Aposelene but enables an approach throughout the entire NRHO. The work takes the simplified dynamics model of the CR3BP to represent Gateway’s dynamics. Building off the relative motion modeling done by Luquette and Sanner, their equations of relative motion are used to model a VV’s approach to the station in the restricted three-body dynamics [34]. The results from this modeling provide the information necessary to answer the four guiding questions to create the desired approach strategy. The strategy is created with a VV operator’s perspective in mind. The desired final result of this thesis is a diagram designed to allow for an easy understanding of the extensive avenues of the strategy to allow for quick decision-making in an operational setting.

5.1.2 Essential Findings

An end-to-end approach strategy enabling a VV to execute an approach phase of a rendezvous operation with the Lunar Gateway is developed. The strategy enables an approach at any

point within Gateway’s NRHO, expanding the limited time-sensitive approaches in today’s literature. The strategy details the optimal approach axes based on Gateway’s location within the NRHO. The approach scheme along each axis is presented with contingent actions prescribed when the vehicle is forced to hold for short and long durations. All segments of the strategy are shown to be safe in the presence of four critical failure modes that may occur during any given approach, bringing the strategy into compliance with international standard requirements. The transfers’ ΔV requirements and contingent actions are optimized, making them feasible to perform by any VV designed to perform a cislunar rendezvous. The entire strategy is presented in a cohesive transit diagram, enabling VV operators to rapidly determine the best approach plan for their approach in both nominal and off-nominal cases.

- Segmenting Gateway’s 9:2 NRHO into regions driven by the orbit’s dynamics and geometry creates regions with consistent behavior and aligns the strategy with previously developed approach strategies presented in current research. The regions include one encompassing Periselene, one encompassing Aposelene, and four that serve as transition regions between the two critical points in the orbit. This approach creates operationally consistent regions where operators can better understand VV relative motion behavior and rendezvous risks.
- Each region has a ΔV -optimal approach axis, which enables efficient station-keeping when approach holds are required. These optimal axes are shown to provide 2.74 m/s in savings compared non optimal axes when holding 5 km away from the station. These savings increase the further the VV is away from Gateway. Not all optimal axes are passively safe, requiring suboptimal axes to be selected to balance approach safety with reducing ΔV requirements. Transfers between axes were shown to be both passively safe and random misfire safe. Two transfers require a “must-complete” operational state to mitigate risk during a partial burn failure.

- Station-keeping is the primary holding strategy for most orbit regions. However, in the Periselene region, characterized by its extreme dynamics, specific alternatives are shown to be safe and more efficient. These alternatives employ a loiter to be performed by the VV, taking it off the approach axis and returning it to the HP after a tuned TOF. The intra-region loiters can save upwards of 42 m/s. For holds that are expected to last for an extended period, including the regions immediately before and after Periselene, a similar loiter can be performed, reducing ΔV requirements by 78 m/s in some cases. These loiter alternatives are shown to be safe in the event of a random misfire or partial burn. Utilizing passive drift on the NRHO to hold was not as efficient as these forced loiter alternatives.
- Two approach schemes enable the VV approach throughout the NRHO while preserving operational symmetry. An “all-in-one” approach is the most time efficient but is unsafe in all cases and cannot be adopted. A more patient “one HP per” approach is safe in all failure modes, providing a feasible transfer strategy to go from HP to HP, bringing the VV closer to the station.
- The approaches developed in the CR3BP dynamics model are, on average, more ΔV efficient when realized in a full-ephemeris dynamics model simulated within STK. Some cases had 191% ΔV difference between CR3BP and full ephemeris implementations, showing a real-world implementation will likely be more fuel efficient. These realized transfers remain passively safe during departure and arrival burn failures.
- The transfer loiters and station-keeping instances shown to be safe and ΔV -optimal for each instance of the approach around the entire NRHO create a transit diagram representing the entire adopted approach strategy. The diagram has a design focus on making approach strategy identification easy and streamlined for operators of VVs. Operators can place themselves in their applicable state and stage in the approach

scheme, see the best nominal plan, and identify contingency actions should they be required.

5.2 Limitations

This section acknowledges the limitations of the presented work. The simplifications were made primarily in the dynamics modeling and the methods used to construct and analyze the trajectories of the approach strategy.

5.2.1 Dynamics Simplifications

The dynamics modeling of the NRHO and relative motion implemented the circular restricted assumptions to the three-body problem. The CR3BP reduces the bodies to point masses and makes the mass of the VV negligible compared to the primaries. Furthermore, it assumes the bodies lie in planar circular orbits around the system's barycenter. These are not the case in the real world. The Moon and Earth have nonuniform gravitational fields and lie on elliptical orbits that are not coplanar—without correction, even imposing just an eccentricity of 0.001 to the Moon's orbit into the CR3BP EOM results in the reference NRHO breaking down [32]. The actual eccentricity of the Moon is 0.0549 [18]. These simplifications were partially addressed by implementing the approach strategies within a full ephemeris dynamics model that accounted for these nuances in real-world dynamics. However, more effort is needed to study the impacts of the simplifications on the potential implementation of the strategy in a real mission.

Additionally, modeling with these assumptions reduces the NRHO to a strictly periodic orbit. The Gateway's NRHO, as referred to within this work, is classified as a 9:2 NRHO. This

resonance structure means Gateway completes nine revolutions around the Moon for every two revolutions the Moon completes around the Earth, creating nine distinct periods of the NRHO as opposed to the one period instance studied. While the definitions used to segment the orbit into its six regions would remain, the behavior of the VV would change depending on which of the nine revolutions Gateway is currently in. A truly comprehensive approach strategy would need to account for these distinct periods, requiring nine subsets of each transfer and proposed station-keeping strategy/alternative. Furthermore, each proposed action variant must be reevaluated for safety across all failure modes. Doing so would result in a string of nine transit diagrams with modifications to account for the varied behavior driven by the NRHO period that Gateway is within.

This work provided what would be considered a first pass at formulating a comprehensive approach strategy. The simplified dynamics give an initial estimate of what an actual implementation may look like. Further analysis is necessary to address the shortfall in the analysis present because of these simplifications.

5.2.2 Trajectory Construction

The numerical methods used to construct the various transfers are another main area where simplifications were made throughout this analysis. Starting with the single-shooting method, the method's objective function only ensured the transfer started at the desired point and, after the required TOF, ended at the desired target. While this results in a viable transfer between both points, it does not tune the velocity of transfer needed. As seen through Region One's loiter analysis, minor modifications in TOF can cause significant transfer ΔV changes in sensitive regions. Furthermore, multiple burns along a single transfer could reduce a transfer's required ΔV . None of these alternatives are considered through

this work's single-shooting method. Franzini implemented a more robust process in similar studies [19]. Modifications like these can result in more finely tuned trajectories to reduce the strategy's ΔV requirements.

All transfers were modeled with impulsive burns. Impulsive means that each burn executed happened instantaneously without considering how efficiently a VV thruster could impart the required ΔV . This simplification allowed the designed strategy to be generic across all VVs. Every VV will have a unique performance envelope that will dictate burn durations and subsequently alter the exact amount of ΔV required to execute a transfer in an actual application. Other works have taken a more mission-specific approach to developing rendezvous strategies incorporating vehicle specifications into the transfer design [19, 26, 27]. The impulsive modeling can be adapted by all vehicles to approximate the proper ΔV adjustment to make the results accurate. STK's maneuver summary report from this thesis's full ephemeris dynamics realization portion approximates finite burn durations and ΔV change between the finite and impulsive modeling. No generic finite estimates for the 500 kg spacecraft were longer than 14.5 seconds.

VVs approaching Gateway may consider using low-thrust propulsion such as ion or Hall effect thrusters. The impulsive modeling does not incorporate the nuances of these continuous thrust transfers. However, the required ΔV for the impulsive trajectories can be used to check their feasibility for a low-thrust spacecraft. Using Northrop Grumman's Mission Extension Vehicle (MEV), a geostationary orbit satellite servicing spacecraft capable of RPOD, as a performance baseline, one can gauge the feasibility of a low-thrust implementation of the proposed transfers [3]. MEV-1 had a mass of 2330 kg, and let us assume the two thrusters were capable of 580 mN of thrust [2]. Using the following equation:

$$t = \frac{\Delta V m}{T}$$

where ΔV is required ΔV for a transfer, m is the mass of spacecraft, and T is engine thrust, one can approximate the thrust duration, t , required for a low-thrust vehicle. Using this equation for the most expensive transfer of 21.70 m/s that has a TOF of 3.85 h, the required thrust would take just over 12 hours or roughly three times the transfer's duration. This requirement is not achievable, but this is the most demanding burn in the strategy near Periselene. The second highest Periselene region burn requires 5.00 m/s of ΔV . This transfer would require 2.79 hours of thrust or 72.5% of the transfer to require constant thrusting. Not optimal but not unachievable. All 16 transfers remaining are not as demanding and are feasible for a low-thrust vehicle by this approximation.

5.3 Suggested Continuations

This section proposes two avenues for which one could make improvements and continue the presented work. One considers iterating the chosen strategy again to look for improvements in ΔV efficiency, and the other takes a natural progression of the work into more realistic dynamic modeling.

5.3.1 Revisions to Presented Work

The work followed a natural progression, making strategy selections based on the analysis presented. However, one could more finely tune the choices made. For instance, consider the selection of suboptimal axes. The axes were more or less randomly selected near the optimal until a safe alternative appeared. An iterative scheme could be developed to analyze all available suboptimal axes. Each safe axis's ΔV would be recorded and the minimum selected. Safe suboptimal axes were selected for the proposed strategy, but it is unknown if

they are global minimums across all safe axes.

The region-to-region transfer results had non-negligible ΔV requirements. These numbers could be reduced by tuning the axes further. A trade between ΔV required to hold for a given axis can be balanced with the required ΔV to transfer with the neighboring region's axes. This ends up causing a balancing act between all six axes, but it could result in significant reductions in the region-to-region transfer costs, further optimizing the overall strategy.

Lastly, one could dive into a more combinatorial approach to designing approach schemes. For example, performing two transfers in one region and the third in the next would result in a faster approach. The author believes that this reduces the operational applicability of the overall strategy approach, as some combinations will be unsafe. However, there are certainly more time-efficient combinations that remain safe. Combinations like this could be explored to find the most time-efficient path to approach Gateway.

5.3.2 Natural Next Steps

Building off this work naturally entails addressing the limitations of the present work. These include but are not limited to, implementing the strategy in the elliptical restricted dynamics and more testing in a full ephemeris model. Innocenti's work showed that his proposed strategies became safer in more realistic dynamics modeling [27]. These models could potentially reveal the "all-in-one" approach scheme to be safe for some regions. Such a result would open up more avenues for approaching the station and make the strategy more time-efficient. A complete ephemeris study could build out the nine revolution-specific diagrams, giving the strategy complete coverage across the NRHO.

Modeling in more realistic dynamics would produce more realistic estimates for ΔV requirements.

Building on this train of thought brings the work into studies implementing finite and low-thrust vehicles into the transfer construction. Franzini explored both areas in his work [18, 19]. These methods can be adopted into the trajectory construction process to create more finely tuned strategies for a specific mission attempting a rendezvous with Gateway.

As was discussed in Chapter 3, this thesis only focused on the trajectory design of the approach phase. The strategy can be expanded to incorporate guidance and control elements as Innocenti did with his strategy or to incorporate the transfer phase into the strategy similar to Ueda's work with invariant manifolds to reduce significant phasing maneuver costs [26, 45]. Guidance and control aspects are as important as the trajectories themselves in RPOD and cannot be ignored when implementing a comprehensive approach strategy. Positional and velocity errors accumulate much more rapidly in the Periselene region. If the vehicle's guidance system cannot correct these errors fast enough, it may lead to the strategies for these regions being too risky to consider. Concepts like phasing manifolds reduce the time-sensitive nature and applicability of the strategy but are a standard tool being studied to reduce ΔV costs for cislunar missions.

All of these are enticing avenues to consider exploring. Each builds off the present work and either improves the accuracy of the current results, ΔV efficiency, and or applicability. More work is needed to make this strategy executable by a real-world mission. However, the work presented serves as a solid first pass in enabling time-sensitive approaches with the Lunar Gateway.

5.4 Conclusion

This work presented a safety-driven, time-sensitive rendezvous approach strategy with the Lunar Gateway. The currently-proposed strategies were discussed, and their limitations were

identified. The thesis addressed the present hole in time-sensitive strategies necessitating an approach with the Gateway outside the Aposelene region. The work emphasized operational applicability and trajectory safety, only considering options that were shown to be entirely safe and strategies that fell in line with current rendezvous operational standards.

The work defined six unique regions of the orbit to design region-specific strategies blended to define a strategy for the entire orbit. Axes within each region were identified that enable safe yet ΔV -efficient station-keeping throughout each region. Safe alternatives were identified and adopted for regions with high station-keeping costs to minimize the holding costs for these instances. Transfers between HPs and Regions were constructed, allowing a VV to effectively hold an HP around the entire NRHO and hop HP to HP to approach the station. These approach schemes were realized within a full ephemeris dynamics model to gauge the impacts the CR3BP simplifications had on the strategy design results. The identified strategy was implemented within an operationally framed transit diagram to enable the efficient execution of the strategy in an operational setting.

The results of this thesis contribute to the growing work addressing Gateway RPOD. Should the Lunar Gateway program continue as currently proposed, the strategies developed in this work can help seed future missions' rendezvous with the station. The hope is that a time-sensitive rendezvous will never be required, but if an instance arises, these approaches can help make one feasible.

Bibliography

- [1] NASA says a design error is behind the failure of a 2015 SpaceX mission. URL <https://qz.com/1227488/elon-musk-spacex-nasa-says-a-design-error-is-behind-the-failure-of-the-2015-crs-7-r>
- [2] XR-5 hall thruster - electric propulsion thruster | SatCatalog. URL <https://www.satcatalog.com/component/xr-5-hall-thruster/>.
- [3] MEV-1 & 2 (mission extension vehicle-1 and -2). URL <https://www.eoportal.org/satellite-missions/mev-1>.
- [4] Moon to mars architecture - white papers - why NRHO: The artemis orbit - NASA. URL <https://www.nasa.gov/moontomarsarchitecture-whitepapers/>.
- [5] Russian spacecraft progress m-27m 'out of control'. URL <https://www.bbc.com/news/world-europe-32517447>.
- [6] Jordan S. Abell, Peter Z. Schulte, Fred D. Clark, Peter T. Spehar, and David C. Woffinden. Orion GN&c sequencing for off-nominal rendezvous, proximity operations, and docking. URL <https://ntrs.nasa.gov/citations/20205011555>. NTRS Author Affiliations: Draper Laboratory, Johnson Space Center NTRS Report/Patent Number: AAS 21-439 NTRS Document ID: 20205011555 NTRS Research Center: Johnson Space Center (JSC).
- [7] Buzz Aldrin. Line-of-sight guidance techniques for manned orbital rendezvous. URL <https://dspace.mit.edu/handle/1721.1/12652>. Accepted: 2008-10-02T19:16:59Z.

- [8] ANSYS. Ansys STK | digital mission engineering software, 2024. URL <https://www.ansys.com/products/missions/ansys-stk>.
- [9] Massachusetts Bay Transportation Authority. Maps | MBTA. URL <https://www.mbta.com/maps>.
- [10] Eric Berger. Starliner’s flight to the space station was far wilder than most of us thought. URL <https://arstechnica.com/space/2025/04/the-harrowing-story-of-what-flying-starliner-was-like-when-its-thrusters-failed/>.
- [11] Nicoletta Bloise, Elisa Capello, Matteo Dentis, and Elisabetta Punta. Obstacle avoidance with potential field applied to a rendezvous maneuver. 7(10):1042. ISSN 2076-3417. doi: 10.3390/app7101042. URL <https://www.mdpi.com/2076-3417/7/10/1042>. Number: 10 Publisher: Multidisciplinary Digital Publishing Institute.
- [12] Lorenzo Bucci, Lavagna Michèle, and Florian Renk. Relative dynamics analysis and rendezvous techniques for lunar near rectilinear halo orbits — IAF digital library. In *IAC 2017 congress proceedings*. International Astronautical Federation. URL <https://dl.iafastro.directory/event/IAC-2017/paper/40894/>.
- [13] W. H. Clohessy and R. S. Wiltshire. Terminal guidance system for satellite rendezvous. 27(9):653–658. doi: 10.2514/8.8704. URL <https://arc.aiaa.org/doi/10.2514/8.8704>. Publisher: American Institute of Aeronautics and Astronautics.
- [14] ESA. How much does it cost? URL https://www.esa.int/Science_Exploration/Human_and_Robotic_Exploration/International_Space_Station/How_much_does_it_cost.
- [15] Dan Falk. NASA’s deep space gateway seen as key to bold plan

- for mars and beyond. URL <https://www.nbcnews.com/mach/science/nasa-s-deep-space-gateway-seen-key-bold-plan-mars-ncna838056>.
- [16] Wigbert Fehse. *Automated Rendezvous and Docking of Spacecraft*. Cambridge Aerospace Series. Cambridge University Press. ISBN 978-0-521-82492-7. doi: 10.1017/CBO9780511543388. URL <https://www.cambridge.org/core/books/automated-rendezvous-and-docking-of-spacecraft/73C7A1056AF42242D7B5549E8BB1FE17>.
- [17] Giovanni Fereoli, Hanspeter Schaub, and Pierluigi Di Lizia. Meta-reinforcement learning for spacecraft proximity operations guidance and control in cislunar space. pages 1–13. ISSN 0022-4650. doi: 10.2514/1.A36100. URL <https://arc.aiaa.org/doi/10.2514/1.A36100>. Publisher: American Institute of Aeronautics and Astronautics.
- [18] Giovanni Franzini and Mario Innocenti. Relative motion dynamics in the restricted three-body problem. 56(5):1322–1337. ISSN 0022-4650. doi: 10.2514/1.A34390. URL <https://arc.aiaa.org/doi/10.2514/1.A34390>. Publisher: American Institute of Aeronautics and Astronautics.
- [19] Giovanni Franzini, Mario Innocenti, and Massimo Casasco. Impulsive rendezvous maneuvers in the restricted three-body problem. In *AIAA Scitech 2019 Forum*, AIAA SciTech Forum. American Institute of Aeronautics and Astronautics, . doi: 10.2514/6.2019-1429. URL <https://arc.aiaa.org/doi/10.2514/6.2019-1429>.
- [20] Giovanni Franzini, Mario Innocenti, and Massimo Casasco. An adjoint-based method for continuous-thrust relative maneuver computation in the restricted three-body problem. In *2021 American Control Conference (ACC)*, pages 4276–4281, . doi: 10.23919/ACC50511.2021.9482823. URL <https://ieeexplore.ieee.org/document/9482823/?arnumber=9482823>. ISSN: 2378-5861.

- [21] Robert B. Friend. Orbital express program summary and mission overview. In *Sensors and Systems for Space Applications II*, volume 6958, pages 11–21. SPIE. doi: 10.1117/12.783792. URL <https://www.spiedigitallibrary.org/conference-proceedings-of-spie/6958/695803/Orbital-Express-program-summary-and-mission-overview/10.1117/12.783792.full>.
- [22] John L. Goodman. History of space shuttle rendezvous. URL <https://ntrs.nasa.gov/citations/20110023479>. NTRS Author Affiliations: United Space Alliance NTRS Report/Patent Number: JSC-CN-24483 NTRS Document ID: 20110023479 NTRS Research Center: Johnson Space Center (JSC).
- [23] William Harwood. NASA: No danger to space station after supply rocket blows up - CBS news. URL <https://www.cbsnews.com/news/rocket-crash-no-immediate-threat-to-station-but-cause-is-unknown/>.
- [24] The MathWorks Inc. fsolve, 2024. URL <https://www.mathworks.com/help/optim/ug/fsolve.html>.
- [25] The MathWorks Inc. Ode78, 2024. URL <https://www.mathworks.com/help/matlab/ref/ode78.html>.
- [26] Mario Innocenti, Giordana Bucchioni, Giovanni Franzini, Michele Galullo, Fabio D’Onofrio, Alexander Cropp, and Massimo Casasco. Dynamics and control analysis during rendezvous in non-keplerian earth—moon orbits. 3, . ISSN 2673-5075. doi: 10.3389/frspt.2022.929179. URL <https://www.frontiersin.org/journals/space-technologies/articles/10.3389/frspt.2022.929179/full>. Publisher: Frontiers.

- [27] Mario Innocenti, Fabio D’Onofrio, and Giordana Bucchioni. Failure mitigation during rendezvous in cislunar orbit. In *AIAA SCITECH 2022 Forum*, AIAA SciTech Forum. American Institute of Aeronautics and Astronautics, . doi: 10.2514/6.2022-0861. URL <https://arc.aiaa.org/doi/10.2514/6.2022-0861>.
- [28] IRSIS. International deep space interoperability standards. URL <https://internationaldeepspacestandards.com/>.
- [29] Wang Sang Koon, Martin W. Lo, Jerrold E. Marsden, and Shane D. Ross. Dynamical systems, the three-body problem and space mission design. pages 1167–1181. ISBN 978-981-02-4359-3. doi: 10.1142/9789812792617_0222. URL https://www.worldscientific.com/doi/10.1142/9789812792617_0222.
- [30] Diane S. Koons and Craig Schreiber. Risk mitigation approach to commercial resupply to the international space station. URL <https://ntrs.nasa.gov/citations/20100014822>. NTRS Author Affiliations: NASA Johnson Space Center, NASA Kennedy Space Center NTRS Report/Patent Number: JSC-CN-19846 NTRS Document ID: 20100014822 NTRS Research Center: Johnson Space Center (JSC).
- [31] Jet Propulsion Laboratory. Navigation and ancillary information facility - DSG, . URL https://naif.jpl.nasa.gov/pub/naif/misc/MORE_PROJECTS/DSG/.
- [32] Jet Propulsion Laboratory. Three-body periodic orbits, . URL https://ssd.jpl.nasa.gov/tools/periodic_orbits.html.
- [33] David E. Lee. White paper: Gateway destination orbit model: A continuous 15 year NRHO reference trajectory. URL <https://ntrs.nasa.gov/citations/20190030294>. NTRS Author Affiliations: NASA Johnson Space Center NTRS Report/Patent Number: JSC-E-DAA-TN72594 NTRS Document ID: 20190030294 NTRS Research Center: Johnson Space Center (JSC).

- [34] Richard J. Luquette and Robert M. Sanner. Linear state-space representation of the dynamics of relative motion, based on restricted three body dynamics. URL <https://ntrs.nasa.gov/citations/20040027695>. NTRS Author Affiliations: NASA Goddard Space Flight Center, Maryland Univ. NTRS Document ID: 20040027695 NTRS Research Center: Goddard Space Flight Center (GSFC).
- [35] Kuljit Mand. Rendezvous and proximity operations at the earth-moon l2 lagrange point: Navigation analysis for preliminary trajectory design.
- [36] Piero Miotto. Designing and validating proximity operations rendezvous and approach trajectories for the cygnus mission. In *AIAA Guidance, Navigation, and Control Conference*, Guidance, Navigation, and Control and Co-located Conferences. American Institute of Aeronautics and Astronautics. doi: 10.2514/6.2010-8446. URL <https://doi.org/10.2514/6.2010-8446>.
- [37] Ryo Nakamura, Junji Kikuchi, Takahiro Sasaki, Yuki Matsumoto, Moeko Hidaka, Naomi Murakami, Satoshi Ueda, and Naoki Satoh. Rendezvous trajectory design of logistics resupply missions to the lunar gateway in near-rectilinear halo orbit. 10 (2):144–154. ISSN 2468-8967. doi: 10.1016/j.jsse.2023.03.001. URL <https://www.sciencedirect.com/science/article/pii/S2468896723000277>.
- [38] NASA. Gateway space station - NASA. URL <https://www.nasa.gov/reference/gateway-about/>.
- [39] Michael Neufeld. The world's first space rendezvous. URL <https://airandspace.si.edu/stories/editorial/worlds-first-space-rendezvous>.
- [40] C. Sagan. *Cosmos*. Ballantine Books, 1980. ISBN 9780345331359.

- [41] Yuki Sato, Kenji Kitamura, and Takeya Shima. Spacecraft rendezvous utilizing invariant manifolds for a halo orbit. 58(5):261–269. doi: 10.2322/tjsass.58.261.
- [42] Michael Sheetz. Northrop grumman MEV-1 spacecraft services intelsat 901 satellite. URL <https://www.cnbc.com/2020/04/17/northrop-grumman-mev-1-spacecraft-services-intelsat-901-satellite.html>.
- [43] Gail Skowran and Faisal Ali. Significant incidents & close calls in human spaceflight. URL <https://sma.nasa.gov/SignificantIncidents/>.
- [44] N.G. Tyson. *Death By Black Hole: And Other Cosmic Quandaries*. WW Norton, 2007. ISBN 9780393062243.
- [45] Satoshi Ueda, Naomi Murakami, and Toshinori Ikenaga. A study on rendezvous trajectory design utilizing invariant manifolds of cislunar periodic orbits. In *AIAA Guidance, Navigation, and Control Conference*, AIAA SciTech Forum. American Institute of Aeronautics and Astronautics. doi: 10.2514/6.2017-1729. URL <https://arc.aiaa.org/doi/10.2514/6.2017-1729>.
- [46] Jen Wang. New space policy directive calls for human expansion across solar system - NASA. URL <https://www.nasa.gov/news-release/new-space-policy-directive-calls-for-human-expansion-across-solar-system/>.
Section: Commercial Space.
- [47] A. Weir. *The Martian: A Novel*. Random House Publishing Group, 2014. ISBN 9780804139021.
- [48] A. Weir. *Project Hail Mary: A Novel*. Random House Publishing Group, 2021. ISBN 9780593135204.

- [49] James R. Wertz and Robert Bell. Autonomous rendezvous and docking technologies — status and prospects | microcosm. Microcosm Inc. URL <https://smad.com/autonomous-rendezvous-docking-technologies-status-prospects/>.
- [50] P.H. Whipple. Some characteristics of coelliptic orbits - case 610.

Appendices

Appendix A

CR3BP 9:2 NRHO Reference Orbit

Look Up Table

Appendix A lists the states of the 9:2 NRHO CR3BP propagated reference orbit as discussed in Section 3.3.

Table A.1: 9:2 NRHO CR3BP Reference Orbit

Time (TU)	x (LU)	y (LU)	z (LU)	\dot{x} (LU/TU)	\dot{y} (LU/TU)	\dot{z} (LU/TU)
0.000000e+00	1.018993e+00	-2.848416e-27	-1.799231e-01	-3.215774e-13	-9.656383e-02	-4.865318e-12
1.471120e-03	1.018993e+00	-1.420568e-04	-1.799225e-01	-1.831493e-04	-9.656337e-02	7.562487e-04
2.942240e-03	1.018993e+00	-2.841122e-04	-1.799209e-01	-3.662983e-04	-9.656198e-02	1.512502e-03
4.413361e-03	1.018992e+00	-4.261649e-04	-1.799181e-01	-5.494468e-04	-9.655966e-02	2.268764e-03
5.884481e-03	1.018991e+00	-5.682135e-04	-1.799142e-01	-7.325944e-04	-9.655641e-02	3.025040e-03
7.355601e-03	1.018990e+00	-7.102566e-04	-1.799092e-01	-9.157410e-04	-9.655224e-02	3.781335e-03
8.826721e-03	1.018988e+00	-8.522929e-04	-1.799031e-01	-1.098886e-03	-9.654714e-02	4.537652e-03
1.029784e-02	1.018987e+00	-9.943211e-04	-1.798958e-01	-1.282030e-03	-9.654112e-02	5.293996e-03
1.176896e-02	1.018985e+00	-1.136340e-03	-1.798875e-01	-1.465171e-03	-9.653416e-02	6.050373e-03
1.324008e-02	1.018982e+00	-1.278347e-03	-1.798780e-01	-1.648311e-03	-9.652628e-02	6.806786e-03
1.471120e-02	1.018980e+00	-1.420343e-03	-1.798675e-01	-1.831447e-03	-9.651747e-02	7.563240e-03
1.618232e-02	1.018977e+00	-1.562324e-03	-1.798558e-01	-2.014582e-03	-9.650774e-02	8.319740e-03
1.765344e-02	1.018974e+00	-1.704291e-03	-1.798430e-01	-2.197713e-03	-9.649707e-02	9.076290e-03
1.912456e-02	1.018970e+00	-1.846242e-03	-1.798291e-01	-2.380840e-03	-9.648548e-02	9.832895e-03
2.059568e-02	1.018967e+00	-1.988174e-03	-1.798141e-01	-2.563965e-03	-9.647296e-02	1.058956e-02
2.206680e-02	1.018963e+00	-2.130088e-03	-1.797979e-01	-2.747085e-03	-9.645951e-02	1.134629e-02
2.353792e-02	1.018959e+00	-2.271981e-03	-1.797807e-01	-2.930201e-03	-9.644513e-02	1.210308e-02
2.500904e-02	1.018954e+00	-2.413852e-03	-1.797623e-01	-3.113313e-03	-9.642982e-02	1.285995e-02
2.648016e-02	1.018950e+00	-2.555700e-03	-1.797428e-01	-3.296420e-03	-9.641358e-02	1.361690e-02
2.795128e-02	1.018945e+00	-2.697524e-03	-1.797222e-01	-3.479522e-03	-9.639642e-02	1.437393e-02
2.942240e-02	1.018939e+00	-2.839321e-03	-1.797005e-01	-3.662619e-03	-9.637832e-02	1.513105e-02
3.089352e-02	1.018934e+00	-2.981091e-03	-1.796777e-01	-3.845710e-03	-9.635929e-02	1.588826e-02
3.236464e-02	1.018928e+00	-3.122833e-03	-1.796538e-01	-4.028796e-03	-9.633933e-02	1.664557e-02
3.383577e-02	1.018922e+00	-3.264544e-03	-1.796287e-01	-4.211875e-03	-9.631844e-02	1.740297e-02
3.530689e-02	1.018916e+00	-3.406224e-03	-1.796026e-01	-4.394948e-03	-9.629662e-02	1.816048e-02
3.677801e-02	1.018909e+00	-3.547872e-03	-1.795753e-01	-4.578014e-03	-9.627387e-02	1.891811e-02
3.824913e-02	1.018902e+00	-3.689485e-03	-1.795469e-01	-4.761074e-03	-9.625018e-02	1.967584e-02
3.972025e-02	1.018895e+00	-3.831062e-03	-1.795174e-01	-4.944126e-03	-9.622556e-02	2.043370e-02

Time (TU)	x (LU)	y (LU)	z (LU)	\dot{x} (LU/TU)	\dot{y} (LU/TU)	\dot{z} (LU/TU)
4.119137e-02	1.018888e+00	-3.972603e-03	-1.794868e-01	-5.127171e-03	-9.620001e-02	2.119168e-02
4.266249e-02	1.018880e+00	-4.114106e-03	-1.794551e-01	-5.310208e-03	-9.617352e-02	2.194979e-02
4.413361e-02	1.018872e+00	-4.255568e-03	-1.794222e-01	-5.493236e-03	-9.614610e-02	2.270803e-02
4.560473e-02	1.018864e+00	-4.396990e-03	-1.793883e-01	-5.676257e-03	-9.611775e-02	2.346641e-02
4.707585e-02	1.018855e+00	-4.538369e-03	-1.793532e-01	-5.859269e-03	-9.608846e-02	2.422494e-02
4.854697e-02	1.018846e+00	-4.679705e-03	-1.793170e-01	-6.042272e-03	-9.605823e-02	2.498361e-02
5.001809e-02	1.018837e+00	-4.820995e-03	-1.792797e-01	-6.225266e-03	-9.602707e-02	2.574243e-02
5.148921e-02	1.018828e+00	-4.962239e-03	-1.792412e-01	-6.408250e-03	-9.599497e-02	2.650142e-02
5.296033e-02	1.018819e+00	-5.103435e-03	-1.792017e-01	-6.591225e-03	-9.596193e-02	2.726056e-02
5.443145e-02	1.018809e+00	-5.244582e-03	-1.791610e-01	-6.774189e-03	-9.592795e-02	2.801987e-02
5.590257e-02	1.018799e+00	-5.385678e-03	-1.791193e-01	-6.957143e-03	-9.589304e-02	2.877935e-02
5.737369e-02	1.018788e+00	-5.526722e-03	-1.790764e-01	-7.140087e-03	-9.585718e-02	2.953901e-02
5.884481e-02	1.018778e+00	-5.667712e-03	-1.790323e-01	-7.323019e-03	-9.582039e-02	3.029885e-02
6.031593e-02	1.018767e+00	-5.808648e-03	-1.789872e-01	-7.505941e-03	-9.578265e-02	3.105887e-02
6.178705e-02	1.018756e+00	-5.949527e-03	-1.789410e-01	-7.688851e-03	-9.574397e-02	3.181908e-02
6.325817e-02	1.018744e+00	-6.090349e-03	-1.788936e-01	-7.871749e-03	-9.570435e-02	3.257949e-02
6.472929e-02	1.018732e+00	-6.231112e-03	-1.788451e-01	-8.054635e-03	-9.566379e-02	3.334010e-02
6.620041e-02	1.018720e+00	-6.371815e-03	-1.787955e-01	-8.237509e-03	-9.562228e-02	3.410092e-02
6.767153e-02	1.018708e+00	-6.512455e-03	-1.787448e-01	-8.420370e-03	-9.557983e-02	3.486194e-02
6.914265e-02	1.018696e+00	-6.653033e-03	-1.786929e-01	-8.603218e-03	-9.553643e-02	3.562318e-02
7.061377e-02	1.018683e+00	-6.793546e-03	-1.786400e-01	-8.786053e-03	-9.549208e-02	3.638464e-02
7.208489e-02	1.018670e+00	-6.933993e-03	-1.785859e-01	-8.968875e-03	-9.544679e-02	3.714633e-02
7.355601e-02	1.018656e+00	-7.074373e-03	-1.785307e-01	-9.151682e-03	-9.540055e-02	3.790824e-02
7.502713e-02	1.018643e+00	-7.214684e-03	-1.784743e-01	-9.334476e-03	-9.535336e-02	3.867039e-02
7.649825e-02	1.018629e+00	-7.354925e-03	-1.784169e-01	-9.517255e-03	-9.530522e-02	3.943278e-02
7.796937e-02	1.018615e+00	-7.495094e-03	-1.783583e-01	-9.700019e-03	-9.525613e-02	4.019541e-02
7.944049e-02	1.018600e+00	-7.635191e-03	-1.782986e-01	-9.882768e-03	-9.520609e-02	4.095829e-02
8.091161e-02	1.018586e+00	-7.775213e-03	-1.782378e-01	-1.006550e-02	-9.515509e-02	4.172142e-02
8.238273e-02	1.018571e+00	-7.915160e-03	-1.781759e-01	-1.024822e-02	-9.510314e-02	4.248482e-02
8.385385e-02	1.018556e+00	-8.055029e-03	-1.781128e-01	-1.043092e-02	-9.505024e-02	4.324848e-02
8.532497e-02	1.018540e+00	-8.194820e-03	-1.780486e-01	-1.061361e-02	-9.499638e-02	4.401240e-02
8.679609e-02	1.018524e+00	-8.334531e-03	-1.779833e-01	-1.079628e-02	-9.494156e-02	4.477661e-02
8.826721e-02	1.018508e+00	-8.474160e-03	-1.779169e-01	-1.097893e-02	-9.488578e-02	4.554109e-02
8.973833e-02	1.018492e+00	-8.613707e-03	-1.778493e-01	-1.116157e-02	-9.482905e-02	4.630586e-02
9.120945e-02	1.018476e+00	-8.753170e-03	-1.777806e-01	-1.134419e-02	-9.477135e-02	4.707091e-02
9.268057e-02	1.018459e+00	-8.892547e-03	-1.777108e-01	-1.152679e-02	-9.471270e-02	4.783627e-02
9.415169e-02	1.018442e+00	-9.031837e-03	-1.776399e-01	-1.170937e-02	-9.465308e-02	4.860192e-02
9.562281e-02	1.018424e+00	-9.171038e-03	-1.775678e-01	-1.189193e-02	-9.459250e-02	4.936788e-02
9.709393e-02	1.018407e+00	-9.310150e-03	-1.774946e-01	-1.207448e-02	-9.453095e-02	5.013414e-02
9.856505e-02	1.018389e+00	-9.449171e-03	-1.774203e-01	-1.225701e-02	-9.446843e-02	5.090073e-02
1.000362e-01	1.018371e+00	-9.588098e-03	-1.773449e-01	-1.243951e-02	-9.440495e-02	5.166763e-02
1.015073e-01	1.018352e+00	-9.726932e-03	-1.772683e-01	-1.262200e-02	-9.434050e-02	5.243486e-02
1.029784e-01	1.018333e+00	-9.865670e-03	-1.771906e-01	-1.280447e-02	-9.427508e-02	5.320242e-02
1.044495e-01	1.018315e+00	-1.000431e-02	-1.771118e-01	-1.298692e-02	-9.420869e-02	5.397032e-02
1.059207e-01	1.018295e+00	-1.014285e-02	-1.770318e-01	-1.316934e-02	-9.414132e-02	5.473857e-02
1.073918e-01	1.018276e+00	-1.028130e-02	-1.769507e-01	-1.335175e-02	-9.407298e-02	5.550715e-02
1.088629e-01	1.018256e+00	-1.041964e-02	-1.768685e-01	-1.353414e-02	-9.400367e-02	5.627610e-02
1.103340e-01	1.018236e+00	-1.055788e-02	-1.767851e-01	-1.371650e-02	-9.393338e-02	5.704540e-02
1.118051e-01	1.018216e+00	-1.069601e-02	-1.767007e-01	-1.389884e-02	-9.386211e-02	5.781506e-02
1.132763e-01	1.018195e+00	-1.083404e-02	-1.766150e-01	-1.408116e-02	-9.378986e-02	5.858509e-02
1.147474e-01	1.018174e+00	-1.097197e-02	-1.765283e-01	-1.426346e-02	-9.371663e-02	5.935550e-02
1.162185e-01	1.018153e+00	-1.110978e-02	-1.764404e-01	-1.444573e-02	-9.364242e-02	6.012629e-02

Time (TU)	x (LU)	y (LU)	z (LU)	\dot{x} (LU/TU)	\dot{y} (LU/TU)	\dot{z} (LU/TU)
1.176896e-01	1.018132e+00	-1.124748e-02	-1.763514e-01	-1.462798e-02	-9.356722e-02	6.089747e-02
1.191607e-01	1.018110e+00	-1.138508e-02	-1.762612e-01	-1.481021e-02	-9.349104e-02	6.166903e-02
1.206319e-01	1.018088e+00	-1.152256e-02	-1.761699e-01	-1.499241e-02	-9.341387e-02	6.244099e-02
1.221030e-01	1.018066e+00	-1.165992e-02	-1.760775e-01	-1.517459e-02	-9.333571e-02	6.321336e-02
1.235741e-01	1.018043e+00	-1.179717e-02	-1.759839e-01	-1.535675e-02	-9.325656e-02	6.398613e-02
1.250452e-01	1.018021e+00	-1.193430e-02	-1.758892e-01	-1.553888e-02	-9.317642e-02	6.475932e-02
1.265163e-01	1.017998e+00	-1.207132e-02	-1.757934e-01	-1.572099e-02	-9.309528e-02	6.553293e-02
1.279875e-01	1.017974e+00	-1.220821e-02	-1.756964e-01	-1.590307e-02	-9.301315e-02	6.630696e-02
1.294586e-01	1.017951e+00	-1.234499e-02	-1.755983e-01	-1.608512e-02	-9.293002e-02	6.708142e-02
1.309297e-01	1.017927e+00	-1.248163e-02	-1.754991e-01	-1.626715e-02	-9.284590e-02	6.785632e-02
1.324008e-01	1.017903e+00	-1.261816e-02	-1.753987e-01	-1.644915e-02	-9.276077e-02	6.863167e-02
1.338719e-01	1.017879e+00	-1.275456e-02	-1.752971e-01	-1.663112e-02	-9.267464e-02	6.940746e-02
1.353431e-01	1.017854e+00	-1.289083e-02	-1.751944e-01	-1.681307e-02	-9.258750e-02	7.018371e-02
1.368142e-01	1.017829e+00	-1.302697e-02	-1.750906e-01	-1.699499e-02	-9.249936e-02	7.096041e-02
1.382853e-01	1.017804e+00	-1.316299e-02	-1.749857e-01	-1.717689e-02	-9.241021e-02	7.173759e-02
1.397564e-01	1.017779e+00	-1.329887e-02	-1.748796e-01	-1.735875e-02	-9.232006e-02	7.251523e-02
1.412275e-01	1.017753e+00	-1.343461e-02	-1.747723e-01	-1.754058e-02	-9.222888e-02	7.329336e-02
1.426987e-01	1.017727e+00	-1.357022e-02	-1.746639e-01	-1.772239e-02	-9.213670e-02	7.407196e-02
1.441698e-01	1.017701e+00	-1.370570e-02	-1.745544e-01	-1.790417e-02	-9.204350e-02	7.485106e-02
1.456409e-01	1.017674e+00	-1.384104e-02	-1.744437e-01	-1.808592e-02	-9.194928e-02	7.563066e-02
1.471120e-01	1.017648e+00	-1.397624e-02	-1.743318e-01	-1.826763e-02	-9.185405e-02	7.641076e-02
1.485831e-01	1.017621e+00	-1.411129e-02	-1.742189e-01	-1.844932e-02	-9.175779e-02	7.719137e-02
1.500543e-01	1.017593e+00	-1.424621e-02	-1.741047e-01	-1.863098e-02	-9.166050e-02	7.797249e-02
1.515254e-01	1.017566e+00	-1.438098e-02	-1.739894e-01	-1.881260e-02	-9.156219e-02	7.875413e-02
1.529965e-01	1.017538e+00	-1.451561e-02	-1.738730e-01	-1.899420e-02	-9.146286e-02	7.953631e-02
1.544676e-01	1.017510e+00	-1.465009e-02	-1.737554e-01	-1.917576e-02	-9.136249e-02	8.031901e-02
1.559387e-01	1.017482e+00	-1.478442e-02	-1.736367e-01	-1.935729e-02	-9.126109e-02	8.110226e-02
1.574099e-01	1.017453e+00	-1.491860e-02	-1.735168e-01	-1.953879e-02	-9.115865e-02	8.188605e-02
1.588810e-01	1.017424e+00	-1.505263e-02	-1.733958e-01	-1.972025e-02	-9.105518e-02	8.267040e-02
1.603521e-01	1.017395e+00	-1.518650e-02	-1.732736e-01	-1.990169e-02	-9.095067e-02	8.345531e-02
1.618232e-01	1.017366e+00	-1.532023e-02	-1.731502e-01	-2.008308e-02	-9.084511e-02	8.424079e-02
1.632943e-01	1.017336e+00	-1.545379e-02	-1.730257e-01	-2.026445e-02	-9.073852e-02	8.502683e-02
1.647655e-01	1.017306e+00	-1.558720e-02	-1.729001e-01	-2.044578e-02	-9.063087e-02	8.581346e-02
1.662366e-01	1.017276e+00	-1.572045e-02	-1.727732e-01	-2.062707e-02	-9.052218e-02	8.660068e-02
1.677077e-01	1.017245e+00	-1.585354e-02	-1.726453e-01	-2.080833e-02	-9.041244e-02	8.738848e-02
1.691788e-01	1.017215e+00	-1.598646e-02	-1.725161e-01	-2.098956e-02	-9.030164e-02	8.817689e-02
1.706499e-01	1.017184e+00	-1.611923e-02	-1.723858e-01	-2.117074e-02	-9.018979e-02	8.896590e-02
1.721211e-01	1.017152e+00	-1.625182e-02	-1.722544e-01	-2.135189e-02	-9.007687e-02	8.975553e-02
1.735922e-01	1.017121e+00	-1.638425e-02	-1.721217e-01	-2.153301e-02	-8.996290e-02	9.054578e-02
1.750633e-01	1.017089e+00	-1.651651e-02	-1.719879e-01	-2.171409e-02	-8.984786e-02	9.133666e-02
1.765344e-01	1.017057e+00	-1.664861e-02	-1.718530e-01	-2.189513e-02	-8.973176e-02	9.212817e-02
1.780055e-01	1.017025e+00	-1.678053e-02	-1.717169e-01	-2.207613e-02	-8.961458e-02	9.292032e-02
1.794767e-01	1.016992e+00	-1.691227e-02	-1.715796e-01	-2.225709e-02	-8.949634e-02	9.371312e-02
1.809478e-01	1.016959e+00	-1.704385e-02	-1.714412e-01	-2.243802e-02	-8.937702e-02	9.450658e-02
1.824189e-01	1.016926e+00	-1.717524e-02	-1.713015e-01	-2.261890e-02	-8.925662e-02	9.530070e-02
1.838900e-01	1.016892e+00	-1.730646e-02	-1.711608e-01	-2.279975e-02	-8.913514e-02	9.609549e-02
1.853611e-01	1.016859e+00	-1.743750e-02	-1.710188e-01	-2.298056e-02	-8.901258e-02	9.689096e-02
1.868323e-01	1.016825e+00	-1.756836e-02	-1.708757e-01	-2.316132e-02	-8.888893e-02	9.768711e-02
1.883034e-01	1.016791e+00	-1.769903e-02	-1.707314e-01	-2.334205e-02	-8.876419e-02	9.848396e-02
1.897745e-01	1.016756e+00	-1.782952e-02	-1.705859e-01	-2.352273e-02	-8.863836e-02	9.928151e-02
1.912456e-01	1.016721e+00	-1.795982e-02	-1.704393e-01	-2.370337e-02	-8.851144e-02	1.000798e-01
1.927167e-01	1.016686e+00	-1.808994e-02	-1.702915e-01	-2.388397e-02	-8.838342e-02	1.008787e-01

Time (TU)	x (LU)	y (LU)	z (LU)	\dot{x} (LU/TU)	\dot{y} (LU/TU)	\dot{z} (LU/TU)
1.941879e-01	1.016651e+00	-1.821987e-02	-1.701425e-01	-2.406453e-02	-8.825429e-02	1.016784e-01
1.956590e-01	1.016616e+00	-1.834961e-02	-1.699923e-01	-2.424504e-02	-8.812407e-02	1.024788e-01
1.971301e-01	1.016580e+00	-1.847915e-02	-1.698409e-01	-2.442551e-02	-8.799273e-02	1.032800e-01
1.986012e-01	1.016544e+00	-1.860850e-02	-1.696884e-01	-2.460594e-02	-8.786029e-02	1.040819e-01
2.000724e-01	1.016507e+00	-1.873766e-02	-1.695347e-01	-2.478632e-02	-8.772673e-02	1.048846e-01
2.015435e-01	1.016471e+00	-1.886661e-02	-1.693798e-01	-2.496666e-02	-8.759205e-02	1.056880e-01
2.030146e-01	1.016434e+00	-1.899537e-02	-1.692238e-01	-2.514696e-02	-8.745626e-02	1.064922e-01
2.044857e-01	1.016397e+00	-1.912393e-02	-1.690665e-01	-2.532720e-02	-8.731934e-02	1.072971e-01
2.059568e-01	1.016359e+00	-1.925229e-02	-1.689081e-01	-2.550740e-02	-8.718129e-02	1.081029e-01
2.074280e-01	1.016322e+00	-1.938044e-02	-1.687484e-01	-2.568756e-02	-8.704211e-02	1.089094e-01
2.088991e-01	1.016284e+00	-1.950839e-02	-1.685876e-01	-2.586767e-02	-8.690180e-02	1.097168e-01
2.103702e-01	1.016246e+00	-1.963612e-02	-1.684256e-01	-2.604773e-02	-8.676035e-02	1.105250e-01
2.118413e-01	1.016207e+00	-1.976365e-02	-1.682624e-01	-2.622774e-02	-8.661776e-02	1.113339e-01
2.133124e-01	1.016169e+00	-1.989097e-02	-1.680980e-01	-2.640770e-02	-8.647402e-02	1.121438e-01
2.147836e-01	1.016130e+00	-2.001808e-02	-1.679325e-01	-2.658762e-02	-8.632914e-02	1.129544e-01
2.162547e-01	1.016090e+00	-2.014497e-02	-1.677657e-01	-2.676748e-02	-8.618310e-02	1.137659e-01
2.177258e-01	1.016051e+00	-2.027165e-02	-1.675977e-01	-2.694730e-02	-8.603591e-02	1.145782e-01
2.191969e-01	1.016011e+00	-2.039811e-02	-1.674286e-01	-2.712707e-02	-8.588756e-02	1.153914e-01
2.206680e-01	1.015971e+00	-2.052435e-02	-1.672582e-01	-2.730678e-02	-8.573804e-02	1.162055e-01
2.221392e-01	1.015931e+00	-2.065037e-02	-1.670867e-01	-2.748645e-02	-8.558736e-02	1.170205e-01
2.236103e-01	1.015890e+00	-2.077617e-02	-1.669139e-01	-2.766606e-02	-8.543550e-02	1.178363e-01
2.250814e-01	1.015849e+00	-2.090174e-02	-1.667400e-01	-2.784562e-02	-8.528247e-02	1.186530e-01
2.265525e-01	1.015808e+00	-2.102709e-02	-1.665648e-01	-2.802512e-02	-8.512826e-02	1.194707e-01
2.280236e-01	1.015767e+00	-2.115221e-02	-1.663885e-01	-2.820458e-02	-8.497287e-02	1.202893e-01
2.294948e-01	1.015725e+00	-2.127710e-02	-1.662109e-01	-2.838398e-02	-8.481629e-02	1.211087e-01
2.309659e-01	1.015683e+00	-2.140176e-02	-1.660321e-01	-2.856333e-02	-8.465852e-02	1.219292e-01
2.324370e-01	1.015641e+00	-2.152619e-02	-1.658522e-01	-2.874262e-02	-8.449955e-02	1.227505e-01
2.339081e-01	1.015599e+00	-2.165038e-02	-1.656710e-01	-2.892185e-02	-8.433938e-02	1.235729e-01
2.353792e-01	1.015556e+00	-2.177433e-02	-1.654886e-01	-2.910103e-02	-8.417801e-02	1.243961e-01
2.368504e-01	1.015513e+00	-2.189805e-02	-1.653050e-01	-2.928016e-02	-8.401542e-02	1.252204e-01
2.383215e-01	1.015470e+00	-2.202153e-02	-1.651202e-01	-2.945923e-02	-8.385163e-02	1.260456e-01
2.397926e-01	1.015426e+00	-2.214476e-02	-1.649341e-01	-2.963824e-02	-8.368661e-02	1.268719e-01
2.412637e-01	1.015383e+00	-2.226775e-02	-1.647469e-01	-2.981719e-02	-8.352037e-02	1.276991e-01
2.427348e-01	1.015339e+00	-2.239050e-02	-1.645584e-01	-2.999608e-02	-8.335291e-02	1.285273e-01
2.442060e-01	1.015294e+00	-2.251300e-02	-1.643687e-01	-3.017492e-02	-8.318421e-02	1.293566e-01
2.456771e-01	1.015250e+00	-2.263525e-02	-1.641778e-01	-3.035369e-02	-8.301428e-02	1.301869e-01
2.471482e-01	1.015205e+00	-2.275724e-02	-1.639857e-01	-3.053241e-02	-8.284310e-02	1.310183e-01
2.486193e-01	1.015160e+00	-2.287899e-02	-1.637923e-01	-3.071106e-02	-8.267068e-02	1.318506e-01
2.500904e-01	1.015115e+00	-2.300048e-02	-1.635977e-01	-3.088966e-02	-8.249700e-02	1.326841e-01
2.515616e-01	1.015069e+00	-2.312171e-02	-1.634019e-01	-3.106819e-02	-8.232207e-02	1.335186e-01
2.530327e-01	1.015023e+00	-2.324269e-02	-1.632049e-01	-3.124666e-02	-8.214588e-02	1.343543e-01
2.545038e-01	1.014977e+00	-2.336341e-02	-1.630066e-01	-3.142507e-02	-8.196842e-02	1.351910e-01
2.559749e-01	1.014931e+00	-2.348386e-02	-1.628071e-01	-3.160341e-02	-8.178969e-02	1.360288e-01
2.574460e-01	1.014884e+00	-2.360405e-02	-1.626064e-01	-3.178169e-02	-8.160969e-02	1.368677e-01
2.589172e-01	1.014837e+00	-2.372398e-02	-1.624044e-01	-3.195991e-02	-8.142840e-02	1.377078e-01
2.603883e-01	1.014790e+00	-2.384363e-02	-1.622012e-01	-3.213806e-02	-8.124582e-02	1.385490e-01
2.618594e-01	1.014743e+00	-2.396302e-02	-1.619968e-01	-3.231614e-02	-8.106195e-02	1.393914e-01
2.633305e-01	1.014695e+00	-2.408214e-02	-1.617911e-01	-3.249416e-02	-8.087678e-02	1.402349e-01
2.648016e-01	1.014647e+00	-2.420098e-02	-1.615842e-01	-3.267211e-02	-8.069031e-02	1.410796e-01
2.662728e-01	1.014599e+00	-2.431954e-02	-1.613760e-01	-3.284999e-02	-8.050252e-02	1.419255e-01
2.677439e-01	1.014551e+00	-2.443783e-02	-1.611666e-01	-3.302781e-02	-8.031342e-02	1.427726e-01
2.692150e-01	1.014502e+00	-2.455585e-02	-1.609559e-01	-3.320556e-02	-8.012300e-02	1.436208e-01

Time (TU)	x (LU)	y (LU)	z (LU)	\dot{x} (LU/TU)	\dot{y} (LU/TU)	\dot{z} (LU/TU)
2.706861e-01	1.014453e+00	-2.467358e-02	-1.607440e-01	-3.338324e-02	-7.993125e-02	1.444704e-01
2.721572e-01	1.014404e+00	-2.479102e-02	-1.605309e-01	-3.356084e-02	-7.973817e-02	1.453211e-01
2.736284e-01	1.014354e+00	-2.490818e-02	-1.603165e-01	-3.373838e-02	-7.954375e-02	1.461731e-01
2.750995e-01	1.014304e+00	-2.502506e-02	-1.601008e-01	-3.391585e-02	-7.934798e-02	1.470263e-01
2.765706e-01	1.014254e+00	-2.514164e-02	-1.598839e-01	-3.409324e-02	-7.915086e-02	1.478809e-01
2.780417e-01	1.014204e+00	-2.525794e-02	-1.596657e-01	-3.427056e-02	-7.895238e-02	1.487367e-01
2.795128e-01	1.014154e+00	-2.537394e-02	-1.594462e-01	-3.444781e-02	-7.875254e-02	1.495938e-01
2.809840e-01	1.014103e+00	-2.548965e-02	-1.592255e-01	-3.462499e-02	-7.855133e-02	1.504522e-01
2.824551e-01	1.014052e+00	-2.560506e-02	-1.590036e-01	-3.480209e-02	-7.834874e-02	1.513119e-01
2.839262e-01	1.014000e+00	-2.572017e-02	-1.587803e-01	-3.497911e-02	-7.814477e-02	1.521729e-01
2.853973e-01	1.013949e+00	-2.583498e-02	-1.585558e-01	-3.515606e-02	-7.793940e-02	1.530354e-01
2.868684e-01	1.013897e+00	-2.594948e-02	-1.583301e-01	-3.533294e-02	-7.773264e-02	1.538991e-01
2.883396e-01	1.013845e+00	-2.606368e-02	-1.581030e-01	-3.550974e-02	-7.752447e-02	1.547643e-01
2.898107e-01	1.013792e+00	-2.617758e-02	-1.578747e-01	-3.568645e-02	-7.731489e-02	1.556308e-01
2.912818e-01	1.013740e+00	-2.629116e-02	-1.576451e-01	-3.586309e-02	-7.710390e-02	1.564987e-01
2.927529e-01	1.013687e+00	-2.640443e-02	-1.574143e-01	-3.603966e-02	-7.689148e-02	1.573681e-01
2.942240e-01	1.013634e+00	-2.651739e-02	-1.571821e-01	-3.621614e-02	-7.667762e-02	1.582389e-01
2.956952e-01	1.013580e+00	-2.663004e-02	-1.569487e-01	-3.639254e-02	-7.646233e-02	1.591111e-01
2.971663e-01	1.013527e+00	-2.674236e-02	-1.567140e-01	-3.656886e-02	-7.624559e-02	1.599848e-01
2.986374e-01	1.013473e+00	-2.685437e-02	-1.564780e-01	-3.674510e-02	-7.602739e-02	1.608600e-01
3.001085e-01	1.013419e+00	-2.696605e-02	-1.562407e-01	-3.692125e-02	-7.580773e-02	1.617366e-01
3.015796e-01	1.013364e+00	-2.707741e-02	-1.560021e-01	-3.709733e-02	-7.558660e-02	1.626148e-01
3.030508e-01	1.013309e+00	-2.718845e-02	-1.557622e-01	-3.727331e-02	-7.536399e-02	1.634944e-01
3.045219e-01	1.013254e+00	-2.729915e-02	-1.555211e-01	-3.744922e-02	-7.513989e-02	1.643756e-01
3.059930e-01	1.013199e+00	-2.740953e-02	-1.552786e-01	-3.762503e-02	-7.491431e-02	1.652584e-01
3.074641e-01	1.013144e+00	-2.751957e-02	-1.550348e-01	-3.780077e-02	-7.468721e-02	1.661427e-01
3.089352e-01	1.013088e+00	-2.762927e-02	-1.547898e-01	-3.797641e-02	-7.445861e-02	1.670286e-01
3.104064e-01	1.013032e+00	-2.773864e-02	-1.545434e-01	-3.815197e-02	-7.422849e-02	1.679161e-01
3.118775e-01	1.012976e+00	-2.784767e-02	-1.542957e-01	-3.832743e-02	-7.399684e-02	1.688052e-01
3.133486e-01	1.012919e+00	-2.795636e-02	-1.540467e-01	-3.850281e-02	-7.376366e-02	1.696959e-01
3.148197e-01	1.012862e+00	-2.806470e-02	-1.537964e-01	-3.867810e-02	-7.352893e-02	1.705883e-01
3.162908e-01	1.012805e+00	-2.817270e-02	-1.535448e-01	-3.885330e-02	-7.329264e-02	1.714824e-01
3.177620e-01	1.012748e+00	-2.828034e-02	-1.532919e-01	-3.902840e-02	-7.305480e-02	1.723781e-01
3.192331e-01	1.012691e+00	-2.838764e-02	-1.530376e-01	-3.920342e-02	-7.281538e-02	1.732755e-01
3.207042e-01	1.012633e+00	-2.849458e-02	-1.527821e-01	-3.937834e-02	-7.257438e-02	1.741746e-01
3.221753e-01	1.012575e+00	-2.860117e-02	-1.525252e-01	-3.955316e-02	-7.233179e-02	1.750755e-01
3.236464e-01	1.012516e+00	-2.870740e-02	-1.522670e-01	-3.972789e-02	-7.208760e-02	1.759781e-01
3.251176e-01	1.012458e+00	-2.881327e-02	-1.520074e-01	-3.990253e-02	-7.184180e-02	1.768824e-01
3.265887e-01	1.012399e+00	-2.891878e-02	-1.517465e-01	-4.007707e-02	-7.159438e-02	1.777886e-01
3.280598e-01	1.012340e+00	-2.902392e-02	-1.514843e-01	-4.025151e-02	-7.134533e-02	1.786965e-01
3.295309e-01	1.012281e+00	-2.912869e-02	-1.512208e-01	-4.042585e-02	-7.109465e-02	1.796063e-01
3.310020e-01	1.012221e+00	-2.923309e-02	-1.509559e-01	-4.060009e-02	-7.084231e-02	1.805179e-01
3.324732e-01	1.012161e+00	-2.933712e-02	-1.506896e-01	-4.077424e-02	-7.058831e-02	1.814314e-01
3.339443e-01	1.012101e+00	-2.944078e-02	-1.504220e-01	-4.094828e-02	-7.033265e-02	1.823467e-01
3.354154e-01	1.012041e+00	-2.954406e-02	-1.501531e-01	-4.112222e-02	-7.007530e-02	1.832639e-01
3.368865e-01	1.011980e+00	-2.964696e-02	-1.498828e-01	-4.129606e-02	-6.981626e-02	1.841831e-01
3.383577e-01	1.011919e+00	-2.974947e-02	-1.496112e-01	-4.146979e-02	-6.955552e-02	1.851042e-01
3.398288e-01	1.011858e+00	-2.985161e-02	-1.493382e-01	-4.164342e-02	-6.929307e-02	1.860272e-01
3.412999e-01	1.011797e+00	-2.995335e-02	-1.490639e-01	-4.181695e-02	-6.902889e-02	1.869522e-01
3.427710e-01	1.011735e+00	-3.005470e-02	-1.487882e-01	-4.199037e-02	-6.876297e-02	1.878792e-01
3.442421e-01	1.011673e+00	-3.015567e-02	-1.485111e-01	-4.216368e-02	-6.849531e-02	1.888082e-01
3.457133e-01	1.011611e+00	-3.025623e-02	-1.482326e-01	-4.233688e-02	-6.822589e-02	1.897393e-01

Time (TU)	x (LU)	y (LU)	z (LU)	\dot{x} (LU/TU)	\dot{y} (LU/TU)	\dot{z} (LU/TU)
3.471844e-01	1.011549e+00	-3.035640e-02	-1.479528e-01	-4.250997e-02	-6.795470e-02	1.906724e-01
3.486555e-01	1.011486e+00	-3.045617e-02	-1.476716e-01	-4.268296e-02	-6.768172e-02	1.916076e-01
3.501266e-01	1.011423e+00	-3.055554e-02	-1.473891e-01	-4.285583e-02	-6.740695e-02	1.925449e-01
3.515977e-01	1.011360e+00	-3.065450e-02	-1.471051e-01	-4.302859e-02	-6.713037e-02	1.934843e-01
3.530689e-01	1.011296e+00	-3.075305e-02	-1.468198e-01	-4.320124e-02	-6.685197e-02	1.944259e-01
3.545400e-01	1.011233e+00	-3.085119e-02	-1.465331e-01	-4.337378e-02	-6.657173e-02	1.953696e-01
3.560111e-01	1.011169e+00	-3.094892e-02	-1.462450e-01	-4.354620e-02	-6.628965e-02	1.963156e-01
3.574822e-01	1.011105e+00	-3.104623e-02	-1.459555e-01	-4.371850e-02	-6.600571e-02	1.972637e-01
3.589533e-01	1.011040e+00	-3.114312e-02	-1.456646e-01	-4.389069e-02	-6.571990e-02	1.982141e-01
3.604245e-01	1.010975e+00	-3.123959e-02	-1.453723e-01	-4.406276e-02	-6.543220e-02	1.991667e-01
3.618956e-01	1.010910e+00	-3.133564e-02	-1.450786e-01	-4.423471e-02	-6.514260e-02	2.001216e-01
3.633667e-01	1.010845e+00	-3.143126e-02	-1.447835e-01	-4.440654e-02	-6.485109e-02	2.010789e-01
3.648378e-01	1.010780e+00	-3.152645e-02	-1.444869e-01	-4.457824e-02	-6.455765e-02	2.020384e-01
3.663089e-01	1.010714e+00	-3.162120e-02	-1.441890e-01	-4.474983e-02	-6.426226e-02	2.030004e-01
3.677801e-01	1.010648e+00	-3.171552e-02	-1.438897e-01	-4.492130e-02	-6.396492e-02	2.039647e-01
3.692512e-01	1.010582e+00	-3.180940e-02	-1.435889e-01	-4.509264e-02	-6.366560e-02	2.049314e-01
3.707223e-01	1.010515e+00	-3.190284e-02	-1.432867e-01	-4.526385e-02	-6.336430e-02	2.059006e-01
3.721934e-01	1.010449e+00	-3.199583e-02	-1.429831e-01	-4.543494e-02	-6.306099e-02	2.068722e-01
3.736645e-01	1.010382e+00	-3.208838e-02	-1.426780e-01	-4.560590e-02	-6.275567e-02	2.078463e-01
3.751357e-01	1.010315e+00	-3.218047e-02	-1.423716e-01	-4.577673e-02	-6.244831e-02	2.088230e-01
3.766068e-01	1.010247e+00	-3.227212e-02	-1.420636e-01	-4.594743e-02	-6.213890e-02	2.098021e-01
3.780779e-01	1.010179e+00	-3.236330e-02	-1.417543e-01	-4.611801e-02	-6.182743e-02	2.107839e-01
3.795490e-01	1.010111e+00	-3.245403e-02	-1.414434e-01	-4.628845e-02	-6.151387e-02	2.117682e-01
3.810201e-01	1.010043e+00	-3.254429e-02	-1.411312e-01	-4.645875e-02	-6.119821e-02	2.127552e-01
3.824913e-01	1.009975e+00	-3.263408e-02	-1.408175e-01	-4.662892e-02	-6.088043e-02	2.137448e-01
3.839624e-01	1.009906e+00	-3.272341e-02	-1.405023e-01	-4.679896e-02	-6.056052e-02	2.147372e-01
3.854335e-01	1.009837e+00	-3.281227e-02	-1.401857e-01	-4.696886e-02	-6.023846e-02	2.157322e-01
3.869046e-01	1.009768e+00	-3.290065e-02	-1.398676e-01	-4.713862e-02	-5.991422e-02	2.167300e-01
3.883757e-01	1.009698e+00	-3.298855e-02	-1.395480e-01	-4.730825e-02	-5.958780e-02	2.177306e-01
3.898469e-01	1.009629e+00	-3.307597e-02	-1.392269e-01	-4.747773e-02	-5.925917e-02	2.187339e-01
3.913180e-01	1.009559e+00	-3.316290e-02	-1.389044e-01	-4.764707e-02	-5.892832e-02	2.197401e-01
3.927891e-01	1.009488e+00	-3.324935e-02	-1.385804e-01	-4.781627e-02	-5.859522e-02	2.207492e-01
3.942602e-01	1.009418e+00	-3.333530e-02	-1.382549e-01	-4.798533e-02	-5.825985e-02	2.217612e-01
3.957313e-01	1.009347e+00	-3.342076e-02	-1.379279e-01	-4.815423e-02	-5.792221e-02	2.227762e-01
3.972025e-01	1.009276e+00	-3.350572e-02	-1.375995e-01	-4.832300e-02	-5.758225e-02	2.237941e-01
3.986736e-01	1.009205e+00	-3.359018e-02	-1.372695e-01	-4.849161e-02	-5.723998e-02	2.248150e-01
4.001447e-01	1.009134e+00	-3.367413e-02	-1.369380e-01	-4.866008e-02	-5.689535e-02	2.258389e-01
4.016158e-01	1.009062e+00	-3.375758e-02	-1.366050e-01	-4.882839e-02	-5.654836e-02	2.268659e-01
4.030869e-01	1.008990e+00	-3.384051e-02	-1.362705e-01	-4.899656e-02	-5.619899e-02	2.278960e-01
4.045581e-01	1.008918e+00	-3.392293e-02	-1.359345e-01	-4.916457e-02	-5.584720e-02	2.289293e-01
4.060292e-01	1.008845e+00	-3.400483e-02	-1.355969e-01	-4.933242e-02	-5.549298e-02	2.299657e-01
4.075003e-01	1.008773e+00	-3.408620e-02	-1.352579e-01	-4.950013e-02	-5.513630e-02	2.310054e-01
4.089714e-01	1.008700e+00	-3.416705e-02	-1.349173e-01	-4.966767e-02	-5.477715e-02	2.320483e-01
4.104425e-01	1.008626e+00	-3.424737e-02	-1.345751e-01	-4.983505e-02	-5.441550e-02	2.330945e-01
4.119137e-01	1.008553e+00	-3.432715e-02	-1.342314e-01	-5.000228e-02	-5.405132e-02	2.341441e-01
4.133848e-01	1.008479e+00	-3.440640e-02	-1.338862e-01	-5.016934e-02	-5.368459e-02	2.351970e-01
4.148559e-01	1.008405e+00	-3.448510e-02	-1.335394e-01	-5.033624e-02	-5.331529e-02	2.362533e-01
4.163270e-01	1.008331e+00	-3.456326e-02	-1.331911e-01	-5.050298e-02	-5.294339e-02	2.373131e-01
4.177981e-01	1.008257e+00	-3.464087e-02	-1.328412e-01	-5.066955e-02	-5.256887e-02	2.383763e-01
4.192693e-01	1.008182e+00	-3.471793e-02	-1.324897e-01	-5.083595e-02	-5.219169e-02	2.394431e-01
4.207404e-01	1.008107e+00	-3.479443e-02	-1.321367e-01	-5.100218e-02	-5.181184e-02	2.405135e-01
4.222115e-01	1.008032e+00	-3.487037e-02	-1.317821e-01	-5.116825e-02	-5.142928e-02	2.415875e-01

Time (TU)	x (LU)	y (LU)	z (LU)	\dot{x} (LU/TU)	\dot{y} (LU/TU)	\dot{z} (LU/TU)
4.236826e-01	1.007957e+00	-3.494575e-02	-1.314259e-01	-5.133414e-02	-5.104400e-02	2.426651e-01
4.251537e-01	1.007881e+00	-3.502056e-02	-1.310681e-01	-5.149986e-02	-5.065595e-02	2.437465e-01
4.266249e-01	1.007805e+00	-3.509479e-02	-1.307087e-01	-5.166540e-02	-5.026512e-02	2.448316e-01
4.280960e-01	1.007729e+00	-3.516845e-02	-1.303477e-01	-5.183077e-02	-4.987147e-02	2.459205e-01
4.295671e-01	1.007653e+00	-3.524152e-02	-1.299852e-01	-5.199596e-02	-4.947498e-02	2.470132e-01
4.310382e-01	1.007576e+00	-3.531401e-02	-1.296210e-01	-5.216097e-02	-4.907561e-02	2.481098e-01
4.325093e-01	1.007499e+00	-3.538591e-02	-1.292552e-01	-5.232580e-02	-4.867334e-02	2.492104e-01
4.339805e-01	1.007422e+00	-3.545722e-02	-1.288877e-01	-5.249044e-02	-4.826812e-02	2.503149e-01
4.354516e-01	1.007345e+00	-3.552793e-02	-1.285187e-01	-5.265491e-02	-4.785994e-02	2.514235e-01
4.369227e-01	1.007267e+00	-3.559803e-02	-1.281480e-01	-5.281918e-02	-4.744876e-02	2.525361e-01
4.383938e-01	1.007189e+00	-3.566753e-02	-1.277756e-01	-5.298327e-02	-4.703455e-02	2.536529e-01
4.398649e-01	1.007111e+00	-3.573642e-02	-1.274017e-01	-5.314717e-02	-4.661727e-02	2.547739e-01
4.413361e-01	1.007033e+00	-3.580469e-02	-1.270260e-01	-5.331087e-02	-4.619688e-02	2.558991e-01
4.428072e-01	1.006954e+00	-3.587234e-02	-1.266488e-01	-5.347439e-02	-4.577337e-02	2.570286e-01
4.442783e-01	1.006876e+00	-3.593937e-02	-1.262698e-01	-5.363771e-02	-4.534668e-02	2.581625e-01
4.457494e-01	1.006797e+00	-3.600576e-02	-1.258892e-01	-5.380083e-02	-4.491678e-02	2.593007e-01
4.472205e-01	1.006717e+00	-3.607152e-02	-1.255069e-01	-5.396375e-02	-4.448364e-02	2.604434e-01
4.486917e-01	1.006638e+00	-3.613664e-02	-1.251229e-01	-5.412648e-02	-4.404722e-02	2.615906e-01
4.501628e-01	1.006558e+00	-3.620112e-02	-1.247372e-01	-5.428900e-02	-4.360747e-02	2.627424e-01
4.516339e-01	1.006478e+00	-3.626494e-02	-1.243498e-01	-5.445132e-02	-4.316437e-02	2.638988e-01
4.531050e-01	1.006398e+00	-3.632811e-02	-1.239608e-01	-5.461343e-02	-4.271787e-02	2.650600e-01
4.545761e-01	1.006317e+00	-3.639063e-02	-1.235700e-01	-5.477534e-02	-4.226793e-02	2.662258e-01
4.560473e-01	1.006237e+00	-3.645247e-02	-1.231774e-01	-5.493704e-02	-4.181452e-02	2.673965e-01
4.575184e-01	1.006156e+00	-3.651365e-02	-1.227832e-01	-5.509852e-02	-4.135757e-02	2.685720e-01
4.589895e-01	1.006075e+00	-3.657416e-02	-1.223872e-01	-5.525979e-02	-4.089707e-02	2.697525e-01
4.604606e-01	1.005993e+00	-3.663398e-02	-1.219895e-01	-5.542085e-02	-4.043295e-02	2.709380e-01
4.619317e-01	1.005912e+00	-3.669312e-02	-1.215901e-01	-5.558169e-02	-3.996518e-02	2.721286e-01
4.634029e-01	1.005830e+00	-3.675157e-02	-1.211889e-01	-5.574231e-02	-3.949371e-02	2.733243e-01
4.648740e-01	1.005748e+00	-3.680932e-02	-1.207859e-01	-5.590272e-02	-3.901849e-02	2.745252e-01
4.663451e-01	1.005665e+00	-3.686637e-02	-1.203811e-01	-5.606289e-02	-3.853948e-02	2.757314e-01
4.678162e-01	1.005583e+00	-3.692271e-02	-1.199746e-01	-5.622284e-02	-3.805662e-02	2.769430e-01
4.692874e-01	1.005500e+00	-3.697834e-02	-1.195663e-01	-5.638257e-02	-3.756988e-02	2.781599e-01
4.707585e-01	1.005417e+00	-3.703324e-02	-1.191562e-01	-5.654207e-02	-3.707919e-02	2.793824e-01
4.722296e-01	1.005333e+00	-3.708743e-02	-1.187443e-01	-5.670133e-02	-3.658450e-02	2.806104e-01
4.737007e-01	1.005250e+00	-3.714088e-02	-1.183306e-01	-5.686036e-02	-3.608577e-02	2.818441e-01
4.751718e-01	1.005166e+00	-3.719360e-02	-1.179150e-01	-5.701916e-02	-3.558293e-02	2.830835e-01
4.766430e-01	1.005082e+00	-3.724557e-02	-1.174977e-01	-5.717771e-02	-3.507594e-02	2.843287e-01
4.781141e-01	1.004998e+00	-3.729680e-02	-1.170785e-01	-5.733603e-02	-3.456474e-02	2.855799e-01
4.795852e-01	1.004913e+00	-3.734727e-02	-1.166574e-01	-5.749411e-02	-3.404926e-02	2.868369e-01
4.810563e-01	1.004829e+00	-3.739698e-02	-1.162345e-01	-5.765194e-02	-3.352946e-02	2.881001e-01
4.825274e-01	1.004744e+00	-3.744592e-02	-1.158098e-01	-5.780952e-02	-3.300526e-02	2.893693e-01
4.839986e-01	1.004659e+00	-3.749409e-02	-1.153831e-01	-5.796686e-02	-3.247662e-02	2.906448e-01
4.854697e-01	1.004573e+00	-3.754147e-02	-1.149546e-01	-5.812394e-02	-3.194346e-02	2.919266e-01
4.869408e-01	1.004488e+00	-3.758807e-02	-1.145242e-01	-5.828077e-02	-3.140572e-02	2.932149e-01
4.884119e-01	1.004402e+00	-3.763387e-02	-1.140919e-01	-5.843734e-02	-3.086334e-02	2.945096e-01
4.898830e-01	1.004316e+00	-3.767887e-02	-1.136577e-01	-5.859366e-02	-3.031625e-02	2.958109e-01
4.913542e-01	1.004229e+00	-3.772307e-02	-1.132215e-01	-5.874971e-02	-2.976438e-02	2.971189e-01
4.928253e-01	1.004143e+00	-3.776645e-02	-1.127835e-01	-5.890550e-02	-2.920766e-02	2.984337e-01
4.942964e-01	1.004056e+00	-3.780900e-02	-1.123435e-01	-5.906103e-02	-2.864601e-02	2.997553e-01
4.957675e-01	1.003969e+00	-3.785073e-02	-1.119015e-01	-5.921628e-02	-2.807938e-02	3.010840e-01
4.972386e-01	1.003882e+00	-3.789162e-02	-1.114576e-01	-5.937127e-02	-2.750767e-02	3.024198e-01
4.987098e-01	1.003794e+00	-3.793166e-02	-1.110117e-01	-5.952598e-02	-2.693081e-02	3.037627e-01

Time (TU)	x (LU)	y (LU)	z (LU)	\dot{x} (LU/TU)	\dot{y} (LU/TU)	\dot{z} (LU/TU)
5.001809e-01	1.003707e+00	-3.797085e-02	-1.105639e-01	-5.968042e-02	-2.634873e-02	3.051130e-01
5.016520e-01	1.003619e+00	-3.800918e-02	-1.101140e-01	-5.983458e-02	-2.576134e-02	3.064707e-01
5.031231e-01	1.003531e+00	-3.804664e-02	-1.096622e-01	-5.998845e-02	-2.516856e-02	3.078359e-01
5.045942e-01	1.003442e+00	-3.808323e-02	-1.092083e-01	-6.014205e-02	-2.457031e-02	3.092087e-01
5.060654e-01	1.003354e+00	-3.811893e-02	-1.087524e-01	-6.029535e-02	-2.396649e-02	3.105894e-01
5.075365e-01	1.003265e+00	-3.815374e-02	-1.082945e-01	-6.044837e-02	-2.335703e-02	3.119779e-01
5.090076e-01	1.003176e+00	-3.818765e-02	-1.078345e-01	-6.060110e-02	-2.274182e-02	3.133744e-01
5.104787e-01	1.003087e+00	-3.822065e-02	-1.073724e-01	-6.075353e-02	-2.212078e-02	3.147790e-01
5.119498e-01	1.002997e+00	-3.825273e-02	-1.069083e-01	-6.090566e-02	-2.149381e-02	3.161919e-01
5.134210e-01	1.002907e+00	-3.828389e-02	-1.064421e-01	-6.105749e-02	-2.086081e-02	3.176132e-01
5.148921e-01	1.002817e+00	-3.831411e-02	-1.059738e-01	-6.120902e-02	-2.022169e-02	3.190431e-01
5.163632e-01	1.002727e+00	-3.834338e-02	-1.055034e-01	-6.136025e-02	-1.957633e-02	3.204815e-01
5.178343e-01	1.002637e+00	-3.837170e-02	-1.050309e-01	-6.151116e-02	-1.892463e-02	3.219288e-01
5.193054e-01	1.002546e+00	-3.839906e-02	-1.045562e-01	-6.166176e-02	-1.826649e-02	3.233850e-01
5.207766e-01	1.002455e+00	-3.842544e-02	-1.040794e-01	-6.181205e-02	-1.760180e-02	3.248503e-01
5.222477e-01	1.002364e+00	-3.845085e-02	-1.036004e-01	-6.196202e-02	-1.693043e-02	3.263249e-01
5.237188e-01	1.002273e+00	-3.847525e-02	-1.031193e-01	-6.211167e-02	-1.625227e-02	3.278088e-01
5.251899e-01	1.002182e+00	-3.849866e-02	-1.026359e-01	-6.226100e-02	-1.556721e-02	3.293023e-01
5.266610e-01	1.002090e+00	-3.852105e-02	-1.021504e-01	-6.241000e-02	-1.487511e-02	3.308054e-01
5.281322e-01	1.001998e+00	-3.854242e-02	-1.016626e-01	-6.255867e-02	-1.417586e-02	3.323185e-01
5.296033e-01	1.001906e+00	-3.856276e-02	-1.011726e-01	-6.270700e-02	-1.346932e-02	3.338415e-01
5.310744e-01	1.001814e+00	-3.858205e-02	-1.006804e-01	-6.285500e-02	-1.275535e-02	3.353748e-01
5.325455e-01	1.001721e+00	-3.860028e-02	-1.001858e-01	-6.300266e-02	-1.203383e-02	3.369184e-01
5.340166e-01	1.001628e+00	-3.861745e-02	-9.968905e-02	-6.314998e-02	-1.130461e-02	3.384726e-01
5.354878e-01	1.001535e+00	-3.863354e-02	-9.918997e-02	-6.329695e-02	-1.056754e-02	3.400376e-01
5.369589e-01	1.001442e+00	-3.864854e-02	-9.868858e-02	-6.344357e-02	-9.822477e-03	3.416134e-01
5.384300e-01	1.001349e+00	-3.866244e-02	-9.818486e-02	-6.358984e-02	-9.069265e-03	3.432004e-01
5.399011e-01	1.001255e+00	-3.867522e-02	-9.767879e-02	-6.373575e-02	-8.307749e-03	3.447987e-01
5.413722e-01	1.001161e+00	-3.868688e-02	-9.717037e-02	-6.388130e-02	-7.537764e-03	3.464085e-01
5.428434e-01	1.001067e+00	-3.869739e-02	-9.665957e-02	-6.402649e-02	-6.759144e-03	3.480300e-01
5.443145e-01	1.000973e+00	-3.870676e-02	-9.614638e-02	-6.417132e-02	-5.971718e-03	3.496634e-01
5.457856e-01	1.000878e+00	-3.871496e-02	-9.563077e-02	-6.431577e-02	-5.175308e-03	3.513090e-01
5.472567e-01	1.000783e+00	-3.872198e-02	-9.511274e-02	-6.445985e-02	-4.369733e-03	3.529669e-01
5.487278e-01	1.000688e+00	-3.872781e-02	-9.459225e-02	-6.460356e-02	-3.554804e-03	3.546375e-01
5.501990e-01	1.000593e+00	-3.873244e-02	-9.406930e-02	-6.474688e-02	-2.730330e-03	3.563209e-01
5.516701e-01	1.000498e+00	-3.873584e-02	-9.354386e-02	-6.488982e-02	-1.896110e-03	3.580173e-01
5.531412e-01	1.000402e+00	-3.873801e-02	-9.301592e-02	-6.503237e-02	-1.051940e-03	3.597271e-01
5.546123e-01	1.000307e+00	-3.873893e-02	-9.248545e-02	-6.517453e-02	-1.976088e-04	3.614504e-01
5.560834e-01	1.000211e+00	-3.873859e-02	-9.195244e-02	-6.531630e-02	6.671021e-04	3.631875e-01
5.575546e-01	1.000114e+00	-3.873696e-02	-9.141686e-02	-6.545767e-02	1.542417e-03	3.649388e-01
5.590257e-01	1.000018e+00	-3.873404e-02	-9.087870e-02	-6.559863e-02	2.428568e-03	3.667043e-01
5.604968e-01	9.999214e-01	-3.872981e-02	-9.033792e-02	-6.573919e-02	3.325795e-03	3.684846e-01
5.619679e-01	9.998246e-01	-3.872425e-02	-8.979452e-02	-6.587934e-02	4.234343e-03	3.702797e-01
5.634390e-01	9.997276e-01	-3.871735e-02	-8.924846e-02	-6.601907e-02	5.154468e-03	3.720901e-01
5.649102e-01	9.996303e-01	-3.870908e-02	-8.869973e-02	-6.615839e-02	6.086434e-03	3.739160e-01
5.663813e-01	9.995329e-01	-3.869943e-02	-8.814830e-02	-6.629728e-02	7.030512e-03	3.757577e-01
5.678524e-01	9.994353e-01	-3.868839e-02	-8.759415e-02	-6.643575e-02	7.986983e-03	3.776156e-01
5.693235e-01	9.993374e-01	-3.867593e-02	-8.703726e-02	-6.657379e-02	8.956137e-03	3.794900e-01
5.707946e-01	9.992394e-01	-3.866203e-02	-8.647759e-02	-6.671140e-02	9.938274e-03	3.813812e-01
5.722658e-01	9.991412e-01	-3.864668e-02	-8.591514e-02	-6.684857e-02	1.093371e-02	3.832896e-01
5.737369e-01	9.990427e-01	-3.862986e-02	-8.534986e-02	-6.698529e-02	1.194275e-02	3.852155e-01
5.752080e-01	9.989441e-01	-3.861154e-02	-8.478173e-02	-6.712158e-02	1.296574e-02	3.871594e-01

Time (TU)	x (LU)	y (LU)	z (LU)	\dot{x} (LU/TU)	\dot{y} (LU/TU)	\dot{z} (LU/TU)
5.766791e-01	9.988452e-01	-3.859170e-02	-8.421073e-02	-6.725741e-02	1.400303e-02	3.891215e-01
5.781502e-01	9.987462e-01	-3.857033e-02	-8.363683e-02	-6.739279e-02	1.505496e-02	3.911022e-01
5.796214e-01	9.986470e-01	-3.854740e-02	-8.306000e-02	-6.752771e-02	1.612191e-02	3.931021e-01
5.810925e-01	9.985475e-01	-3.852289e-02	-8.248022e-02	-6.766217e-02	1.720425e-02	3.951215e-01
5.825636e-01	9.984479e-01	-3.849677e-02	-8.189745e-02	-6.779617e-02	1.830239e-02	3.971607e-01
5.840347e-01	9.983480e-01	-3.846903e-02	-8.131167e-02	-6.792969e-02	1.941673e-02	3.992204e-01
5.855058e-01	9.982480e-01	-3.843963e-02	-8.072284e-02	-6.806274e-02	2.054770e-02	4.013008e-01
5.869770e-01	9.981478e-01	-3.840856e-02	-8.013094e-02	-6.819531e-02	2.169575e-02	4.034025e-01
5.884481e-01	9.980474e-01	-3.837579e-02	-7.953592e-02	-6.832740e-02	2.286132e-02	4.055260e-01
5.899192e-01	9.979467e-01	-3.834129e-02	-7.893777e-02	-6.845901e-02	2.404490e-02	4.076718e-01
5.913903e-01	9.978459e-01	-3.830504e-02	-7.833644e-02	-6.859012e-02	2.524698e-02	4.098404e-01
5.928614e-01	9.977449e-01	-3.826700e-02	-7.773191e-02	-6.872074e-02	2.646808e-02	4.120323e-01
5.943326e-01	9.976437e-01	-3.822715e-02	-7.712413e-02	-6.885086e-02	2.770872e-02	4.142480e-01
5.958037e-01	9.975424e-01	-3.818546e-02	-7.651308e-02	-6.898048e-02	2.896947e-02	4.164882e-01
5.972748e-01	9.974408e-01	-3.814191e-02	-7.589871e-02	-6.910960e-02	3.025090e-02	4.187534e-01
5.987459e-01	9.973390e-01	-3.809645e-02	-7.528099e-02	-6.923820e-02	3.155362e-02	4.210443e-01
6.002171e-01	9.972371e-01	-3.804906e-02	-7.465989e-02	-6.936629e-02	3.287824e-02	4.233614e-01
6.016882e-01	9.971349e-01	-3.799970e-02	-7.403535e-02	-6.949385e-02	3.422542e-02	4.257054e-01
6.031593e-01	9.970326e-01	-3.794835e-02	-7.340734e-02	-6.962090e-02	3.559584e-02	4.280770e-01
6.046304e-01	9.969301e-01	-3.789496e-02	-7.277583e-02	-6.974742e-02	3.699022e-02	4.304769e-01
6.061015e-01	9.968274e-01	-3.783950e-02	-7.214076e-02	-6.987341e-02	3.840928e-02	4.329058e-01
6.075727e-01	9.967245e-01	-3.778194e-02	-7.150210e-02	-6.999887e-02	3.985380e-02	4.353644e-01
6.090438e-01	9.966214e-01	-3.772223e-02	-7.085980e-02	-7.012379e-02	4.132458e-02	4.378536e-01
6.105149e-01	9.965182e-01	-3.766034e-02	-7.021382e-02	-7.024817e-02	4.282247e-02	4.403740e-01
6.119860e-01	9.964148e-01	-3.759622e-02	-6.956410e-02	-7.037200e-02	4.434835e-02	4.429267e-01
6.134571e-01	9.963111e-01	-3.752984e-02	-6.891060e-02	-7.049528e-02	4.590312e-02	4.455123e-01
6.149283e-01	9.962073e-01	-3.746115e-02	-6.825328e-02	-7.061802e-02	4.748777e-02	4.481319e-01
6.163994e-01	9.961034e-01	-3.739010e-02	-6.759207e-02	-7.074020e-02	4.910328e-02	4.507863e-01
6.178705e-01	9.959992e-01	-3.731666e-02	-6.692694e-02	-7.086182e-02	5.075073e-02	4.534766e-01
6.193416e-01	9.958949e-01	-3.724076e-02	-6.625782e-02	-7.098289e-02	5.243120e-02	4.562036e-01
6.208127e-01	9.957904e-01	-3.716238e-02	-6.558466e-02	-7.110338e-02	5.414587e-02	4.589686e-01
6.222839e-01	9.956857e-01	-3.708144e-02	-6.490740e-02	-7.122332e-02	5.589594e-02	4.617724e-01
6.237550e-01	9.955808e-01	-3.699790e-02	-6.422599e-02	-7.134268e-02	5.768269e-02	4.646164e-01
6.252261e-01	9.954758e-01	-3.691170e-02	-6.354037e-02	-7.146148e-02	5.950747e-02	4.675016e-01
6.266972e-01	9.953705e-01	-3.682279e-02	-6.285047e-02	-7.157970e-02	6.137168e-02	4.704293e-01
6.281683e-01	9.952652e-01	-3.673111e-02	-6.215623e-02	-7.169735e-02	6.327680e-02	4.734008e-01
6.296395e-01	9.951596e-01	-3.663660e-02	-6.145759e-02	-7.181443e-02	6.522440e-02	4.764174e-01
6.311106e-01	9.950539e-01	-3.653918e-02	-6.075448e-02	-7.193093e-02	6.721613e-02	4.794805e-01
6.325817e-01	9.949480e-01	-3.643881e-02	-6.004682e-02	-7.204685e-02	6.925371e-02	4.825915e-01
6.340528e-01	9.948419e-01	-3.633540e-02	-5.933455e-02	-7.216219e-02	7.133897e-02	4.857519e-01
6.355239e-01	9.947356e-01	-3.622889e-02	-5.861760e-02	-7.227695e-02	7.347384e-02	4.889634e-01
6.369951e-01	9.946292e-01	-3.611920e-02	-5.789588e-02	-7.239114e-02	7.566037e-02	4.922276e-01
6.384662e-01	9.945226e-01	-3.600625e-02	-5.716932e-02	-7.250474e-02	7.790071e-02	4.955463e-01
6.399373e-01	9.944159e-01	-3.588997e-02	-5.643783e-02	-7.261778e-02	8.019715e-02	4.989211e-01
6.414084e-01	9.943090e-01	-3.577026e-02	-5.570134e-02	-7.273023e-02	8.255209e-02	5.023541e-01
6.428795e-01	9.942019e-01	-3.564705e-02	-5.495976e-02	-7.284212e-02	8.496811e-02	5.058472e-01
6.443507e-01	9.940947e-01	-3.552023e-02	-5.421299e-02	-7.295343e-02	8.744793e-02	5.094025e-01
6.458218e-01	9.939873e-01	-3.538972e-02	-5.346094e-02	-7.306417e-02	8.999443e-02	5.130222e-01
6.472929e-01	9.938797e-01	-3.525542e-02	-5.270352e-02	-7.317435e-02	9.261069e-02	5.167085e-01
6.487640e-01	9.937720e-01	-3.511720e-02	-5.194063e-02	-7.328398e-02	9.529997e-02	5.204640e-01
6.502351e-01	9.936641e-01	-3.497498e-02	-5.117216e-02	-7.339304e-02	9.806577e-02	5.242910e-01
6.517063e-01	9.935560e-01	-3.482863e-02	-5.039800e-02	-7.350156e-02	1.009118e-01	5.281924e-01

Time (TU)	x (LU)	y (LU)	z (LU)	\dot{x} (LU/TU)	\dot{y} (LU/TU)	\dot{z} (LU/TU)
6.531774e-01	9.934478e-01	-3.467803e-02	-4.961805e-02	-7.360954e-02	1.038420e-01	5.321708e-01
6.546485e-01	9.933395e-01	-3.452306e-02	-4.883219e-02	-7.371699e-02	1.068606e-01	5.362292e-01
6.561196e-01	9.932309e-01	-3.436358e-02	-4.804029e-02	-7.382390e-02	1.099722e-01	5.403708e-01
6.575907e-01	9.931222e-01	-3.419945e-02	-4.724224e-02	-7.393030e-02	1.131817e-01	5.445989e-01
6.590619e-01	9.930134e-01	-3.403052e-02	-4.643791e-02	-7.403620e-02	1.164941e-01	5.489168e-01
6.605330e-01	9.929044e-01	-3.385664e-02	-4.562715e-02	-7.414160e-02	1.199153e-01	5.533282e-01
6.620041e-01	9.927953e-01	-3.367764e-02	-4.480984e-02	-7.424652e-02	1.234511e-01	5.578371e-01
6.634752e-01	9.926860e-01	-3.349336e-02	-4.398581e-02	-7.435097e-02	1.271080e-01	5.624475e-01
6.649463e-01	9.925765e-01	-3.330360e-02	-4.315493e-02	-7.445496e-02	1.308931e-01	5.671637e-01
6.664175e-01	9.924669e-01	-3.310817e-02	-4.231703e-02	-7.455852e-02	1.348140e-01	5.719904e-01
6.678886e-01	9.923571e-01	-3.290687e-02	-4.147194e-02	-7.466166e-02	1.388788e-01	5.769323e-01
6.693597e-01	9.922472e-01	-3.269948e-02	-4.061949e-02	-7.476439e-02	1.430964e-01	5.819947e-01
6.708308e-01	9.921372e-01	-3.248577e-02	-3.975951e-02	-7.486674e-02	1.474764e-01	5.871831e-01
6.723019e-01	9.920269e-01	-3.226549e-02	-3.889179e-02	-7.496872e-02	1.520294e-01	5.925032e-01
6.737731e-01	9.919166e-01	-3.203837e-02	-3.801615e-02	-7.507036e-02	1.567668e-01	5.979614e-01
6.752442e-01	9.918061e-01	-3.180415e-02	-3.713238e-02	-7.517168e-02	1.617010e-01	6.035641e-01
6.767153e-01	9.916954e-01	-3.156251e-02	-3.624025e-02	-7.527269e-02	1.668457e-01	6.093185e-01
6.781864e-01	9.915846e-01	-3.131313e-02	-3.533954e-02	-7.537342e-02	1.722159e-01	6.152321e-01
6.796575e-01	9.914736e-01	-3.105569e-02	-3.443001e-02	-7.547390e-02	1.778281e-01	6.213128e-01
6.811287e-01	9.913625e-01	-3.078979e-02	-3.351140e-02	-7.557413e-02	1.837004e-01	6.275692e-01
6.825998e-01	9.912513e-01	-3.051506e-02	-3.258346e-02	-7.567414e-02	1.898529e-01	6.340105e-01
6.840709e-01	9.911399e-01	-3.023105e-02	-3.164589e-02	-7.577393e-02	1.963077e-01	6.406465e-01
6.855420e-01	9.910283e-01	-2.993731e-02	-3.069842e-02	-7.587352e-02	2.030894e-01	6.474875e-01
6.870131e-01	9.909167e-01	-2.963334e-02	-2.974072e-02	-7.597291e-02	2.102257e-01	6.545447e-01
6.884843e-01	9.908048e-01	-2.931859e-02	-2.877248e-02	-7.607207e-02	2.177469e-01	6.618302e-01
6.899554e-01	9.906928e-01	-2.899247e-02	-2.779334e-02	-7.617098e-02	2.256877e-01	6.693566e-01
6.914265e-01	9.905807e-01	-2.865434e-02	-2.680295e-02	-7.626961e-02	2.340864e-01	6.771376e-01
6.928976e-01	9.904684e-01	-2.830349e-02	-2.580091e-02	-7.636786e-02	2.429868e-01	6.851877e-01
6.943687e-01	9.903560e-01	-2.793914e-02	-2.478682e-02	-7.646564e-02	2.524382e-01	6.935223e-01
6.958399e-01	9.902434e-01	-2.756046e-02	-2.376025e-02	-7.656279e-02	2.624968e-01	7.021580e-01
6.973110e-01	9.901307e-01	-2.716649e-02	-2.272075e-02	-7.665909e-02	2.732266e-01	7.111120e-01
6.987821e-01	9.900179e-01	-2.675619e-02	-2.166782e-02	-7.675423e-02	2.847013e-01	7.204026e-01
7.002532e-01	9.899049e-01	-2.632842e-02	-2.060097e-02	-7.684780e-02	2.970056e-01	7.300486e-01
7.017243e-01	9.897918e-01	-2.588188e-02	-1.951966e-02	-7.693925e-02	3.102379e-01	7.400698e-01
7.031955e-01	9.896785e-01	-2.541511e-02	-1.842332e-02	-7.702781e-02	3.245129e-01	7.504856e-01
7.046666e-01	9.895652e-01	-2.492650e-02	-1.731135e-02	-7.711245e-02	3.399647e-01	7.613153e-01
7.061377e-01	9.894517e-01	-2.441420e-02	-1.618313e-02	-7.719177e-02	3.567518e-01	7.725770e-01
7.076088e-01	9.893380e-01	-2.387611e-02	-1.503802e-02	-7.726387e-02	3.750624e-01	7.842858e-01
7.090799e-01	9.892243e-01	-2.330982e-02	-1.387535e-02	-7.732616e-02	3.951216e-01	7.964523e-01
7.105511e-01	9.891105e-01	-2.271258e-02	-1.269444e-02	-7.737508e-02	4.172007e-01	8.090789e-01
7.120222e-01	9.889967e-01	-2.208117e-02	-1.149463e-02	-7.740570e-02	4.416295e-01	8.221552e-01
7.134933e-01	9.888828e-01	-2.141185e-02	-1.027526e-02	-7.741114e-02	4.688123e-01	8.356503e-01
7.149644e-01	9.887689e-01	-2.070021e-02	-9.035766e-03	-7.738169e-02	4.992494e-01	8.495009e-01
7.164355e-01	9.886552e-01	-1.994104e-02	-7.775703e-03	-7.730349e-02	5.335660e-01	8.635930e-01
7.179067e-01	9.885415e-01	-1.912805e-02	-6.494843e-03	-7.715645e-02	5.725505e-01	8.777318e-01
7.193778e-01	9.884282e-01	-1.825368e-02	-5.193337e-03	-7.691101e-02	6.172071e-01	8.915941e-01
7.208489e-01	9.883153e-01	-1.730867e-02	-3.871950e-03	-7.652285e-02	6.688256e-01	9.046484e-01
7.223200e-01	9.882031e-01	-1.628161e-02	-2.532459e-03	-7.592426e-02	7.290726e-01	9.160218e-01
7.237911e-01	9.880921e-01	-1.515828e-02	-1.178310e-03	-7.500955e-02	8.001024e-01	9.242709e-01
7.252623e-01	9.879827e-01	-1.392089e-02	1.842805e-04	-7.361021e-02	8.846695e-01	9.269859e-01
7.267334e-01	9.878759e-01	-1.254708e-02	1.544443e-03	-7.145227e-02	9.861663e-01	9.201013e-01
7.282045e-01	9.877730e-01	-1.100919e-02	2.883427e-03	-6.808496e-02	1.108356e+00	8.967247e-01

Time (TU)	x (LU)	y (LU)	z (LU)	\dot{x} (LU/TU)	\dot{y} (LU/TU)	\dot{z} (LU/TU)
7.296756e-01	9.876765e-01	-9.274385e-03	4.169192e-03	-6.277209e-02	1.254164e+00	8.453235e-01
7.311468e-01	9.875899e-01	-7.308115e-03	5.348024e-03	-5.437530e-02	1.422055e+00	7.477018e-01
7.326179e-01	9.875187e-01	-5.086106e-03	6.334593e-03	-4.141893e-02	1.597775e+00	5.798143e-01
7.340890e-01	9.874708e-01	-2.621495e-03	7.010358e-03	-2.287402e-02	1.743264e+00	3.242231e-01
7.355601e-01	9.874536e-01	-1.772540e-11	7.253892e-03	-1.225207e-10	1.801941e+00	2.265661e-09
7.370312e-01	9.874708e-01	2.621495e-03	7.010358e-03	2.287402e-02	1.743264e+00	-3.242231e-01
7.385024e-01	9.875187e-01	5.086106e-03	6.334593e-03	4.141893e-02	1.597775e+00	-5.798143e-01
7.399735e-01	9.875899e-01	7.308115e-03	5.348024e-03	5.437530e-02	1.422055e+00	-7.477018e-01
7.414446e-01	9.876765e-01	9.274385e-03	4.169192e-03	6.277209e-02	1.254164e+00	-8.453235e-01
7.429157e-01	9.877730e-01	1.100919e-02	2.883427e-03	6.808496e-02	1.108356e+00	-8.967247e-01
7.443868e-01	9.878759e-01	1.254708e-02	1.544443e-03	7.145227e-02	9.861663e-01	-9.201013e-01
7.458580e-01	9.879827e-01	1.392089e-02	1.842805e-04	7.361021e-02	8.846695e-01	-9.269859e-01
7.473291e-01	9.880921e-01	1.515828e-02	-1.178310e-03	7.500955e-02	8.001024e-01	-9.242709e-01
7.488002e-01	9.882031e-01	1.628161e-02	-2.532459e-03	7.592426e-02	7.290726e-01	-9.160218e-01
7.502713e-01	9.883153e-01	1.730867e-02	-3.871950e-03	7.652285e-02	6.688256e-01	-9.046484e-01
7.517424e-01	9.884282e-01	1.825368e-02	-5.193337e-03	7.691101e-02	6.172071e-01	-8.915941e-01
7.532136e-01	9.885415e-01	1.912805e-02	-6.494843e-03	7.715645e-02	5.725505e-01	-8.777318e-01
7.546847e-01	9.886552e-01	1.994104e-02	-7.775703e-03	7.730349e-02	5.335660e-01	-8.635930e-01
7.561558e-01	9.887689e-01	2.070021e-02	-9.035766e-03	7.738169e-02	4.992494e-01	-8.495009e-01
7.576269e-01	9.888828e-01	2.141185e-02	-1.027526e-02	7.741114e-02	4.688123e-01	-8.356503e-01
7.590980e-01	9.889967e-01	2.208117e-02	-1.149463e-02	7.740570e-02	4.416295e-01	-8.221552e-01
7.605692e-01	9.891105e-01	2.271258e-02	-1.269444e-02	7.737508e-02	4.172007e-01	-8.090789e-01
7.620403e-01	9.892243e-01	2.330982e-02	-1.387535e-02	7.732616e-02	3.951216e-01	-7.964523e-01
7.635114e-01	9.893380e-01	2.387611e-02	-1.503802e-02	7.726387e-02	3.750624e-01	-7.842858e-01
7.649825e-01	9.894517e-01	2.441420e-02	-1.618313e-02	7.719177e-02	3.567518e-01	-7.725770e-01
7.664536e-01	9.895652e-01	2.492650e-02	-1.731135e-02	7.711245e-02	3.399647e-01	-7.613153e-01
7.679248e-01	9.896785e-01	2.541511e-02	-1.842332e-02	7.702781e-02	3.245129e-01	-7.504856e-01
7.693959e-01	9.897918e-01	2.588188e-02	-1.951966e-02	7.693925e-02	3.102379e-01	-7.400698e-01
7.708670e-01	9.899049e-01	2.632842e-02	-2.060097e-02	7.684780e-02	2.970056e-01	-7.300486e-01
7.723381e-01	9.900179e-01	2.675619e-02	-2.166782e-02	7.675423e-02	2.847013e-01	-7.204026e-01
7.738092e-01	9.901307e-01	2.716649e-02	-2.272075e-02	7.665909e-02	2.732266e-01	-7.111120e-01
7.752804e-01	9.902434e-01	2.756046e-02	-2.376025e-02	7.656279e-02	2.624968e-01	-7.021580e-01
7.767515e-01	9.903560e-01	2.793914e-02	-2.478682e-02	7.646564e-02	2.524382e-01	-6.935223e-01
7.782226e-01	9.904684e-01	2.830349e-02	-2.580091e-02	7.636786e-02	2.429868e-01	-6.851877e-01
7.796937e-01	9.905807e-01	2.865434e-02	-2.680295e-02	7.626961e-02	2.340864e-01	-6.771376e-01
7.811648e-01	9.906928e-01	2.899247e-02	-2.779334e-02	7.617098e-02	2.256877e-01	-6.693566e-01
7.826360e-01	9.908048e-01	2.931859e-02	-2.877248e-02	7.607207e-02	2.177469e-01	-6.618302e-01
7.841071e-01	9.909167e-01	2.963334e-02	-2.974072e-02	7.597291e-02	2.102257e-01	-6.545447e-01
7.855782e-01	9.910283e-01	2.993731e-02	-3.069842e-02	7.587352e-02	2.030894e-01	-6.474875e-01
7.870493e-01	9.911399e-01	3.023105e-02	-3.164589e-02	7.577393e-02	1.963077e-01	-6.406465e-01
7.885204e-01	9.912513e-01	3.051506e-02	-3.258346e-02	7.567414e-02	1.898529e-01	-6.340105e-01
7.899916e-01	9.913625e-01	3.078979e-02	-3.351140e-02	7.557413e-02	1.837004e-01	-6.275692e-01
7.914627e-01	9.914736e-01	3.105569e-02	-3.443001e-02	7.547390e-02	1.778281e-01	-6.213128e-01
7.929338e-01	9.915846e-01	3.131313e-02	-3.533954e-02	7.537342e-02	1.722159e-01	-6.152321e-01
7.944049e-01	9.916954e-01	3.156251e-02	-3.624025e-02	7.527269e-02	1.668457e-01	-6.093185e-01
7.958760e-01	9.918061e-01	3.180415e-02	-3.713238e-02	7.517168e-02	1.617010e-01	-6.035641e-01
7.973472e-01	9.919166e-01	3.203837e-02	-3.801615e-02	7.507036e-02	1.567668e-01	-5.979614e-01
7.988183e-01	9.920269e-01	3.226549e-02	-3.889179e-02	7.496872e-02	1.520294e-01	-5.925032e-01
8.002894e-01	9.921372e-01	3.248577e-02	-3.975951e-02	7.486674e-02	1.474764e-01	-5.871831e-01
8.017605e-01	9.922472e-01	3.269948e-02	-4.061949e-02	7.476439e-02	1.430964e-01	-5.819947e-01
8.032316e-01	9.923571e-01	3.290687e-02	-4.147194e-02	7.466166e-02	1.388788e-01	-5.769323e-01
8.047028e-01	9.924669e-01	3.310817e-02	-4.231703e-02	7.455852e-02	1.348140e-01	-5.719904e-01

Time (TU)	x (LU)	y (LU)	z (LU)	\dot{x} (LU/TU)	\dot{y} (LU/TU)	\dot{z} (LU/TU)
8.061739e-01	9.925765e-01	3.330360e-02	-4.315493e-02	7.445496e-02	1.308931e-01	-5.671637e-01
8.076450e-01	9.926860e-01	3.349336e-02	-4.398581e-02	7.435097e-02	1.271080e-01	-5.624475e-01
8.091161e-01	9.927953e-01	3.367764e-02	-4.480984e-02	7.424652e-02	1.234511e-01	-5.578371e-01
8.105872e-01	9.929044e-01	3.385664e-02	-4.562715e-02	7.414160e-02	1.199153e-01	-5.533282e-01
8.120584e-01	9.930134e-01	3.403052e-02	-4.643791e-02	7.403620e-02	1.164941e-01	-5.489168e-01
8.135295e-01	9.931222e-01	3.419945e-02	-4.724224e-02	7.393030e-02	1.131817e-01	-5.445989e-01
8.150006e-01	9.932309e-01	3.436358e-02	-4.804029e-02	7.382390e-02	1.099722e-01	-5.403708e-01
8.164717e-01	9.933395e-01	3.452306e-02	-4.883219e-02	7.371699e-02	1.068606e-01	-5.362292e-01
8.179428e-01	9.934478e-01	3.467803e-02	-4.961805e-02	7.360954e-02	1.038420e-01	-5.321708e-01
8.194140e-01	9.935560e-01	3.482863e-02	-5.039800e-02	7.350156e-02	1.009118e-01	-5.281924e-01
8.208851e-01	9.936641e-01	3.497498e-02	-5.117216e-02	7.339304e-02	9.806577e-02	-5.242910e-01
8.223562e-01	9.937720e-01	3.511720e-02	-5.194063e-02	7.328398e-02	9.529997e-02	-5.204640e-01
8.238273e-01	9.938797e-01	3.525542e-02	-5.270352e-02	7.317435e-02	9.261069e-02	-5.167085e-01
8.252984e-01	9.939873e-01	3.538972e-02	-5.346094e-02	7.306417e-02	8.999443e-02	-5.130222e-01
8.267696e-01	9.940947e-01	3.552023e-02	-5.421299e-02	7.295343e-02	8.744793e-02	-5.094025e-01
8.282407e-01	9.942019e-01	3.564705e-02	-5.495976e-02	7.284212e-02	8.496811e-02	-5.058472e-01
8.297118e-01	9.943090e-01	3.577026e-02	-5.570134e-02	7.273023e-02	8.255209e-02	-5.023541e-01
8.311829e-01	9.944159e-01	3.588997e-02	-5.643783e-02	7.261778e-02	8.019715e-02	-4.989211e-01
8.326540e-01	9.945226e-01	3.600625e-02	-5.716932e-02	7.250474e-02	7.790071e-02	-4.955463e-01
8.341252e-01	9.946292e-01	3.611920e-02	-5.789588e-02	7.239114e-02	7.566037e-02	-4.922276e-01
8.355963e-01	9.947356e-01	3.622889e-02	-5.861760e-02	7.227695e-02	7.347384e-02	-4.889634e-01
8.370674e-01	9.948419e-01	3.633540e-02	-5.933455e-02	7.216219e-02	7.133897e-02	-4.857519e-01
8.385385e-01	9.949480e-01	3.643881e-02	-6.004682e-02	7.204685e-02	6.925371e-02	-4.825915e-01
8.400096e-01	9.950539e-01	3.653918e-02	-6.075448e-02	7.193093e-02	6.721613e-02	-4.794805e-01
8.414808e-01	9.951596e-01	3.663660e-02	-6.145759e-02	7.181443e-02	6.522440e-02	-4.764174e-01
8.429519e-01	9.952652e-01	3.673111e-02	-6.215623e-02	7.169735e-02	6.327680e-02	-4.734008e-01
8.444230e-01	9.953705e-01	3.682279e-02	-6.285047e-02	7.157970e-02	6.137168e-02	-4.704293e-01
8.458941e-01	9.954758e-01	3.691170e-02	-6.354037e-02	7.146148e-02	5.950747e-02	-4.675016e-01
8.473652e-01	9.955808e-01	3.699790e-02	-6.422599e-02	7.134268e-02	5.768269e-02	-4.646164e-01
8.488364e-01	9.956857e-01	3.708144e-02	-6.490740e-02	7.122332e-02	5.589594e-02	-4.617724e-01
8.503075e-01	9.957904e-01	3.716238e-02	-6.558466e-02	7.110338e-02	5.414587e-02	-4.589686e-01
8.517786e-01	9.958949e-01	3.724076e-02	-6.625782e-02	7.098289e-02	5.243120e-02	-4.562036e-01
8.532497e-01	9.959992e-01	3.731666e-02	-6.692694e-02	7.086182e-02	5.075073e-02	-4.534766e-01
8.547208e-01	9.961034e-01	3.739010e-02	-6.759207e-02	7.074020e-02	4.910328e-02	-4.507863e-01
8.561920e-01	9.962073e-01	3.746115e-02	-6.825328e-02	7.061802e-02	4.748777e-02	-4.481319e-01
8.576631e-01	9.963111e-01	3.752984e-02	-6.891060e-02	7.049528e-02	4.590312e-02	-4.455123e-01
8.591342e-01	9.964148e-01	3.759622e-02	-6.956410e-02	7.037200e-02	4.434835e-02	-4.429267e-01
8.606053e-01	9.965182e-01	3.766034e-02	-7.021382e-02	7.024817e-02	4.282247e-02	-4.403740e-01
8.620764e-01	9.966214e-01	3.772223e-02	-7.085980e-02	7.012379e-02	4.132458e-02	-4.378536e-01
8.635476e-01	9.967245e-01	3.778194e-02	-7.150210e-02	6.999887e-02	3.985380e-02	-4.353644e-01
8.650187e-01	9.968274e-01	3.783950e-02	-7.214076e-02	6.987341e-02	3.840928e-02	-4.329058e-01
8.664898e-01	9.969301e-01	3.789496e-02	-7.277583e-02	6.974742e-02	3.699022e-02	-4.304769e-01
8.679609e-01	9.970326e-01	3.794835e-02	-7.340734e-02	6.962090e-02	3.559584e-02	-4.280770e-01
8.694321e-01	9.971349e-01	3.799970e-02	-7.403535e-02	6.949385e-02	3.422542e-02	-4.257054e-01
8.709032e-01	9.972371e-01	3.804906e-02	-7.465989e-02	6.936629e-02	3.287824e-02	-4.233614e-01
8.723743e-01	9.973390e-01	3.809645e-02	-7.528099e-02	6.923820e-02	3.155362e-02	-4.210443e-01
8.738454e-01	9.974408e-01	3.814191e-02	-7.589871e-02	6.910960e-02	3.025090e-02	-4.187534e-01
8.753165e-01	9.975424e-01	3.818546e-02	-7.651308e-02	6.898048e-02	2.896947e-02	-4.164882e-01
8.767877e-01	9.976437e-01	3.822715e-02	-7.712413e-02	6.885086e-02	2.770872e-02	-4.142480e-01
8.782588e-01	9.977449e-01	3.826700e-02	-7.773191e-02	6.872074e-02	2.646808e-02	-4.120323e-01
8.797299e-01	9.978459e-01	3.830504e-02	-7.833644e-02	6.859012e-02	2.524698e-02	-4.098404e-01
8.812010e-01	9.979467e-01	3.834129e-02	-7.893777e-02	6.845901e-02	2.404490e-02	-4.076718e-01

Time (TU)	x (LU)	y (LU)	z (LU)	\dot{x} (LU/TU)	\dot{y} (LU/TU)	\dot{z} (LU/TU)
8.826721e-01	9.980474e-01	3.837579e-02	-7.953592e-02	6.832740e-02	2.286132e-02	-4.055260e-01
8.841433e-01	9.981478e-01	3.840856e-02	-8.013094e-02	6.819531e-02	2.169575e-02	-4.034025e-01
8.856144e-01	9.982480e-01	3.843963e-02	-8.072284e-02	6.806274e-02	2.054770e-02	-4.013008e-01
8.870855e-01	9.983480e-01	3.846903e-02	-8.131167e-02	6.792969e-02	1.941673e-02	-3.992204e-01
8.885566e-01	9.984479e-01	3.849677e-02	-8.189745e-02	6.779617e-02	1.830239e-02	-3.971607e-01
8.900277e-01	9.985475e-01	3.852289e-02	-8.248022e-02	6.766217e-02	1.720425e-02	-3.951215e-01
8.914989e-01	9.986470e-01	3.854740e-02	-8.306000e-02	6.752771e-02	1.612191e-02	-3.931021e-01
8.929700e-01	9.987462e-01	3.857033e-02	-8.363683e-02	6.739279e-02	1.505496e-02	-3.911022e-01
8.944411e-01	9.988452e-01	3.859170e-02	-8.421073e-02	6.725741e-02	1.400303e-02	-3.891215e-01
8.959122e-01	9.989441e-01	3.861154e-02	-8.478173e-02	6.712158e-02	1.296574e-02	-3.871594e-01
8.973833e-01	9.990427e-01	3.862986e-02	-8.534986e-02	6.698529e-02	1.194275e-02	-3.852155e-01
8.988545e-01	9.991412e-01	3.864668e-02	-8.591514e-02	6.684857e-02	1.093371e-02	-3.832896e-01
9.003256e-01	9.992394e-01	3.866203e-02	-8.647759e-02	6.671140e-02	9.938274e-03	-3.813812e-01
9.017967e-01	9.993374e-01	3.867593e-02	-8.703726e-02	6.657379e-02	8.956137e-03	-3.794900e-01
9.032678e-01	9.994353e-01	3.868839e-02	-8.759415e-02	6.643575e-02	7.986983e-03	-3.776156e-01
9.047389e-01	9.995329e-01	3.869943e-02	-8.814830e-02	6.629728e-02	7.030512e-03	-3.757577e-01
9.062101e-01	9.996303e-01	3.870908e-02	-8.869973e-02	6.615839e-02	6.086434e-03	-3.739160e-01
9.076812e-01	9.997276e-01	3.871735e-02	-8.924846e-02	6.601907e-02	5.154468e-03	-3.720901e-01
9.091523e-01	9.998246e-01	3.872425e-02	-8.979452e-02	6.587934e-02	4.234343e-03	-3.702797e-01
9.106234e-01	9.999214e-01	3.872981e-02	-9.033792e-02	6.573919e-02	3.325795e-03	-3.684846e-01
9.120945e-01	1.000018e+00	3.873404e-02	-9.087870e-02	6.559863e-02	2.428568e-03	-3.667043e-01
9.135657e-01	1.000114e+00	3.873696e-02	-9.141686e-02	6.545767e-02	1.542417e-03	-3.649388e-01
9.150368e-01	1.000211e+00	3.873859e-02	-9.195244e-02	6.531630e-02	6.671021e-04	-3.631875e-01
9.165079e-01	1.000307e+00	3.873893e-02	-9.248545e-02	6.517453e-02	-1.976087e-04	-3.614504e-01
9.179790e-01	1.000402e+00	3.873801e-02	-9.301592e-02	6.503237e-02	-1.051940e-03	-3.597271e-01
9.194501e-01	1.000498e+00	3.873584e-02	-9.354386e-02	6.488982e-02	-1.896110e-03	-3.580173e-01
9.209213e-01	1.000593e+00	3.873244e-02	-9.406930e-02	6.474688e-02	-2.730330e-03	-3.563209e-01
9.223924e-01	1.000688e+00	3.872781e-02	-9.459225e-02	6.460356e-02	-3.554804e-03	-3.546375e-01
9.238635e-01	1.000783e+00	3.872198e-02	-9.511274e-02	6.445985e-02	-4.369733e-03	-3.529669e-01
9.253346e-01	1.000878e+00	3.871496e-02	-9.563077e-02	6.431577e-02	-5.175308e-03	-3.513090e-01
9.268057e-01	1.000973e+00	3.870676e-02	-9.614638e-02	6.417132e-02	-5.971718e-03	-3.496634e-01
9.282769e-01	1.001067e+00	3.869739e-02	-9.665957e-02	6.402649e-02	-6.759144e-03	-3.480300e-01
9.297480e-01	1.001161e+00	3.868688e-02	-9.717037e-02	6.388130e-02	-7.537764e-03	-3.464085e-01
9.312191e-01	1.001255e+00	3.867522e-02	-9.767879e-02	6.373575e-02	-8.307749e-03	-3.447987e-01
9.326902e-01	1.001349e+00	3.866244e-02	-9.818486e-02	6.358984e-02	-9.069265e-03	-3.432004e-01
9.341613e-01	1.001442e+00	3.864854e-02	-9.868858e-02	6.344357e-02	-9.822477e-03	-3.416134e-01
9.356325e-01	1.001535e+00	3.863354e-02	-9.918997e-02	6.329695e-02	-1.056754e-02	-3.400376e-01
9.371036e-01	1.001628e+00	3.861745e-02	-9.968905e-02	6.314998e-02	-1.130461e-02	-3.384726e-01
9.385747e-01	1.001721e+00	3.860028e-02	-1.001858e-01	6.300266e-02	-1.203383e-02	-3.369184e-01
9.400458e-01	1.001814e+00	3.858205e-02	-1.006804e-01	6.285500e-02	-1.275535e-02	-3.353748e-01
9.415169e-01	1.001906e+00	3.856276e-02	-1.011726e-01	6.270700e-02	-1.346932e-02	-3.338415e-01
9.429881e-01	1.001998e+00	3.854242e-02	-1.016626e-01	6.255867e-02	-1.417586e-02	-3.323185e-01
9.444592e-01	1.002090e+00	3.852105e-02	-1.021504e-01	6.241000e-02	-1.487511e-02	-3.308054e-01
9.459303e-01	1.002182e+00	3.849866e-02	-1.026359e-01	6.226100e-02	-1.556721e-02	-3.293023e-01
9.474014e-01	1.002273e+00	3.847525e-02	-1.031193e-01	6.211167e-02	-1.625227e-02	-3.278088e-01
9.488725e-01	1.002364e+00	3.845085e-02	-1.036004e-01	6.196202e-02	-1.693043e-02	-3.263249e-01
9.503437e-01	1.002455e+00	3.842544e-02	-1.040794e-01	6.181205e-02	-1.760180e-02	-3.248503e-01
9.518148e-01	1.002546e+00	3.839906e-02	-1.045562e-01	6.166176e-02	-1.826649e-02	-3.233850e-01
9.532859e-01	1.002637e+00	3.837170e-02	-1.050309e-01	6.151116e-02	-1.892463e-02	-3.219288e-01
9.547570e-01	1.002727e+00	3.834338e-02	-1.055034e-01	6.136025e-02	-1.957633e-02	-3.204815e-01
9.562281e-01	1.002817e+00	3.831411e-02	-1.059738e-01	6.120902e-02	-2.022169e-02	-3.190431e-01
9.576993e-01	1.002907e+00	3.828389e-02	-1.064421e-01	6.105749e-02	-2.086081e-02	-3.176132e-01

Time (TU)	x (LU)	y (LU)	z (LU)	\dot{x} (LU/TU)	\dot{y} (LU/TU)	\dot{z} (LU/TU)
9.591704e-01	1.002997e+00	3.825273e-02	-1.069083e-01	6.090566e-02	-2.149381e-02	-3.161919e-01
9.606415e-01	1.003087e+00	3.822065e-02	-1.073724e-01	6.075353e-02	-2.212078e-02	-3.147790e-01
9.621126e-01	1.003176e+00	3.818765e-02	-1.078345e-01	6.060110e-02	-2.274182e-02	-3.133744e-01
9.635837e-01	1.003265e+00	3.815374e-02	-1.082945e-01	6.044837e-02	-2.335703e-02	-3.119779e-01
9.650549e-01	1.003354e+00	3.811893e-02	-1.087524e-01	6.029535e-02	-2.396649e-02	-3.105894e-01
9.665260e-01	1.003442e+00	3.808323e-02	-1.092083e-01	6.014205e-02	-2.457031e-02	-3.092087e-01
9.679971e-01	1.003531e+00	3.804664e-02	-1.096622e-01	5.998845e-02	-2.516856e-02	-3.078359e-01
9.694682e-01	1.003619e+00	3.800918e-02	-1.101140e-01	5.983458e-02	-2.576134e-02	-3.064707e-01
9.709393e-01	1.003707e+00	3.797085e-02	-1.105639e-01	5.968042e-02	-2.634873e-02	-3.051130e-01
9.724105e-01	1.003794e+00	3.793166e-02	-1.110117e-01	5.952598e-02	-2.693081e-02	-3.037627e-01
9.738816e-01	1.003882e+00	3.789162e-02	-1.114576e-01	5.937127e-02	-2.750767e-02	-3.024198e-01
9.753527e-01	1.003969e+00	3.785073e-02	-1.119015e-01	5.921628e-02	-2.807938e-02	-3.010840e-01
9.768238e-01	1.004056e+00	3.780900e-02	-1.123435e-01	5.906103e-02	-2.864601e-02	-2.997553e-01
9.782949e-01	1.004143e+00	3.776645e-02	-1.127835e-01	5.890550e-02	-2.920766e-02	-2.984337e-01
9.797661e-01	1.004229e+00	3.772307e-02	-1.132215e-01	5.874971e-02	-2.976438e-02	-2.971189e-01
9.812372e-01	1.004316e+00	3.767887e-02	-1.136577e-01	5.859366e-02	-3.031625e-02	-2.958109e-01
9.827083e-01	1.004402e+00	3.763387e-02	-1.140919e-01	5.843734e-02	-3.086334e-02	-2.945096e-01
9.841794e-01	1.004488e+00	3.758807e-02	-1.145242e-01	5.828077e-02	-3.140572e-02	-2.932149e-01
9.856505e-01	1.004573e+00	3.754147e-02	-1.149546e-01	5.812394e-02	-3.194346e-02	-2.919266e-01
9.871217e-01	1.004659e+00	3.749409e-02	-1.153831e-01	5.796686e-02	-3.247662e-02	-2.906448e-01
9.885928e-01	1.004744e+00	3.744592e-02	-1.158098e-01	5.780952e-02	-3.300526e-02	-2.893693e-01
9.900639e-01	1.004829e+00	3.739698e-02	-1.162345e-01	5.765194e-02	-3.352946e-02	-2.881001e-01
9.915350e-01	1.004913e+00	3.734727e-02	-1.166574e-01	5.749411e-02	-3.404926e-02	-2.868369e-01
9.930061e-01	1.004998e+00	3.729680e-02	-1.170785e-01	5.733603e-02	-3.456474e-02	-2.855799e-01
9.944773e-01	1.005082e+00	3.724557e-02	-1.174977e-01	5.717771e-02	-3.507594e-02	-2.843287e-01
9.959484e-01	1.005166e+00	3.719360e-02	-1.179150e-01	5.701916e-02	-3.558293e-02	-2.830835e-01
9.974195e-01	1.005250e+00	3.714088e-02	-1.183306e-01	5.686036e-02	-3.608577e-02	-2.818441e-01
9.988906e-01	1.005333e+00	3.708743e-02	-1.187443e-01	5.670133e-02	-3.658450e-02	-2.806104e-01
1.000362e+00	1.005417e+00	3.703324e-02	-1.191562e-01	5.654207e-02	-3.707919e-02	-2.793824e-01
1.001833e+00	1.005500e+00	3.697834e-02	-1.195663e-01	5.638257e-02	-3.756988e-02	-2.781599e-01
1.003304e+00	1.005583e+00	3.692271e-02	-1.199746e-01	5.622284e-02	-3.805662e-02	-2.769430e-01
1.004775e+00	1.005665e+00	3.686637e-02	-1.203811e-01	5.606289e-02	-3.853948e-02	-2.757314e-01
1.006246e+00	1.005748e+00	3.680932e-02	-1.207859e-01	5.590272e-02	-3.901849e-02	-2.745252e-01
1.007717e+00	1.005830e+00	3.675157e-02	-1.211889e-01	5.574231e-02	-3.949371e-02	-2.733243e-01
1.009188e+00	1.005912e+00	3.669312e-02	-1.215901e-01	5.558169e-02	-3.996518e-02	-2.721286e-01
1.010660e+00	1.005993e+00	3.663398e-02	-1.219895e-01	5.542085e-02	-4.043295e-02	-2.709380e-01
1.012131e+00	1.006075e+00	3.657416e-02	-1.223872e-01	5.525979e-02	-4.089707e-02	-2.697525e-01
1.013602e+00	1.006156e+00	3.651365e-02	-1.227832e-01	5.509852e-02	-4.135757e-02	-2.685720e-01
1.015073e+00	1.006237e+00	3.645247e-02	-1.231774e-01	5.493704e-02	-4.181452e-02	-2.673965e-01
1.016544e+00	1.006317e+00	3.639063e-02	-1.235700e-01	5.477534e-02	-4.226793e-02	-2.662258e-01
1.018015e+00	1.006398e+00	3.632811e-02	-1.239608e-01	5.461343e-02	-4.271787e-02	-2.650600e-01
1.019486e+00	1.006478e+00	3.626494e-02	-1.243498e-01	5.445132e-02	-4.316437e-02	-2.638988e-01
1.020957e+00	1.006558e+00	3.620112e-02	-1.247372e-01	5.428900e-02	-4.360747e-02	-2.627424e-01
1.022429e+00	1.006638e+00	3.613664e-02	-1.251229e-01	5.412648e-02	-4.404722e-02	-2.615906e-01
1.023900e+00	1.006717e+00	3.607152e-02	-1.255069e-01	5.396375e-02	-4.448364e-02	-2.604434e-01
1.025371e+00	1.006797e+00	3.600576e-02	-1.258892e-01	5.380083e-02	-4.491678e-02	-2.593007e-01
1.026842e+00	1.006876e+00	3.593937e-02	-1.262698e-01	5.363771e-02	-4.534668e-02	-2.581625e-01
1.028313e+00	1.006954e+00	3.587234e-02	-1.266488e-01	5.347439e-02	-4.577337e-02	-2.570286e-01
1.029784e+00	1.007033e+00	3.580469e-02	-1.270260e-01	5.331087e-02	-4.619688e-02	-2.558991e-01
1.031255e+00	1.007111e+00	3.573642e-02	-1.274017e-01	5.314717e-02	-4.661727e-02	-2.547739e-01
1.032726e+00	1.007189e+00	3.566753e-02	-1.277756e-01	5.298327e-02	-4.703455e-02	-2.536529e-01
1.034198e+00	1.007267e+00	3.559803e-02	-1.281480e-01	5.281918e-02	-4.744876e-02	-2.525361e-01

Time (TU)	x (LU)	y (LU)	z (LU)	\dot{x} (LU/TU)	\dot{y} (LU/TU)	\dot{z} (LU/TU)
1.035669e+00	1.007345e+00	3.552793e-02	-1.285187e-01	5.265491e-02	-4.785994e-02	-2.514235e-01
1.037140e+00	1.007422e+00	3.545722e-02	-1.288877e-01	5.249044e-02	-4.826812e-02	-2.503149e-01
1.038611e+00	1.007499e+00	3.538591e-02	-1.292552e-01	5.232580e-02	-4.867334e-02	-2.492104e-01
1.040082e+00	1.007576e+00	3.531401e-02	-1.296210e-01	5.216097e-02	-4.907561e-02	-2.481098e-01
1.041553e+00	1.007653e+00	3.524152e-02	-1.299852e-01	5.199596e-02	-4.947498e-02	-2.470132e-01
1.043024e+00	1.007729e+00	3.516845e-02	-1.303477e-01	5.183077e-02	-4.987147e-02	-2.459205e-01
1.044495e+00	1.007805e+00	3.509479e-02	-1.307087e-01	5.166540e-02	-5.026512e-02	-2.448316e-01
1.045966e+00	1.007881e+00	3.502056e-02	-1.310681e-01	5.149986e-02	-5.065595e-02	-2.437465e-01
1.047438e+00	1.007957e+00	3.494575e-02	-1.314259e-01	5.133414e-02	-5.104400e-02	-2.426651e-01
1.048909e+00	1.008032e+00	3.487037e-02	-1.317821e-01	5.116825e-02	-5.142928e-02	-2.415875e-01
1.050380e+00	1.008107e+00	3.479443e-02	-1.321367e-01	5.100218e-02	-5.181184e-02	-2.405135e-01
1.051851e+00	1.008182e+00	3.471793e-02	-1.324897e-01	5.083595e-02	-5.219169e-02	-2.394431e-01
1.053322e+00	1.008257e+00	3.464087e-02	-1.328412e-01	5.066955e-02	-5.256887e-02	-2.383763e-01
1.054793e+00	1.008331e+00	3.456326e-02	-1.331911e-01	5.050298e-02	-5.294339e-02	-2.373131e-01
1.056264e+00	1.008405e+00	3.448510e-02	-1.335394e-01	5.033624e-02	-5.331529e-02	-2.362533e-01
1.057735e+00	1.008479e+00	3.440640e-02	-1.338862e-01	5.016934e-02	-5.368459e-02	-2.351970e-01
1.059207e+00	1.008553e+00	3.432715e-02	-1.342314e-01	5.000228e-02	-5.405132e-02	-2.341441e-01
1.060678e+00	1.008626e+00	3.424737e-02	-1.345751e-01	4.983505e-02	-5.441550e-02	-2.330945e-01
1.062149e+00	1.008700e+00	3.416705e-02	-1.349173e-01	4.966767e-02	-5.477715e-02	-2.320483e-01
1.063620e+00	1.008773e+00	3.408620e-02	-1.352579e-01	4.950013e-02	-5.513630e-02	-2.310054e-01
1.065091e+00	1.008845e+00	3.400483e-02	-1.355969e-01	4.933242e-02	-5.549298e-02	-2.299657e-01
1.066562e+00	1.008918e+00	3.392293e-02	-1.359345e-01	4.916457e-02	-5.584720e-02	-2.289293e-01
1.068033e+00	1.008990e+00	3.384051e-02	-1.362705e-01	4.899656e-02	-5.619899e-02	-2.278960e-01
1.069504e+00	1.009062e+00	3.375758e-02	-1.366050e-01	4.882839e-02	-5.654836e-02	-2.268659e-01
1.070976e+00	1.009134e+00	3.367413e-02	-1.369380e-01	4.866008e-02	-5.689535e-02	-2.258389e-01
1.072447e+00	1.009205e+00	3.359018e-02	-1.372695e-01	4.849161e-02	-5.723998e-02	-2.248150e-01
1.073918e+00	1.009276e+00	3.350572e-02	-1.375995e-01	4.832300e-02	-5.758225e-02	-2.237941e-01
1.075389e+00	1.009347e+00	3.342076e-02	-1.379279e-01	4.815423e-02	-5.792221e-02	-2.227762e-01
1.076860e+00	1.009418e+00	3.333530e-02	-1.382549e-01	4.798533e-02	-5.825985e-02	-2.217612e-01
1.078331e+00	1.009488e+00	3.324935e-02	-1.385804e-01	4.781627e-02	-5.859522e-02	-2.207492e-01
1.079802e+00	1.009559e+00	3.316290e-02	-1.389044e-01	4.764707e-02	-5.892832e-02	-2.197401e-01
1.081273e+00	1.009629e+00	3.307597e-02	-1.392269e-01	4.747773e-02	-5.925917e-02	-2.187339e-01
1.082744e+00	1.009698e+00	3.298855e-02	-1.395480e-01	4.730825e-02	-5.958780e-02	-2.177306e-01
1.084216e+00	1.009768e+00	3.290065e-02	-1.398676e-01	4.713862e-02	-5.991422e-02	-2.167300e-01
1.085687e+00	1.009837e+00	3.281227e-02	-1.401857e-01	4.696886e-02	-6.023846e-02	-2.157322e-01
1.087158e+00	1.009906e+00	3.272341e-02	-1.405023e-01	4.679896e-02	-6.056052e-02	-2.147372e-01
1.088629e+00	1.009975e+00	3.263408e-02	-1.408175e-01	4.662892e-02	-6.088043e-02	-2.137448e-01
1.090100e+00	1.010043e+00	3.254429e-02	-1.411312e-01	4.645875e-02	-6.119821e-02	-2.127552e-01
1.091571e+00	1.010111e+00	3.245403e-02	-1.414434e-01	4.628845e-02	-6.151387e-02	-2.117682e-01
1.093042e+00	1.010179e+00	3.236330e-02	-1.417543e-01	4.611801e-02	-6.182743e-02	-2.107839e-01
1.094513e+00	1.010247e+00	3.227212e-02	-1.420636e-01	4.594743e-02	-6.213890e-02	-2.098021e-01
1.095985e+00	1.010315e+00	3.218047e-02	-1.423716e-01	4.577673e-02	-6.244831e-02	-2.088230e-01
1.097456e+00	1.010382e+00	3.208838e-02	-1.426780e-01	4.560590e-02	-6.275567e-02	-2.078463e-01
1.098927e+00	1.010449e+00	3.199583e-02	-1.429831e-01	4.543494e-02	-6.306099e-02	-2.068722e-01
1.100398e+00	1.010515e+00	3.190284e-02	-1.432867e-01	4.526385e-02	-6.336430e-02	-2.059006e-01
1.101869e+00	1.010582e+00	3.180940e-02	-1.435889e-01	4.509264e-02	-6.366560e-02	-2.049314e-01
1.103340e+00	1.010648e+00	3.171552e-02	-1.438897e-01	4.492130e-02	-6.396492e-02	-2.039647e-01
1.104811e+00	1.010714e+00	3.162120e-02	-1.441890e-01	4.474983e-02	-6.426226e-02	-2.030004e-01
1.106282e+00	1.010780e+00	3.152645e-02	-1.444869e-01	4.457824e-02	-6.455765e-02	-2.020384e-01
1.107754e+00	1.010845e+00	3.143126e-02	-1.447835e-01	4.440654e-02	-6.485109e-02	-2.010789e-01
1.109225e+00	1.010910e+00	3.133564e-02	-1.450786e-01	4.423471e-02	-6.514260e-02	-2.001216e-01
1.110696e+00	1.010975e+00	3.123959e-02	-1.453723e-01	4.406276e-02	-6.543220e-02	-1.991667e-01

Time (TU)	x (LU)	y (LU)	z (LU)	\dot{x} (LU/TU)	\dot{y} (LU/TU)	\dot{z} (LU/TU)
1.112167e+00	1.011040e+00	3.114312e-02	-1.456646e-01	4.389069e-02	-6.571990e-02	-1.982141e-01
1.113638e+00	1.011105e+00	3.104623e-02	-1.459555e-01	4.371850e-02	-6.600571e-02	-1.972637e-01
1.115109e+00	1.011169e+00	3.094892e-02	-1.462450e-01	4.354620e-02	-6.628965e-02	-1.963156e-01
1.116580e+00	1.011233e+00	3.085119e-02	-1.465331e-01	4.337378e-02	-6.657173e-02	-1.953696e-01
1.118051e+00	1.011296e+00	3.075305e-02	-1.468198e-01	4.320124e-02	-6.685197e-02	-1.944259e-01
1.119522e+00	1.011360e+00	3.065450e-02	-1.471051e-01	4.302859e-02	-6.713037e-02	-1.934843e-01
1.120994e+00	1.011423e+00	3.055554e-02	-1.473891e-01	4.285583e-02	-6.740695e-02	-1.925449e-01
1.122465e+00	1.011486e+00	3.045617e-02	-1.476716e-01	4.268296e-02	-6.768172e-02	-1.916076e-01
1.123936e+00	1.011549e+00	3.035640e-02	-1.479528e-01	4.250997e-02	-6.795470e-02	-1.906724e-01
1.125407e+00	1.011611e+00	3.025623e-02	-1.482326e-01	4.233688e-02	-6.822589e-02	-1.897393e-01
1.126878e+00	1.011673e+00	3.015567e-02	-1.485111e-01	4.216368e-02	-6.849531e-02	-1.888082e-01
1.128349e+00	1.011735e+00	3.005470e-02	-1.487882e-01	4.199037e-02	-6.876297e-02	-1.878792e-01
1.129820e+00	1.011797e+00	2.995335e-02	-1.490639e-01	4.181695e-02	-6.902889e-02	-1.869522e-01
1.131291e+00	1.011858e+00	2.985161e-02	-1.493382e-01	4.164342e-02	-6.929307e-02	-1.860272e-01
1.132763e+00	1.011919e+00	2.974947e-02	-1.496112e-01	4.146979e-02	-6.955552e-02	-1.851042e-01
1.134234e+00	1.011980e+00	2.964696e-02	-1.498828e-01	4.129606e-02	-6.981626e-02	-1.841831e-01
1.135705e+00	1.012041e+00	2.954406e-02	-1.501531e-01	4.112222e-02	-7.007530e-02	-1.832639e-01
1.137176e+00	1.012101e+00	2.944078e-02	-1.504220e-01	4.094828e-02	-7.033265e-02	-1.823467e-01
1.138647e+00	1.012161e+00	2.933712e-02	-1.506896e-01	4.077424e-02	-7.058831e-02	-1.814314e-01
1.140118e+00	1.012221e+00	2.923309e-02	-1.509559e-01	4.060009e-02	-7.084231e-02	-1.805179e-01
1.141589e+00	1.012281e+00	2.912869e-02	-1.512208e-01	4.042585e-02	-7.109465e-02	-1.796063e-01
1.143060e+00	1.012340e+00	2.902392e-02	-1.514843e-01	4.025151e-02	-7.134533e-02	-1.786965e-01
1.144532e+00	1.012399e+00	2.891878e-02	-1.517465e-01	4.007707e-02	-7.159438e-02	-1.777886e-01
1.146003e+00	1.012458e+00	2.881327e-02	-1.520074e-01	3.990253e-02	-7.184180e-02	-1.768824e-01
1.147474e+00	1.012516e+00	2.870740e-02	-1.522670e-01	3.972789e-02	-7.208760e-02	-1.759781e-01
1.148945e+00	1.012575e+00	2.860117e-02	-1.525252e-01	3.955316e-02	-7.233179e-02	-1.750755e-01
1.150416e+00	1.012633e+00	2.849458e-02	-1.527821e-01	3.937834e-02	-7.257438e-02	-1.741746e-01
1.151887e+00	1.012691e+00	2.838764e-02	-1.530376e-01	3.920342e-02	-7.281538e-02	-1.732755e-01
1.153358e+00	1.012748e+00	2.828034e-02	-1.532919e-01	3.902840e-02	-7.305480e-02	-1.723781e-01
1.154829e+00	1.012805e+00	2.817270e-02	-1.535448e-01	3.885330e-02	-7.329264e-02	-1.714824e-01
1.156300e+00	1.012862e+00	2.806470e-02	-1.537964e-01	3.867810e-02	-7.352893e-02	-1.705883e-01
1.157772e+00	1.012919e+00	2.795636e-02	-1.540467e-01	3.850281e-02	-7.376366e-02	-1.696959e-01
1.159243e+00	1.012976e+00	2.784767e-02	-1.542957e-01	3.832743e-02	-7.399684e-02	-1.688052e-01
1.160714e+00	1.013032e+00	2.773864e-02	-1.545434e-01	3.815197e-02	-7.422849e-02	-1.679161e-01
1.162185e+00	1.013088e+00	2.762927e-02	-1.547898e-01	3.797641e-02	-7.445861e-02	-1.670286e-01
1.163656e+00	1.013144e+00	2.751957e-02	-1.550348e-01	3.780077e-02	-7.468721e-02	-1.661427e-01
1.165127e+00	1.013199e+00	2.740953e-02	-1.552786e-01	3.762503e-02	-7.491431e-02	-1.652584e-01
1.166598e+00	1.013254e+00	2.729915e-02	-1.555211e-01	3.744922e-02	-7.513989e-02	-1.643756e-01
1.168069e+00	1.013309e+00	2.718845e-02	-1.557622e-01	3.727331e-02	-7.536399e-02	-1.634944e-01
1.169541e+00	1.013364e+00	2.707741e-02	-1.560021e-01	3.709733e-02	-7.558660e-02	-1.626148e-01
1.171012e+00	1.013419e+00	2.696605e-02	-1.562407e-01	3.692125e-02	-7.580773e-02	-1.617366e-01
1.172483e+00	1.013473e+00	2.685437e-02	-1.564780e-01	3.674510e-02	-7.602739e-02	-1.608600e-01
1.173954e+00	1.013527e+00	2.674236e-02	-1.567140e-01	3.656886e-02	-7.624559e-02	-1.599848e-01
1.175425e+00	1.013580e+00	2.663004e-02	-1.569487e-01	3.639254e-02	-7.646233e-02	-1.591111e-01
1.176896e+00	1.013634e+00	2.651739e-02	-1.571821e-01	3.621614e-02	-7.667762e-02	-1.582389e-01
1.178367e+00	1.013687e+00	2.640443e-02	-1.574143e-01	3.603966e-02	-7.689148e-02	-1.573681e-01
1.179838e+00	1.013740e+00	2.629116e-02	-1.576451e-01	3.586310e-02	-7.710390e-02	-1.564987e-01
1.181310e+00	1.013792e+00	2.617758e-02	-1.578747e-01	3.568645e-02	-7.731489e-02	-1.556308e-01
1.182781e+00	1.013845e+00	2.606368e-02	-1.581030e-01	3.550974e-02	-7.752447e-02	-1.547643e-01
1.184252e+00	1.013897e+00	2.594948e-02	-1.583301e-01	3.533294e-02	-7.773264e-02	-1.538991e-01
1.185723e+00	1.013949e+00	2.583498e-02	-1.585558e-01	3.515606e-02	-7.793940e-02	-1.530354e-01
1.187194e+00	1.014000e+00	2.572017e-02	-1.587803e-01	3.497911e-02	-7.814477e-02	-1.521729e-01

Time (TU)	x (LU)	y (LU)	z (LU)	\dot{x} (LU/TU)	\dot{y} (LU/TU)	\dot{z} (LU/TU)
1.188665e+00	1.014052e+00	2.560506e-02	-1.590036e-01	3.480209e-02	-7.834874e-02	-1.513119e-01
1.190136e+00	1.014103e+00	2.548965e-02	-1.592255e-01	3.462499e-02	-7.855133e-02	-1.504522e-01
1.191607e+00	1.014154e+00	2.537394e-02	-1.594462e-01	3.444781e-02	-7.875254e-02	-1.495938e-01
1.193078e+00	1.014204e+00	2.525794e-02	-1.596657e-01	3.427056e-02	-7.895238e-02	-1.487367e-01
1.194550e+00	1.014254e+00	2.514164e-02	-1.598839e-01	3.409324e-02	-7.915086e-02	-1.478809e-01
1.196021e+00	1.014304e+00	2.502506e-02	-1.601008e-01	3.391585e-02	-7.934798e-02	-1.470263e-01
1.197492e+00	1.014354e+00	2.490818e-02	-1.603165e-01	3.373838e-02	-7.954375e-02	-1.461731e-01
1.198963e+00	1.014404e+00	2.479102e-02	-1.605309e-01	3.356084e-02	-7.973817e-02	-1.453211e-01
1.200434e+00	1.014453e+00	2.467358e-02	-1.607440e-01	3.338324e-02	-7.993125e-02	-1.444704e-01
1.201905e+00	1.014502e+00	2.455585e-02	-1.609559e-01	3.320556e-02	-8.012300e-02	-1.436208e-01
1.203376e+00	1.014551e+00	2.443783e-02	-1.611666e-01	3.302781e-02	-8.031342e-02	-1.427726e-01
1.204847e+00	1.014599e+00	2.431954e-02	-1.613760e-01	3.284999e-02	-8.050252e-02	-1.419255e-01
1.206319e+00	1.014647e+00	2.420098e-02	-1.615842e-01	3.267211e-02	-8.069031e-02	-1.410796e-01
1.207790e+00	1.014695e+00	2.408214e-02	-1.617911e-01	3.249416e-02	-8.087678e-02	-1.402349e-01
1.209261e+00	1.014743e+00	2.396302e-02	-1.619968e-01	3.231614e-02	-8.106195e-02	-1.393914e-01
1.210732e+00	1.014790e+00	2.384363e-02	-1.622012e-01	3.213806e-02	-8.124582e-02	-1.385490e-01
1.212203e+00	1.014837e+00	2.372398e-02	-1.624044e-01	3.195991e-02	-8.142840e-02	-1.377078e-01
1.213674e+00	1.014884e+00	2.360405e-02	-1.626064e-01	3.178169e-02	-8.160969e-02	-1.368677e-01
1.215145e+00	1.014931e+00	2.348386e-02	-1.628071e-01	3.160341e-02	-8.178969e-02	-1.360288e-01
1.216616e+00	1.014977e+00	2.336341e-02	-1.630066e-01	3.142507e-02	-8.196842e-02	-1.351910e-01
1.218088e+00	1.015023e+00	2.324269e-02	-1.632049e-01	3.124666e-02	-8.214588e-02	-1.343543e-01
1.219559e+00	1.015069e+00	2.312171e-02	-1.634019e-01	3.106819e-02	-8.232207e-02	-1.335186e-01
1.221030e+00	1.015115e+00	2.300048e-02	-1.635977e-01	3.088966e-02	-8.249700e-02	-1.326841e-01
1.222501e+00	1.015160e+00	2.287899e-02	-1.637923e-01	3.071106e-02	-8.267068e-02	-1.318506e-01
1.223972e+00	1.015205e+00	2.275724e-02	-1.639857e-01	3.053241e-02	-8.284310e-02	-1.310183e-01
1.225443e+00	1.015250e+00	2.263525e-02	-1.641778e-01	3.035369e-02	-8.301428e-02	-1.301869e-01
1.226914e+00	1.015294e+00	2.251300e-02	-1.643687e-01	3.017492e-02	-8.318421e-02	-1.293566e-01
1.228385e+00	1.015339e+00	2.239050e-02	-1.645584e-01	2.999608e-02	-8.335291e-02	-1.285273e-01
1.229857e+00	1.015383e+00	2.226775e-02	-1.647469e-01	2.981719e-02	-8.352037e-02	-1.276991e-01
1.231328e+00	1.015426e+00	2.214476e-02	-1.649341e-01	2.963824e-02	-8.368661e-02	-1.268719e-01
1.232799e+00	1.015470e+00	2.202153e-02	-1.651202e-01	2.945923e-02	-8.385163e-02	-1.260456e-01
1.234270e+00	1.015513e+00	2.189805e-02	-1.653050e-01	2.928016e-02	-8.401542e-02	-1.252204e-01
1.235741e+00	1.015556e+00	2.177433e-02	-1.654886e-01	2.910103e-02	-8.417801e-02	-1.243961e-01
1.237212e+00	1.015599e+00	2.165038e-02	-1.656710e-01	2.892185e-02	-8.433938e-02	-1.235729e-01
1.238683e+00	1.015641e+00	2.152619e-02	-1.658522e-01	2.874262e-02	-8.449955e-02	-1.227505e-01
1.240154e+00	1.015683e+00	2.140176e-02	-1.660321e-01	2.856333e-02	-8.465852e-02	-1.219292e-01
1.241625e+00	1.015725e+00	2.127710e-02	-1.662109e-01	2.838398e-02	-8.481629e-02	-1.211087e-01
1.243097e+00	1.015767e+00	2.115221e-02	-1.663885e-01	2.820458e-02	-8.497287e-02	-1.202893e-01
1.244568e+00	1.015808e+00	2.102709e-02	-1.665648e-01	2.802512e-02	-8.512826e-02	-1.194707e-01
1.246039e+00	1.015849e+00	2.090174e-02	-1.667400e-01	2.784562e-02	-8.528247e-02	-1.186530e-01
1.247510e+00	1.015890e+00	2.077617e-02	-1.669139e-01	2.766606e-02	-8.543550e-02	-1.178363e-01
1.248981e+00	1.015931e+00	2.065037e-02	-1.670867e-01	2.748645e-02	-8.558736e-02	-1.170205e-01
1.250452e+00	1.015971e+00	2.052435e-02	-1.672582e-01	2.730678e-02	-8.573804e-02	-1.162055e-01
1.251923e+00	1.016011e+00	2.039811e-02	-1.674286e-01	2.712707e-02	-8.588756e-02	-1.153914e-01
1.253394e+00	1.016051e+00	2.027165e-02	-1.675977e-01	2.694730e-02	-8.603591e-02	-1.145782e-01
1.254866e+00	1.016090e+00	2.014497e-02	-1.677657e-01	2.676748e-02	-8.618310e-02	-1.137659e-01
1.256337e+00	1.016130e+00	2.001808e-02	-1.679325e-01	2.658762e-02	-8.632914e-02	-1.129544e-01
1.257808e+00	1.016169e+00	1.989097e-02	-1.680980e-01	2.640770e-02	-8.647402e-02	-1.121438e-01
1.259279e+00	1.016207e+00	1.976365e-02	-1.682624e-01	2.622774e-02	-8.661776e-02	-1.113339e-01
1.260750e+00	1.016246e+00	1.963612e-02	-1.684256e-01	2.604773e-02	-8.676035e-02	-1.105250e-01
1.262221e+00	1.016284e+00	1.950839e-02	-1.685876e-01	2.586767e-02	-8.690180e-02	-1.097168e-01
1.263692e+00	1.016322e+00	1.938044e-02	-1.687484e-01	2.568756e-02	-8.704211e-02	-1.089094e-01

Time (TU)	x (LU)	y (LU)	z (LU)	\dot{x} (LU/TU)	\dot{y} (LU/TU)	\dot{z} (LU/TU)
1.265163e+00	1.016359e+00	1.925229e-02	-1.689081e-01	2.550740e-02	-8.718129e-02	-1.081029e-01
1.266635e+00	1.016397e+00	1.912393e-02	-1.690665e-01	2.532720e-02	-8.731934e-02	-1.072971e-01
1.268106e+00	1.016434e+00	1.899537e-02	-1.692238e-01	2.514696e-02	-8.745626e-02	-1.064922e-01
1.269577e+00	1.016471e+00	1.886661e-02	-1.693798e-01	2.496666e-02	-8.759205e-02	-1.056880e-01
1.271048e+00	1.016507e+00	1.873766e-02	-1.695347e-01	2.478632e-02	-8.772673e-02	-1.048846e-01
1.272519e+00	1.016544e+00	1.860850e-02	-1.696884e-01	2.460594e-02	-8.786029e-02	-1.040819e-01
1.273990e+00	1.016580e+00	1.847915e-02	-1.698409e-01	2.442551e-02	-8.799273e-02	-1.032800e-01
1.275461e+00	1.016616e+00	1.834961e-02	-1.699923e-01	2.424504e-02	-8.812407e-02	-1.024788e-01
1.276932e+00	1.016651e+00	1.821987e-02	-1.701425e-01	2.406453e-02	-8.825429e-02	-1.016784e-01
1.278403e+00	1.016686e+00	1.808994e-02	-1.702915e-01	2.388397e-02	-8.838342e-02	-1.008787e-01
1.279875e+00	1.016721e+00	1.795982e-02	-1.704393e-01	2.370337e-02	-8.851144e-02	-1.000798e-01
1.281346e+00	1.016756e+00	1.782952e-02	-1.705859e-01	2.352273e-02	-8.863836e-02	-9.928151e-02
1.282817e+00	1.016791e+00	1.769903e-02	-1.707314e-01	2.334205e-02	-8.876419e-02	-9.848396e-02
1.284288e+00	1.016825e+00	1.756836e-02	-1.708757e-01	2.316132e-02	-8.888893e-02	-9.768711e-02
1.285759e+00	1.016859e+00	1.743750e-02	-1.710188e-01	2.298056e-02	-8.901258e-02	-9.689096e-02
1.287230e+00	1.016892e+00	1.730646e-02	-1.711608e-01	2.279975e-02	-8.913514e-02	-9.609549e-02
1.288701e+00	1.016926e+00	1.717524e-02	-1.713015e-01	2.261890e-02	-8.925662e-02	-9.530070e-02
1.290172e+00	1.016959e+00	1.704385e-02	-1.714412e-01	2.243802e-02	-8.937702e-02	-9.450658e-02
1.291644e+00	1.016992e+00	1.691227e-02	-1.715796e-01	2.225709e-02	-8.949634e-02	-9.371312e-02
1.293115e+00	1.017025e+00	1.678053e-02	-1.717169e-01	2.207613e-02	-8.961458e-02	-9.292032e-02
1.294586e+00	1.017057e+00	1.664861e-02	-1.718530e-01	2.189513e-02	-8.973176e-02	-9.212817e-02
1.296057e+00	1.017089e+00	1.651651e-02	-1.719879e-01	2.171409e-02	-8.984786e-02	-9.133666e-02
1.297528e+00	1.017121e+00	1.638425e-02	-1.721217e-01	2.153301e-02	-8.996290e-02	-9.054578e-02
1.298999e+00	1.017152e+00	1.625182e-02	-1.722544e-01	2.135189e-02	-9.007687e-02	-8.975553e-02
1.300470e+00	1.017184e+00	1.611923e-02	-1.723858e-01	2.117074e-02	-9.018979e-02	-8.896590e-02
1.301941e+00	1.017215e+00	1.598646e-02	-1.725161e-01	2.098956e-02	-9.030164e-02	-8.817689e-02
1.303413e+00	1.017245e+00	1.585354e-02	-1.726453e-01	2.080833e-02	-9.041244e-02	-8.738848e-02
1.304884e+00	1.017276e+00	1.572045e-02	-1.727732e-01	2.062707e-02	-9.052218e-02	-8.660068e-02
1.306355e+00	1.017306e+00	1.558720e-02	-1.729001e-01	2.044578e-02	-9.063087e-02	-8.581346e-02
1.307826e+00	1.017336e+00	1.545379e-02	-1.730257e-01	2.026445e-02	-9.073852e-02	-8.502683e-02
1.309297e+00	1.017366e+00	1.532023e-02	-1.731502e-01	2.008308e-02	-9.084511e-02	-8.424079e-02
1.310768e+00	1.017395e+00	1.518650e-02	-1.732736e-01	1.990169e-02	-9.095067e-02	-8.345531e-02
1.312239e+00	1.017424e+00	1.505263e-02	-1.733958e-01	1.972025e-02	-9.105518e-02	-8.267040e-02
1.313710e+00	1.017453e+00	1.491860e-02	-1.735168e-01	1.953879e-02	-9.115865e-02	-8.188605e-02
1.315181e+00	1.017482e+00	1.478442e-02	-1.736367e-01	1.935729e-02	-9.126109e-02	-8.110226e-02
1.316653e+00	1.017510e+00	1.465009e-02	-1.737554e-01	1.917576e-02	-9.136249e-02	-8.031901e-02
1.318124e+00	1.017538e+00	1.451561e-02	-1.738730e-01	1.899420e-02	-9.146286e-02	-7.953631e-02
1.319595e+00	1.017566e+00	1.438098e-02	-1.739894e-01	1.881260e-02	-9.156219e-02	-7.875413e-02
1.321066e+00	1.017593e+00	1.424621e-02	-1.741047e-01	1.863098e-02	-9.166050e-02	-7.797249e-02
1.322537e+00	1.017621e+00	1.411129e-02	-1.742189e-01	1.844932e-02	-9.175779e-02	-7.719137e-02
1.324008e+00	1.017648e+00	1.397624e-02	-1.743318e-01	1.826763e-02	-9.185405e-02	-7.641076e-02
1.325479e+00	1.017674e+00	1.384104e-02	-1.744437e-01	1.808592e-02	-9.194928e-02	-7.563066e-02
1.326950e+00	1.017701e+00	1.370570e-02	-1.745544e-01	1.790417e-02	-9.204350e-02	-7.485106e-02
1.328422e+00	1.017727e+00	1.357022e-02	-1.746639e-01	1.772239e-02	-9.213670e-02	-7.407196e-02
1.329893e+00	1.017753e+00	1.343461e-02	-1.747723e-01	1.754058e-02	-9.222888e-02	-7.329336e-02
1.331364e+00	1.017779e+00	1.329887e-02	-1.748796e-01	1.735875e-02	-9.232006e-02	-7.251523e-02
1.332835e+00	1.017804e+00	1.316299e-02	-1.749857e-01	1.717689e-02	-9.241021e-02	-7.173759e-02
1.334306e+00	1.017829e+00	1.302697e-02	-1.750906e-01	1.699499e-02	-9.249936e-02	-7.096041e-02
1.335777e+00	1.017854e+00	1.289083e-02	-1.751944e-01	1.681307e-02	-9.258750e-02	-7.018371e-02
1.337248e+00	1.017879e+00	1.275456e-02	-1.752971e-01	1.663112e-02	-9.267464e-02	-6.940746e-02
1.338719e+00	1.017903e+00	1.261816e-02	-1.753987e-01	1.644915e-02	-9.276077e-02	-6.863167e-02
1.340191e+00	1.017927e+00	1.248163e-02	-1.754991e-01	1.626715e-02	-9.284590e-02	-6.785632e-02

Time (TU)	x (LU)	y (LU)	z (LU)	\dot{x} (LU/TU)	\dot{y} (LU/TU)	\dot{z} (LU/TU)
1.341662e+00	1.017951e+00	1.234499e-02	-1.755983e-01	1.608512e-02	-9.293002e-02	-6.708142e-02
1.343133e+00	1.017974e+00	1.220821e-02	-1.756964e-01	1.590307e-02	-9.301315e-02	-6.630696e-02
1.344604e+00	1.017998e+00	1.207132e-02	-1.757934e-01	1.572099e-02	-9.309528e-02	-6.553293e-02
1.346075e+00	1.018021e+00	1.193430e-02	-1.758892e-01	1.553888e-02	-9.317642e-02	-6.475932e-02
1.347546e+00	1.018043e+00	1.179717e-02	-1.759839e-01	1.535675e-02	-9.325656e-02	-6.398613e-02
1.349017e+00	1.018066e+00	1.165992e-02	-1.760775e-01	1.517459e-02	-9.333571e-02	-6.321336e-02
1.350488e+00	1.018088e+00	1.152256e-02	-1.761699e-01	1.499241e-02	-9.341387e-02	-6.244099e-02
1.351959e+00	1.018110e+00	1.138508e-02	-1.762612e-01	1.481021e-02	-9.349104e-02	-6.166903e-02
1.353431e+00	1.018132e+00	1.124748e-02	-1.763514e-01	1.462798e-02	-9.356722e-02	-6.089747e-02
1.354902e+00	1.018153e+00	1.110978e-02	-1.764404e-01	1.444573e-02	-9.364242e-02	-6.012629e-02
1.356373e+00	1.018174e+00	1.097197e-02	-1.765283e-01	1.426346e-02	-9.371663e-02	-5.935550e-02
1.357844e+00	1.018195e+00	1.083404e-02	-1.766150e-01	1.408116e-02	-9.378986e-02	-5.858509e-02
1.359315e+00	1.018216e+00	1.069601e-02	-1.767007e-01	1.389884e-02	-9.386211e-02	-5.781506e-02
1.360786e+00	1.018236e+00	1.055788e-02	-1.767851e-01	1.371650e-02	-9.393338e-02	-5.704540e-02
1.362257e+00	1.018256e+00	1.041964e-02	-1.768685e-01	1.353414e-02	-9.400367e-02	-5.627610e-02
1.363728e+00	1.018276e+00	1.028130e-02	-1.769507e-01	1.335175e-02	-9.407298e-02	-5.550715e-02
1.365200e+00	1.018295e+00	1.014285e-02	-1.770318e-01	1.316934e-02	-9.414132e-02	-5.473857e-02
1.366671e+00	1.018315e+00	1.000431e-02	-1.771118e-01	1.298692e-02	-9.420869e-02	-5.397032e-02
1.368142e+00	1.018333e+00	9.865670e-03	-1.771906e-01	1.280447e-02	-9.427508e-02	-5.320242e-02
1.369613e+00	1.018352e+00	9.726932e-03	-1.772683e-01	1.262200e-02	-9.434050e-02	-5.243486e-02
1.371084e+00	1.018371e+00	9.588098e-03	-1.773449e-01	1.243951e-02	-9.440495e-02	-5.166763e-02
1.372555e+00	1.018389e+00	9.449171e-03	-1.774203e-01	1.225701e-02	-9.446843e-02	-5.090073e-02
1.374026e+00	1.018407e+00	9.310150e-03	-1.774946e-01	1.207448e-02	-9.453095e-02	-5.013414e-02
1.375497e+00	1.018424e+00	9.171038e-03	-1.775678e-01	1.189193e-02	-9.459250e-02	-4.936788e-02
1.376969e+00	1.018442e+00	9.031837e-03	-1.776399e-01	1.170937e-02	-9.465308e-02	-4.860192e-02
1.378440e+00	1.018459e+00	8.892547e-03	-1.777108e-01	1.152679e-02	-9.471270e-02	-4.783627e-02
1.379911e+00	1.018476e+00	8.753170e-03	-1.777806e-01	1.134419e-02	-9.477135e-02	-4.707091e-02
1.381382e+00	1.018492e+00	8.613707e-03	-1.778493e-01	1.116157e-02	-9.482905e-02	-4.630586e-02
1.382853e+00	1.018508e+00	8.474160e-03	-1.779169e-01	1.097893e-02	-9.488578e-02	-4.554109e-02
1.384324e+00	1.018524e+00	8.334531e-03	-1.779833e-01	1.079628e-02	-9.494156e-02	-4.477661e-02
1.385795e+00	1.018540e+00	8.194820e-03	-1.780486e-01	1.061361e-02	-9.499638e-02	-4.401240e-02
1.387266e+00	1.018556e+00	8.055029e-03	-1.781128e-01	1.043092e-02	-9.505024e-02	-4.324848e-02
1.388737e+00	1.018571e+00	7.915160e-03	-1.781759e-01	1.024822e-02	-9.510314e-02	-4.248482e-02
1.390209e+00	1.018586e+00	7.775213e-03	-1.782378e-01	1.006550e-02	-9.515509e-02	-4.172142e-02
1.391680e+00	1.018600e+00	7.635191e-03	-1.782986e-01	9.882768e-03	-9.520609e-02	-4.095829e-02
1.393151e+00	1.018615e+00	7.495094e-03	-1.783583e-01	9.700019e-03	-9.525613e-02	-4.019541e-02
1.394622e+00	1.018629e+00	7.354925e-03	-1.784169e-01	9.517255e-03	-9.530522e-02	-3.943278e-02
1.396093e+00	1.018643e+00	7.214684e-03	-1.784743e-01	9.334476e-03	-9.535336e-02	-3.867039e-02
1.397564e+00	1.018656e+00	7.074373e-03	-1.785307e-01	9.151682e-03	-9.540055e-02	-3.790824e-02
1.399035e+00	1.018670e+00	6.933993e-03	-1.785859e-01	8.968875e-03	-9.544679e-02	-3.714633e-02
1.400506e+00	1.018683e+00	6.793546e-03	-1.786400e-01	8.786053e-03	-9.549208e-02	-3.638464e-02
1.401978e+00	1.018696e+00	6.653033e-03	-1.786929e-01	8.603218e-03	-9.553643e-02	-3.562318e-02
1.403449e+00	1.018708e+00	6.512455e-03	-1.787448e-01	8.420370e-03	-9.557983e-02	-3.486194e-02
1.404920e+00	1.018720e+00	6.371815e-03	-1.787955e-01	8.237509e-03	-9.562228e-02	-3.410092e-02
1.406391e+00	1.018732e+00	6.231112e-03	-1.788451e-01	8.054635e-03	-9.566379e-02	-3.334010e-02
1.407862e+00	1.018744e+00	6.090349e-03	-1.788936e-01	7.871749e-03	-9.570435e-02	-3.257949e-02
1.409333e+00	1.018756e+00	5.949527e-03	-1.789410e-01	7.688851e-03	-9.574397e-02	-3.181908e-02
1.410804e+00	1.018767e+00	5.808648e-03	-1.789872e-01	7.505941e-03	-9.578265e-02	-3.105887e-02
1.412275e+00	1.018778e+00	5.667712e-03	-1.790323e-01	7.323020e-03	-9.582039e-02	-3.029885e-02
1.413747e+00	1.018788e+00	5.526722e-03	-1.790764e-01	7.140087e-03	-9.585718e-02	-2.953901e-02
1.415218e+00	1.018799e+00	5.385678e-03	-1.791193e-01	6.957143e-03	-9.589304e-02	-2.877935e-02
1.416689e+00	1.018809e+00	5.244582e-03	-1.791610e-01	6.774189e-03	-9.592795e-02	-2.801987e-02

Time (TU)	x (LU)	y (LU)	z (LU)	\dot{x} (LU/TU)	\dot{y} (LU/TU)	\dot{z} (LU/TU)
1.418160e+00	1.018819e+00	5.103435e-03	-1.792017e-01	6.591225e-03	-9.596193e-02	-2.726056e-02
1.419631e+00	1.018828e+00	4.962239e-03	-1.792412e-01	6.408250e-03	-9.599497e-02	-2.650142e-02
1.421102e+00	1.018837e+00	4.820995e-03	-1.792797e-01	6.225266e-03	-9.602707e-02	-2.574243e-02
1.422573e+00	1.018846e+00	4.679705e-03	-1.793170e-01	6.042272e-03	-9.605823e-02	-2.498361e-02
1.424044e+00	1.018855e+00	4.538369e-03	-1.793532e-01	5.859269e-03	-9.608846e-02	-2.422494e-02
1.425515e+00	1.018864e+00	4.396990e-03	-1.793883e-01	5.676257e-03	-9.611775e-02	-2.346641e-02
1.426987e+00	1.018872e+00	4.255568e-03	-1.794222e-01	5.493236e-03	-9.614610e-02	-2.270803e-02
1.428458e+00	1.018880e+00	4.114106e-03	-1.794551e-01	5.310208e-03	-9.617352e-02	-2.194979e-02
1.429929e+00	1.018888e+00	3.972603e-03	-1.794868e-01	5.127171e-03	-9.620001e-02	-2.119168e-02
1.431400e+00	1.018895e+00	3.831062e-03	-1.795174e-01	4.944126e-03	-9.622556e-02	-2.043370e-02
1.432871e+00	1.018902e+00	3.689485e-03	-1.795469e-01	4.761074e-03	-9.625018e-02	-1.967584e-02
1.434342e+00	1.018909e+00	3.547872e-03	-1.795753e-01	4.578014e-03	-9.627387e-02	-1.891811e-02
1.435813e+00	1.018916e+00	3.406224e-03	-1.796026e-01	4.394948e-03	-9.629662e-02	-1.816048e-02
1.437284e+00	1.018922e+00	3.264544e-03	-1.796287e-01	4.211875e-03	-9.631844e-02	-1.740297e-02
1.438756e+00	1.018928e+00	3.122833e-03	-1.796538e-01	4.028796e-03	-9.633933e-02	-1.664557e-02
1.440227e+00	1.018934e+00	2.981091e-03	-1.796777e-01	3.845710e-03	-9.635929e-02	-1.588826e-02
1.441698e+00	1.018939e+00	2.839321e-03	-1.797005e-01	3.662619e-03	-9.637832e-02	-1.513105e-02
1.443169e+00	1.018945e+00	2.697524e-03	-1.797222e-01	3.479522e-03	-9.639642e-02	-1.437393e-02
1.444640e+00	1.018950e+00	2.555700e-03	-1.797428e-01	3.296420e-03	-9.641358e-02	-1.361690e-02
1.446111e+00	1.018954e+00	2.413852e-03	-1.797623e-01	3.113313e-03	-9.642982e-02	-1.285995e-02
1.447582e+00	1.018959e+00	2.271981e-03	-1.797807e-01	2.930201e-03	-9.644513e-02	-1.210308e-02
1.449053e+00	1.018963e+00	2.130088e-03	-1.797979e-01	2.747085e-03	-9.645951e-02	-1.134629e-02
1.450525e+00	1.018967e+00	1.988174e-03	-1.798141e-01	2.563965e-03	-9.647296e-02	-1.058956e-02
1.451996e+00	1.018970e+00	1.846242e-03	-1.798291e-01	2.380840e-03	-9.648548e-02	-9.832895e-03
1.453467e+00	1.018974e+00	1.704291e-03	-1.798430e-01	2.197713e-03	-9.649707e-02	-9.076290e-03
1.454938e+00	1.018977e+00	1.562324e-03	-1.798558e-01	2.014582e-03	-9.650774e-02	-8.319740e-03
1.456409e+00	1.018980e+00	1.420343e-03	-1.798675e-01	1.831447e-03	-9.651747e-02	-7.563240e-03
1.457880e+00	1.018982e+00	1.278347e-03	-1.798780e-01	1.648311e-03	-9.652628e-02	-6.806786e-03
1.459351e+00	1.018985e+00	1.136340e-03	-1.798875e-01	1.465171e-03	-9.653416e-02	-6.050373e-03
1.460822e+00	1.018987e+00	9.943211e-04	-1.798958e-01	1.282030e-03	-9.654112e-02	-5.293996e-03
1.462294e+00	1.018988e+00	8.522929e-04	-1.799031e-01	1.098886e-03	-9.654714e-02	-4.537652e-03
1.463765e+00	1.018990e+00	7.102566e-04	-1.799092e-01	9.157410e-04	-9.655224e-02	-3.781335e-03
1.465236e+00	1.018991e+00	5.682135e-04	-1.799142e-01	7.325944e-04	-9.655641e-02	-3.025040e-03
1.466707e+00	1.018992e+00	4.261649e-04	-1.799181e-01	5.494468e-04	-9.655966e-02	-2.268764e-03
1.468178e+00	1.018993e+00	2.841122e-04	-1.799209e-01	3.662983e-04	-9.656198e-02	-1.512502e-03
1.469649e+00	1.018993e+00	1.420568e-04	-1.799225e-01	1.831493e-04	-9.656337e-02	-7.562487e-04
1.471120e+00	1.018993e+00	3.986104e-12	-1.799231e-01	1.262589e-11	-9.656383e-02	-2.651104e-11

Appendix B

Loiter Station-Keeping Trade Study

Heat Maps

Appendix B provides the Loiter v. Traditional Station Keeping trade analysis tables as discussed in Section 4.3.2.

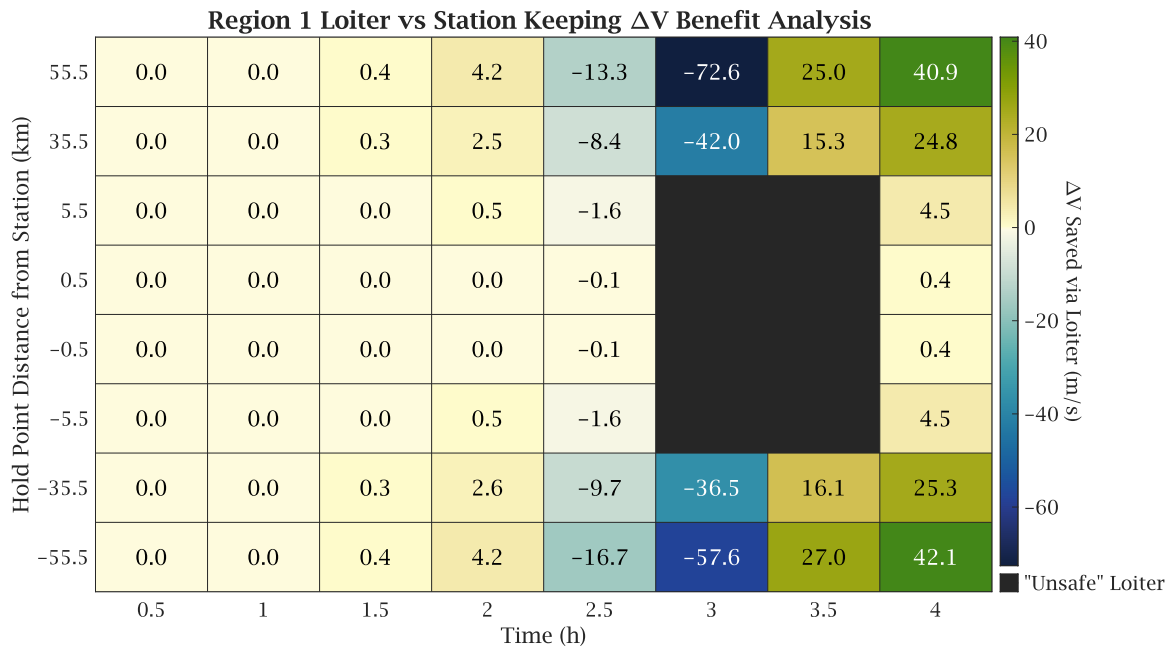


Figure B.1: Region 1 Loiter vs Station Keeping ΔV Benefit Analysis.

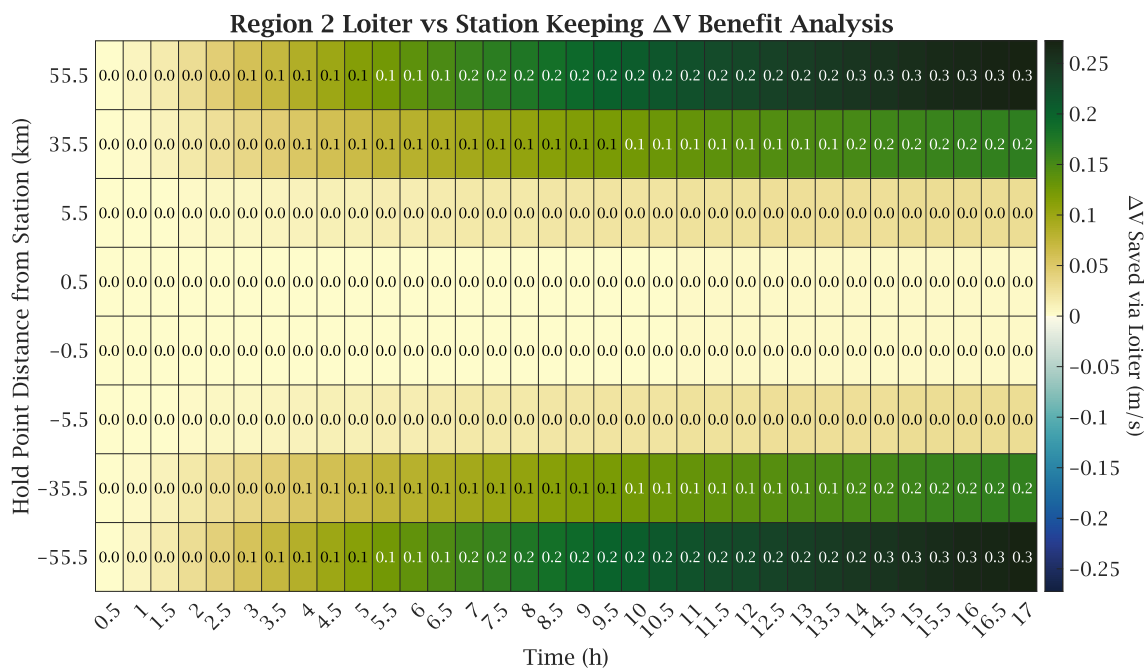


Figure B.2: Region 2 Loiter vs Station Keeping ΔV Benefit Analysis.

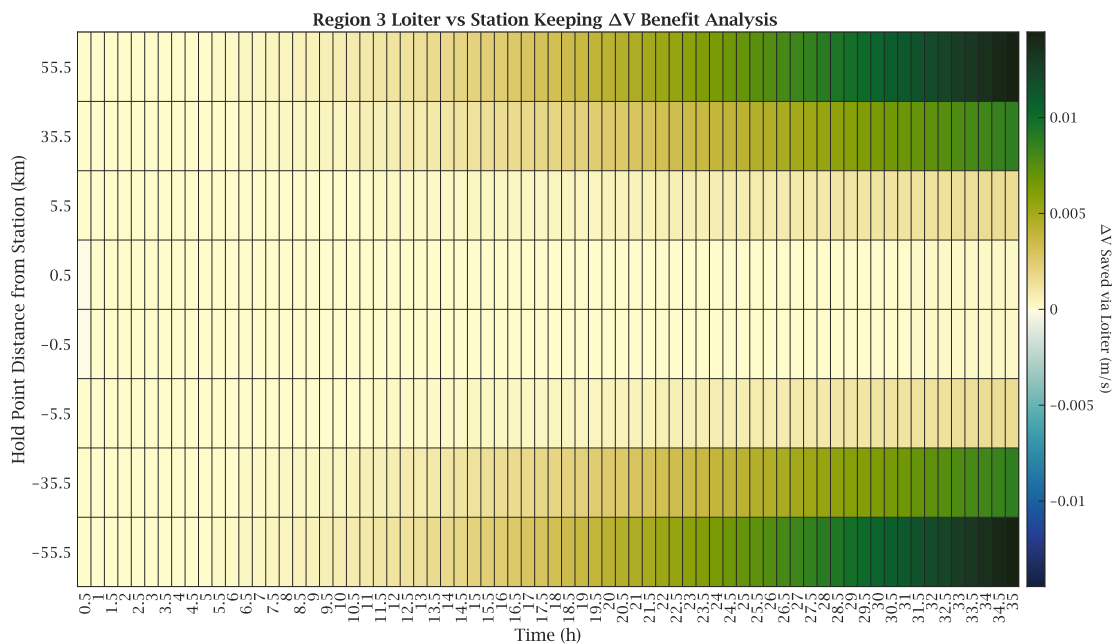


Figure B.3: Region 3 Loiter vs Station Keeping ΔV Benefit Analysis.

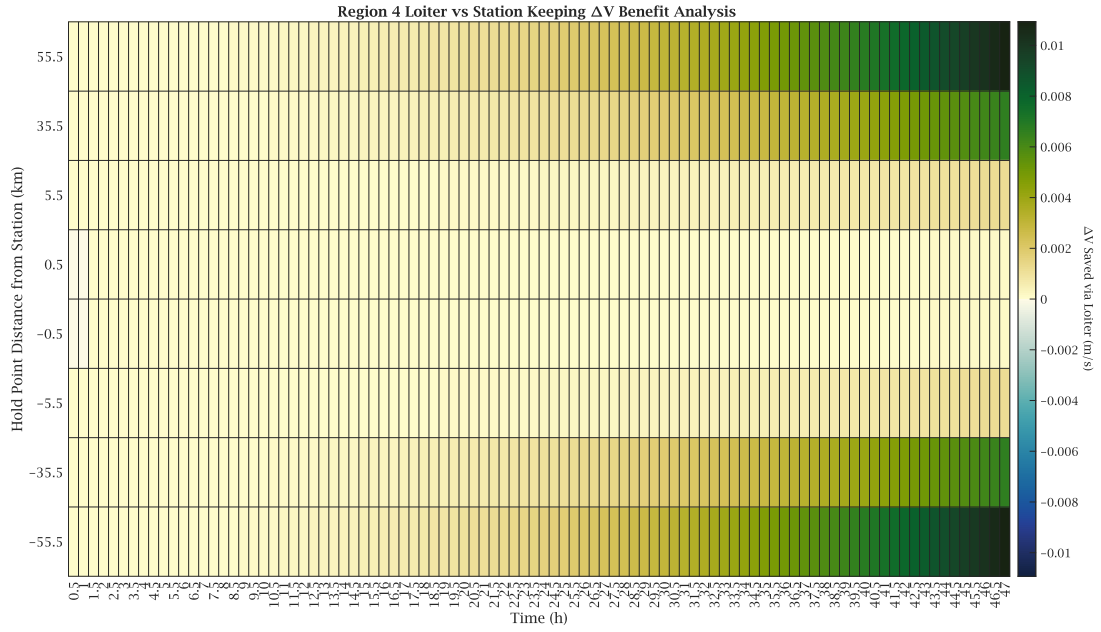


Figure B.4: Region 4 Loiter vs Station Keeping ΔV Benefit Analysis.

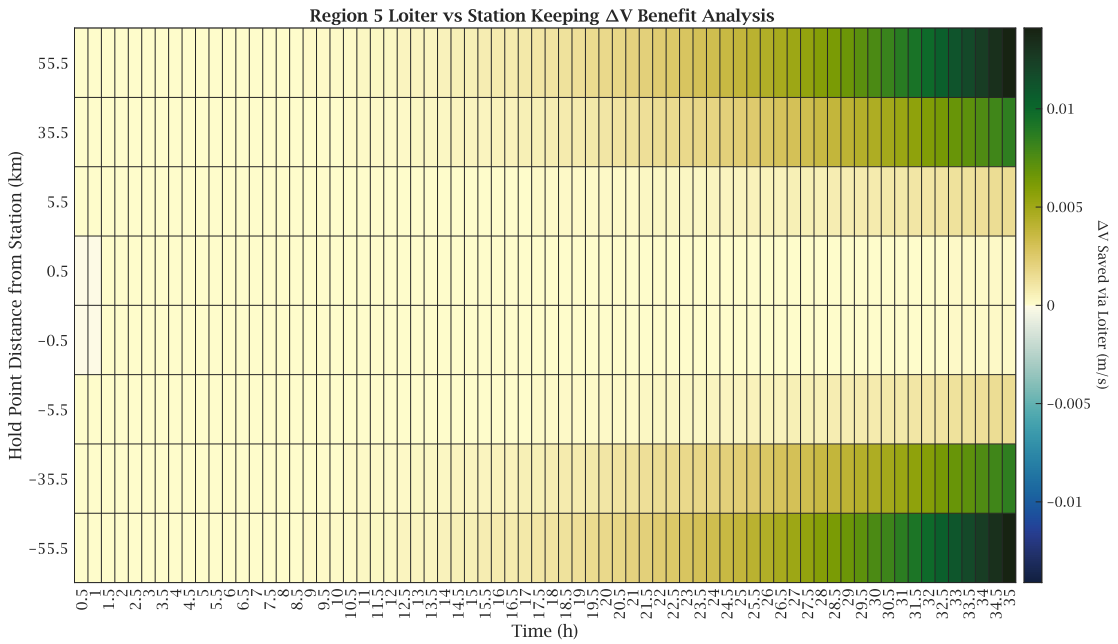


Figure B.5: Region 5 Loiter vs Station Keeping ΔV Benefit Analysis.

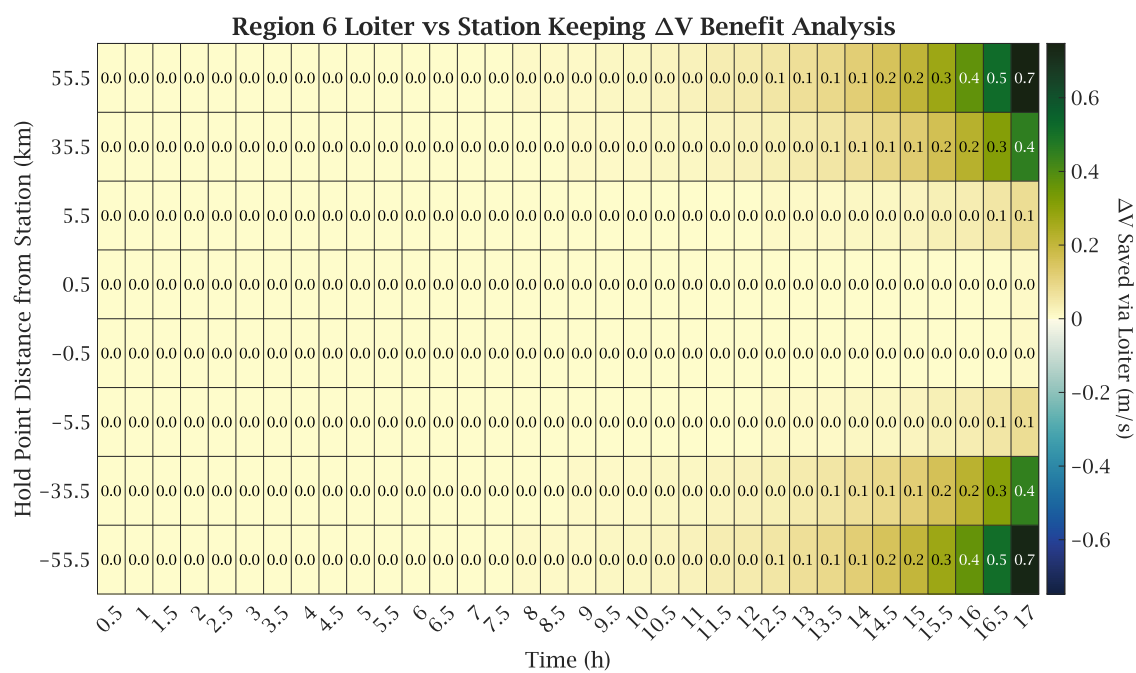
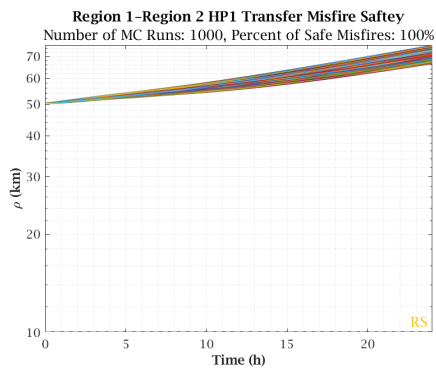


Figure B.6: Region 6 Loiter vs Station Keeping ΔV Benefit Analysis.

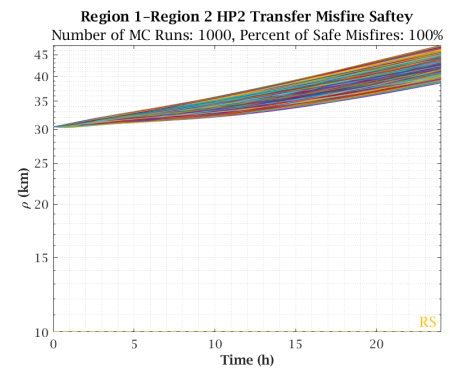
Appendix C

Misfire Safety Monte Carlo Simulation Plots

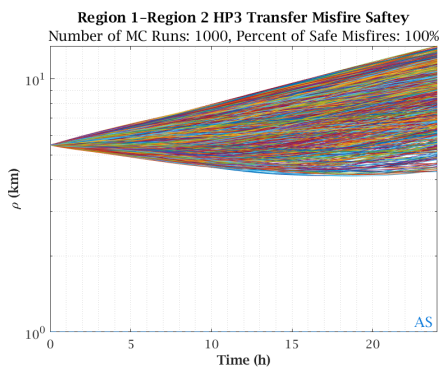
Appendix C provides the Monte Carlo Random Misfire Safety plots as discussed in Sections [4.2.3](#), [4.3.4](#), and [4.4.2](#).



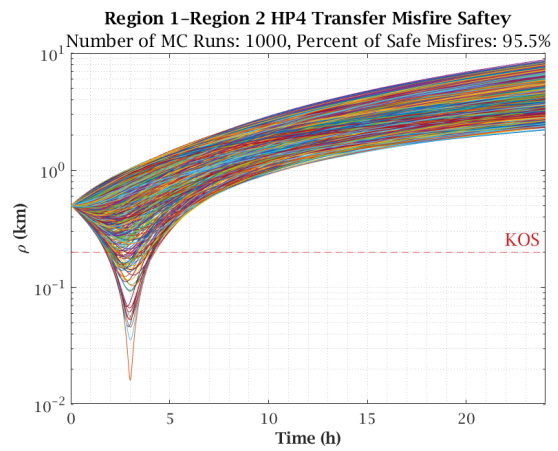
(a) HP1



(b) HP2

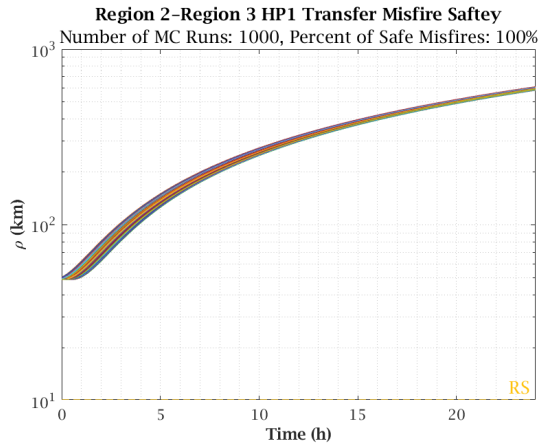


(c) HP3

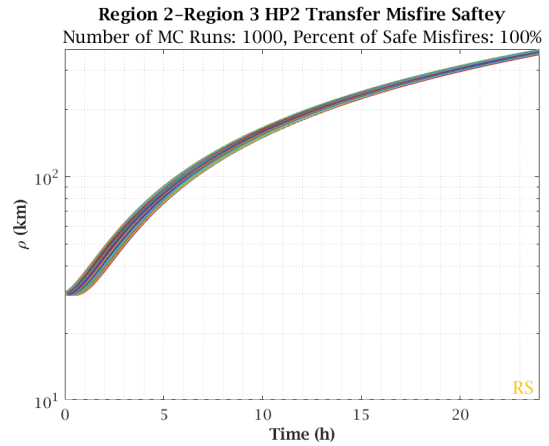


(d) HP4

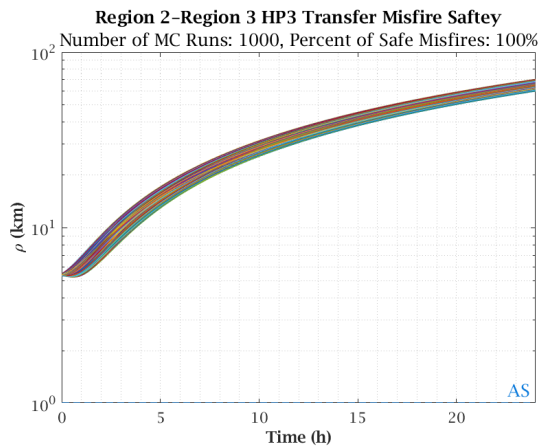
Figure C.1: Region 1 to Region 2 Region-to-Region Transfer Random Misfire Fire Monte Carlo Simulations



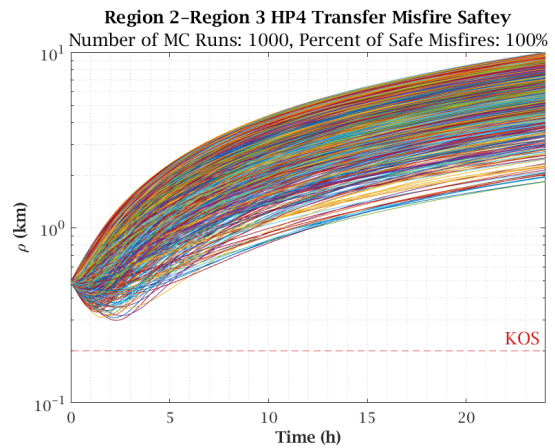
(a) HP1



(b) HP2

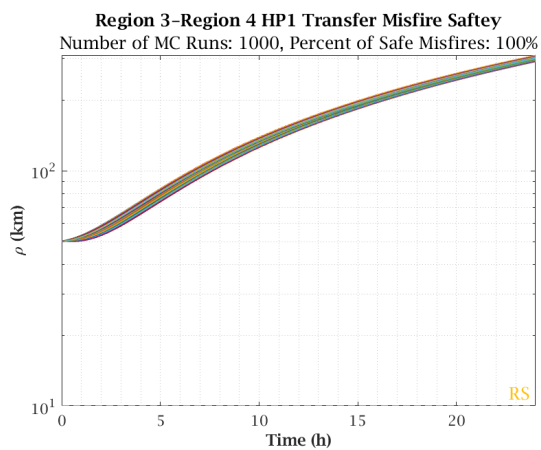


(c) HP3

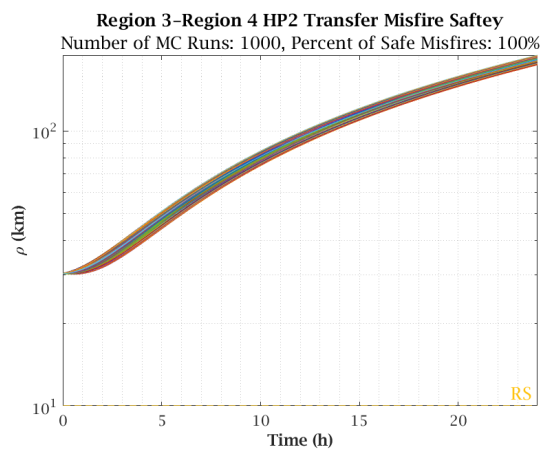


(d) HP4

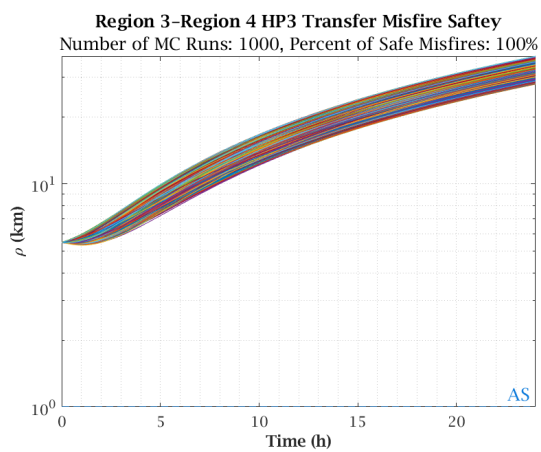
Figure C.2: Region 2 to Region 3 Region-to-Region Transfer Random Misfire Fire Monte Carlo Simulations



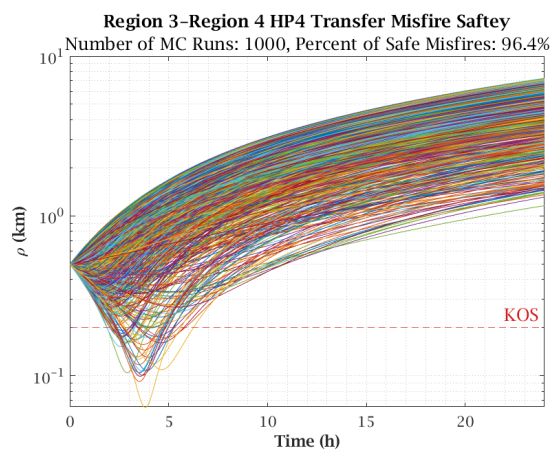
(a) HP1



(b) HP2

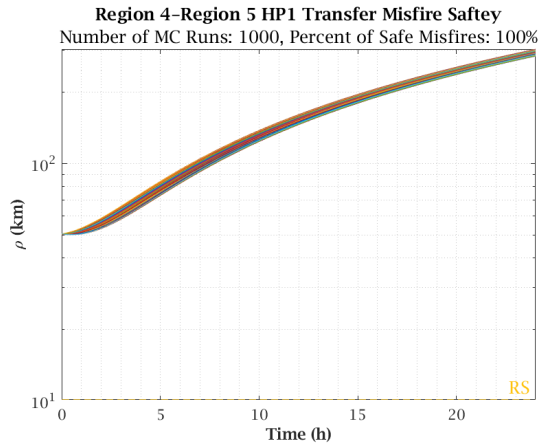


(c) HP3

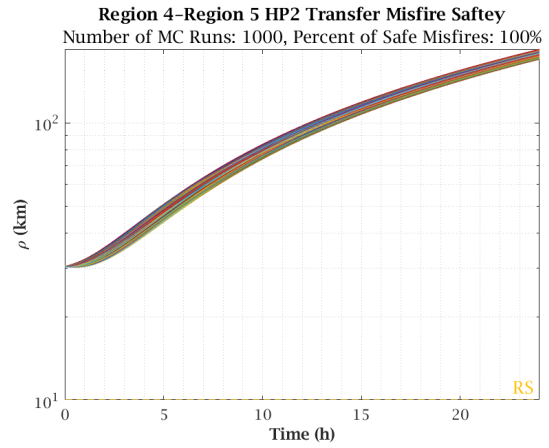


(d) HP4

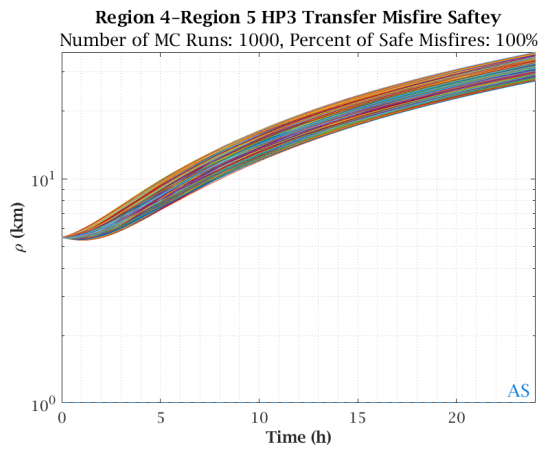
Figure C.3: Region 3 to Region 4 Region-to-Region Transfer Random Misfire Fire Monte Carlo Simulations



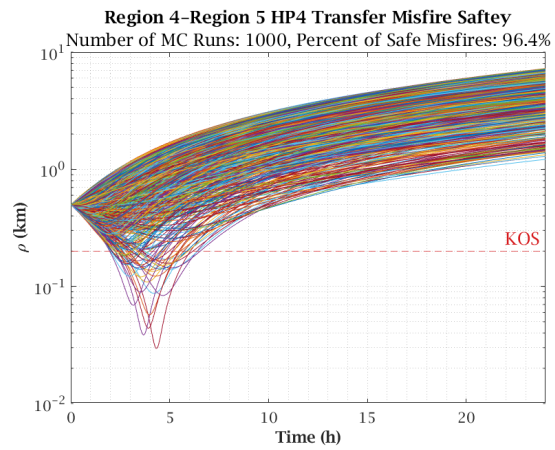
(a) HP1



(b) HP2

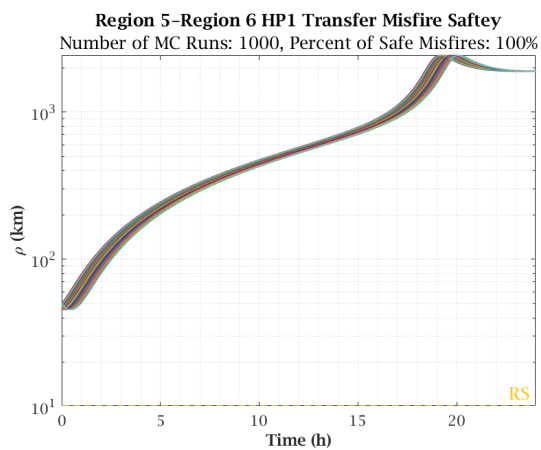


(c) HP3

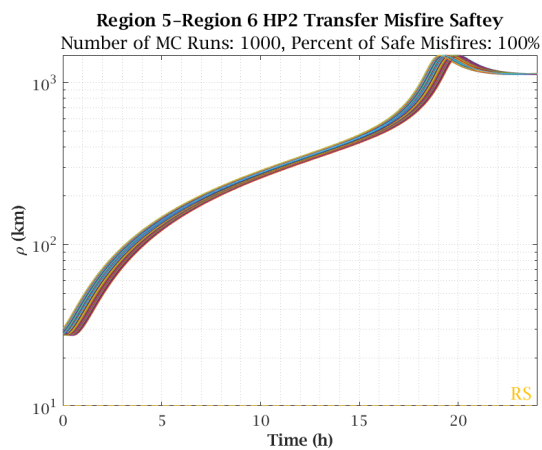


(d) HP4

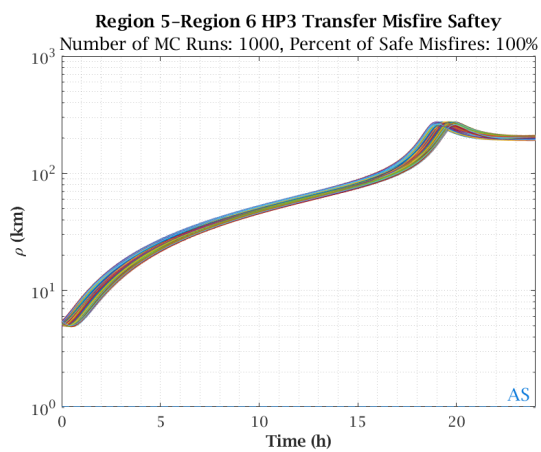
Figure C.4: Region 4 to Region 5 Region-to-Region Transfer Random Misfire Fire Monte Carlo Simulations



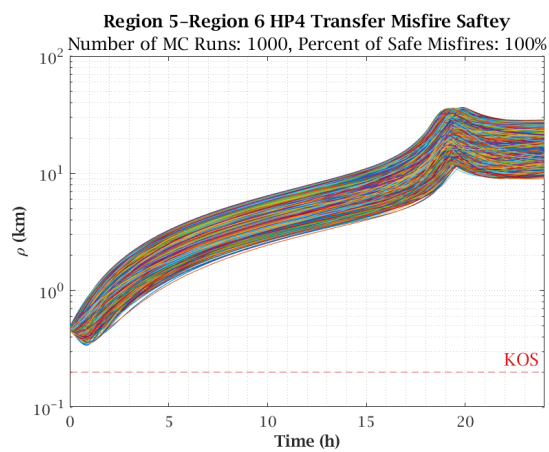
(a) HP1



(b) HP2

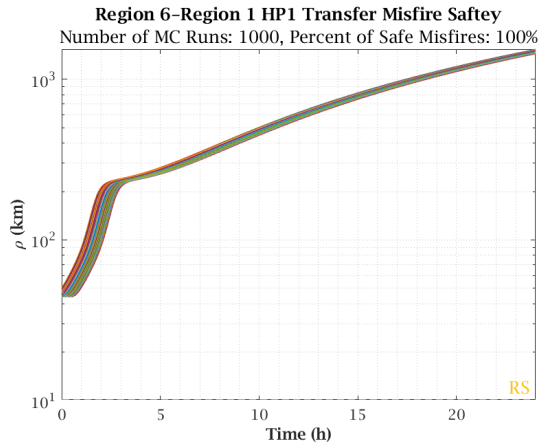


(c) HP3

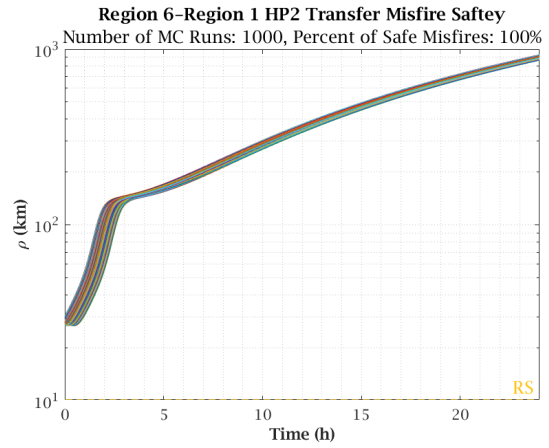


(d) HP4

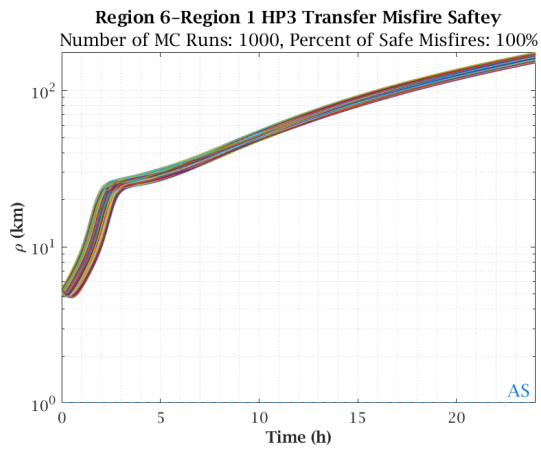
Figure C.5: Region 5 to Region 6 Region-to-Region Transfer Random Misfire Fire Monte Carlo Simulations



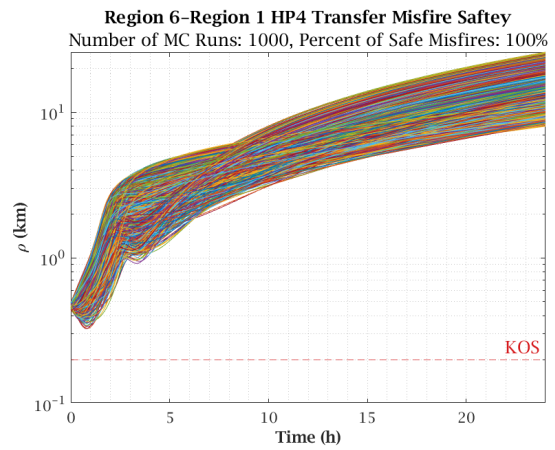
(a) HP1



(b) HP2



(c) HP3



(d) HP4

Figure C.6: Region 6 to Region 1 Region-to-Region Transfer Random Misfire Fire Monte Carlo Simulations

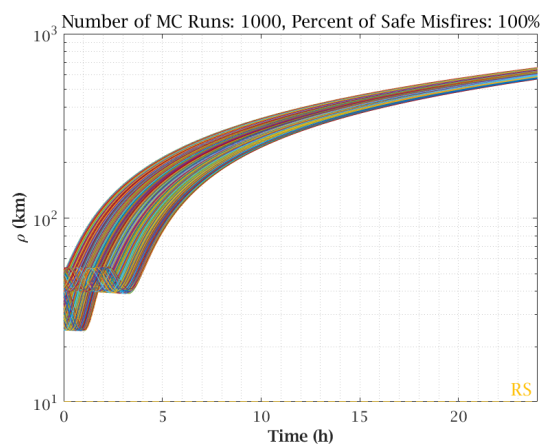
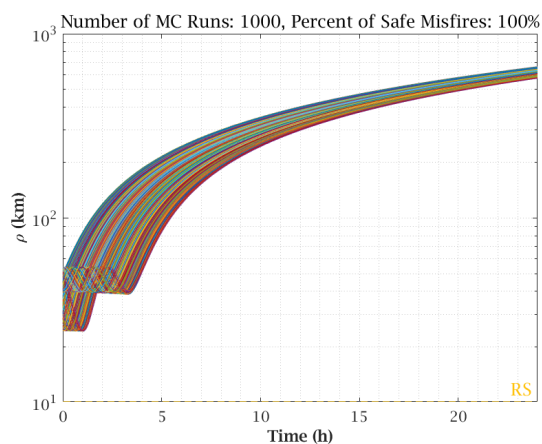
(a) $\rho_0 = -50.5$ (b) $\rho_0 = +50.5$

Figure C.7: Region 1, HP1, 4 Hour Loiter Random Misfire Fire Monte Carlo Simulations

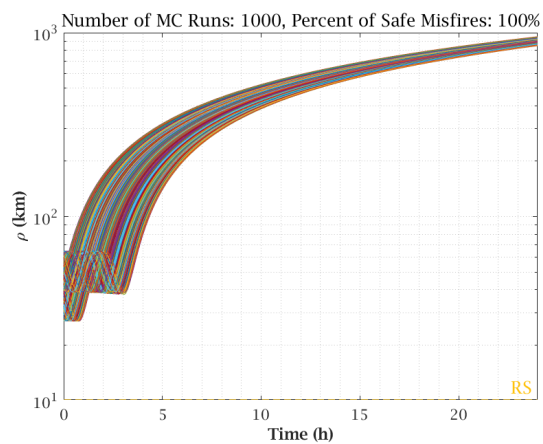
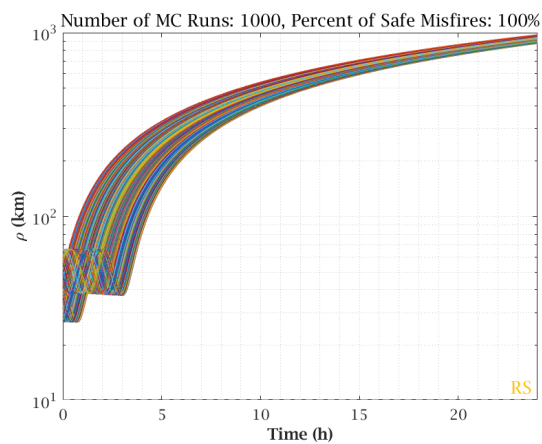
(a) $\rho_0 = -50.5$ (b) $\rho_0 = +50.5$

Figure C.8: Region 1, HP1, 3.5 Hour Loiter Random Misfire Fire Monte Carlo Simulations

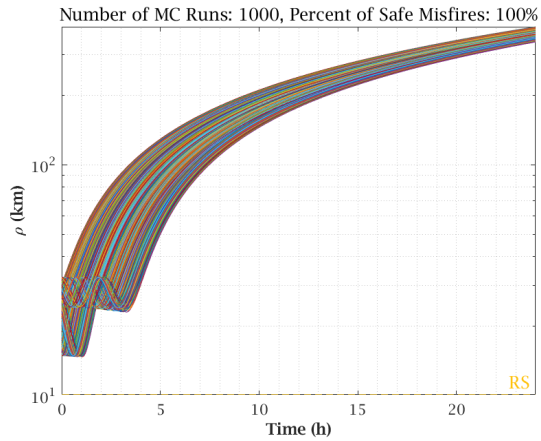
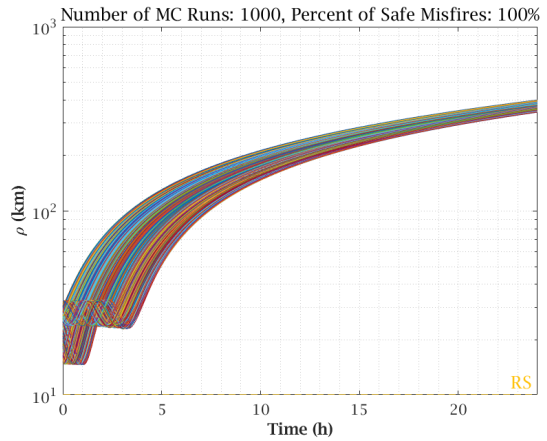
(a) $\rho_0 = -30.5$ (b) $\rho_0 = +30.5$

Figure C.9: Region 1, HP2, 4 Hour Loiter Random Misfire Fire Monte Carlo Simulations

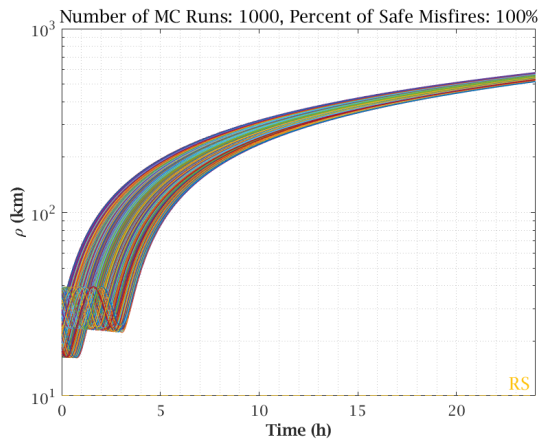
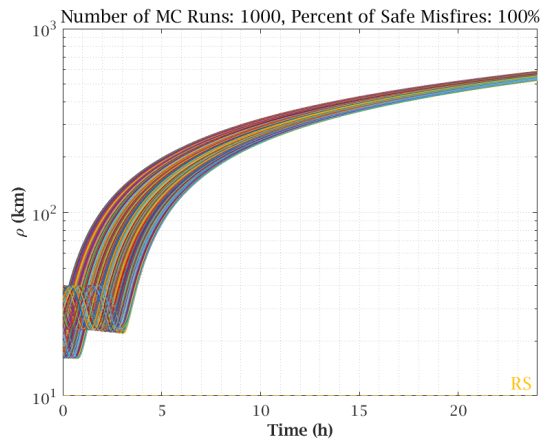
(a) $\rho_0 = -30.5$ (b) $\rho_0 = +30.5$

Figure C.10: Region 1, HP2, 3.5 Hour Loiter Random Misfire Fire Monte Carlo Simulations

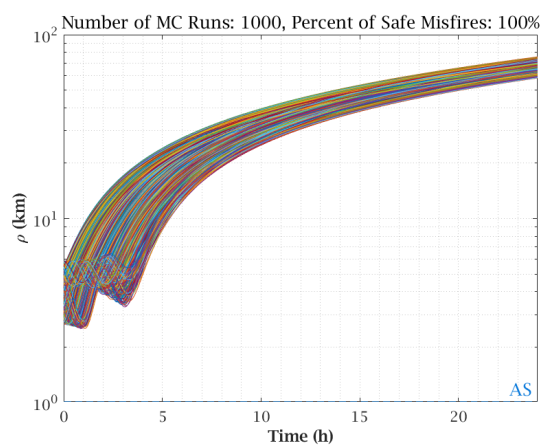
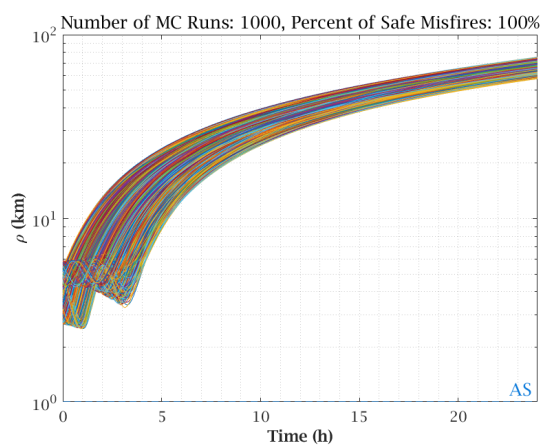
(a) $\rho_0 = -5.5$ (b) $\rho_0 = +5.5$

Figure C.11: Region 1, HP3, 4 Hour Loiter Random Misfire Fire Monte Carlo Simulations

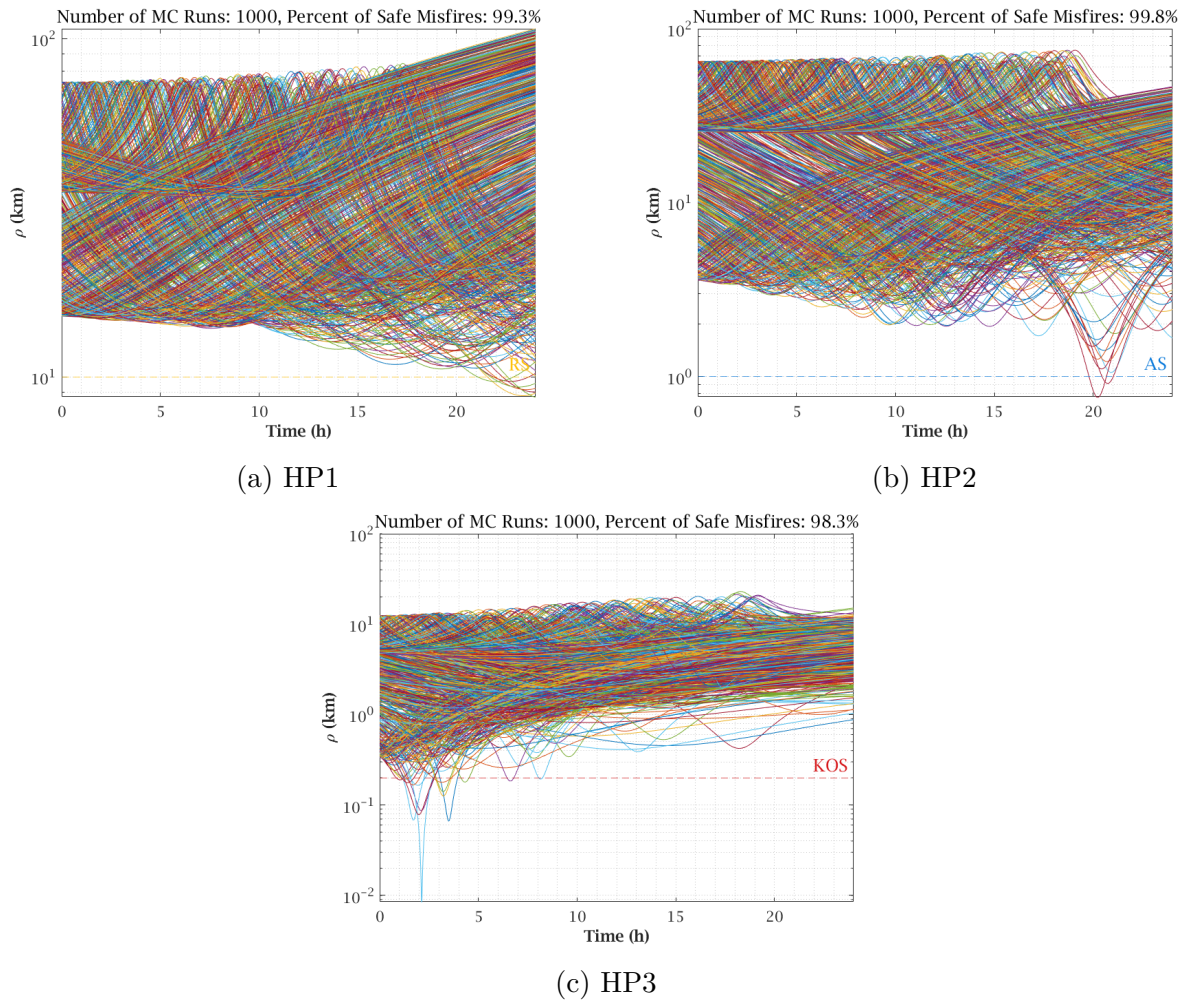
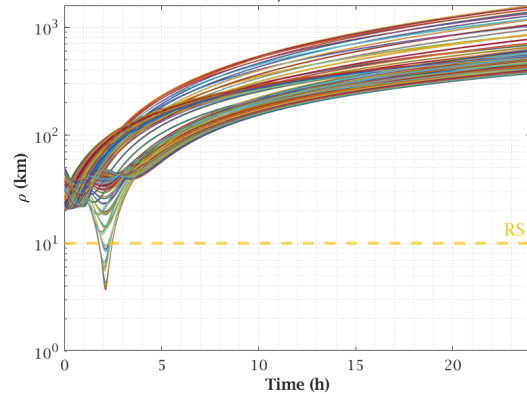


Figure C.12: Region 6 to Region 1 38 Hour Loiter Random Misfire Fire Monte Carlo Simulations

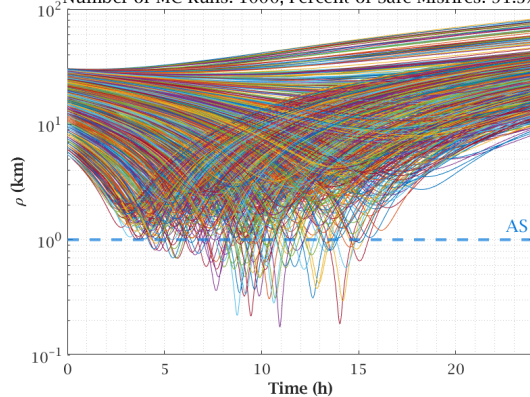
Region 1 "One HP Per" Approach, Transfer 1 Random Misfire Safety

Number of MC Runs: 1000, Percent of Safe Misfires: 96.8%



(a) Transfer 1

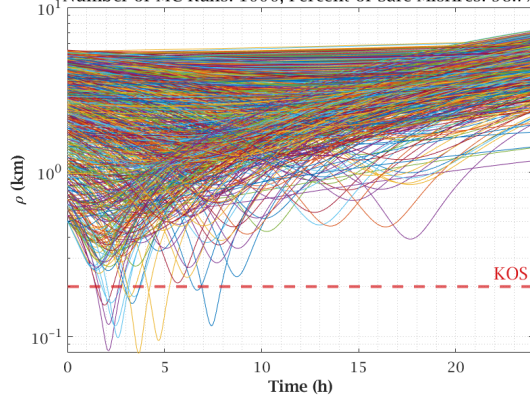
Number of MC Runs: 1000, Percent of Safe Misfires: 91.3%



(b) Transfer 2

Region 1 "One HP Per" Approach, Transfer 3 Random Misfire Safety

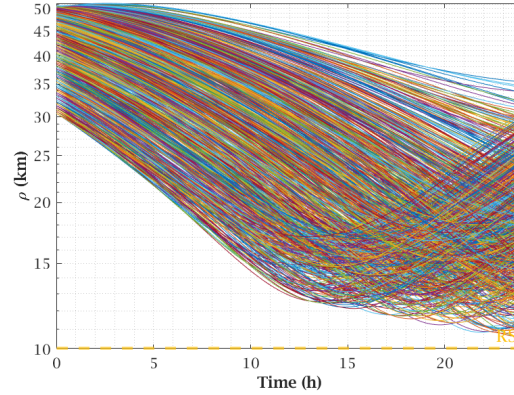
Number of MC Runs: 1000, Percent of Safe Misfires: 98.7%



(c) Transfer 3

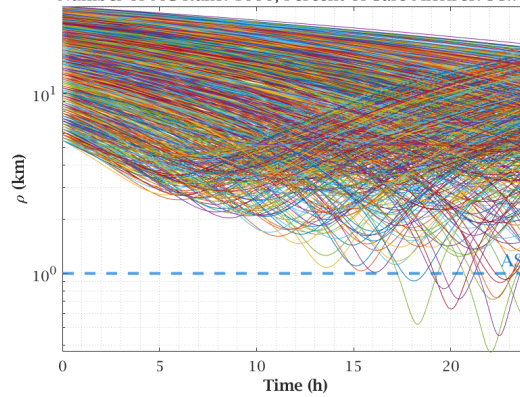
Figure C.13: Region 1 "One HP per" Random Misfire MC Safety Analysis Plots

Region 2 "One HP Per" Approach, Transfer 1 Random Misfire Safety
 Number of MC Runs: 1000, Percent of Safe Misfires: 100%



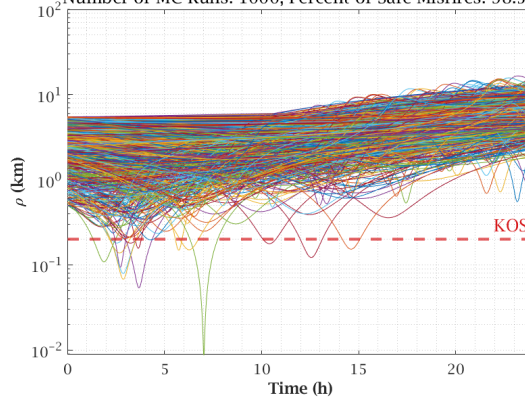
(a) Transfer 1

Region 2 "One HP Per" Approach, Transfer 2 Random Misfire Safety
 Number of MC Runs: 1000, Percent of Safe Misfires: 98.7%



(b) Transfer 2

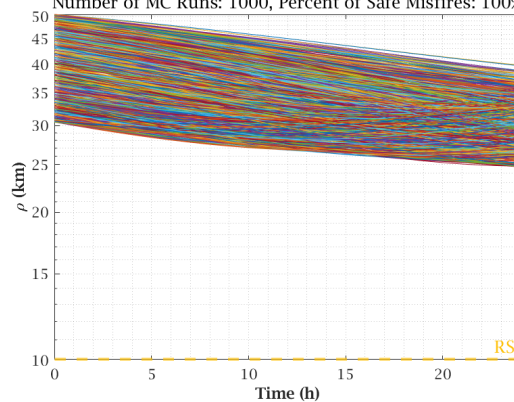
Region 2 "One HP Per" Approach, Transfer 3 Random Misfire Safety
 Number of MC Runs: 1000, Percent of Safe Misfires: 98.5%



(c) Transfer 3

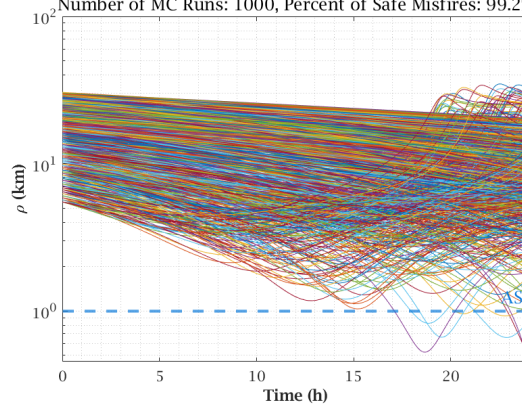
Figure C.14: Region 2 "One HP per" Random Misfire MC Safety Analysis Plots

Region 3 "One HP Per" Approach, Transfer 1 Random Misfire Safety
 Number of MC Runs: 1000, Percent of Safe Misfires: 100%



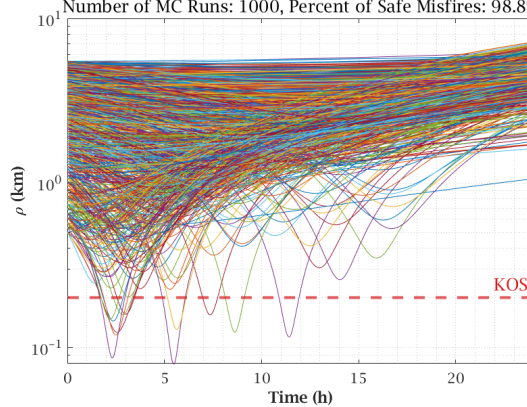
(a) Transfer 1

Region 3 "One HP Per" Approach, Transfer 2 Random Misfire Safety
 Number of MC Runs: 1000, Percent of Safe Misfires: 99.2%



(b) Transfer 2

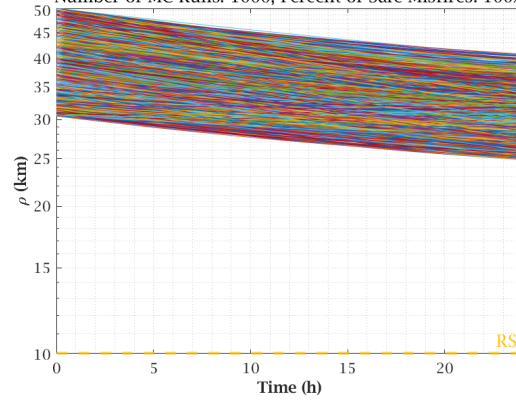
Region 3 "One HP Per" Approach, Transfer 3 Random Misfire Safety
 Number of MC Runs: 1000, Percent of Safe Misfires: 98.8%



(c) Transfer 3

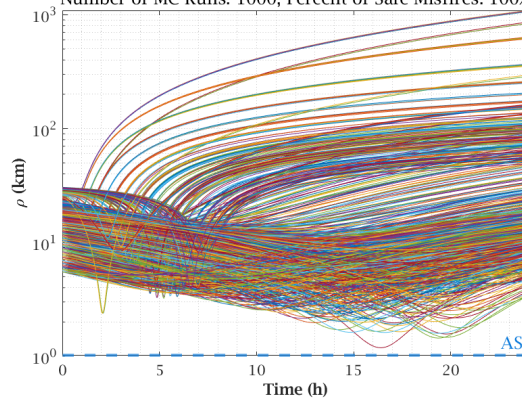
Figure C.15: Region 3 "One HP per" Random Misfire MC Safety Analysis Plots

Region 4 "One HP Per" Approach, Transfer 1 Random Misfire Safety
 Number of MC Runs: 1000, Percent of Safe Misfires: 100%



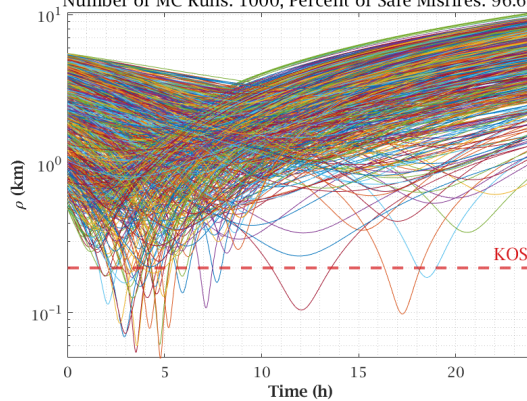
(a) Transfer 1

Region 4 "One HP Per" Approach, Transfer 2 Random Misfire Safety
 Number of MC Runs: 1000, Percent of Safe Misfires: 100%



(b) Transfer 2

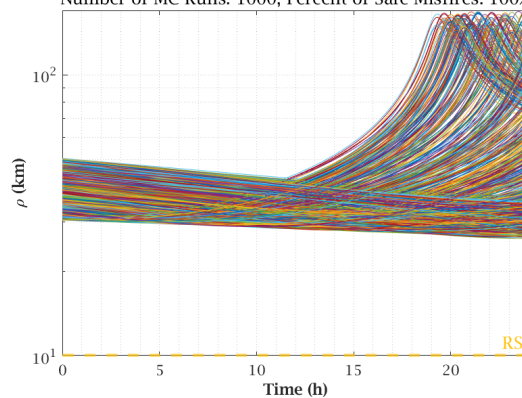
Region 4 "One HP Per" Approach, Transfer 3 Random Misfire Safety
 Number of MC Runs: 1000, Percent of Safe Misfires: 96.6%



(c) Transfer 3

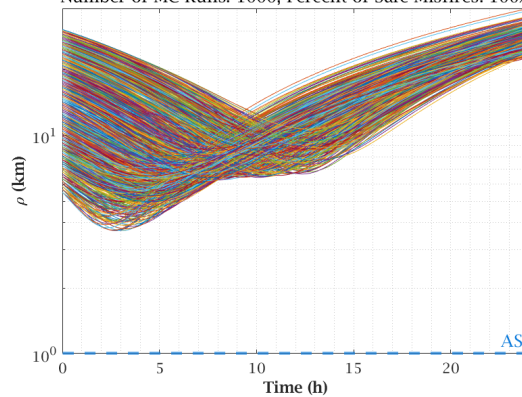
Figure C.16: Region 4 "One HP per" Random Misfire MC Safety Analysis Plots

Region 5 "One HP Per" Approach, Transfer 1 Random Misfire Safety
 Number of MC Runs: 1000, Percent of Safe Misfires: 100%



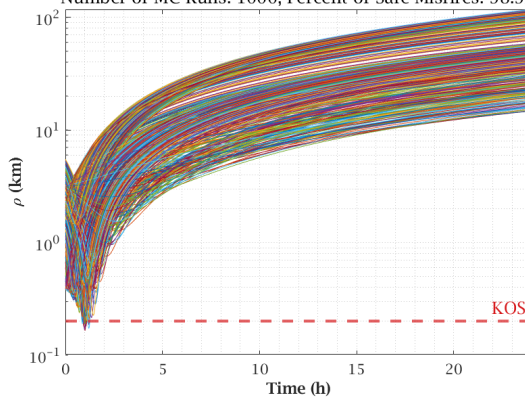
(a) Transfer 1

Region 5 "One HP Per" Approach, Transfer 2 Random Misfire Safety
 Number of MC Runs: 1000, Percent of Safe Misfires: 100%



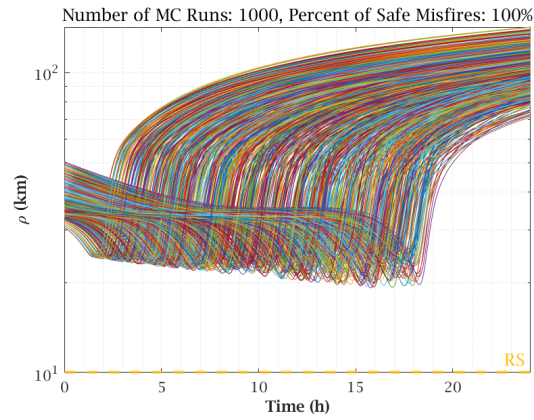
(b) Transfer 2

Region 5 "One HP Per" Approach, Transfer 3 Random Misfire Safety
 Number of MC Runs: 1000, Percent of Safe Misfires: 98.9%



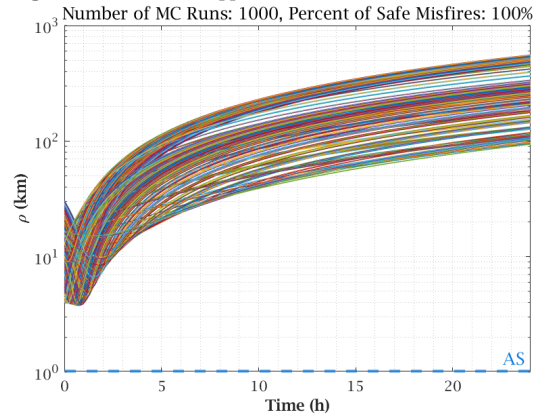
(c) Transfer 3

Figure C.17: Region 5 "One HP per" Random Misfire MC Safety Analysis Plots



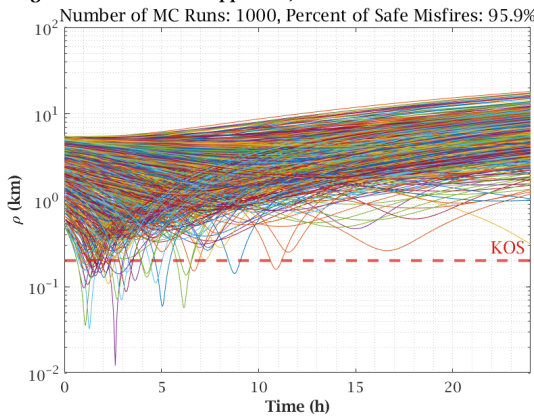
(a) Transfer 1

Region 6 "One HP Per" Approach, Transfer 2 Random Misfire Safety



(b) Transfer 2

Region 6 "One HP Per" Approach, Transfer 3 Random Misfire Safety



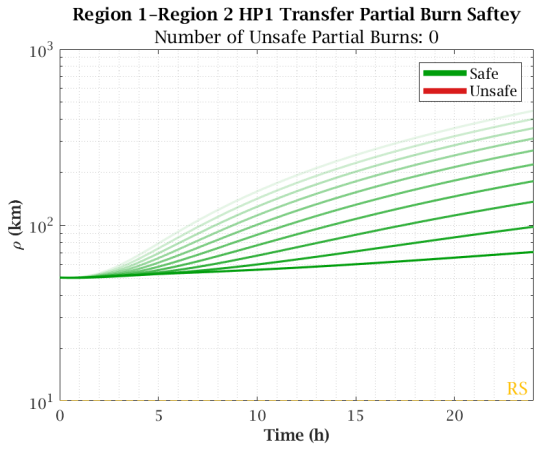
(c) Transfer 3

Figure C.18: Region 6 "One HP per" Random Misfire MC Safety Analysis Plots

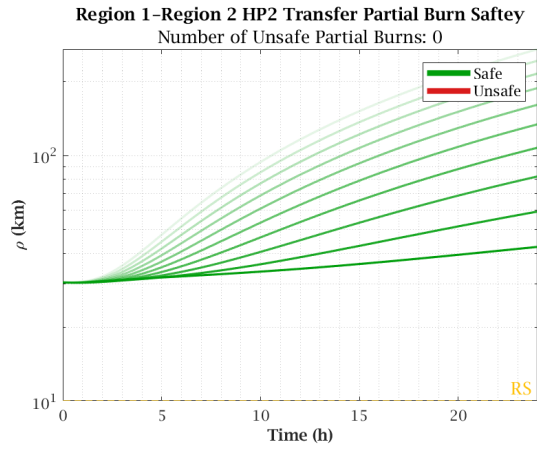
Appendix D

Partial Burn Safety Plots

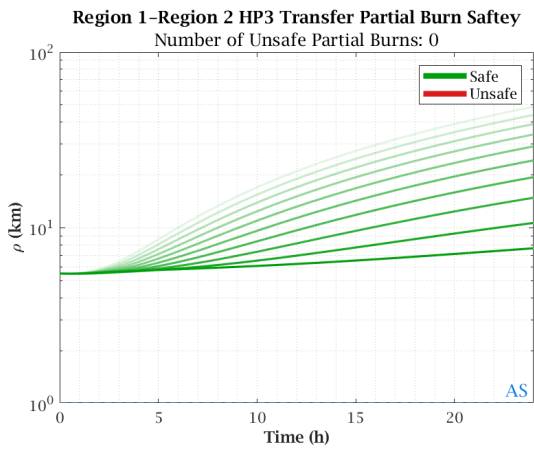
Appendix D provides the Partial Burn Safety plots as discussed in Sections [4.2.3](#), [4.3.4](#), and [4.4.2](#).



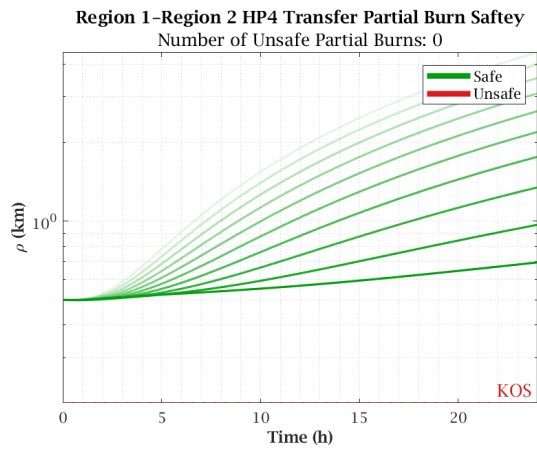
(a) HP1



(b) HP2



(c) HP3



(d) HP4

Figure D.1: Region 1 to Region 2 Region-to-Region Transfer Partial Burn Safety

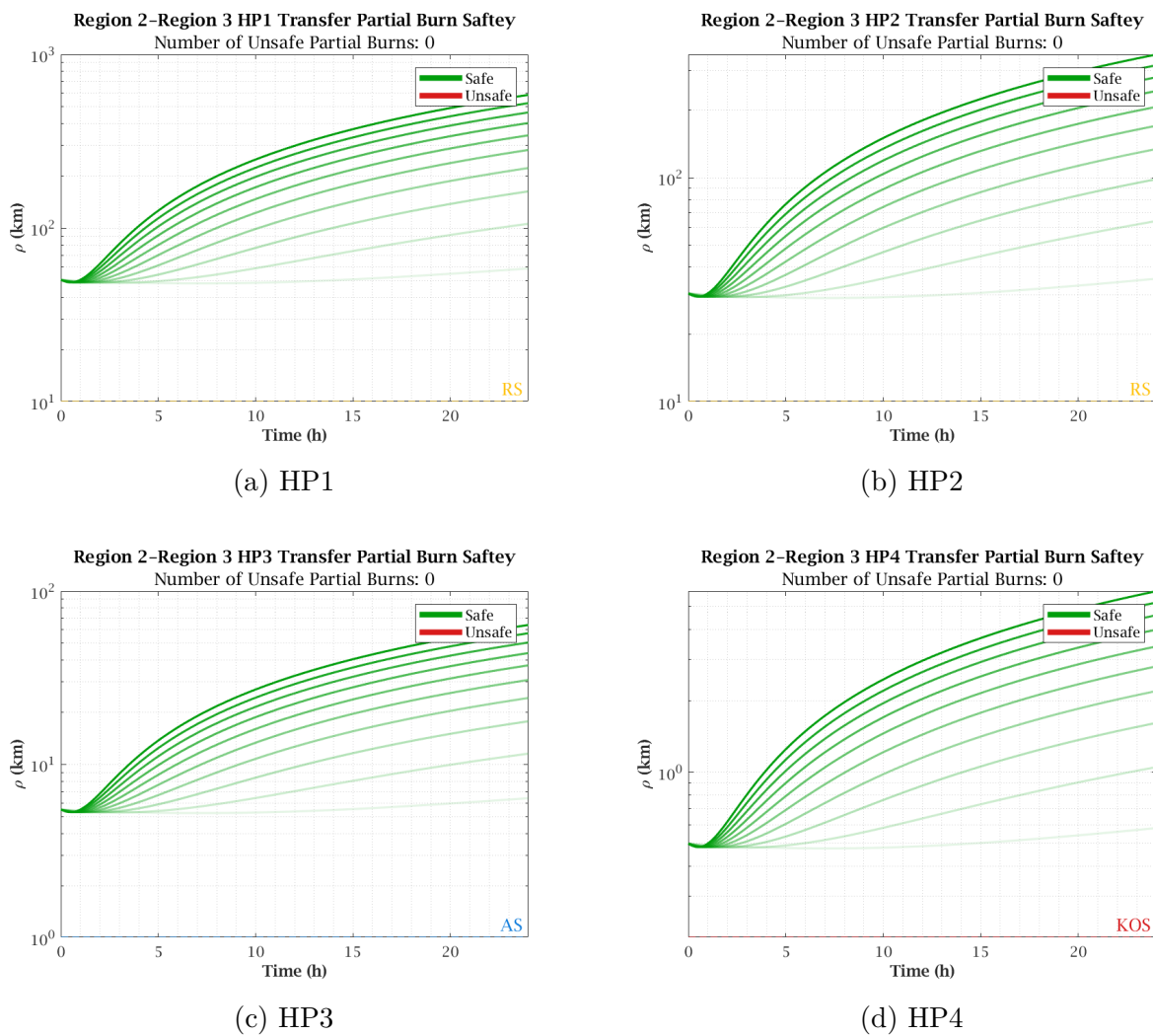
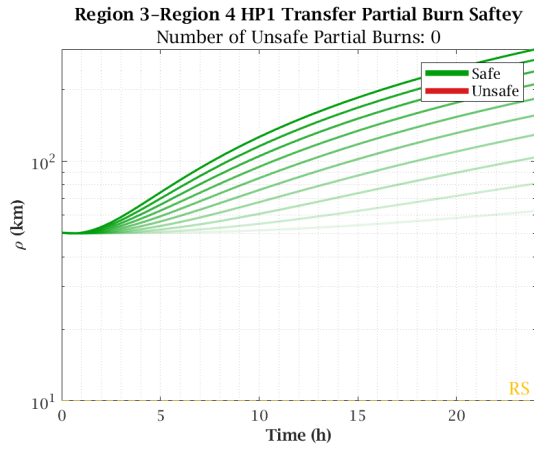
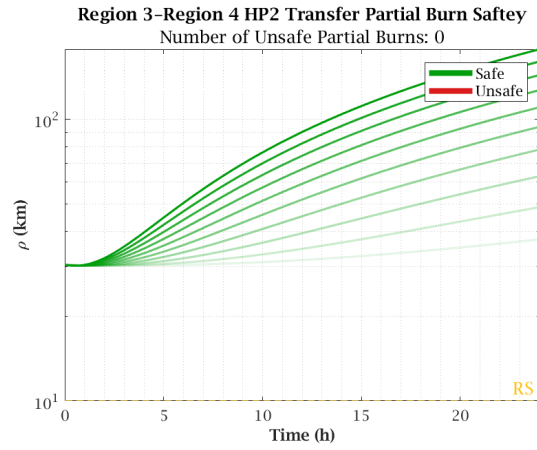


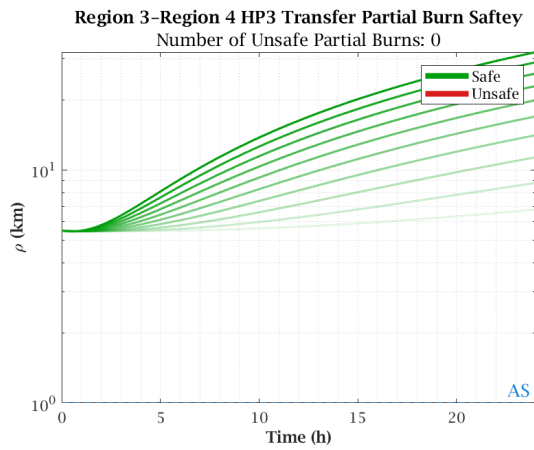
Figure D.2: Region 2 to Region 3 Region-to-Region Transfer Partial Burn Safety



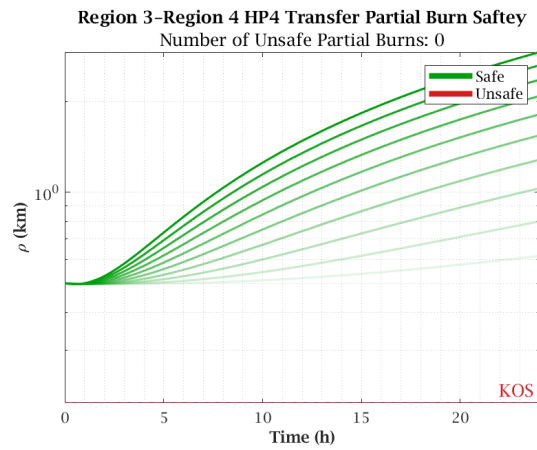
(a) HP1



(b) HP2



(c) HP3



(d) HP4

Figure D.3: Region 3 to Region 4 Region-to-Region Transfer Partial Burn Safety

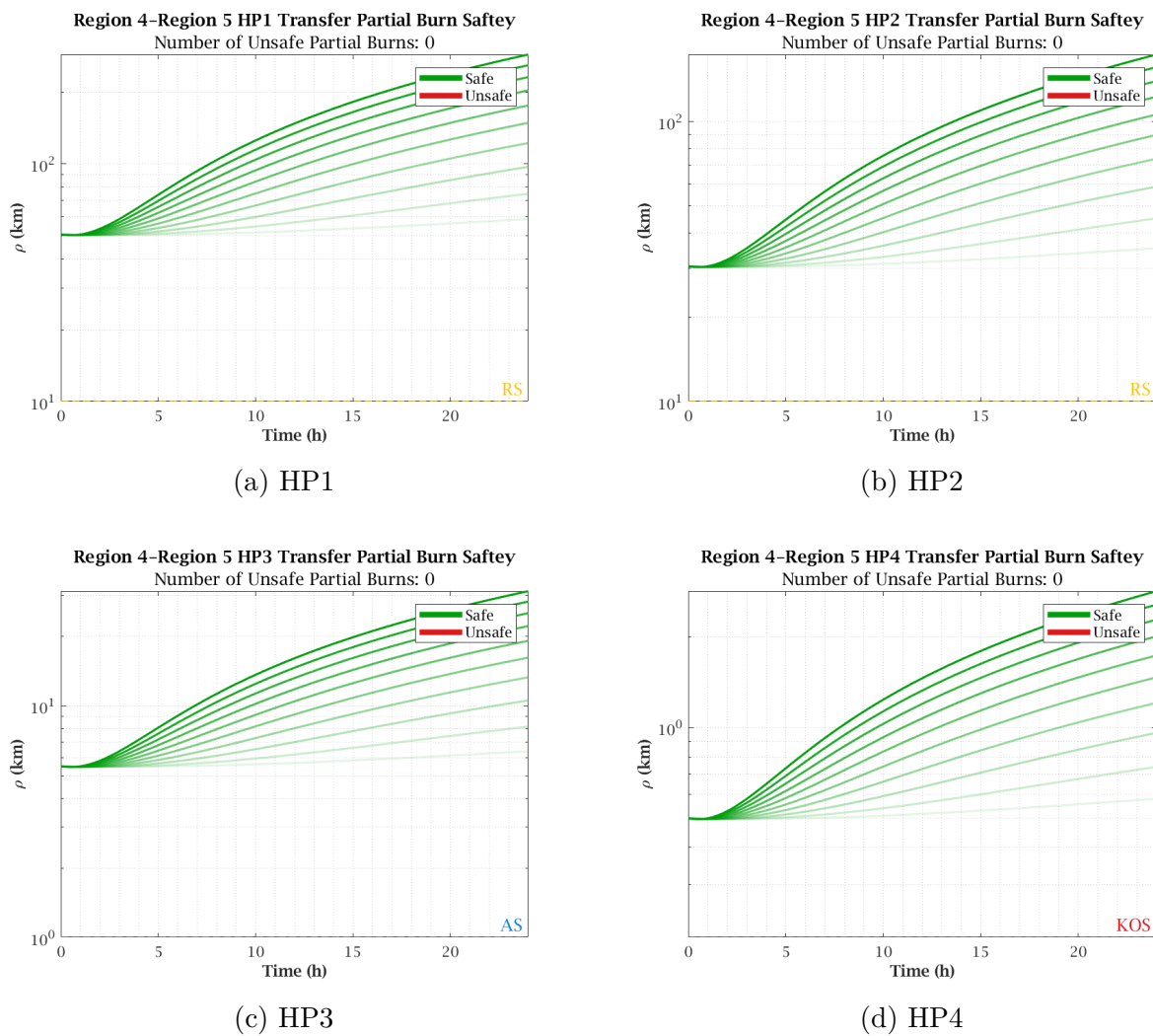
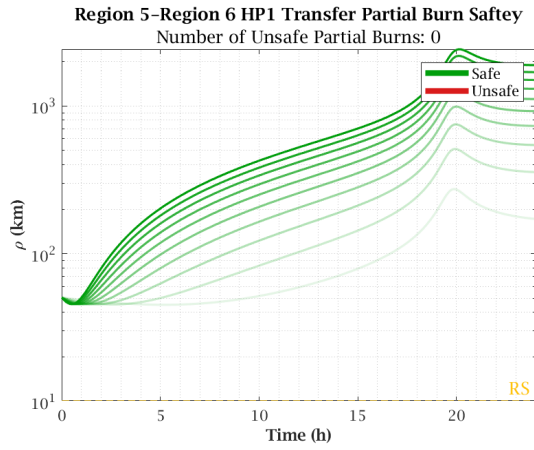
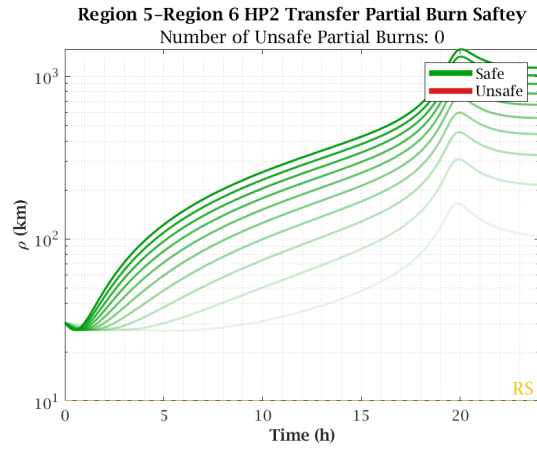


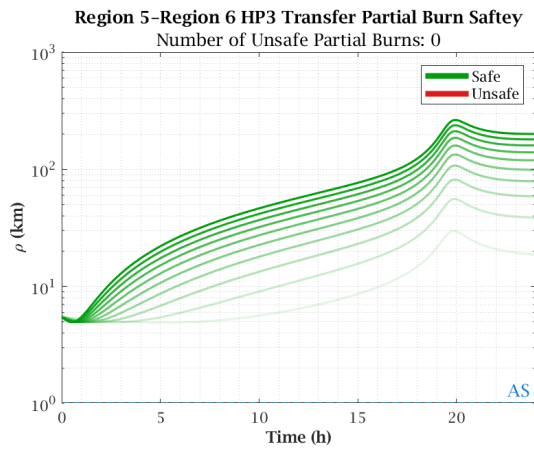
Figure D.4: Region 4 to Region 5 Region-to-Region Transfer Partial Burn Safety



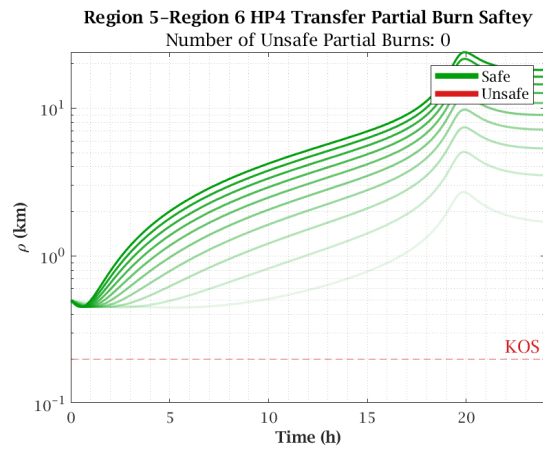
(a) HP1



(b) HP2



(c) HP3



(d) HP4

Figure D.5: Region 5 to Region 6 Region-to-Region Transfer Partial Burn Safety

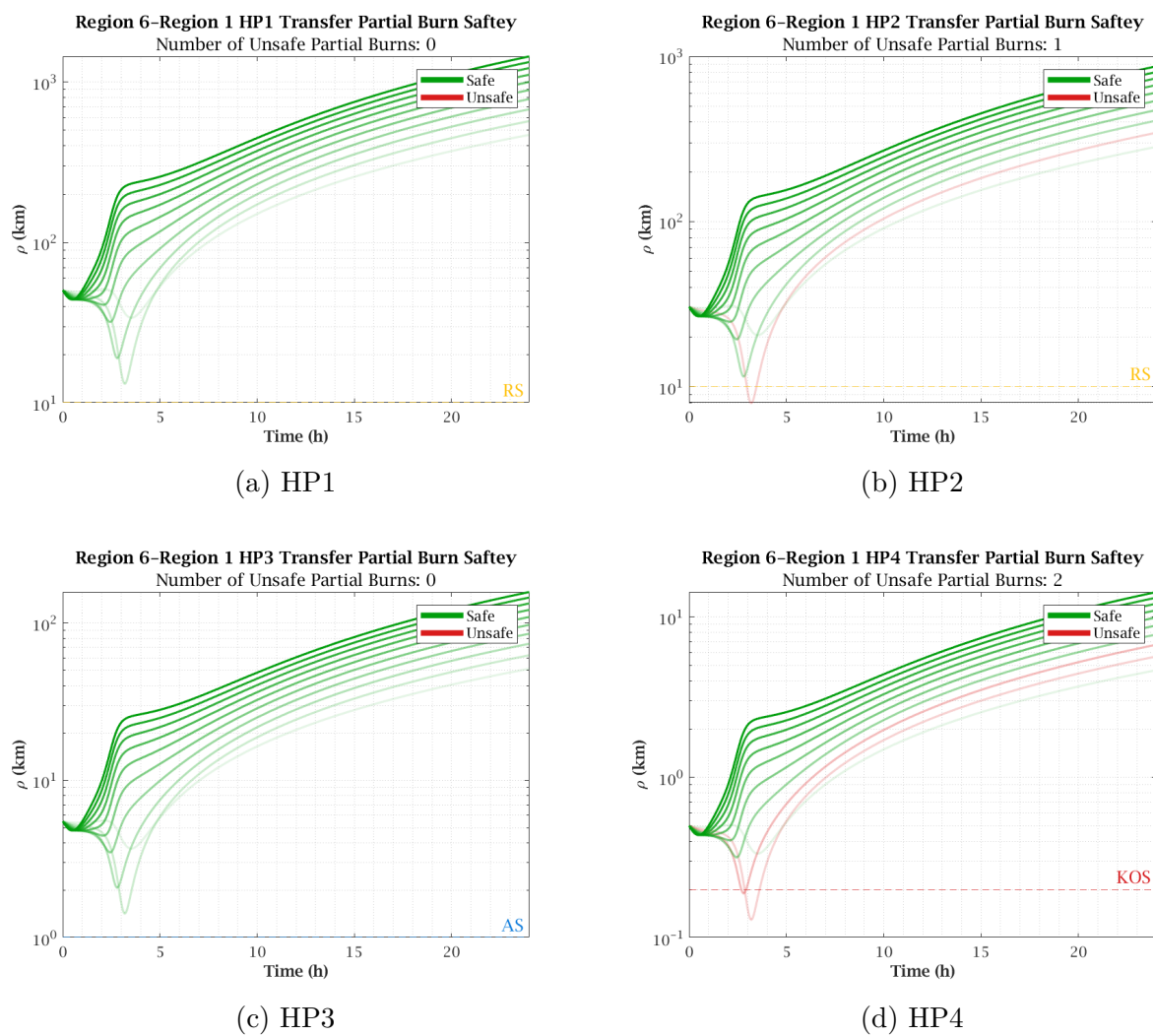
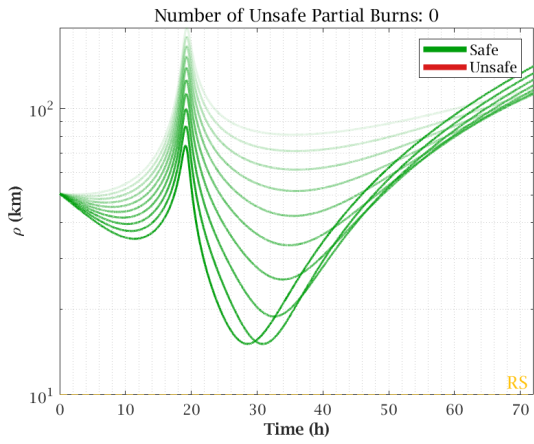
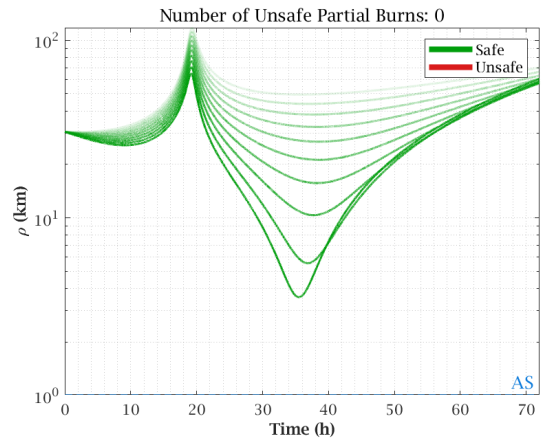


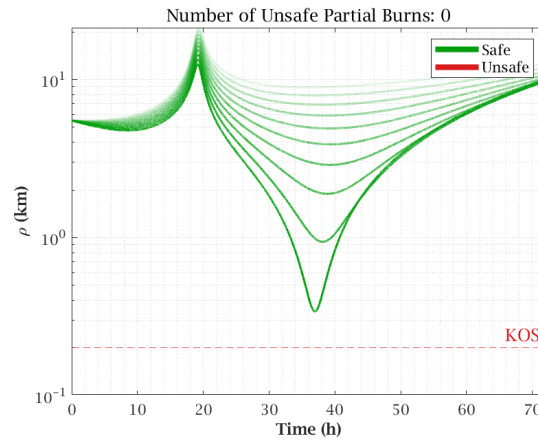
Figure D.6: Region 6 to Region 1 Region-to-Region Transfer Partial Burn Safety



(a) HP1



(b) HP2



(c) HP3

Figure D.7: Region 6 to Region 1 38 Hour Loiter Partial Burn Safety

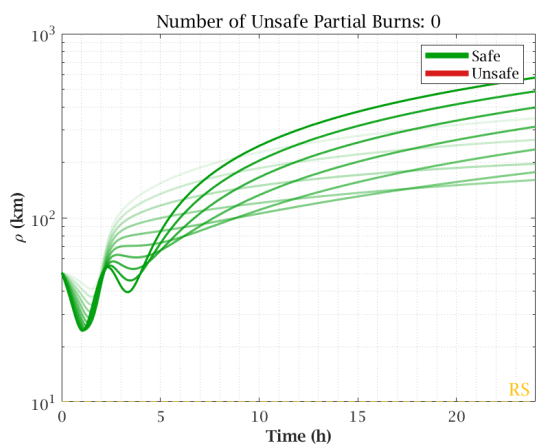
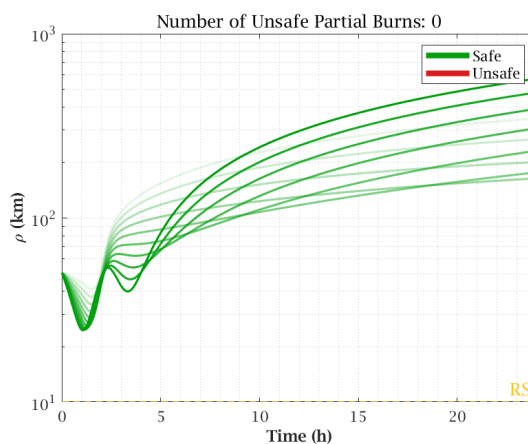
(a) $\rho_0 = -50.5$ (b) $\rho_0 = +50.5$

Figure D.8: Region 1, HP1, 4 Hour Loiter Partial Burn Safety

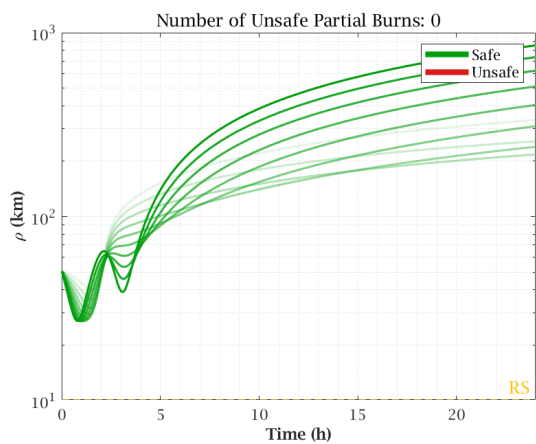
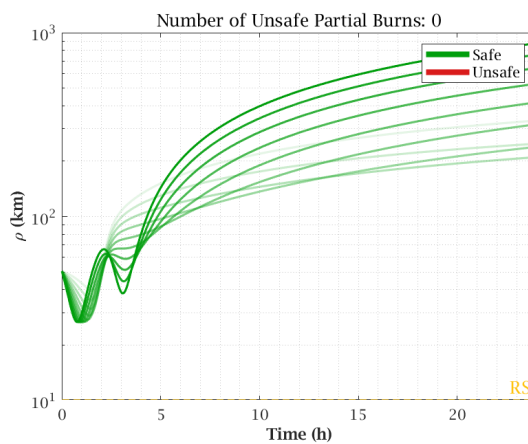
(a) $\rho_0 = -50.5$ (b) $\rho_0 = +50.5$

Figure D.9: Region 1, HP1, 3.5 Hour Loiter Partial Burn Safety

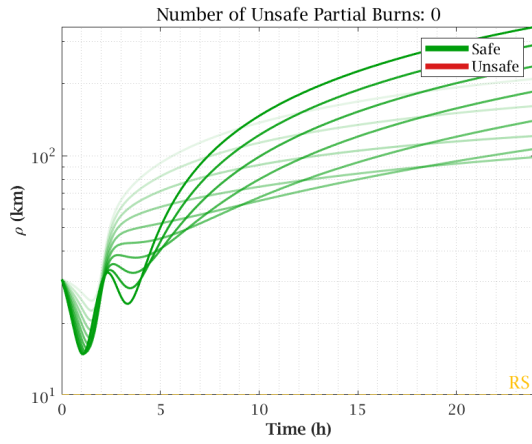
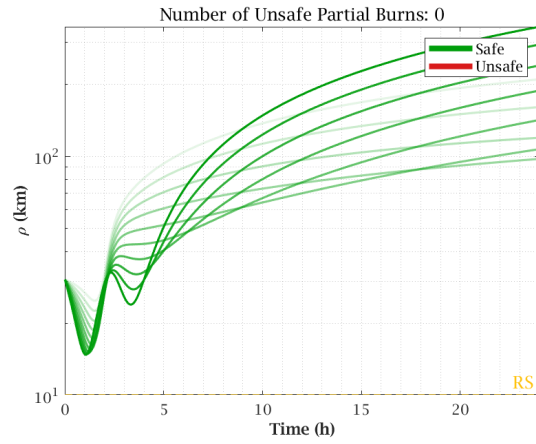
(a) $\rho_0 = -30.5$ (b) $\rho_0 = +30.5$

Figure D.10: Region 1, HP2, 4 Hour Loiter Partial Burn Safety

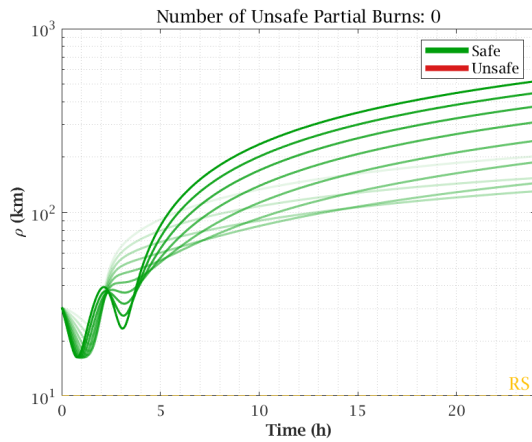
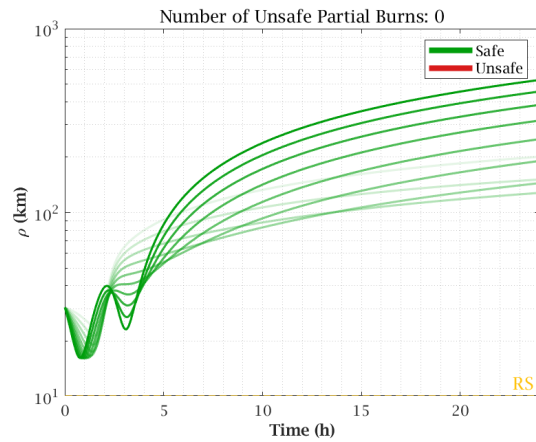
(a) $\rho_0 = -30.5$ (b) $\rho_0 = +30.5$

Figure D.11: Region 1, HP2, 3.5 Hour Loiter Partial Burn Safety

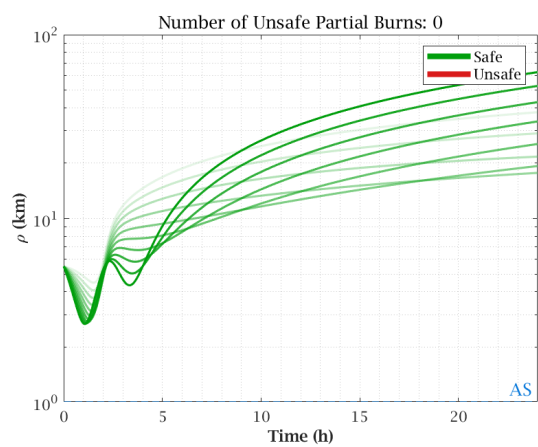
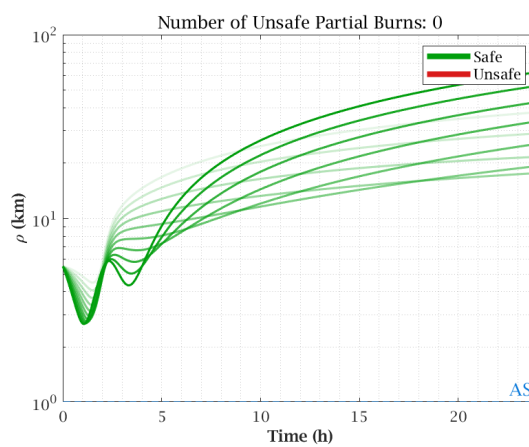
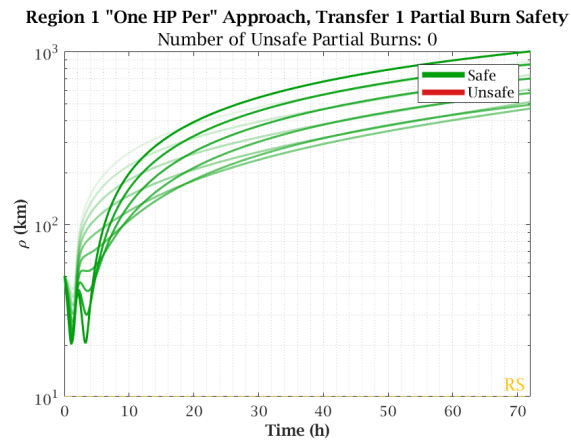
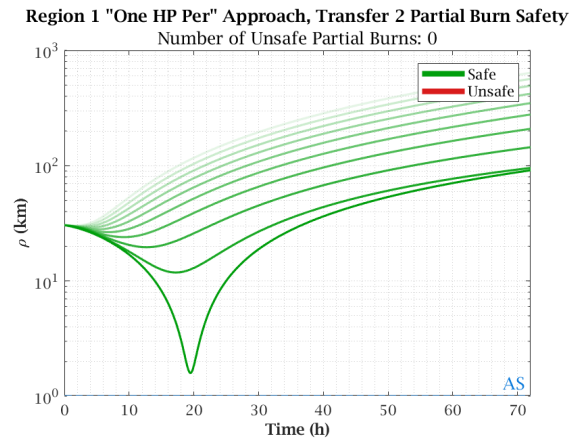
(a) $\rho_0 = -5.5$ (b) $\rho_0 = +5.5$

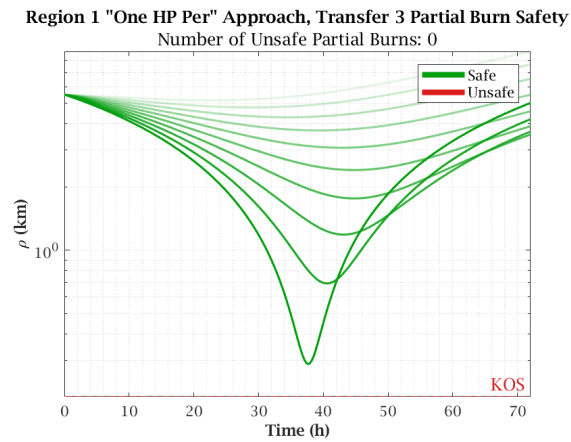
Figure D.12: Region 1, HP3, 4 Hour Loiter Partial Burn Safety



(a) Transfer 1



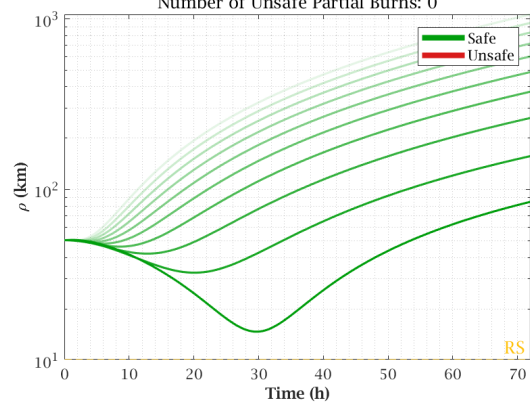
(b) Transfer 2



(c) Transfer 3

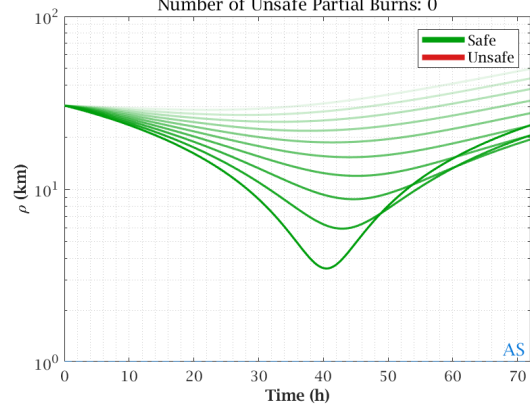
Figure D.13: Region 1 "One HP per" Partial Burn Safety Analysis Plots

Region 2 "One HP Per" Approach, Transfer 1 Partial Burn Safety
Number of Unsafe Partial Burns: 0



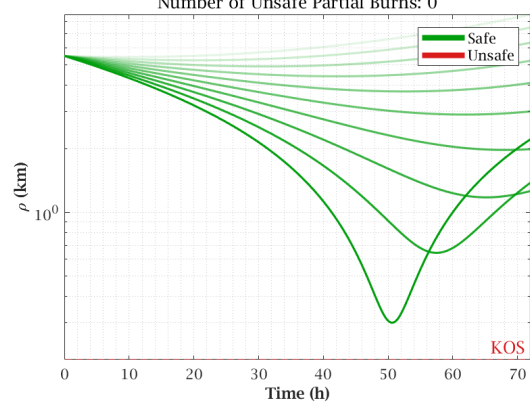
(a) Transfer 1

Region 2 "One HP Per" Approach, Transfer 2 Partial Burn Safety
Number of Unsafe Partial Burns: 0



(b) Transfer 2

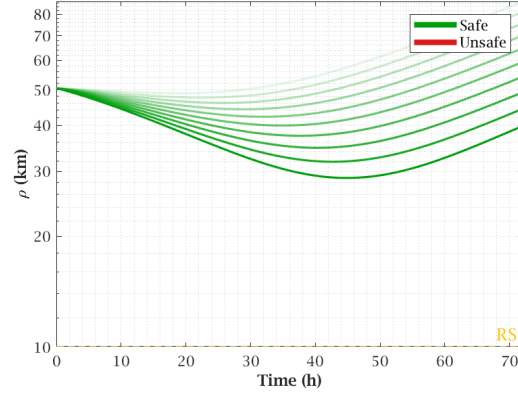
Region 2 "One HP Per" Approach, Transfer 3 Partial Burn Safety
Number of Unsafe Partial Burns: 0



(c) Transfer 3

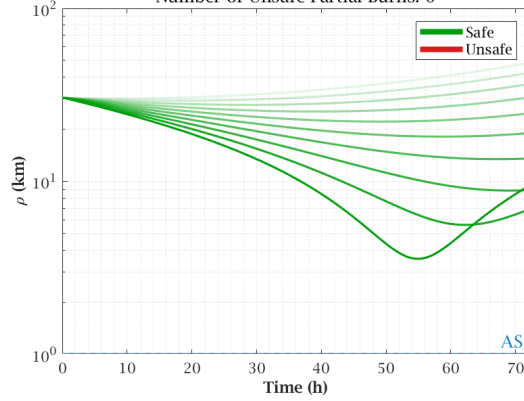
Figure D.14: Region 2 "One HP per" Partial Burn Safety Analysis Plots

Region 3 "One HP Per" Approach, Transfer 1 Partial Burn Safety
 Number of Unsafe Partial Burns: 0



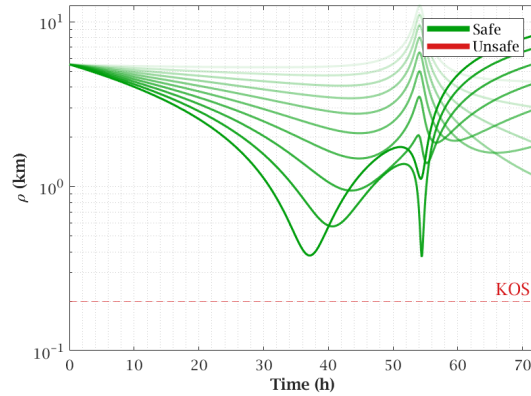
(a) Transfer 1

Region 3 "One HP Per" Approach, Transfer 2 Partial Burn Safety
 Number of Unsafe Partial Burns: 0



(b) Transfer 2

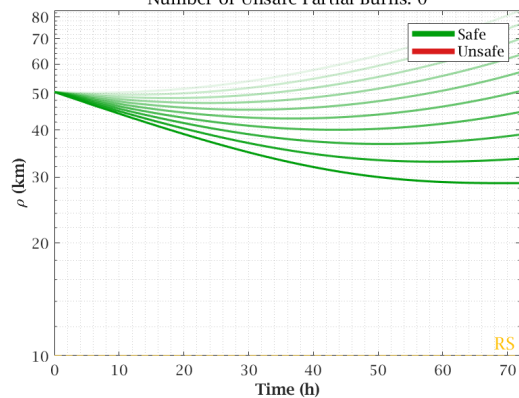
Region 3 "One HP Per" Approach, Transfer 3 Partial Burn Safety
 Number of Unsafe Partial Burns: 0



(c) Transfer 3

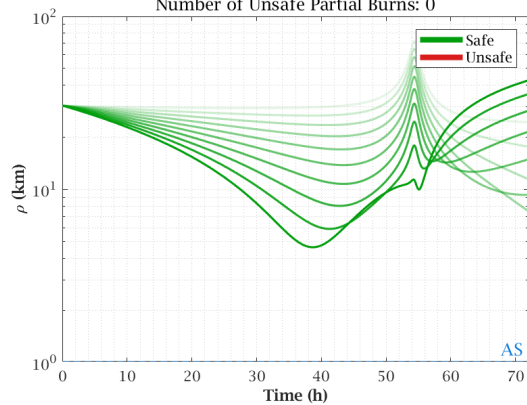
Figure D.15: Region 3 "One HP per" Partial Burn Safety Analysis Plots

Region 4 "One HP Per" Approach, Transfer 1 Partial Burn Safety
Number of Unsafe Partial Burns: 0



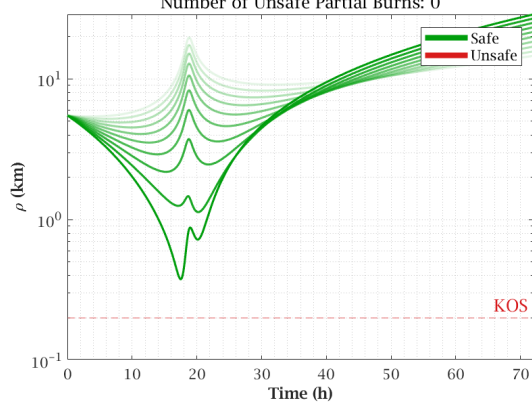
(a) Transfer 1

Region 4 "One HP Per" Approach, Transfer 2 Partial Burn Safety
Number of Unsafe Partial Burns: 0



(b) Transfer 2

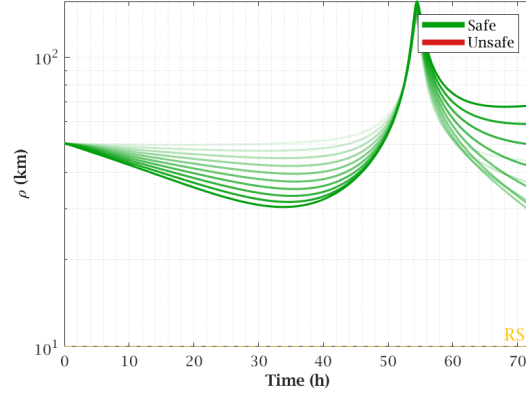
Region 4 "One HP Per" Approach, Transfer 3 Partial Burn Safety
Number of Unsafe Partial Burns: 0



(c) Transfer 3

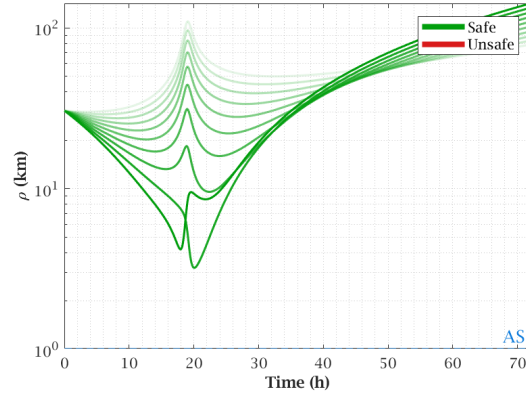
Figure D.16: Region 4 "One HP per" Partial Burn Safety Analysis Plots

Region 5 "One HP Per" Approach, Transfer 1 Partial Burn Safety
 Number of Unsafe Partial Burns: 0



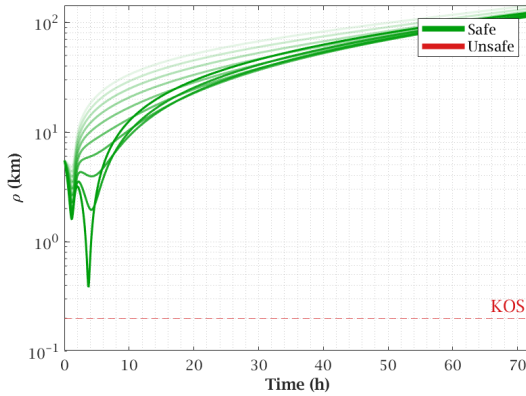
(a) Transfer 1

Region 5 "One HP Per" Approach, Transfer 2 Partial Burn Safety
 Number of Unsafe Partial Burns: 0



(b) Transfer 2

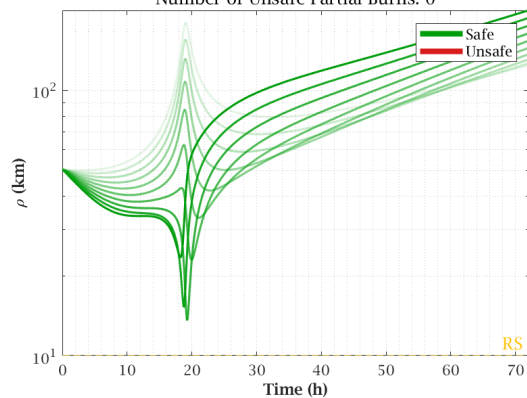
Region 5 "One HP Per" Approach, Transfer 3 Partial Burn Safety
 Number of Unsafe Partial Burns: 0



(c) Transfer 3

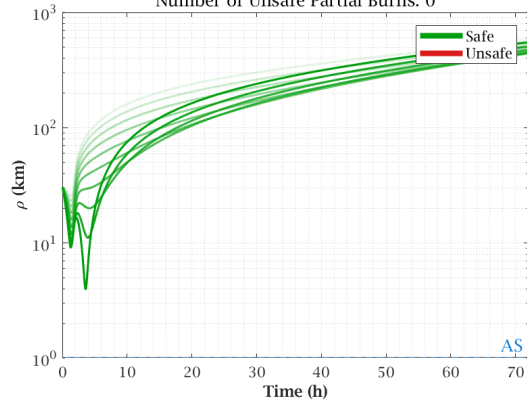
Figure D.17: Region 5 "One HP per" Partial Burn Safety Analysis Plots

Region 6 "One HP Per" Approach, Transfer 1 Partial Burn Safety
Number of Unsafe Partial Burns: 0



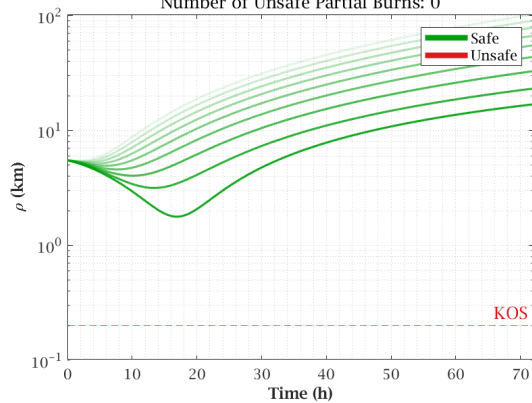
(a) Transfer 1

Region 6 "One HP Per" Approach, Transfer 2 Partial Burn Safety
Number of Unsafe Partial Burns: 0



(b) Transfer 2

Region 6 "One HP Per" Approach, Transfer 3 Partial Burn Safety
Number of Unsafe Partial Burns: 0



(c) Transfer 3

Figure D.18: Region 6 "One HP per" Partial Burn Safety Analysis Plots

Appendix E

“On-Orbit” Loiter TOF Optimization Contour Plots

Appendix E provides the TOF optimization contour plots discussed in Section 4.3.3.

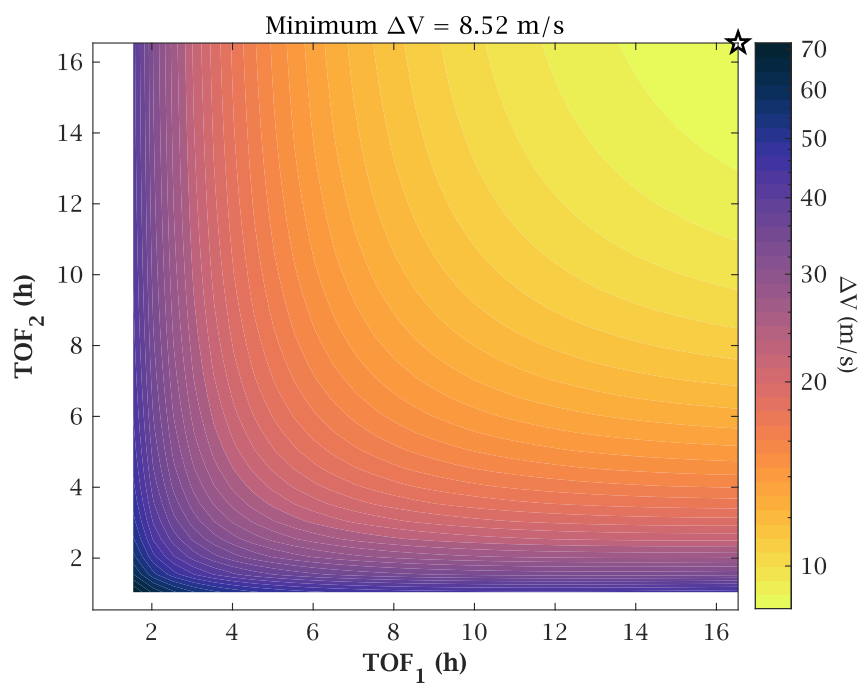


Figure E.1: On Orbit Hold Transfer TOF Optimization: -HP1.

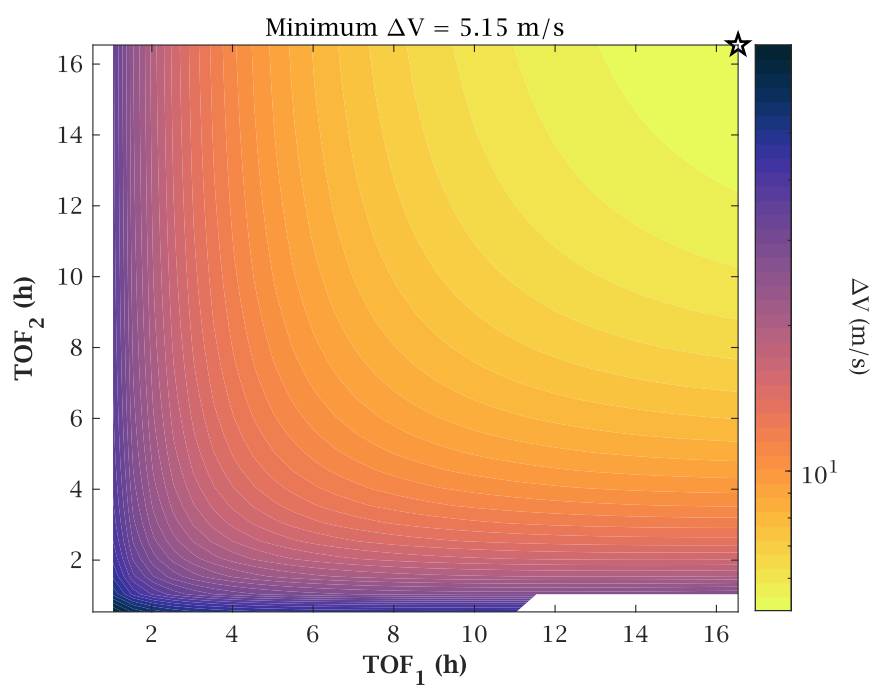


Figure E.2: On Orbit HoldTOF Optimization: -HP2.

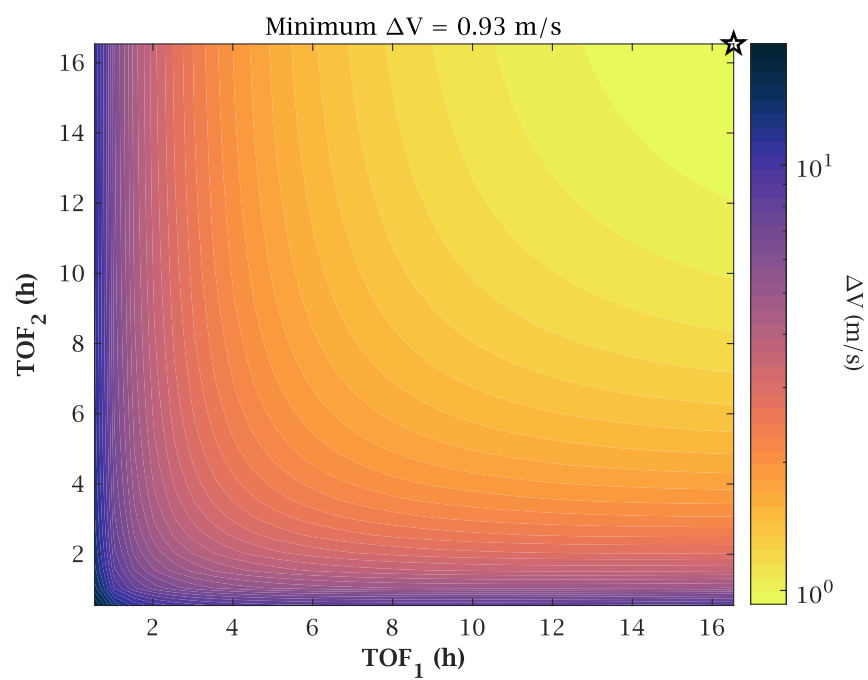


Figure E.3: On Orbit HoldTOF Optimization: -HP3.

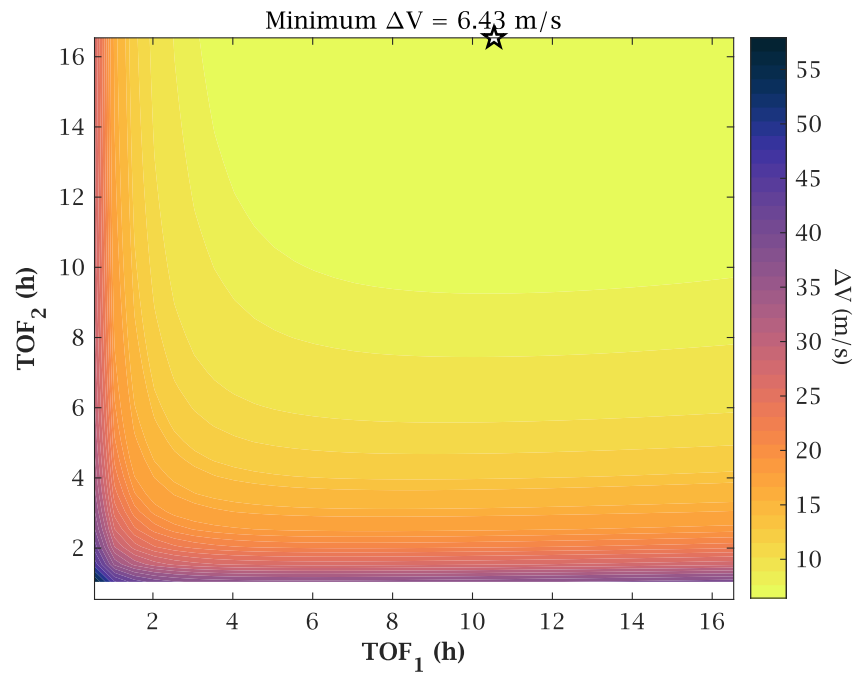


Figure E.4: On Orbit HoldTOF Optimization: +HP1.

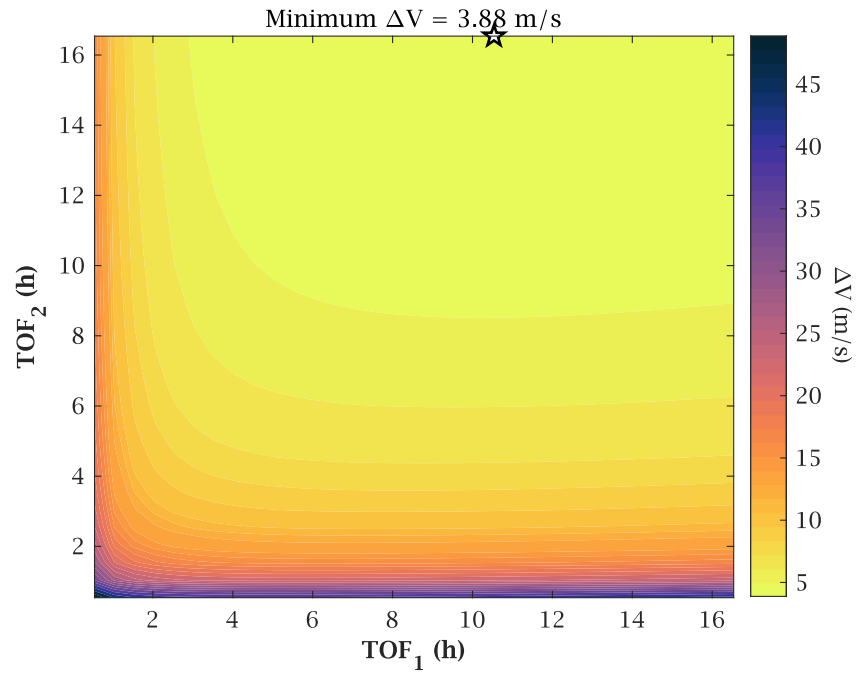


Figure E.5: On Orbit HoldTOF Optimization: +HP2.

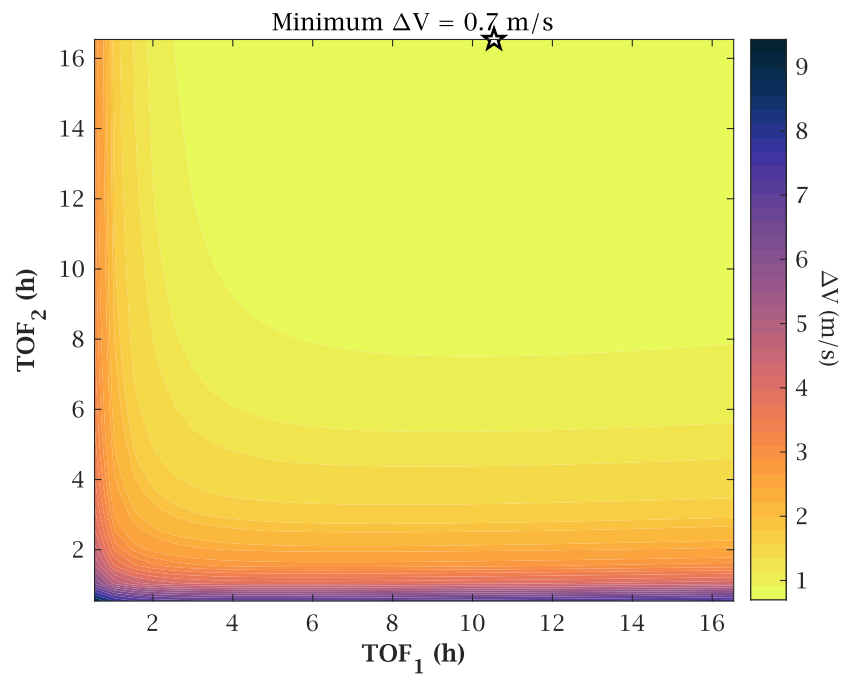
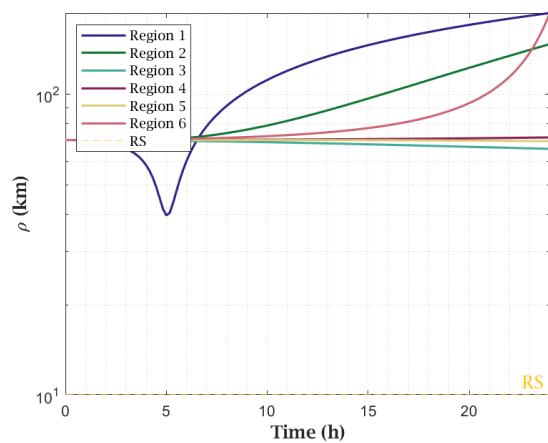


Figure E.6: On Orbit HoldTOF Optimization: +HP3.

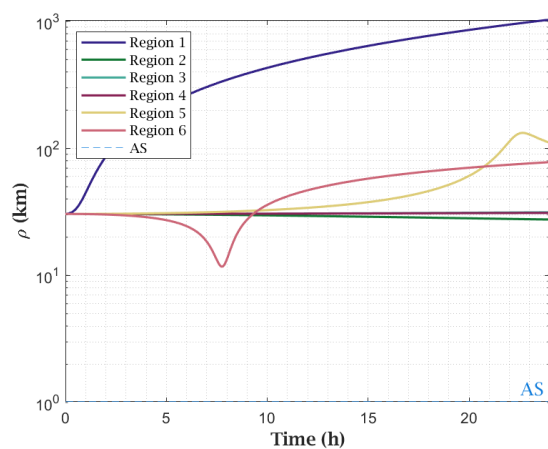
Appendix F

STK “One HP per” Approach Passive Safety Analysis

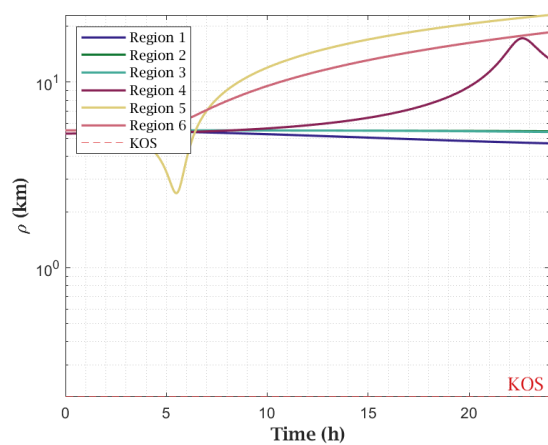
Appendix [F](#) provides the burn transfer safety plots discussed in Section [4.5.1](#).



(a) Transfer 1

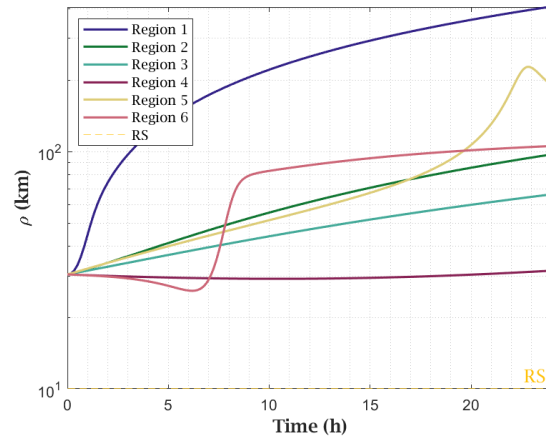


(b) Transfer 2

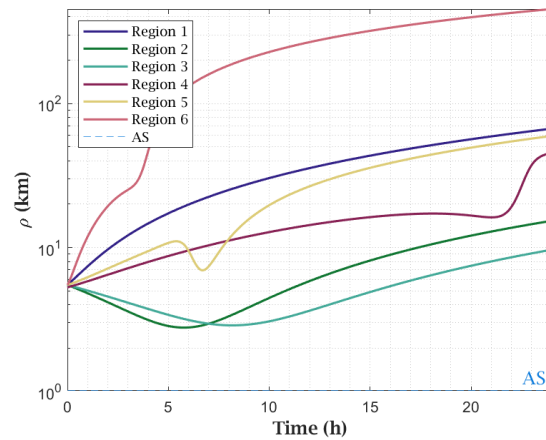


(c) Transfer 3

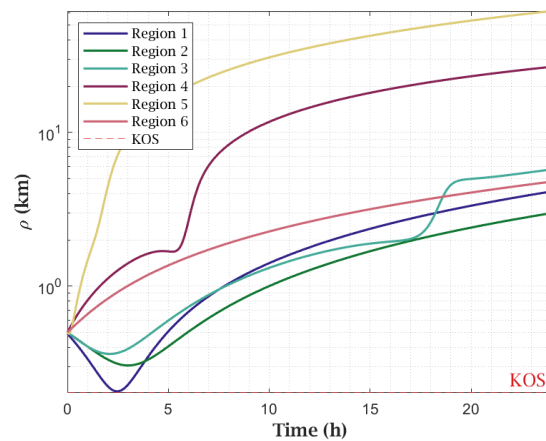
Figure F.1: “One HP per” Full Ephemeris Implementation Approach Transfer Departure Burn Passive Safety Analysis.



(a) Transfer 1



(b) Transfer 2



(c) Transfer 3

Figure F.2: “One HP per” Full Ephemeris Implementation Approach Transfer Arrival Burn Passive Safety Analysis.

Appendix G

Note on Franzini and Innocenti's

LVLH EORM

As noted in Chapter 3, Franzini and Innocenti's EORM were considered for modeling three-body relative motion in this thesis. A complete derivation of their model can be found in their paper, but it results in the Eq. G.1 [18].

$$\begin{aligned} [\ddot{\boldsymbol{\rho}}]_{\mathcal{L}} = & -2\boldsymbol{\Omega}_{l/i}[\dot{\boldsymbol{\rho}}]_{\mathcal{L}} - ([\dot{\boldsymbol{\Omega}}_{l/i}]_{\mathcal{L}} + \boldsymbol{\Omega}_{l/i}^2)\boldsymbol{\rho} + \mu \left(\frac{\mathbf{r}}{r^3} + \frac{\mathbf{r} + \boldsymbol{\rho}}{\|\mathbf{r} + \boldsymbol{\rho}\|^3} \right) \\ & + (1 - \mu) \left(\frac{\mathbf{r} + \mathbf{r}_{em}}{\|\mathbf{r} + \mathbf{r}_{em}\|^3} - \frac{\mathbf{r} + \boldsymbol{\rho} + \mathbf{r}_{em}}{\|\mathbf{r} + \boldsymbol{\rho} + \mathbf{r}_{em}\|^3} \right) \end{aligned} \quad (\text{G.1})$$

Where $\boldsymbol{\Omega}_{l/i}$ and $\dot{\boldsymbol{\Omega}}_{l/i}$ are the skew-symmetric matrices containing the angular velocity and acceleration terms of the target with respect to the Moon. The author was able to verify all positional derivatives used in this equation against other works to ensure their accuracy. However, these terms could not be accurately computed when implementing these equations.

The author believes the error in his work is due to the computation of the jerk term within the angular acceleration matrix, but implementing alternatives to calculate the jerk, like finite differencing, did not resolve the issues. No works to date that have implemented these equations have produced a figure or table to compare these terms against making reproduction challenging.

This model has led to exciting work that has been published in literature by various independent research groups. However, attempts to implement this model during the research for this thesis resulted in extreme inaccuracies in chaser motion. In some cases, the chaser was able to accelerate up to $100\times$ the speed of light in under three weeks. The author hopes future reproductions of Franzini and Innocenti's work will provide clearer insights into the angular terms to identify the root cause of the failed attempts to recreate their work.